CANADIAN THESES

THÈSES CANADIENNES

NOTICE

The quality of this microfiche is heavily dependent upon the quality of the original thesis submitted for microfilming. Every effort has been made to ensure the highest quality of reproduction possible.

If pages are missing, contact the university which granted the degree.

Some pages may have indistinct print especially if the original pages were typed with a poor typewriter ribbon or if the university sent us an inferior photocopy.

Previously copyrighted materials (journal articles, published tests, etc.) are not filmed.

Reproduction in full or in part of this film is governed by the Canadian Copyright Act, R.S.C. 1970, c. C-30. Please read the authorization forms which accompany this thesis.

AVIS

La qualité de cette microfiche dépend grandement de la qualité de la thèse soumise au microfilmage. Nous avons tout fait pour assurer une qualité supérieure de reproduction.

S'il manque des pages, veuillez communiquer avec l'université qui a conféré le grade.

La qualité d'impression de certaines pages peut laisser à désirer, surtout si les pages originales ont été dactylographiées à l'aide d'un ruban usé ou si l'université nous a fait parvenir une photocopie de qualité inférieure.

Les documents qui font déjà l'objet d'un droit d'auteur (articles de revue, examens publiés, etc.) ne sont pas microfilmés.

La reproduction, même partielle, de ce microfilm est soumise à la Loi canadienne sur le droit d'auteur, SRC 1970, c. C-30. Veuillez prendre connaissance des formules d'autorisation qui accompagnent cette thèse.

THIS DISSERTATION
HAS BEEN MICROFILMED
EXACTLY AS RECEIVED

LA THÈSE A ÉTÉ
MICROFILMÉE TELLE QUE
NOUS L'AVONS REÇUE

Canada

IMMERSED SURFACE HEAT TRANSFER IN A VIBRATED FLUIDIZED BED

by

KARUN MALHOTRA

A thesis submitted to the
Faculty of Graduate Studies and Research
of McGill University
in partial fulfillment of the requirements for
the degree of Master of Engineering

Thesis Supervisor: Dr. A.S. Mujumdar
Department of Chemical Engineering
McGill University
Montreal, Quebec,
Canada.

" When you can measure what you are speaking about and express it in numbers, you know something about it; but when you cannot measure it, when you cannot express it in numbers, your knowledge is of a meager and unsatisfactory kind: it may be the beginning of knowledge, but you have scarcely, in your thoughts, advanced to the stage of science "

- Lord Kelvin

ABSTRACT

Results of an experimental study of the flow characteristics and immersed-surface heat transfer rates in a vertically vibrated aerated bed of model particles are presented and discussed. Variables examined included vibrational acceleration (0-4 times gravity), vibration frequency (0-105 rad/s), vibration amplitude ($0-4.25\times10^{-3}$ m), air flow (0-0.60 m/s), surface stickiness (0-0.006 kg glycerine/ kg dry particles), particle moisture content (0-0.40 kg water/ kg dry particles), particle size (0.325×10^{-3}-2.36×10^{-3} m), bed height (80×10^{-3}-130×10^{-3} m) and cylinder diameter (25×10^{-3}-38.1×10^{-3} m). Glass ballotini and molecular sieve particles were used as model particles.

The flow experiments were performed in a two-dimensional bed (0.20 m x 0.05 m). The effect of vibration on fluidization and mixing characteristics for beds of dry and sticky particles is examined. The effects of the various parameters on the fluidized bed pressure drop are also discussed briefly. Flow visualization studies were performed to observe flow patterns around horizontal, rigidly mounted immersed circular cylinders.

A parametric study of the effect of vibration on surface-to-bed heat transfer is presented. Application of vibration was found to enhance heat transfer rates severalfold. Development of particle-free air gaps around immersed cylinders were observed to affect the heat transfer rate. A dramatic increase in the heat transfer rate was found to occur during removal of surface moisture for molecular sieve particles. Below

the critical moisture content the heat transfer rate approaches rapidly that for completely dry beds under identical operating conditions. Finally, a physical model based on the observed mixing and flow patterns in a VFB and on existing theories on contact heat transfer is proposed to predict the average surface-to-bed heat transfer coefficient in a VFB.

RESUME

Les résultats d'une étude expérimentale des caractéristiques aérodynamiques et des vitesses du transfert de chaleur de surfaces immergées dans un lit aéré en vibration verticale pour de particules modèls sont présentés et discutés. Les variables étudiées induent l'accélération des vîbrations (0-4 fois la gravité), la fréquence de vibration (0-105 rad/s), l'amplitude de vibration ($0-4.25\times10^{-3}$ m), la vîtesse de l'air (0-0.60 m/s), l'adhésivité de la surface (0-0.006 kg glycerine/kg particules sâches), lateneur enhumidité des particules (0-0.4 kg eau/kg particules séches), la grosseur des particules (0.325×10^{-3}- 2.36×10^{-3} m), la hauteur du lit (80×10^{-3}-130×10^{-3} m) et le diamètre des cylindre (25×10^{-3}-38.1×10^{-3} m). Duverre ballotini et de la sidérose moléculaire étaient utilisés comme particules modèles.

Les expériences aérodynamiques furent faites dans un lit á deux dimensions (0.20 m x 0.05 m). L'effet de la vibration sur la fluidisation et sur les caractéristiqués de mélange pour des lits de particules séches et collantes a été étudié. Les effets des différents paramètres sur la chute de pression des lit fluidisés sont aussi brievèment discutés. Des études de visualisation aérodynamique furent exécuté pour observer les diagrammes d'ecoulement á l'entour de cylindres circulaires immergès et monté rigidement.

Une étude de l'effet de la vibration sur le transfert de chaleur de la surface au lit présenteé. Il a été trouvé que l'utilisation des vibrations augmente grandement le transfert de

chaleur. La vitesse du transfert de chaleur est affectée par le développment de trous d'air sans particules á l'entour des cylindres immergés.

Une augmentation marquée dans la vitesse du transfert de chaleur a été observée lorsque l'humidité de surface est eliminée des particules moleculaire de sidérose. Au-dessous du taux d'humiditécritique, la vitesse du transfert de chaleur approche rapidement celur obtenu pour des lits complètment secs dans des conditions sinilaires. Finalement, un modèle physique basé sur le mélange observé et les diagrammes découlement dans un LFV et sur les theories existantes décrivant le transfert de chaleur de contact est proposé pour prédire le coefficient moyen du transfert de chaleur de la surface au lit dans un LFV.

ACKNOWLEDGEMENTS

The author wishes to express his sincere gratitude to his thesis advisor, Dr. A.S. Mujumdar for his constant advice, instruction and valuable guidance during this project.

Thanks are due to Mr A. Krish, Mr J.Dumont, Mr W. Greenland and Mr A. Gagnon for their help in fabrication and modification of the experimental setup; to Mr Louis Law, Miss Rosalba Lozada, Mr Richard Figueredo and Mr Ziaie Babak for lending a helping hand with the experimentation. Special thanks are due to Union Carbide, Alabama, U.S.A. for supplying molecular sieve particles and Mr J.A. Cripps of Union Carbide, Toronto, Canada, for providing relevant information on the properties of molecular sieve particles.

TABLE OF CONTENTS

LIST OF FIGURES

LIST OF TABLES

NOMENCLATURE

A	Amplitude of vibration, m
A_b	Cross-sectional area of bed, m^2
Ac	Surface area of the immersed heater, m^2
a	Empirical constant, (Equation 5.3.11)
C_f	Specific heat of fluid, J/kgK
Cp	Specific heat of particles, J/kgK
Cs	Specific heat of emulsion, J/kgK
D	Cylinder diameter, m
dp	Average particle diameter, m
F_h	Adhesion force, N/m^2
Fv	Vibration factor, -
f	Frequency of vibration, Hz
f_B	Local bubble frequency, Hz
g	Acceleration due to gravity, m/s^2
H	Height of the bed, m
h	Average surface-to-bed overall heat transfer coefficient, W/m^2K
h°	Average surface-to-bed overall heat transfer coefficient in presence of surface moisture, W/m^2K
hc	Particle contact heat transfer coefficient, W/m^2K
hcm	Maximum heat transfer coefficient for a CFB, W/m^2K
he	Particle convective heat transfer coefficient, W/m^2K
he'	Particle convective heat transfer coefficient for a CFB, W/m^2K
hg	Gas convective heat transfer coefficient, W/m^2K
hmax	Maximum overall surface-to-bed heat transfer coefficient, W/m^2K

ho	Average surface-to-bed heat transfer coefficient for non-vibrated beds, W/m^2K
hp	Surface-to-particle heat transfer coefficient, W/m^2K
hs	Surface-to-bed heat transfer coefficient, W/m^2K
hv	Heat transfer coefficient for air gaps, W/m^2K
hr	Radiation heat transfer coefficient, W/m^2K
Kc	Thermal conductivity of cylinder, W/mK
K_f	Thermal conductivity of fluid, W/mK
Kp	Thermal conductivity of particles, W/mK
Ks	Effective bed thermal conductivity, W/mK
Ks°	Effective bed thermal conductivity of a non-aerated, non-vibrated bed, W/mK
Kw	Thermal conductivity of water, W/mK
L	Length of heater, m
M	Mass of bed, kg
m	Molecular weight of the fluid, kg/kgmole
ΔP	Bed pressure drop, N/m^2
ΔPmf	Bed pressure drop at minimum fluidization, N/m^2
ΔPo	Orifice pressure drop, N/m^2
p	Absolute pressure, N/m^2
Q	Heat input to the bed, W
R	Universal gas constant, J/kgmol K
R_k	Thermal resistance to particle contact heat transfer, m^2K/W
S	Local gap width between the surfaces of wall and sphere, m
T	Average fluid temperature, K
T_b	Average bed temperature, K
Ts	Average surface temperature, K

ΔT	Temperature drop ($T_s - T_b$), K
t	Particle contact time, s
t'	Modified particle contact time, s
te	Flight time, s
t_i	Time period of one oscillation, s
tp	Packet residence time, s
U	Superficial air velocity through the bed, m/s
U'	Fluctuating component of air velocity, m/s
Umf	Minimum fluidization velocity for non-vibrated bed, m/s
Umm	Minimum mixing velocity, m/s
Uopt	Air velocity for maximum heat transfer in a CFB, m/s
Up	Particle velocity, m/s
X	Moisture/stickiness content of particles, kg water/ glycerine per kg dry particles
Xc	Critical moisture content of particles, kg water per kg dry particles
Xe	Equilbrium moisture content of particles, kg water per kg dry particles
Y	Maximum gap width around immersed cylinder, m

Greek letters

δ	Total roughness of the wall surface and the sphere, m
Λ	Mean free path of gas molecules, m
ε_h	Heat transfer enhancement factor, h/ho, -
θ	Extent of coverage of particle free air gaps around the immersed circular cylinder, °
ϕ	Particle shape factor, -
ψ	Void fraction, -

ψ_o	Void fraction for non-aerated, non-vibrated bed, -
μ	Viscosity of fluid, Pa.s
ρ_b	Bulk density of the bed, kg/m³
ρ	Density of fluid, kg/m³
ρ_p	Particle density, kg/m³
ω	Angular frequency of vibration, rad/s
Γmax	Value of Γ at hmax
Γ	Extended vibrational acceleration number, -
γ	Accomodation coefficient

Dimensionless Numbers

Ar	Archimedes number, $gdp^3(\rho_p/\rho - 1)(\rho/\mu)^2$
Bi	Biot number, hD/Kc
N	(Nu - Nu°)/(Numax - Nu°)
Nu	Nusselt number, hD/Ks
Numax	Maximum Nusselt number, hmax D/Ks
Nu°	Nusselt number at Γ=0, hoD/Ks
Pr	Prandtl number, $Cp\mu/K$
Re	Reynolds number, $DU\rho/\mu$
Rep	Particle Reynolds number, $dpU\rho/\mu$
Γ	Vibrational acceleration number, $A\omega^2/g$

Note: Since this thesis is typed on a word processor (McGill MUSIC SCRIPT) lower case characters are used instead of subscripts.

CHAPTER 1

INTRODUCTION

Certain drawbacks of conventional fluidized beds, viz gas bypassing, rapid solid mixing, attrition and entrainment of friable materials have a negative effect upon the contact between phases and the productivity of some industrial processes. To improve performance of fluidized beds many modifications have evolved. These include fluidization by gas under pressure, fluidization with impulsed circulation of fluid, fluidization with simultaneously flowing liquids and gases, fluidization in centrifugal field, improving hydraulic resistance of the distributor, use of baffles and fluidization in conical vessels etc. One of the most successful modification has been the application of vertical and horizontal vibration to fluidized beds.

The application of vibrated fluidized beds (VFB) in practice has grown substantially during the last two decades. Application of mechanical vibration facilitates fluidization of sticky or agglomerating solids which cannot be fluidized conventionally. It is noteworthy that it is also possible to " pseudo-fluidize " beds of solids at vibrational accelerations in excess of gravity without the aid of air flow. Such systems can be used for heating, cooling or coating applications, and also for vacuum contact drying of wet, sticky granular media.

The major application of vibrated fluidized beds remains in the area of drying. VFB's are also used frequently for

granulation (e.g." instantizing" spray dried product). Some of the applications include the drying of granulated fertilisers, polymer chips, inorganic and organic chemicals, pharmaceuticals, food products (e.g. sugar, cocoa, coffee), asbestos fibres, clay etc. In addition, a growing interest in utilising mechanical vibration to improve fluid bed processing in such diverse applications as calcination, exothermic gas-solid reactions, polymer coating, metal sintering and steaming of pulp and wood have been reported by Gupta (1979). Vibrating equipment has also proven economical in duties such as moistening, aspirating, pickling, separating and dewatering.

An industrial VFB is typically a long horizontal rectangular trough which is vibrated at a slight angle to the vertical to permit conveying of solids along the trough. The degree of vibration required depends upon the material being processed, its particle size, its readiness to fluidize and the desired rate of feed along the trough. The combination of air and vibration reduces the fluidizing velocity requirement substantially and hence tends to minimize the fines entrainment. VFB's are mounted on well-designed resonance springs to minimize power consumption. The operating costs can be reduced by selecting optimum vibrating parameters as shown by Erdesz and Ormos (1984). They reported that in batch-operated systems the optimum vibrating parameters are in the Γ=1-5 range. A number of commercial VFB systems have been illustrated by Shah and Goel (1980), Danielsen and Hovmand (1978), Pye (1974), Engelmann (1958) and Hastani et al (1984).

Despite the marginally increased equipment complexity due to added vibrational motion, the VFB offers several advantages accounting for its growing commercial success. These include:

1. Easier control of residence time by manipulating vibrational parameters (amplitude and frequency of vibration) without affecting the gas flow rates. In continuous operation, plug-flow conditions can be achieved thereby making it ideal for the processing of heat sensitive materials.

2. Reduced air requirements for fluidization at reasonable vibrational acceleration levels (may be as low as 20 per cent of the minimum fluidization requirement in a conventional non-vibrated bed) resulting in a remarkable reduction in the bed pressure drop. This leads to a reduction in bed size, air-ducts and dust collecting equipment (due to considerable reduction in entrainment as well as reduced air volumes).

3. Ability to handle polydisperse materials. The wide particle size distribution of some products makes the choice of the operating velocity in conventional fluidized beds very difficult. In a VFB the material is transported and " pseudo-fluidized" by vibration and therefore gas flowrates can be chosen relatively independently.

4. More efficient and uniform drying of sticky, pasty or agglomerating particles due to better quality fluidization,

achieved with the help of mechanical agitation.

5. Drying, cooling and conveying can be carried out in the same equipment simultaneously.

6. Vibration eliminates " deadzones " within the dryer, resulting in more hygienic operations for food products by reducing the risk of bacterial growth.

Other features of VFB include higher heat and mass transfer rates, gentler handling of friable materials, ease of closed cycle drying and recovery of organic solvents (Danielsen and Hovmand (1978)) and an overall more economic operation as compared to conventional drying equipment.

Heat transfer between submerged surfaces and VFB is an area of significant industrial interest especially in the design of energy-efficient thermal processing of hard-to-fluidize, polydisperse and/or sticky granular solids. Sometimes it is necessary to supply supplemental heat when the fluidizing air must be at lower temperature or if the air flowrate must be low for process reasons. The heat exchange surfaces may be plane, vertical panels or multiple tubes arranged horizontally or vertically. Since the bed depth is limited due to rapid attenuation of vibrational energy within the bed, vertical tube arrangements appear to have little industrial potential in VFB applications.

Rigidly mounted horizontal tubes allow more heat exchange

surface to be packed in a given VFB while permitting use of deeper beds as the tubes impart additional vibrational energy within the bed itself. Suspended heat transfer surfaces appear to be more interesting for practical considerations. Work is in progress to evaluate these (Kwamya and Mujumdar (1984)).

A major part of all published work on immersed surface-to-bed heat transfer in VFB's is in Russian and is reviewed fully by Pakowski et al (1984). Pakowski and Mujumdar (1982) reported for the first time a dramatic diminution in cylinder heat transfer from a horizontal cylinder to a vibrated bed of sticky glass ballotini particles. It was shown that this reduction was caused by inhibition of particle mixing and formation of larger air gaps around the cylinder as compared to beds of dry ballotini. Surface stickiness was induced by coating the glass ballotini particles with controlled amounts of glycerine.

This project deals with immersed surface-to-bed heat transfer in a VFB of dry and wet (sticky) particles. Since the heat transfer process is governed by the bed aerodynamics, flow behaviour of dry and sticky particles in a VFB, including the effect of various pertinent parameters (e.g. amplitude and frequency of vibration, particle size, bed height, aeration rate and moisture content) on the flow past a cylinder immersed in a VFB, has also been examined. A flow visualization study was conducted in a two-dimensional bed to examine particle free air gaps around immersed horizontal cylinders in a VFB of dry and sticky particles. The cylinders were in all cases described in

this thesis, mounted rigidly to the vessel walls i.e. the heat exchange surface also acts as a vibrator.

The main objectives of this project were twofold:

1. To perform heat transfer experiments with rigidly-mounted horizontal circular cylinders immersed in a VFB and study the effect of vibrational amplitude and frequency, aeration rate, particle size and type, moisture and stickiness on the heat transfer rate from the immersed cylinder to the bed.

2. To examine the flow and mixing behaviour of dry and sticky particles in a VFB with immersed horizontal cylinder in order to explain the heat transfer results.

This thesis is divided into two main sections- aerodynamics and heat transfer. Chapter 4 deals with aerodynamics and includes the effect of vibrational acceleration on fluidization curves for dry and sticky particles; bed pressure drop; mixing; flow patterns around immersed cylinders and extended vibrational acceleration number. Chapter 5 presents a parametric study of average surface- to-bed heat transfer coefficient and a physical model based on the observed mixing characteristics of the bed and particle free air gaps around the cylinder. Chapter 2 briefly surveys the available relevant literature on the subject, while Chapter 3 describes the experimental facility and procedures.

CHAPTER 2

REVIEW OF RELATED LITERATURE

2.1 INTRODUCTION

As discussed in the preceding chapter fluidization of solids with the aid of mechanical vibration has been one of the most successful operations commercially. Intense research and development activity in conventional fluidized beds (CFB's) started in the late fifties, after pioneering work in the theoretical modelling of the formation, stability and size of bubbles in conventional fluidized beds (CFB) by Kunii and Levenspiel (1967), Harrison and Leung (1961) amongst others, was completed. The understanding of the flow mechanism in CFB's helped in the development of modifications to improve the performance of fluidized beds.

Most of the available literature on VFB research and development is from East European countries, the USSR and Japan. Gupta (1979) reported that about 75% of retrieved literature citations (in 1978) were in Russian; about 15 percent in Polish, Rumanian and Japanese while less than 10 percent of the citations were from English speaking parts of the world.

Bratu and Jinescu (1971), Bretsznajder et al (1963), Bukarwa et al (1969), Chelenov and Mikhailov (1965), Yamazaki et al (1974) and Gutman (1974) are some of the early workers in the field of vibrated fluidized beds. Apart from trade literature (Engelmann (1958), Pye (1974)) only one paper (Danielsenand Hovmand (1980)) appears to have been

published by a manufacturer of VFB equipment.

Despite the widespread interest in the VFB process, the complexity of the phenomenon has defied all attempts at understanding the basic mechanism. The design parameters of VFB's have been attempted to be correlated with the vibratory acceleration, $\omega^2 A$ (Bratu and Jinescu (1971), Yamazaki et al (1974), Erdesz and Ormos (1984), Pakowski and Mujumdar (1982)), vibration velocity, ωA (Bretsznajder (1963)) and the vibration intensity, $\omega^3 A$ (Gupta (1979)).

Gupta (1979) has listed factors, some of which are unique to VFB literature which make it difficult to review the subject critically. These include: incomplete reporting of experimental procedures, incomplete definitions of certain terms, lack of specification on the mode of vibration employed and lack of information on the basis of comparison of VFB's with other contactors (e.g. packed beds or CFB's).

This chapter is devoted to a brief survey of the relevant literature on the aerodynamic, flow and heat transfer characteristics of the VFB. A comprehensive review of the literature can be found in Pakowski et al (1984).

2.2 AERODYNAMICS AND FLOW

2.2.1 Operating Regimes

If vibration acceleration applied to the bed of particles is strong enough, it may evoke a state corresponding to particulate fluidization. This state of " pseudo fluidization " can also be achieved by a combined effect of air flow and

vibration. Based on the range of operating conditions, aerated vibrated beds have been classified (Pakowski et al (1984)) as:

(i) Vibrated bed - all beds of particles without forced gas flow for $\Gamma>1$

(ii) Vibro-fluidized bed- all beds of particles with gas velocity $U/Umf<1$ and $\Gamma>1$

(iii) Vibrated-fluid bed - all beds of particles with gas velocity $U/Umf>1$ irrespective of the vibrational acceleration.

Bratu and Jinescu (1971) defined differently three regimes of operation of an aerated vibrated bed depending on the magnitude of the vertical component of the vibrational acceleration only, without considering the influence of air flow.

In this study the term vibrated fluidized bed (VFB) is used over the entire range of operating parameters i.e. $\Gamma\geq0$ and $U/Umf\geq0$. It should be pointed out that the term "fluidization" is used rather loosely in this report; it corresponds to the state of a well mixed bed and not with $U/Umf>1$ as for conventional fluidized beds. This is in accord with the generally accepted terminology used in the pertinent literature.

2.2.2 Bed Characteristics

Application of vibration improves bed homogeneity and stability (Bratu and Jinescu (1971), Gupta (1979)),

probably due to the fact that high frequency vibration prevents possible coalescence of bubbles resulting in a more uniform bed. On the other hand, excessive vibration has been shown (Gupta (1979)) to deteriorate the bed structure. The term excessive is a relative one; it depends for a given bed of particles, upon the air flow rate through the bed i.e. a combined action of high vibration intensity and air flow results in deterioration of the bed structure.

The effect of vibration on bed porosity has been reviewed by Gupta (1979) and Pakowski et al (1984). Both reduction and increase in bed porosity with vibration have been reported in Gupta's review. The discrepancy in the above results is attributed to the basis of comparison i.e. a reduction in bed porosity was observed as compared to a conventional fluidized bed while an increase was observed when compared to a packed bed.

Figure 2-1 illustrates the fact that the bed compacts for $A\omega^2/g<1$ and expands for $A\omega^2/g>1$. These curves were reported by Pakowski et al (1984) for quartz sand layers (dp=0.210 - 0.355 mm, H=40 mm) for non vibrated beds. Furthermore, they found that bed expansion is a stronger function of the vibration amplitude than of frequency.

2.2.3 Mixing and Flow Characteristics

Particle mixing and flow patterns are of great importance for modelling drying and heat transfer processes in a VFB.

An improvement in the bed fluidity due to breaking up of

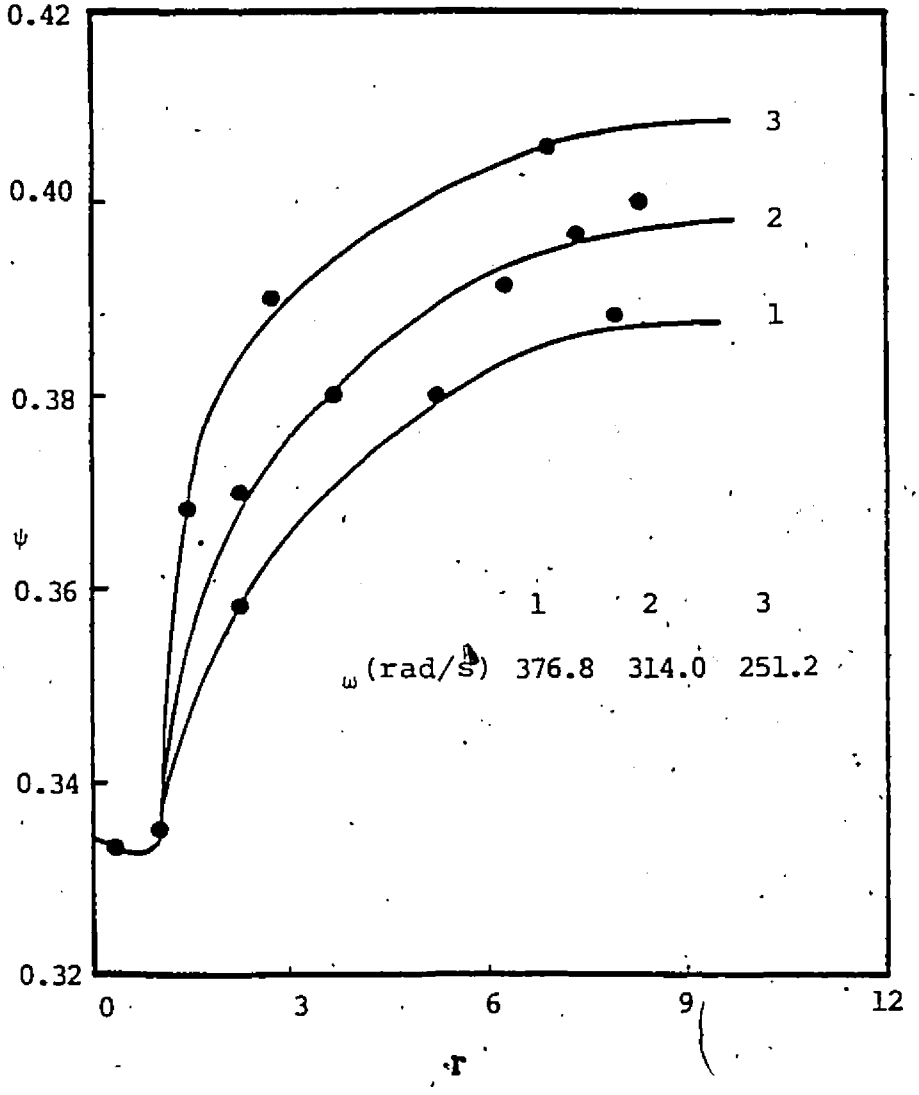

Figure 2-1 Bed porosity in a VFB

interparticle forces (for fine, agglomerating or sticky particles) by vibration is reported by Gupta (1979). Experiments of Chelenov and Mikhailov (1965) have shown that extensive solid mixing takes place in a VFB resulting in an isothermal bed.

Pakowski and Mujumdar (1982) observed circulatory mixing patterns in a VFB fitted with an immersed horizontal tube (Figure 2-2). The intensity of the circulatory streams depends on Γ and U/Umf and the angular velocities of circulation as high as 0.17 s^{-1} were observed by Pakowski and Mujumdar (1982). Similar circulation patterns of solids i.e. from the centre of the bed towards the walls and then down the wall towards the distributor have been reported by Bretsznajder et al (1963).

To achieve efficient solids mixing in a CFB, operating velocities are usually 2-5 times Umf (Kunii and Levenspiel (1967)); similar conditions for solids mixing can be achieved in a VFB by simply vibrating the bed at sufficiently high frequency and/or amplitude. Gupta (1979) and Gupta and Mujumdar (1980) differentiated this phenomenon from ordinary gas fluidization by labelling it "pseudo-fluidization". Figure 2-3 shows the experimentally observed (Gupta (1979)) combinations of vibration and amplitude that generate this state of pseudo-fluidization in the absence of air flow. Gupta and Mujumdar (1980) proposed that pseudo-fluidization occurs when

$$(A\omega^2/g)_{rms} \geq 1$$

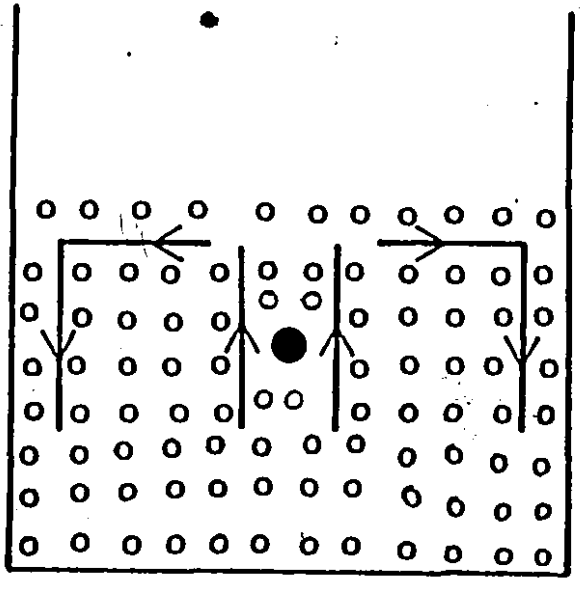

Figure 2-2 Circulatory patterns in a VFB with a horizontally immersed cylinder

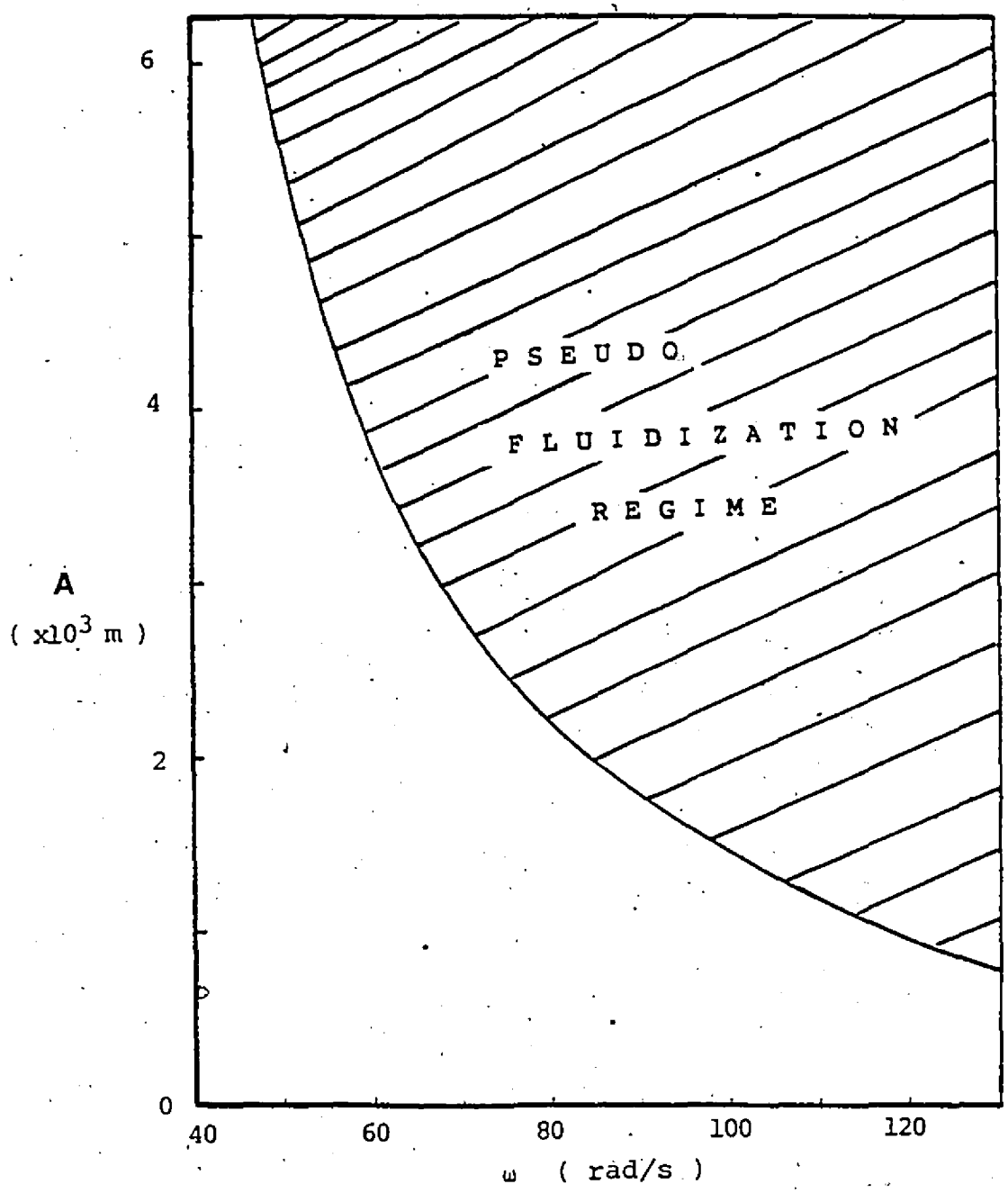

Figure 2-3 Map for onset of pseudo-fluidization

Gupta and Mujumdar (1980) further investigated the effect of air flow on the phenomenon of pseudo-fluidization; their observations are presented in Figure 2-4. It should be pointed out that this figure is a qualitative one based on visual observations with no quantitative measure for the onset of mixing.

An empirical correlation for their newly defined minimum mixing velocity, Umm (minimum air velocity at which solids mixing commences in presence of vibration) is expressed by Gupta and Mujumdar (1980) as follows:

$$Umm/Umf = 1.952 - 0.275\ \Gamma - 0.686\ \Gamma^2$$

in the range

$$0 \leq \Gamma \leq 4$$

$$12.5\times10^{-3} \leq H \leq 75\times10^{-3}\ m$$

$$2.2\times10^{-3} \leq dp \leq 3.9\times10^{-3}\ m$$

$$550 \leq \rho_b \leq 890\ kg/m^3$$

$$0.77 \leq \phi \leq 1.00$$

Pakowski and Mujumdar (1982) observed bed separation from the supporting plate at $\Gamma \geq 1$. They also reported bed separation at the surface of the immersed horizontal heater forming air gaps above the heater when the bed is ascending and below the heater when it is descending. Such situations increase the heater-to-bed resistance causing the heat transfer coefficient to drop.

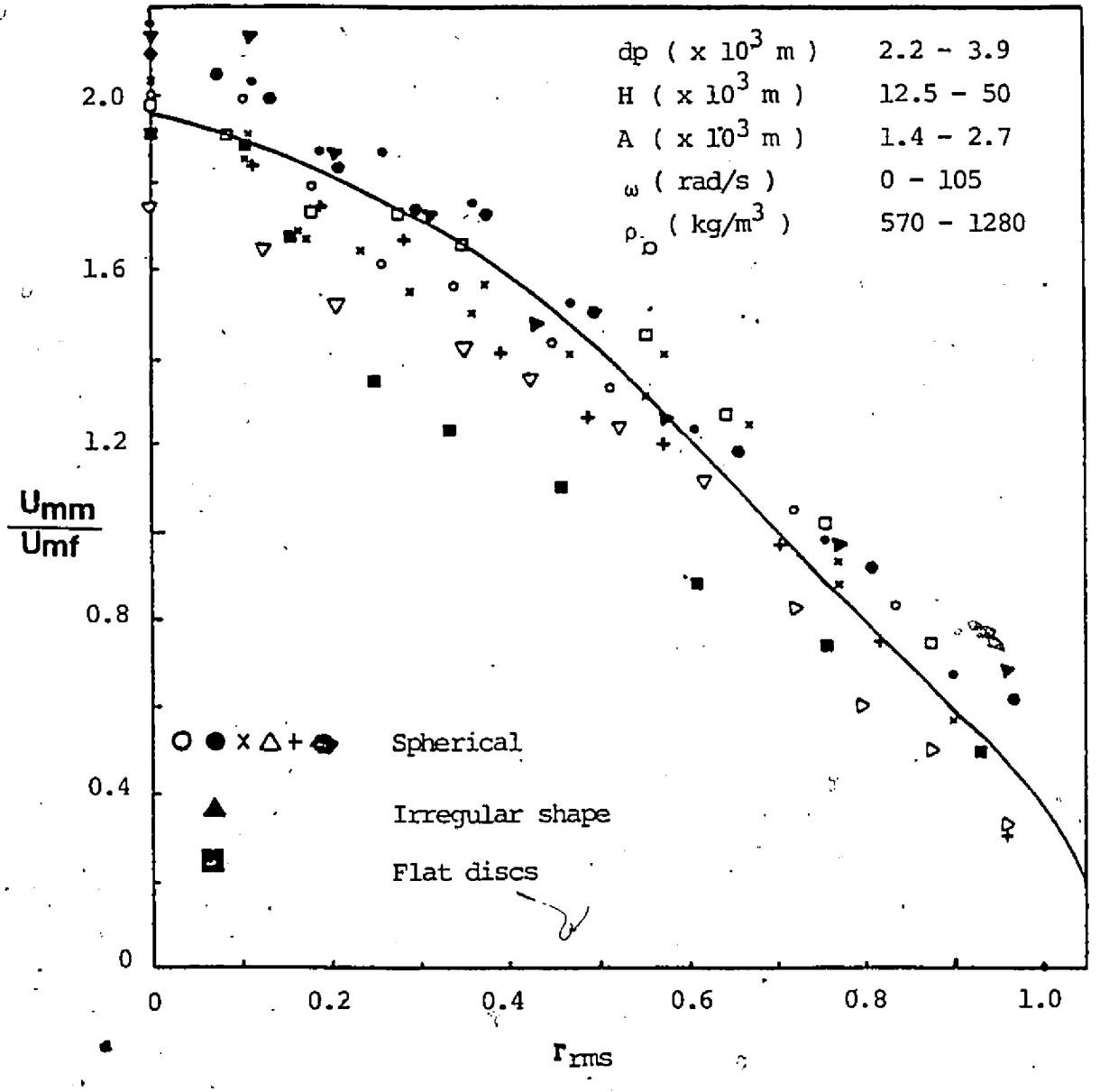

Figure 2-4 Minimum mixing velocity as a function of vibrational acceleration

At high vibrational acceleration levels and air velocities in the neighbourhood of the minimum fluidization velocity, beds of the smaller particles (dp=0.454 mm) displayed presence of attached air bubbles on the upper surface of the immersed horizontal cylinder (Pakowski and Mujumdar (1982)) as shown in Figure 2-5. Visual observations of the bubble pattern of the overall bed indicated that higher air velocities (i.e. velocities in excess of 1.4Umf) tend to reduce the average bubble size and thus improve the bed structure.

Pakowski and Mujumdar (1982), while studying the effect of surface stickiness on heat transfer, observed permanent air gaps around immersed heater surface. They proposed an explanation in terms of increased internal friction of the bed reflected by the increased angle of repose of the sticky particles, which impedes the collapse of the bed around the heater after the gap is formed. This makes the air gap more stable until finally at higher levels of stickiness, the gap is permanently formed so that the heater oscillates creating an oval space, contacting the bed fully only in the uppermost and lowermost configurations. This phenomenon is crucially important in determining the surface-to-bed heat transfer as will be discussed fully in Chapter 5.

2.2.4 Bed Pressure Drop

The effect of vibrational parameters on the bed pressure drop has been studied by Bretsznajder et al (1963), Chelenov

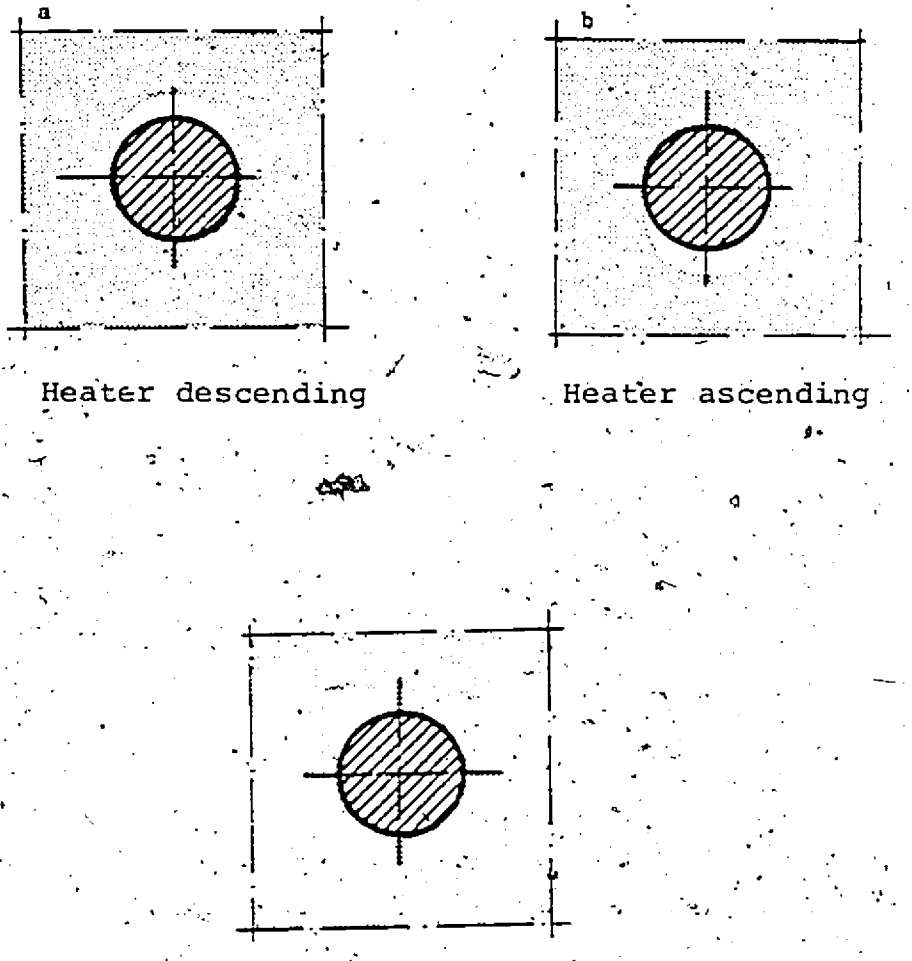

Figure 2-5 Air gap formation around a horizontally immersed cylinder in a VFB

and Mikhailov (1965), Bratu and Jinescu (1971), Gupta and Mujumdar (1980) and Erdesz and Ormos (1984). All these studies show a strong dependence of bed pressure drop on vibration parameters, A and ω.

Upto 35 percent reduction in bed pressure drop has been reported by Bratu and Jinescu (1971) as a consequence of vibration. Gupta and Mujumdar (1980) found the VFB pressure drop to be lower than the pressure drop in a non-vibrated bed over the entire range of operating conditions used in their study (A=0-4.25 mm, ω=0-105 rad/s). The minimum fluidization pressure drop was found to decrease with an increase in frequency and amplitude. They confined their attention to shallow beds (25-50 mm).

More recently Erdesz and Ormos (1984) performed hydrodynamic experiments with sand particles in the range Γ=0-13.4 (A=0.6-1.85 mm). They observed that in the presence of vibration the characteristic pressure peak of gas fluidization is missing and the relative bed expansion is linear. Contrary to Gupta and Mujumdar's (1980) observations they reported bed compaction (higher pressure drop) at lower intensities of vibration ($\Gamma \leq 1$) followed by expansion at higher vibrational accelerations.

A considerable attenuation of the effect of vibration on ΔP_{mf} with increase in the bed height is reported by Gupta and Mujumdar (1980). They reported almost no effect of vibration on ΔP_{mf} for bed heights in excess of 50 mm.

Erdesz and Ormos (1984) observed that with increasing

particle size the pressure reducing effects of vibration are hindered. On the contrary, Gupta and Mujumdar (1980) reported larger sized particles to be affected to a greater extent by vibration than smaller ones. It should however be noted, that the bed heights and particle density in Erdesz and Ormos's study were twice as much as compared to Gupta and Mujumdar.

An interesting result presented by Erdesz and Ormos (1984) is a reduction in the minimum fluidization pressure drop (over the entire range) with less permeable support plates i.e. higher support resistance. Pakowski et al (1984) have indicated that the design of the gas distributor grid and measuring technique can effect the pressure drop measured in fluidized beds. Erdesz and Ormos (1984) have not stated the technique used in the measurement of the bed pressure drop.

Gupta and Mujumdar (1980) conducted experiments to determine the effect of vibration on the fluidization of sticky materials commonly encountered in drying applications. For this purpose they mixed dry particles with controlled amounts of oil. Severe gas channelling and no fluidization was observed by them under conditions of no vibration. With vibration it was possible to fluidize the bed and ΔP_{mf} decreased with an increase in vibration frequency, although it was always higher when compared to ΔP_{mf} for a dry bed. This can be attributed to the momentum lost in overcoming surface forces of interparticle adhesion due to the presence of the oil film.

In conclusion it can be stated that the effect of vertical sinusoidal vibration on bed pressure drop has been

investigated experimentally by many researchers. Bed height, particle size, particle density and surface properties have been reported to exert first order effects. In addition, vibration aids in fluidization of sticky and agglomerating solids.

2.3 HEAT TRANSFER

This section reviews primarily the contact heat transfer process from immersed surfaces in a VFB. A brief review on the convective heat transfer in a VFB, effect of vibrational parameters, mechanism of heat transfer in a VFB and drying is also presented. Finally, a section on heat transfer in a granular bed (packed, agitated or fluidized) is presented. This section is further discussed in depth in Chapter 5 where it is used to propose a model for immersed surface heat transfer in a VFB.

2.3.1 Introduction

A comprehensive review of the available world literature on heat transfer in VFB's is available in Pakowski et al (1984). Not much progress has been reported since in the area of surface-to-bed heat transfer in VFB's except by Pakowski and Mujumdar (1982), Ringer and Mujumdar (1982, 1984a, 1984b), Mujumdar and Pakowski (1983) and Malhotra and Mujumdar (1984). A brief outline of the relevant literature is presented in the following text.

Despite the fact that the major application of VFB is in the drying of granular solids, the bulk of literature pertains

to heat transfer between a heating surface and the conventional fluidized bed. Included in this area of research are:

(a) heat transfer from plate heaters (horizontal or vertical)

(b) heat transfer from the walls of the vessel

(c) heat transfer from the distributor to the bed

(d) heat transfer from coaxial rods

(e) heat transfer from immersed objects i.e. spheres, tubes.

Studies have been conducted with both aerated and non-aerated beds, with vibration being imparted only to the bed, only to the heater or to both simultaneously. In scope of the present work the review is focussed primarily at surface-to-bed heat transfer from immersed tubes or heaters attached rigidly to the vibrating bed.

2.3.2 Contact Heat Transfer

Heat transfer by contact is a commonly employed mode of heat supply in non-aerated vibrated beds. Limitations on air flow and temperature make it the only feasible way of supplying sufficient heat in some drying processes. In contrast vibrated fluidized beds use this type of heat as an auxilliary source of heat, because of the low aeration rates ($U/Umf \leq 1$) commonly employed.

In discussion of contact heat transfer from vertical heaters it is necessary to distinguish between two distinct cases; the heater may be attached to the vibrating vessel or it may be suspended into the bed. Strumillo and Pakowski (1980)

have performed heat transfer studies in a bed with only the vessel bottom (i.e. distributor) vibrating.

The dependence of contact heat transfer coefficient on vibrational acceleration has been shown to follow an S-shaped curve (Pakowski et al (1984)). This shape of the curves has been attributed to the following two processes:

(i) scouring of the gas film from the heater surface by the bed particles.

(ii) transport of heat outside the heater zone by circulation of solids.

For vertical heaters, Pakowski et al (1984) reported an increase in both processes when $A\omega^2/g$ is increased. At high levels of vibration a state is reached when the bed inertia prevails and the bed no more pulsates but remains in a kind of suspended state. Circulatory motions also decrease. As a result heat transfer coefficient decreases or remains constant. For heated bottom plates when $A\omega^2/g$ increases a point is reached when the bed starts to separate from the heater. This air gap then isolates the the bed from the heater to a great extent causing in many cases heat transfer coefficient to drop.

Bretsznajder et al (1963) reported an increase of 17-19 times in heat transfer due to vibration for aluminium, kaolin and zinc and 9 times for graphite as compared to non-vibrated packed beds. A different critical value of vibration velocity corresponding to the onset of "fluidization" was reported by them for various materials, below which vibration did not

improve h.

A model for heat transfer from a vertical heater is described in Pakowski et al (1984). It assumes that particles in their vibrating motion scour a gas film from the heater which results in reduction of the heat transfer resistance. Correlations for calculating the average film thickness have also been presented by Pakowski et al (1984).

Flow of gas through the vibrated bed upto a certain velocity increases the heat transfer coefficient. For U>Umf, h in conventional fluidized beds increases because of more vigorous mixing in the bed; in VFB h tends to a value which is independent of vibration frequency but depends on particle diameter and vibration amplitude. Recently Ringer and Mujumdar (1982 , 1984a, 1984b) presented some results on the flow and immersed-surface heat transfer in a vertically vibrated VFB. They provided a simple design chart to enable selection of the range of gas velocity and vibrational acceleration in which both contact heat transfer and transportation properties of the bed are the best.

A simple model for evaluating the heat transfer coefficient in VFB on the basis of the heat transfer coefficient in a conventional non-vibrated fluidized bed, time of flight of the bed, time period of oscillations and bed pressure drop has been proposed by Ringer and Mujumdar (1982, 1984b).

Experimental results for heat transfer from immersed horizontal cylinders in a VFB have been reported by Mujumdar and

Pakowski (1983), Pakowski and Mujumdar (1982) and Malhotra and Mujumdar (1984). Surprisingly, no prior studies could be found in the literature on heat transfer from rigidly mounted horizontal tubes immersed in a VFB, even though such an arrangement allows more heat exchange surface to be packed in a given VFB while permitting use of deeper beds as the tubes impart additional vibrational energy within the bed itself.

Mujumdar and Pakowski, (1983) performed experiments with glass ballotini in a VFB vibrated at a constant amplitude of 4.25 mm. They reported a significant enhancement in heat transfer rate in presence of vibration and more so at lower aeration rates. The heat transfer coefficient for non-aerated beds becomes nearly independent of vibrational acceleration when the latter is above about 1.5 times gravity. A set of experimental curves for a bed of dry glass ballotini as reported by Mujumdar and Pakowski (1983) are reproduced in Figure 2-6.

It can be seen from Figure 2-6 that superposition of air flow makes the transition from fixed bed to vibrofluidized one to occur at lower values of Γ. The influence of gas flow on the heat transfer coefficient is significant only in the range $U/Umf<1$. A 10-20 percent rise in peak heat transfer coefficient at $U/Umf=1.2$ in a VFB as compared to corresponding value for a non-vibrated bed can be seen from Figure 2-6. The mark z on the figure corresponds to the heat transfer coefficient in fluid beds predicted by Zabrodski's (1966) correlation.

Pakowski and Mujumdar (1982) and Mujumdar and Pakowski (1983) proposed the following empirical correlation obtained

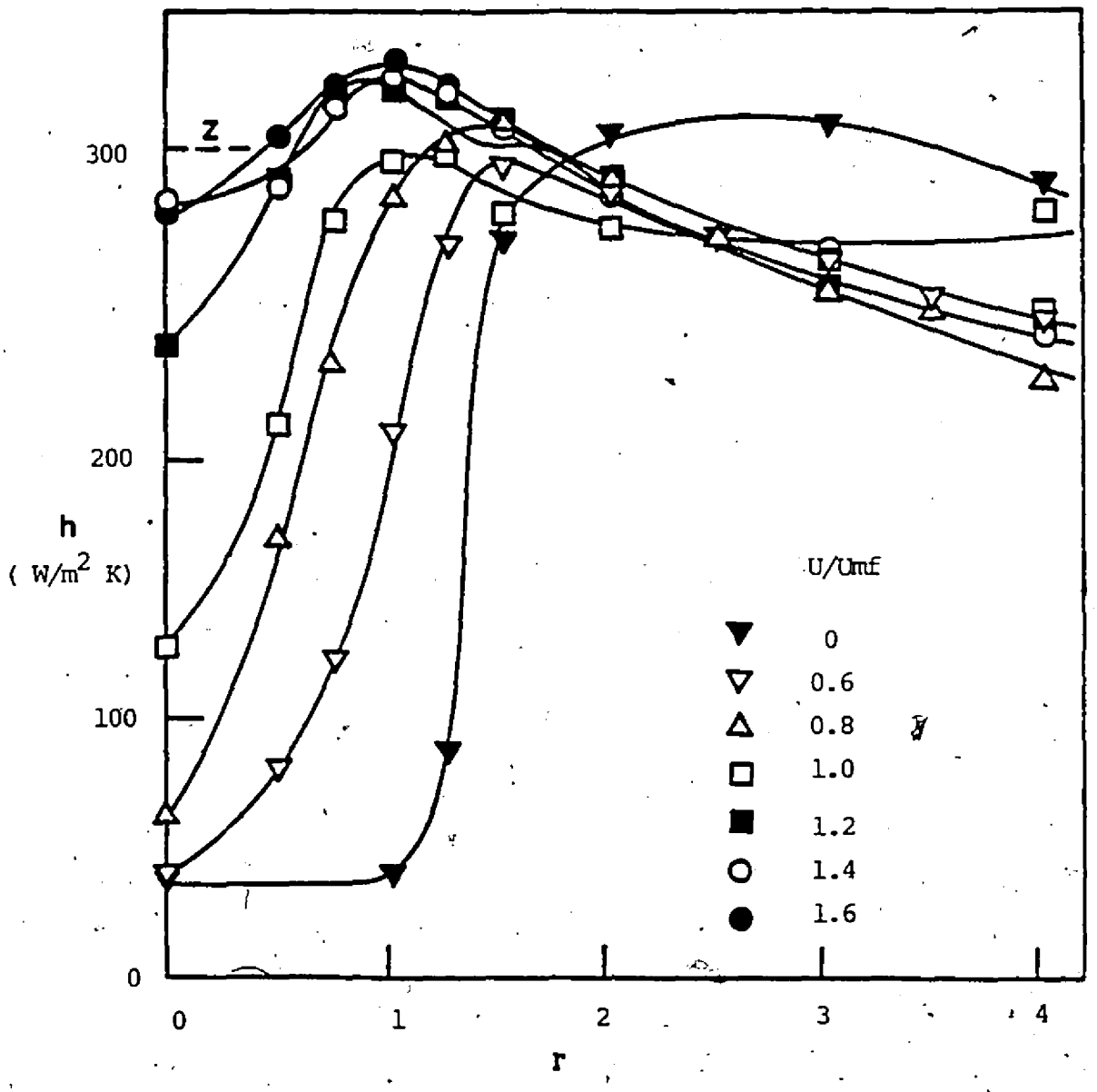

Figure 2-6 A typical h versus r plot for a bed of dry glass ballotini

from their experiments with beds of dry glass ballotini:

$$Nu = C_1 (C_2 U/Umf)^{C_3 - C_4 r}$$

With constants C_1 = 2.27, C_2 =0.67, C_3 =2.63 and C_4 =1.95, this equation describes the heat transfer coefficient for glass ballotini, dp=0.454 mm in the range U/Umf=0.6-1.2 with 20% accuracy. With constants C_1 =2.20, C_2 =0.55, C_3 =1.35 and C_4 =0.98 it describes heat transfer coefficient for larger ballotini (dp=0.667 mm) in the range U/Umf=0.4-1.2 with same accuracy as before. This equation is not general enough to be useful.

Visual observations made during the experiments by Mujumdar and Pakowski (1983) showed an increase in bed circulatory motion with an increase in U/Umf and r. For r≥1 and U/Umf≥0 they reported gap formation around the heater surface which inhibits the heat transfer process. A similar behaviour was also observed by Bukareva et al (1965) in non-aerated beds if the vibration frequency was high enough.

Pakowski and Mujumdar (1982) studied the effect of surface stickiness on heat transfer for glass ballotini and reported a dramatic drop in heat transfer coefficient with addition of minute quantities of glycerine. A typical h versus r plot for a sticky bed is illustrated in Figure 2.7. Surface stickiness(or presence of surface moisture) decreases the degree of mixing in the bed as observed visually by Pakowski and Mujumdar (1982). Although surface stickiness has been

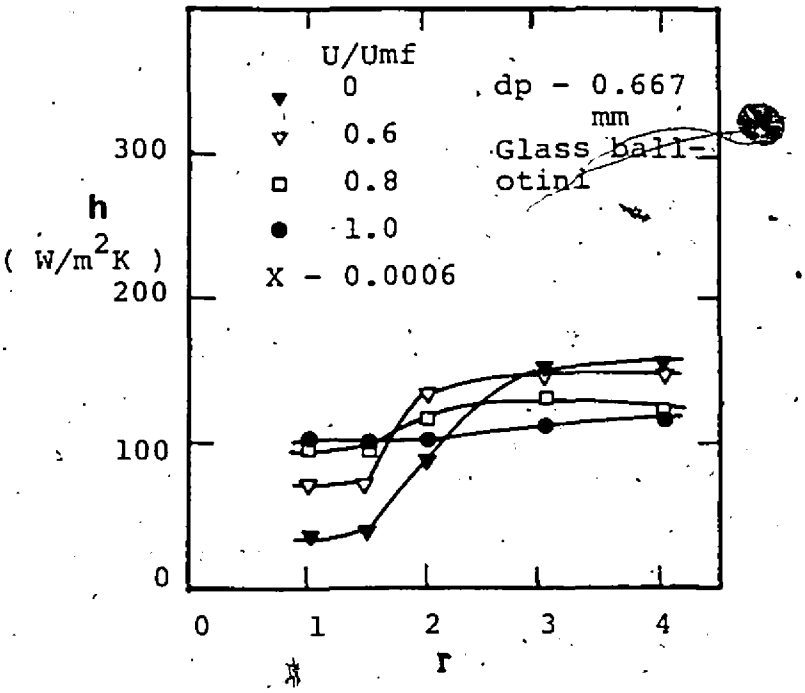

Figure 2-7 A typical h versus Γ plot for a bed of sticky glass ballotini

recognized to be an important particle characteristic (Varsayni and Puskas-Nadai (1977)) surprisingly no other report on the effect of stickiness on heat transfer in VFB's has appeared in open literature. It is not clear how the particle stickiness can be quantified.

2.3.3 Convective Heat Transfer

Convective heat transfer from a hot gas to the bed is perhaps the most commonly employed method of heat supply in a drying process. The factors affecting this process have been classified into the following four categories by Pakowski et al (1984):

(i) disturbances of a boundary layer around particles or their agglomerates (positive or negative effect)
(ii) backmixing of gas (negative effect)
(iii) changes to total area exposed to heat transfer (positive effect)
(iv) equalization of bed temperatures by internal mixing (positive effect).

The extent to which these phenomena contribute to the total heat transfer coefficient, h, depends on the range of vibrational acceleration and gas flow rate as well as on the bed porosity (which in turn is affected by the former parameters).

A number of correlations relating h and Γ for convective heat transfer in a VFB for different materials (coal, cereals,

polymers etc) have been reviewed by Pakowski et al (1984). A typical correlation for $\Gamma<6$ obtained by drying of calcium carbonate spheres in the constant rate period is shown below:

$$Nup = 0.827\ Rep^{1.04}\ (\ dp/H\ )^{1.17}\ (\ \Gamma\ )^{0.483}$$

2.3.4 Effect of Vibrational Parameters

The degree of influence of vibration on heat transfer has been found to depend on the relative magnitude of vibration velocity, Af, air flow rate, U, and the minimum fluidization velocity, Umf. Gupta (1979) reported that at large air flow rates, the effect of vibration is not important in the estimation of h, while Yamazaki et al (1974) found h to improve with air flow rate upto $U/Umf \leq 1$ and then stabilize. Gupta (1979) from his literature survey presented the correlation

$$h/ho = 1.1(2\pi Af/U)^{0.4} \quad \text{for } 2\pi Af>U$$

with h depending on the moisture content of solid, indicating the influence of mass transfer on heat transfer performance.

Pakowski et al (1984) also reported that vibration greatly influences heat transfer in VFB's of fine particles. Heat transfer in beds of large particles increases slightly with an increase in vibration and can even decrease under some conditions.

2.3.5 Mechanism of Heat Transfer

Various mechanisms have been proposed to explain the surface-to-bed heat transfer phenomena in VFB's. Gutman (1976) successfully modified the film model for vibrated non-aerated beds while Mickley and Fairbanks (1955) model for unsteady state heat conduction has been shown (Gupta (1979)) to predict fairly accurately for aerated beds.

Yamazaki et al (1974) modelled the VFB on the assumption that vibration results in pulsation of air flow below the distributor and this pulsating component acts as an additional air velocity over and above the mean velocity. This effective air velocity, (U + U') was used in the equation for non-vibrated beds and found to give good agreement between predicted and experimental values. Thus, the vibration velocity may be considered equivalent to an increase in gas velocity.

Recently Ringer and Mujumdar (1982) presented a calculation model for surface-to-particle heat transfer coefficient. For the purpose of modelling they assumed that bed mixing governs heat transfer rate and is a result of the operating forces during one cycle of the particle and conveyor motion. The final equation obtained by them is:

$$h/hcm = 0.8te/ti + (\Delta P/\Delta Pmf)(1-0.8te/ti)$$

where hcm is the maximum heat transfer coefficient for a non-vibrated bed, te is the flight time of the bed and ti the time period of oscillation. The above model matched quite well

with the experimentally obtained results of Ringer and Mujumdar (1982) for vertically suspended immersed cylinders.

2.3.6 Drying

Drying in VFB's has been studied by Jinescu et al (1982), Chelenov and Mikhailov (1965), Kazachinskaya and Bilyk (1975), Gupta and Mujumdar (1980), Suzuki et al (1980a, 1980b, 1980c, 1984) among others. An extensive review is available in Pakowski et al (1984). Almost all the prior work has been in the area of convective drying.

Vibration has been found to affect drying rates in a fluidized bed in a complex way. For operation at $A\omega^2/g \geq 1$, both improvement and impairment in heat transfer has been reported with an optimum value of A and ω existing for all the materials investigated.

The amplitude of vibration has been reported to influence drying rate more strongly than the vibration frequency. A reduction in Xc for smaller particles has also been reported. The other variables affecting the drying rate are: bed height, particle size, aeration rate and the interparticle forces of adhesion and cohesion.

Recently Suzuki et al (1984) studied freeze drying of granular materials in a VFB. They reported uniform bed temperatures and thorough mixing induced by vibration. The overall heat transfer coeffitient between the heater and the bed was found to depend upon the bed moisture content; the value of h decreased from 300-500 W/m^2K in the initial period of drying

to 60-80 W/m²K in the latter half of the drying period.

In modelling the drying process it is essential to know the thermal conductivities of the wet particles. A number of correlations to determine the thermal conductivity of wet and porous particles have been given by Catala and Maupsey (1981), Cermak (1981a, 1981b), Kendall (1980), Toei (1984) and Szentgyorgyi et al (1981) among others.

2.3.7 Surface-to-Bed Heat Transfer in a Granular Bed

The wall-to-bed average heat transfer coefficient is defined as:

$$h = Q/(Ac(Ts - T_b))$$

where Q/Ac is the heat flux through the surface area of the heat exchanger element, Ts the average surface temperature and T_b the average bed temperature at a sufficient distance from the heated (or cooled) surface.

Most authors of the more recent literature (Martin (1981), Baskakov et al (1973), Adams (1981a, 1981b, 1982a, 1982b, 1982c, 1984), Abubakar et al (1983), Ozkaynak and Chen (1980), Heyde and Klocke (1980), Schlunder (1982), Bock (1981a, 1981b), Bock and Molerus (1980), etc) agree that the wall-to-bed heat transfer is composed of three parallel mechanisms: Particle convection, Gas convection and Radiation.

$$h = he + hg + hr$$

Particle convection denotes the mechanism of energy transfer through the moving particles: Heat is transferred to a particle during its contact with the heated surface mainly by conduction through the gaseous gap in the vicinity of the contact point increasing the particle's internal energy. By the random motion of the particles that surplus of internal energy is carried out into the bulk of the bed where it is transferred (instantaneously) to the gas and the other particles. The most important parameter in evaluation of he is the particle-surface contact time, which varies greatly depending upon the type of granular bed (i.e. packed, fluidized or agitated).

Gas convection is the direct wall-to-gas heat transfer over those parts of the surface which are not in contact with particles. The gas convection component increases with increasing gas velocity. In fluidized beds of large particles ($d_p \geq 3$ mm), which consequently need higher gas velocities to be fluidized, the gas convective component becomes the dominant mechanism.

The radiative component of heat transfer is directly proportional to the fourth power of ($T_s - T_b$) and becomes important only for higher temperatures (> 800 K) and is therefore not discussed here.

The particle and gas convective heat transfer mechanisms are discussed in depth in Chapter 5.

CHAPTER 3

EXPERIMENTAL APPARATUS AND PROCEDURES

3.1 THE APPARATUS

A schematic sketch of the apparatus and instrumentation used for the experimental work is shown in Figure 3-1.

Different fluidized beds were used for the flow and heat transfer studies. For the flow and pressure drop experiments, a two-dimensional fluidized bed of a rectangular cross-section, 0.202 m X 0.05 m was used. An isometric sketch of the bed is shown in Figure 3-2. The heat transfer experiments were conducted in a vessel of square cross-section, 0.202 m X 0.202 m (Figure 3-3). Both beds were constructed from plexi-glas to allow visual observation.

The two-dimensional vibrated fluidized bed (VFB) was used primarily to examine the flow and bed circulation patterns around the rigidly mounted, horizontal circular cylinders. To reduce the effect of three-dimensionality, one side of the bed (along the axis of the cylinder) was made very small, although it could not be made very thin due to possible wall effects. (The ratio of depth of the bed to average size of the largest particle should be greater than 50 for wall effects to vanish). The top of the bed had a circular outlet that was connected by a flexible hose to a dry gas air flowmeter.

Two perforated plate air distributors with 4 % free area (1 mm diameter holes on 4.76 mm triangular pitch) and 18 % free area (1.6 mm diameter holes on 3.60 mm triangular pitch)

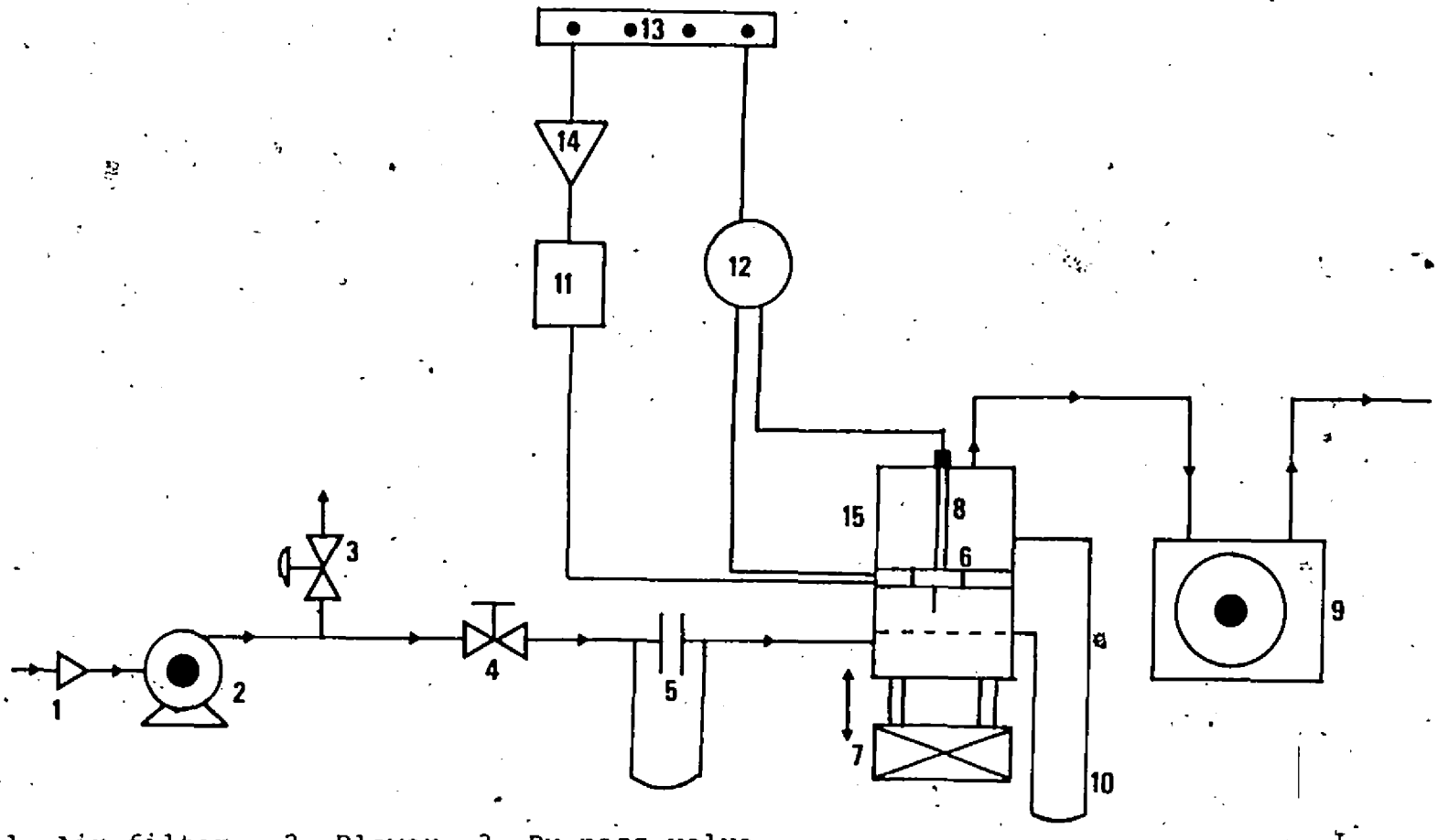

1. Air filter 2. Blower 3. By-pass valve
4. Control valve 5. Orifice meter 6. Heater
7. Vibratory mechanism 8. Bed thermocouples
9. Dry gas flowmeter 10. U-tube manometer
11. Wattmeter 12. Digital thermometer 13. Power source
14. Voltage regulator 15. The VFB

Figure 3-1 Experimental Setup

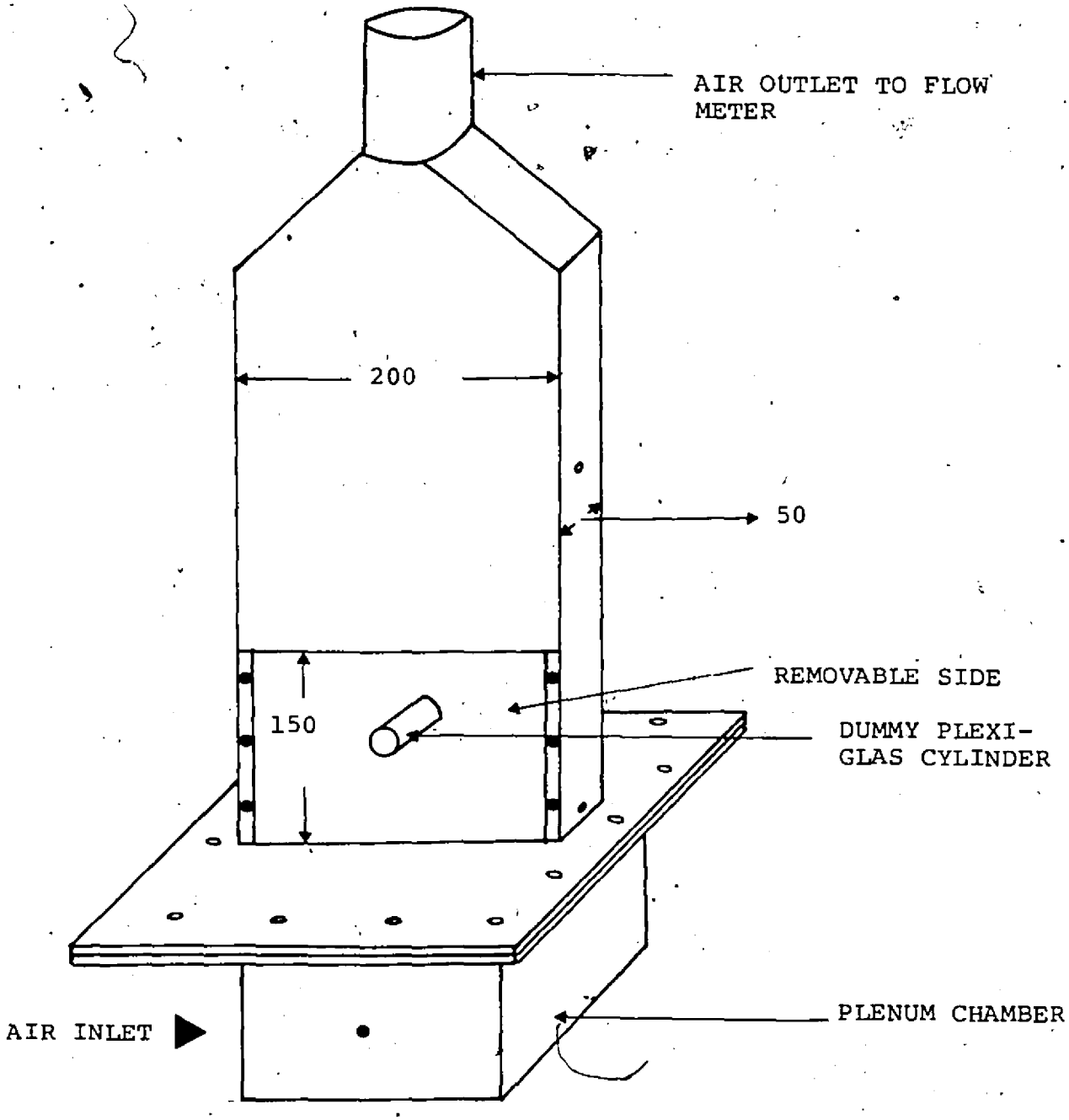

MATERIAL: PLEXI-GLAS

Note: All dimensions in mm

Figure 3-2 Isometric sketch of the two-dimensional fluidized bed

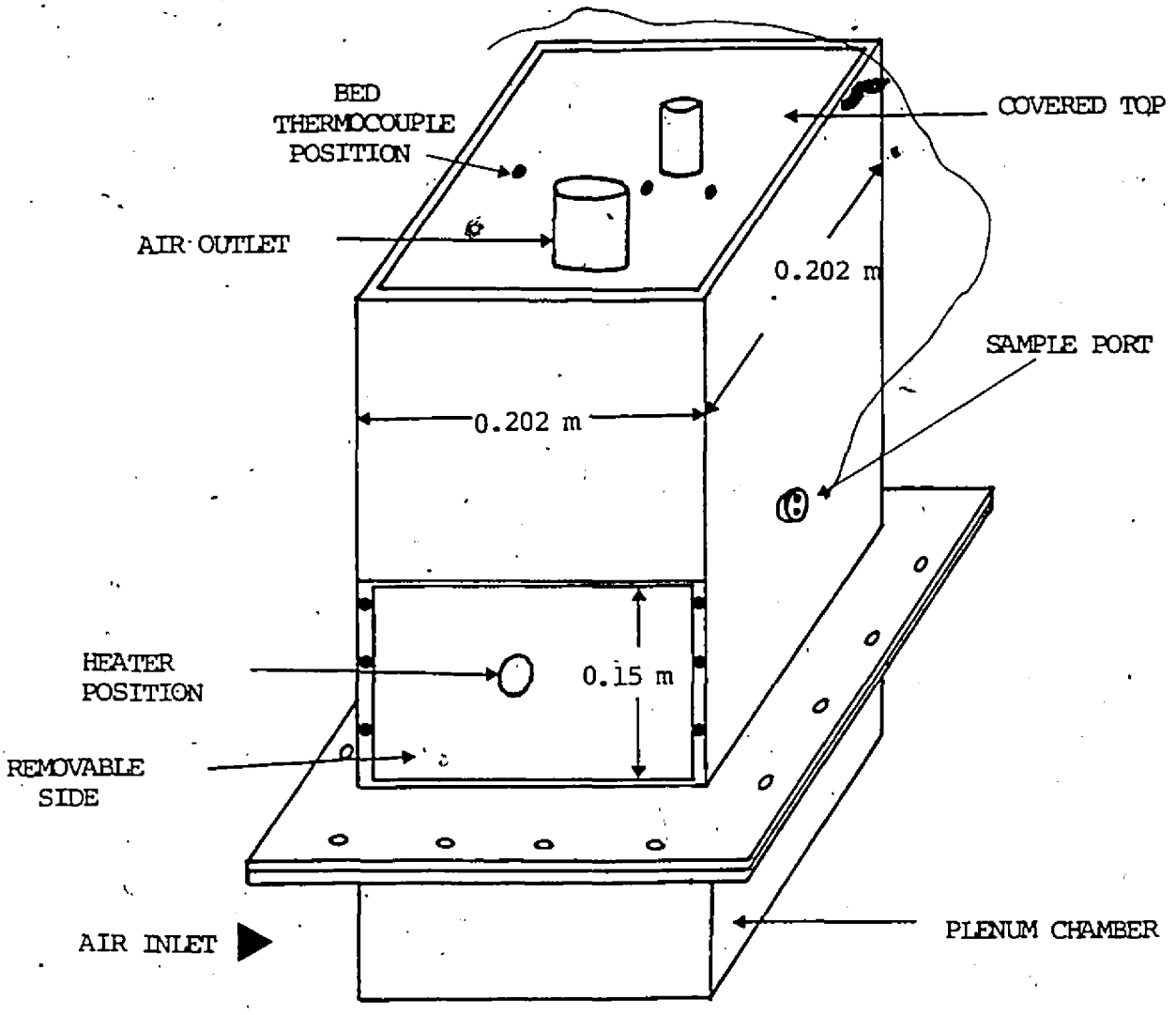

MATERIAL OF CONSTRUCTION : PLEXI-GLAS

NOTE: DRAWING NOT TO SCALE

Figure 3-3 Isometric sketch of the bed used for heat transfer experiments

were used. A very fine nylon mesh (250 mesh) was fitted on the distributor to prevent particle leakage. The flow patterns around rigidly-mounted horizontal cylinders were visually observed and/or photographed using a 35 mm still camera. The cylinder was always located in the middle of the bed.

The square vessel used for the heat transfer experiments had three removable sides and two sampling ports as shown in 3-3. One side of the bed was used to discharge the material while the other two were used to change the heater. The sampling ports were used to collect samples for moisture determination. This bed also had two circular outlets on the top surface which could be connected to the air flowmeter. The outlets were found to have no measurable or visible effect on the particle flow patterns inside the bed.

Cylindrical heaters were used as the immersed heat source. An exploded assembly of the test cylinder is shown in Figure 3-4. The assembly consisted of a copper cylinder imbedded with a 140 ohm, cartridge heater, and extended on both sides by Teflon tubes of same diameter to minimize axial heat losses (estimated to be less than 0.5%). The heater temperatures were measured by 5 thermocouples (Teflon-coated Iron-Constantan of nominal size 0.43 mm) mounted flush with the heater surface along its circumference. The bed temperature was measured at three locations in the bed with bare thermocouples (Teflon-coated Iron-Constantan of nominal size 1.3 mm). The cylinder axis was always located 60 mm above the distributor plate. Two thermocouples were located in the bed, each one 40 mm

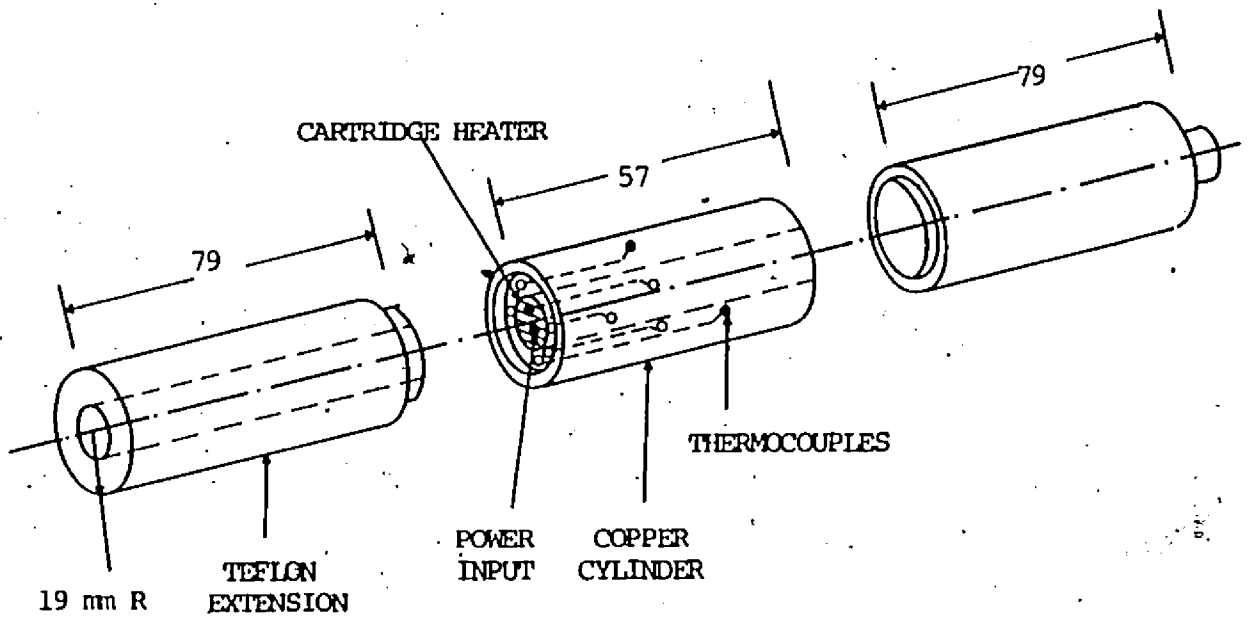

NOTE: ALL DIMENSIONS IN MM

Figure 3-4 Exploded assembly of the circular cylinder

on either side of the cylinder axis and at the same height. The third thermocouple to monitor the bed temperature was placed 60 mm from the cylinder axis on the horizontal plane and 40 mm below it.

All thermocouple readings were monitored on an electronic digital thermometer (Omega type 2160-A). The thermometer had a reading rate of 2.5 readings per second and a response time to rated accuracy of less than 2 seconds. The temperature range of the thermometer was -74.4 to 537.7°C, resolution and repeatability was 0.11°C with a maximum error of ± 0.67°C (including reference junction and conformity error). A selector switch was used to scan the readings of all the thermocouples.

The power input to the heater was varied with a 0-140 volts AC voltage regulator and measured on an AC/DC type single phase wattmeter (Yokogawa Electric Works, Tokyo, Japan). It had a power factor of 1.0 and an accuracy of ± 0.5%.

The whole bed was vibrated nearly sinusoidally in the vertical plane by means of an eccentric mechanism which converted the rotary motion of an electric motor to linear motion. The amplitude of the system could be varied by adjusting the eccentricity of the drive system. The frequency of vibration was varied continuously with a 1 hp DC motor controlled by a silicon controlled rectifier (SCR) variable-speed RATIOTROL drive, manufactured by M/S Boston Gears. The motor had a maximum rating of 1050 RPM. The motor RPM, i.e. frequency of vibration, was measured using a pre-calibrated digital tachometer.

A 2 hp (Canadian Blower and Forge Co. Ltd) blower fitted with an air filter, was used to supply atmospheric air to the system. The blower was connected to the VFB by a series of flexible and rigid pipes. A by-pass valve was used primarily to control the air flow; finer control was obtained by manipulating the line pressure drop downstream of the bed. A calibrated orifice plate was used to measure air flow rates (superficial air velocity in the bed) above 0.0085 m^3/s, while lower air flowrates were measured on a pre-calibrated dry gas flowmeter (Canadian Meter Co.). The pressure drop across the orifice plate was measured by an inclined manometer (M/S Wilh Lambrecht KG, Golligen) with a manometric fluid (Meriam red) of specific gravity 1.0. The maximum possible error (at an inclination of 30°) in the pressure drop reading was estimated to be ±4.9 N/m^2

The bed pressure drop was measured on a U-tube manometer with a manometric liquid of specific gravity 1.0. One pressure tap was located flush with the distributor surface, while the other one was well above the bed height, flush with the bed walls. Thus, the bed pressure drop was measured directly.

The levelled bed height was measured by means of graduated tapes on the sides of the bed. The particle size and shape were determined from microscopic analysis of a random sample of particles. The particle density and properties were supplied by the manufacturer, while the bulk density was calculated from the weight of given volume of sample. A weighing balance (OHAUSS Cent-O-Gram ; accuracy ± 0.01 gm) was

TABLE 3.1 (a)

PHYSICAL PROPERTIES OF MODEL PARTICLES

TYPE	dp (mm)	ρ_p (kg/m^3)	ρ_b (kg/m^3)	ψ	ϕ	Cp (J/kgK)	Kp (W/mK)	Xc	Xe *	Umf (m/s)
Glass ballotini	0.325	2480	1375	0.44	0.95	753.12	0.837	—	—	0.085
Glass ballotini	0.454	2470	1385	0.44	0.95	753.12	0.837	—	—	0.146
Glass ballotini	0.595	2480	1405	0.43	0.95	753.12	0.837	—	—	0.201
Glass ballotini	0.667	2470	1405	0.43	0.95	753.12	0.837	—	—	0.276
Glass ballotini	1.017	2480	1415	0.43	0.95	753.12	0.837	—	—	0.365
Molecular sieve	1.4	1250	750	0.40	1.00	962.00	0.589	0.24	0.16	0.363
Molecular sieve	2.36	1250	740	0.40	1.00	962.00	0.589	0.24	0.16	0.485

* at 300 K

TABLE 3.1 (b)

Aerodynamic and Thermal Classification of Model Particles *

Type of Particle	dp (mm)	Aerodynamic Group	Thermal Group	Rep
Glass ballotini	0.325	B	small/large	0-1.6
Glass ballotini	0.454	B	small/large	0-3.9
Glass ballotini	0.595	B	small	0-7.1
Glass ballotini	0.667	B/D	large	0-10.9
Glass ballotini	1.017	D	large	0-21.9
Molecular sieve	1.4	D	large	0-30.4
Molecular sieve	2.36	D	large	0-67.4

* - Refer to Appendices B and C for definitions.

TABLE 3.2

Range of Operating Parameters

VARIABLE	RANGE OF OPERATION		UNITS
	MINIMUM	MAXIMUM	
Vibration amplitude, A	0	4.25×10^{-3}	m
Vibration frequency, ω	0	105	rad/s
Bed height, H	80×10^{-3}	130×10^{-3}	m
Mean particle size, dp	0.325×10^{-3}	2.36×10^{-3}	m
Bulk density ρ_b	760	1425	kg/m^3
Particle density ρ_p	1250	2480	kg/m^3
U/Umf	0	1.2	-
Particle spherecity	0.95	1.0	-
Particle surface	dry	wet/sticky	-
Bed Area, Ac	0.20x0.05	0.202x0.202	m^2
Vibration number, Γ	0		-

used for moisture determination. The wet samples were bone-dried in an electric oven at 200°C for 45 minutes and weighed immediately thereafter.

For inducing surface stickiness in glass ballotini, glycerine (vapour pressure 1mm Hg at 120°C) was mixed with dry glass ballotini in a double cone mixer for 6 hours. Molecular sieve particles were saturated with water by dipping them overnight in water and then draining off the excess water.

Table 3.1 shows the properties of the model particles used, while Table 3.2 shows the range of operating parameters used in the study.

3.2 DATA ACQUISITION

3.2.1 Flow Visualization and Pressure Drop

The objective of this part of the project was to examine the size and shape of the time-averaged particle free air gaps around immersed circular cylinders and study the effects of pertinent parameters thereon. Time-averaged (0.5 to 3 second exposure) and instantaneous (1/250 to 1/30 second exposure) photographs were also taken for some runs. The bed pressure was recorded for all the runs.

The experimental procedure adapted is described briefly in the following. After fixing the test cylinder rigidly to the bed at appropriate distance above the distributor, the bed was filled with particles to the desired level. The air by-pass valve was opened before switching the blower on and the air

flowrate set to the desired value. The vibratory mechanism was then adjusted to achieve the lowest value of vibrational acceleration (eg. 325 RPM for 4.25 mm amplitude of vibration) and set into operation. The bed pressure drop and flow patterns around the immersed cylinder(s) were then recorded (photographed ,if desired). The frequency of vibration was then set to the next higher value. For a different set of experiment , the air flowrate was changed to another pre-selected value and similar procedure as before followed. On completion of the experiments, the vibratory mechanism was switched off first, followed by the blower. The particles discharged from the bed were then weighed. In situations where the bed pressure drop fluctuated, the lower and upper limits of fluctuations were recorded.

3.2.2 Heat Transfer

Heat transfer experiments were performed to examine the effect of vibrational amplitude and frequency, particle size and type, moisture content and cylinder size on the average surface-to-bed heat transfer coefficient. The experimental procedure followed is briefly described in the following paragraph.

The particles were weighed carefully and then charged into the bed and the air flow set to the desired U/Umf ratio. After adjusting the frequency of vibration , the heater was turned on. Steady state thermocouple readings were recorded when the heater and bed temperature changes were less than 0.1°C over

5 minutes (under conditions of poor mixing in the bed this took more than an hour, while with good mixing in the bed it was obtained typically within fifteen minutes). The heat input and bed pressure drop readings were noted. The frequency of vibration was then changed to the next higher level and the aforementioned procedure followed. Note: For experiments with wet particles, samples were withdrawn every 7-10 minutes while simultaneously the thermocouple and power readings were recorded. The samples were later analysed for their moisture content.

During the course of an experiment, the air flow changes due to changes in the bed pressure drop; this was corrected continuously by adjusting the bypass valve to ensure the same U/Umf in a given run.

3.3 CALIBRATION

3.3.1 Orifice Calibration

As mentioned earlier, flow rates above 0.0085 m^3/s were measured using a flat plate type orifice. The orifice plate, (38.1 mm diameter) was placed in the 108 mm diameter air duct. The upstream pressure tap was located two pipe radii from the orifice plate, while the downstream one was one pipe radius distant. Measurements were made with an inclined- tube manometer. A precalibrated dry gas flowmeter was used to calibrate the orificemeter. Pressure fluctuations transmitted by vibration of the bed did not effect the manometer reading. The orifice calibration curve for the 0.202 m X 0.202 m bed (all

the flow experiments in the two dimensional bed were performed with the flowmeter) shown in Figure 3-5 is represented by:

$$U\ (\ m/s) = 0.022\ (\ \Delta Po\ (\ N/m^2))^{1/2}$$

3.3.2 Wattmeter Calibration

The wattmeter was calibrated using a precalibrated digital multimeter. The power factor and the resistance of the heater were measured. The wattmeter has two ranges, 0-24 W and 0-120 W. The calibration curve for the lower range is given in Figure 3-6. The relationship obtained was,

Actual Power = 1.267 X wattmeter reading

The wattmeter was accurate in the larger range.

3.4 DATA REDUCTION

3.4.1 Flow and Pressure Drop

Firstly, the minimum fluidization velocities for all model particles used (dry as well as wet) were determined using the ΔP versus U data at $r=0$. Figure 3-7 shows a typical ΔP versus U curve for a bed of dry particles which was used to obtain the minimum fluidization velocity. The raw data obtained was plotted as ΔP versus r at constant U/Umf as shown in Figure 3-8. Subsequent analysis and cross-plots were obtained from the above curves. Approximate shapes and sizes of air gaps around the immersed cylinders were recorded concurrently.

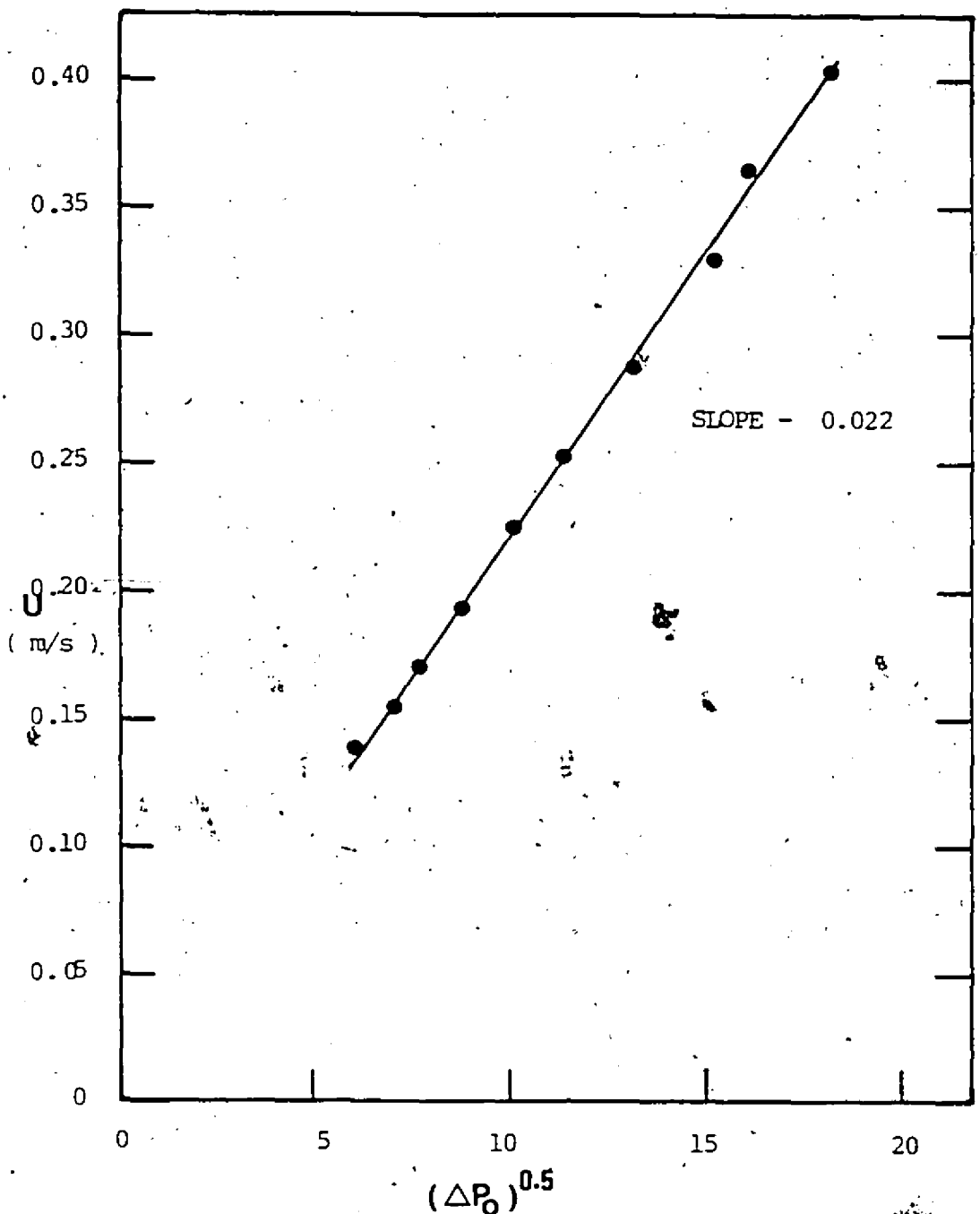

Figure 3-5. Orifice calibration curve

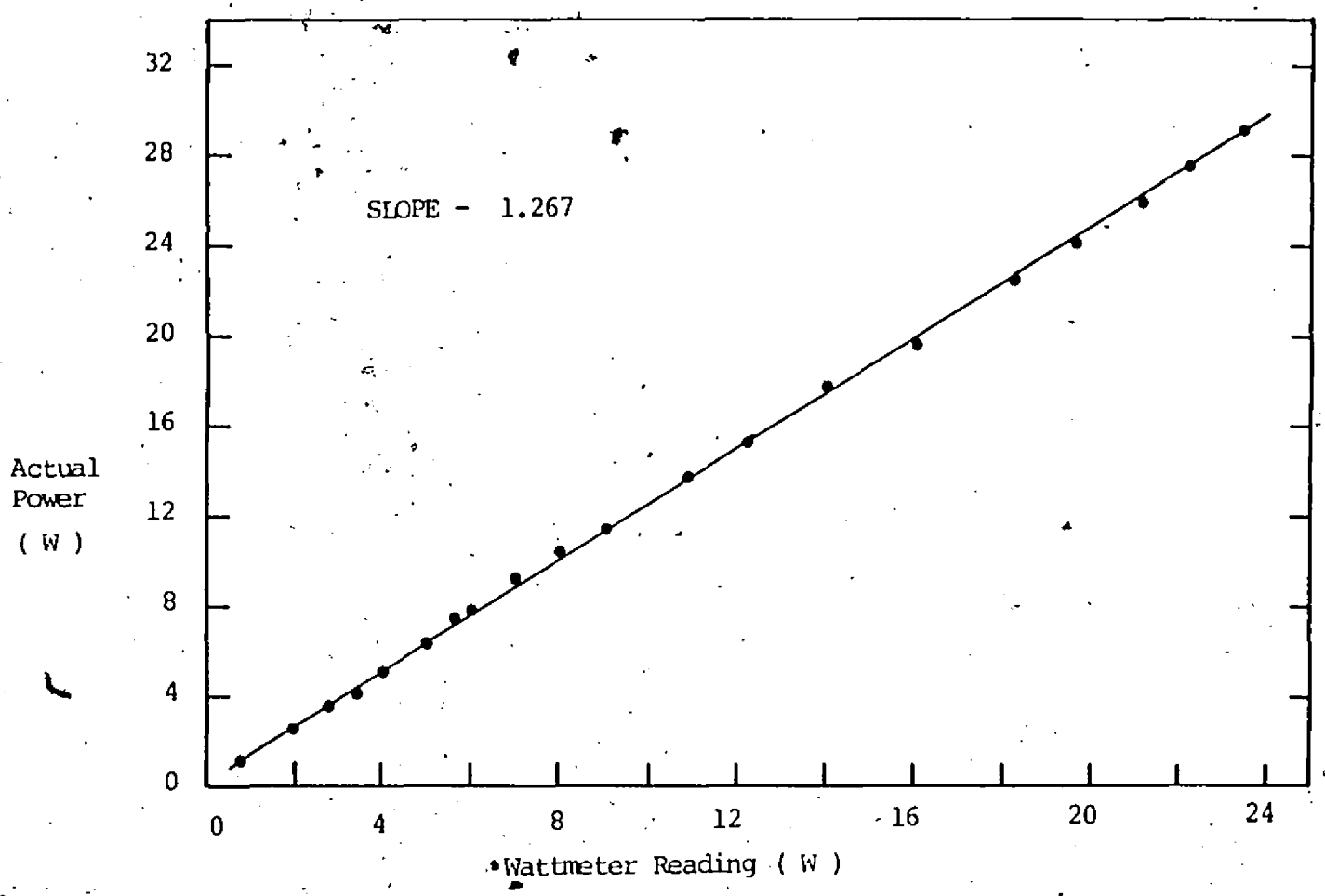

Figure 3-6 Wattmeter calibration curve

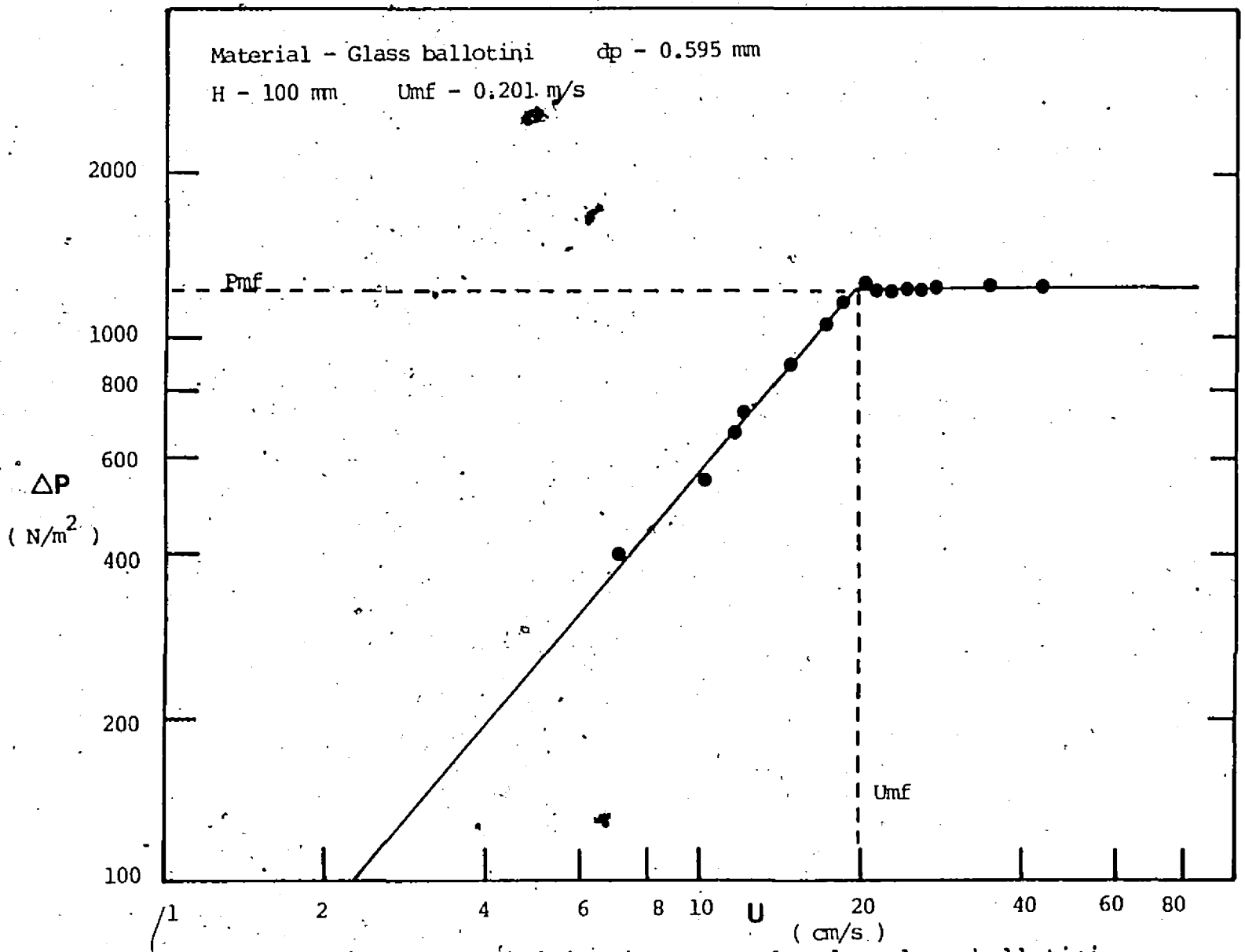

Figure 3-7 Fluidization curve for dry glass ballotini

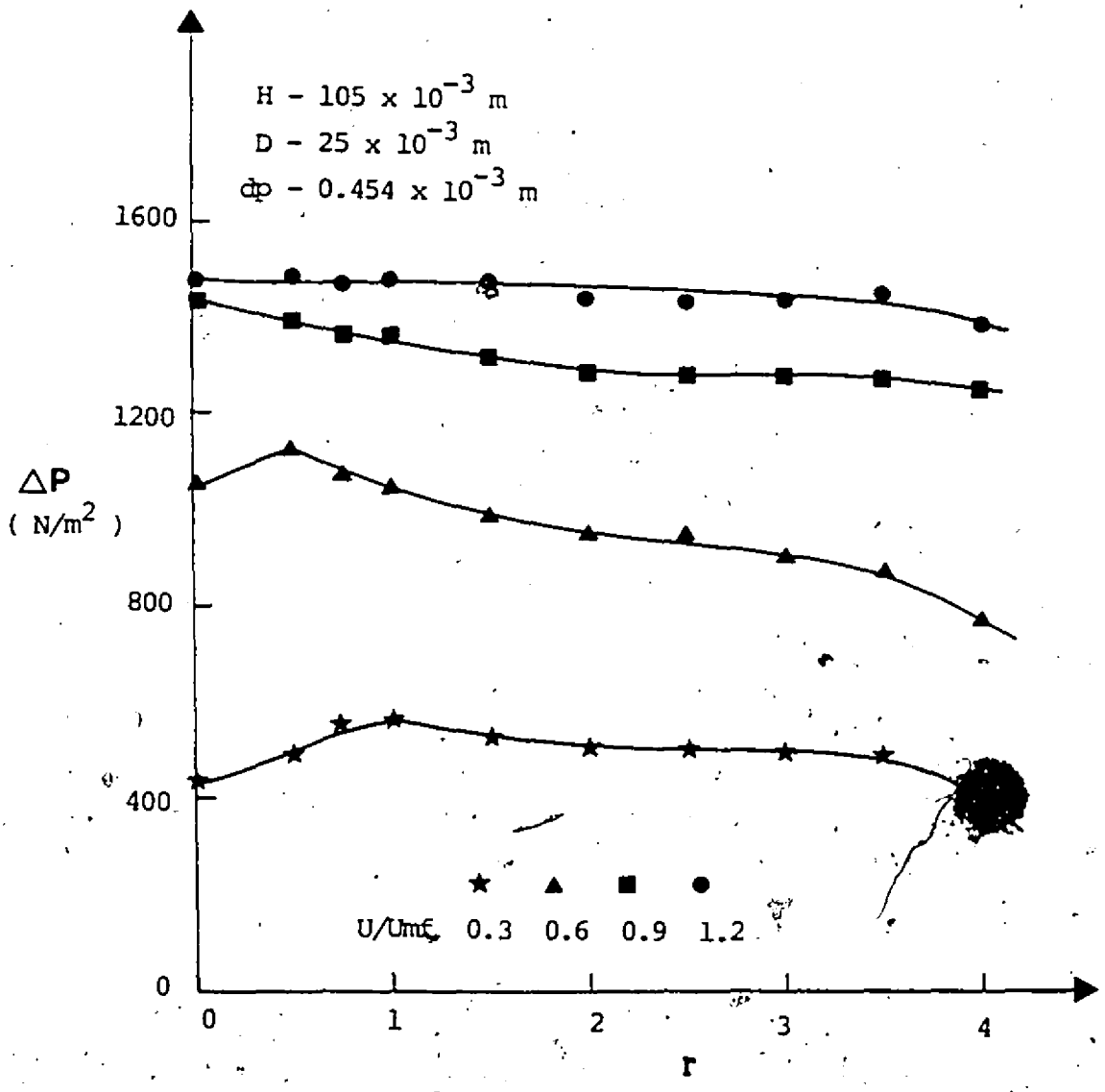

Figure 3-8 A typical ΔP versus r plot

3.4.2 Heat Transfer

A sample data sheet used in heat transfer experiments is shown in Appendix D. All five heater thermocouples were used in determining the average cylinder temperature. A minor temperature variation around the cylinder was noted which is a result of the expected peripheral variations in the heat transfer coefficient around the cylinder surface. The objective of this work was to examine only the average heat transfer rate for immersed cylinders. The Biot number (h D/Kc) was found to be less than 0.02 which allowed assumption of a uniform temperature in the cylinder.

The choice of the bed temperature to be used in the definition of h was dependent on the mixing conditions in the bed. Figure 3-9 shows a " mixing regime map " for a bed of dry particles. This map was obtained from detailed temperature surveys of the bed temperature at various locations (thermocouple number 33, 35, 37 in the data sheet- 35 being the farthest from the heater). In the region I of Figure 3-9 the difference in the temperature between the thermocouples nearest to and farthest from the heater was significant (greater than 5°C with heating input of 3-4 W). Such large temperature variations indicated that the bed was poorly mixed. Region II was a transition phase during which time the bed mixing was classified moderate and the temperature variation was typically below 1.5°C with a heat input of 7-8 W. Region III of the map was considered well-mixed with temperature variations of less than 0.25°C. It must be pointed out that the boundary between

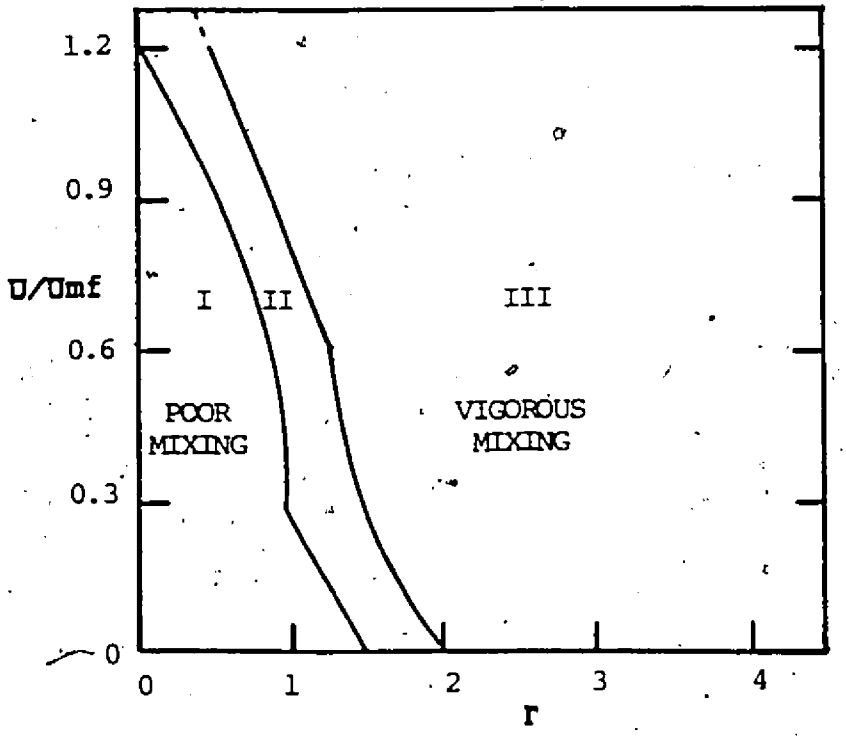

Figure 3-9 Map showing mixing characteristics for a bed of dry particles

regions I and II was noted to be a sharp one, while the one between II and III was not sharp.

In region I the bed temperature used in calculating h was represented by the thermocouple farthest (number 35) from the heater, while in the other two flow regimes, the average of all the bed thermocouples was selected as the appropriate bed temperature. It may be noted that for similar measurements in conventional fluidized beds, the bed temperatures are normally measured by two to three thermocouples, one each located well above and below the immersed surface, as reported by Grewal and Saxena (1980, 1983), Chandran et al (1980) and Goel et al (1984).

The average heat transfer coefficient was calculated for different conditions of U/Umf and r and the raw data plotted as shown in Figure 3-10. Subsequent data for cross- plots and dimensionless plots were extracted from similar graphs. For runs with wet molecular sieve particles, h versus X was plotted for given conditions of U and r. The bed was always in region III of Figure 3- 9 for experiments with wet particles (because of the obvious particle sampling problem when the bed is not well-mixed).

3.5 EXPERIMENTAL UNCERTAINTY

The estimated maximum errors and experimental uncertainties for both independent and dependent variables are

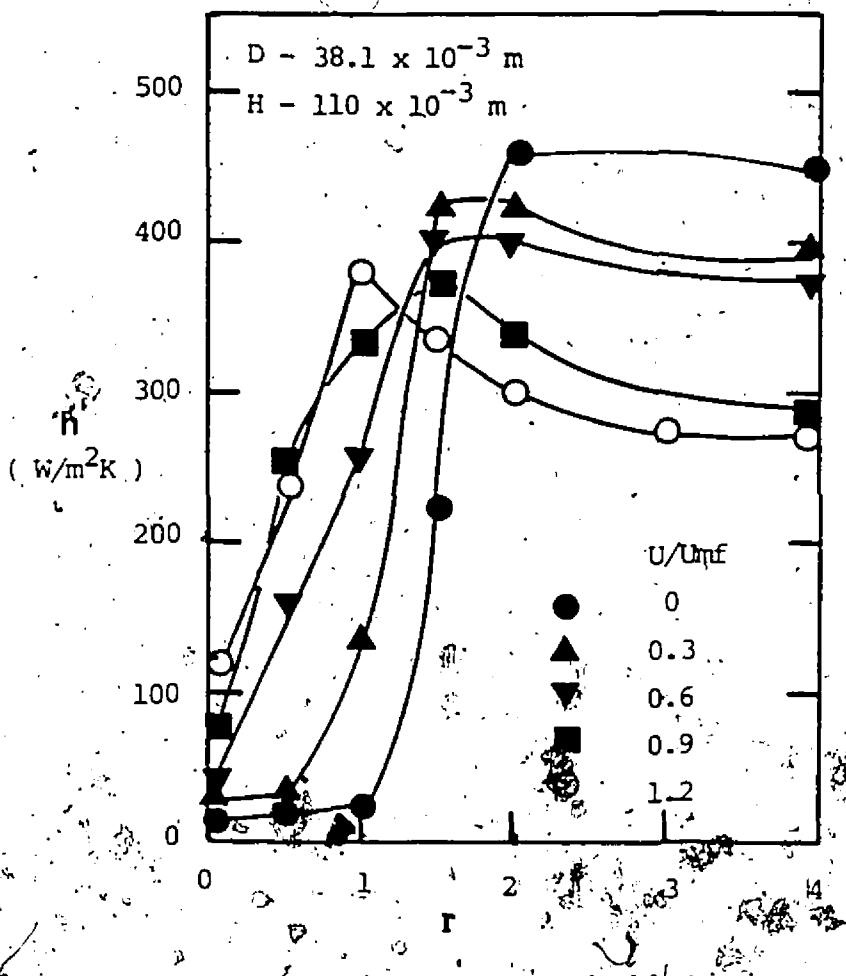

Material - Glass ballotini

Figure 3-10 A typical h versus r plot for dry beds

tabulated in Table 3.3. The determination of these experimental uncertainties is also explained in Appendix A. The reproducability of the heat transfer runs was ±3%.

TABLE 3.3

Experimental Uncertainty for Independent and Dependent Variables

VARIABLE	EXPERIMENTAL UNCERTAINTY
Vibration amplitude, A	$\pm 0.1 \times 10^{-3}$ m
Vibration frequency, ω	±0.3 rad/s
Bed height, H	$\pm 0.2 \times 10^{-3}$ m
Particle size, dp	±5%
Bulk density, ρ_b	±25 kg/m³
Air velocity, U	±0.55% - ±1.67%
Moisture content, $\bar{X}$	±0.4%
Bed pressure drop, ΔP	±9.81 N/m²
Vibration number, $\Gamma = A\omega^2/g$	±0.109
U/Umf	±0.77% - ±2.36%
ΔT ($T_s - T_b$)	±1°C
Heat input, Q	±0.5%
Overall heat transfer coefficient, h	±8%

CHAPTER 4

RESULTS AND DISCUSSION- AERODYNAMIC ASPECTS

4.1 INTRODUCTION

Among the numerous advantages of a VFB are its ability to pseudo-fluidize solids at low aeration rates (U<Umf), difficult-to-fluidize sticky or wet particles, gentle handling etc. This chapter presents results on the fluidization and mixing characteristics of dry and sticky particles in a vibrated fluidized bed.

It is often impossible to supply adequate heat for drying of particulates in a directly heated (i.e. purely convective dryer) dryer. It is then necessary to install heat exchange surfaces within the bed of particles to supply additional heat directly. The flow patterns around these immersed surfaces and mixing patterns in the bed play an important role in determining the surface-to-bed heat transfer.

Since the rigidly mounted immersed heat transfer surfaces within the bed act as distributed vibrators and impart additional energy to it, the results of bed pressure drop with immersed cylinders are also presented. It should be noted that all the results in this chapter are for a VFB fitted with a 4% free area distributor plate.

Finally the extended vibrational acceleration number proposed by Ringer and Mujumdar (1982) to evaluate the minimum fluidization velocity in presence of vibration is briefly discussed.

4.2 FLOW RESULTS

4.2.1 Dry Particles

Figures 4-1 and 4-2 present typical ΔP versus U data for dry glass ballotini (dp=0.454 mm and dp=0.667 mm). The curves for $\Gamma = 0$ are those for conventional fluidization. As Γ increases the pressure drop initially rises above the $\Gamma=0$ curve and then crosses it over. The maximum positive deviation for glass ballotini particles from the $\Gamma = 0$ curve occurs at $\Gamma=0.5$ in the range U/Umf=0.6-0.7. With an increase in Γ, this deviation from the $\Gamma=0$ curve becomes small until at higher Γ's the entire pressure drop curve is below the $\Gamma=0$ curve.

The initial surge in the bed pressure drop due to vibration is ascribed to compaction of the bed as observed visually too. Up to $\Gamma=1-1.5$ the bed compacts; above this value, it expands if the vibrational intensity is high enough ($\Gamma \geq 2$). A similar finding has been reported by Erdesz and Ormos (1984) who carried out their experiments in a bed of sand particles (dp= 0.15-0.6 mm), 100-120 mm high and with amplitudes upto 1.85 mm. They reported compaction in all cases for $\Gamma<1$ and U/Umf<1. The above results were also verified for molecular sieve particles (A=2.75 mm) as shown in Figure 4-3.

From Figures 4-1 and 4-2 it can be seen that for smaller glass ballotini (dp=0.454 mm), application of vibration over the entire Γ range increased the bed pressure drop for U/Umf<0.6-0.7. For larger ballotini (dp=0.667 mm) the bed expands beyond $\Gamma>2$ i.e. for $\Gamma>2$ the bed pressure drop is always lower than for a non-vibrated bed. This result suggests that

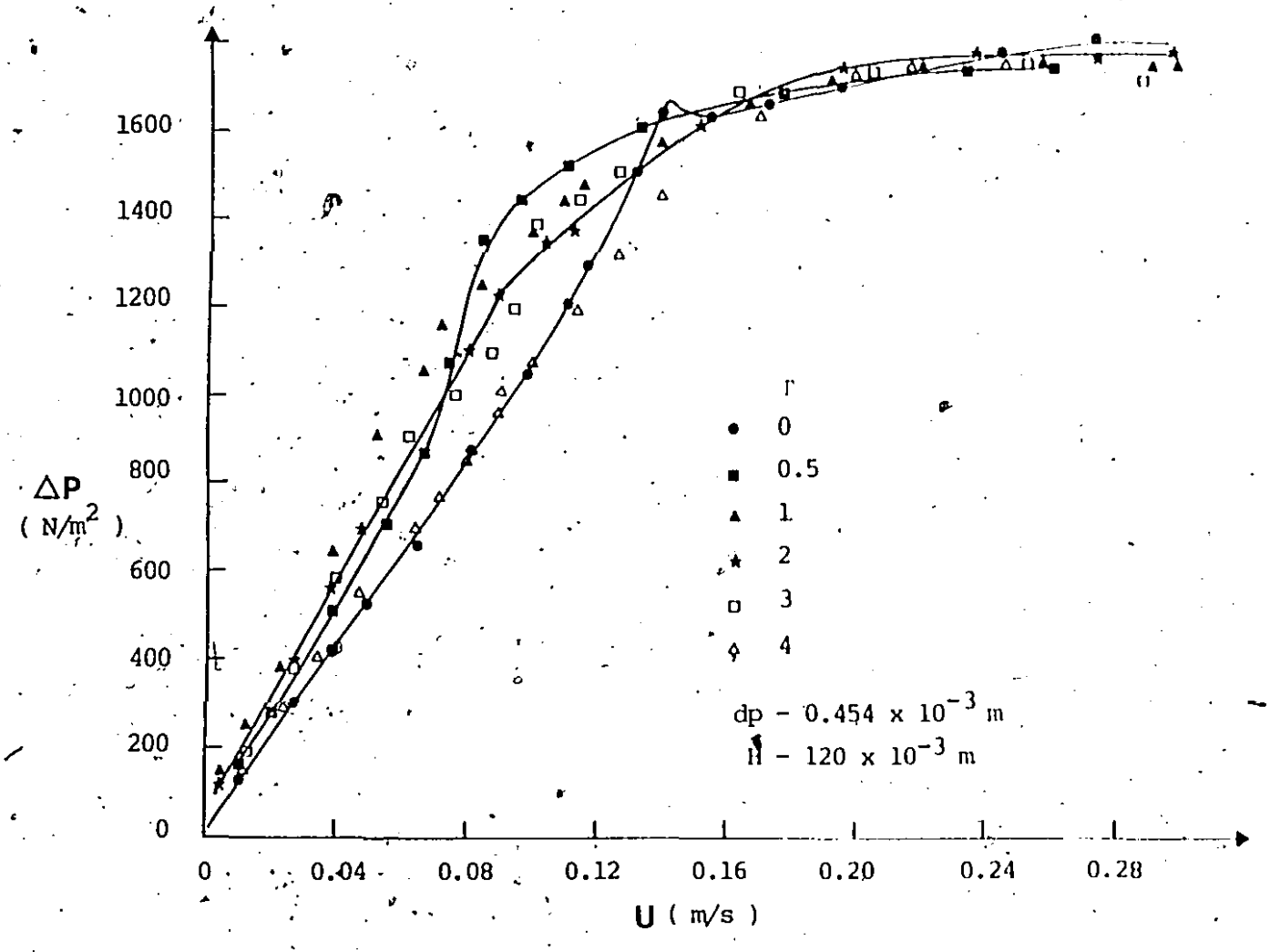

Figure 4-1 Effect of vibrational acceleration on a bed of dry glass ballotini at A=4.25 mm

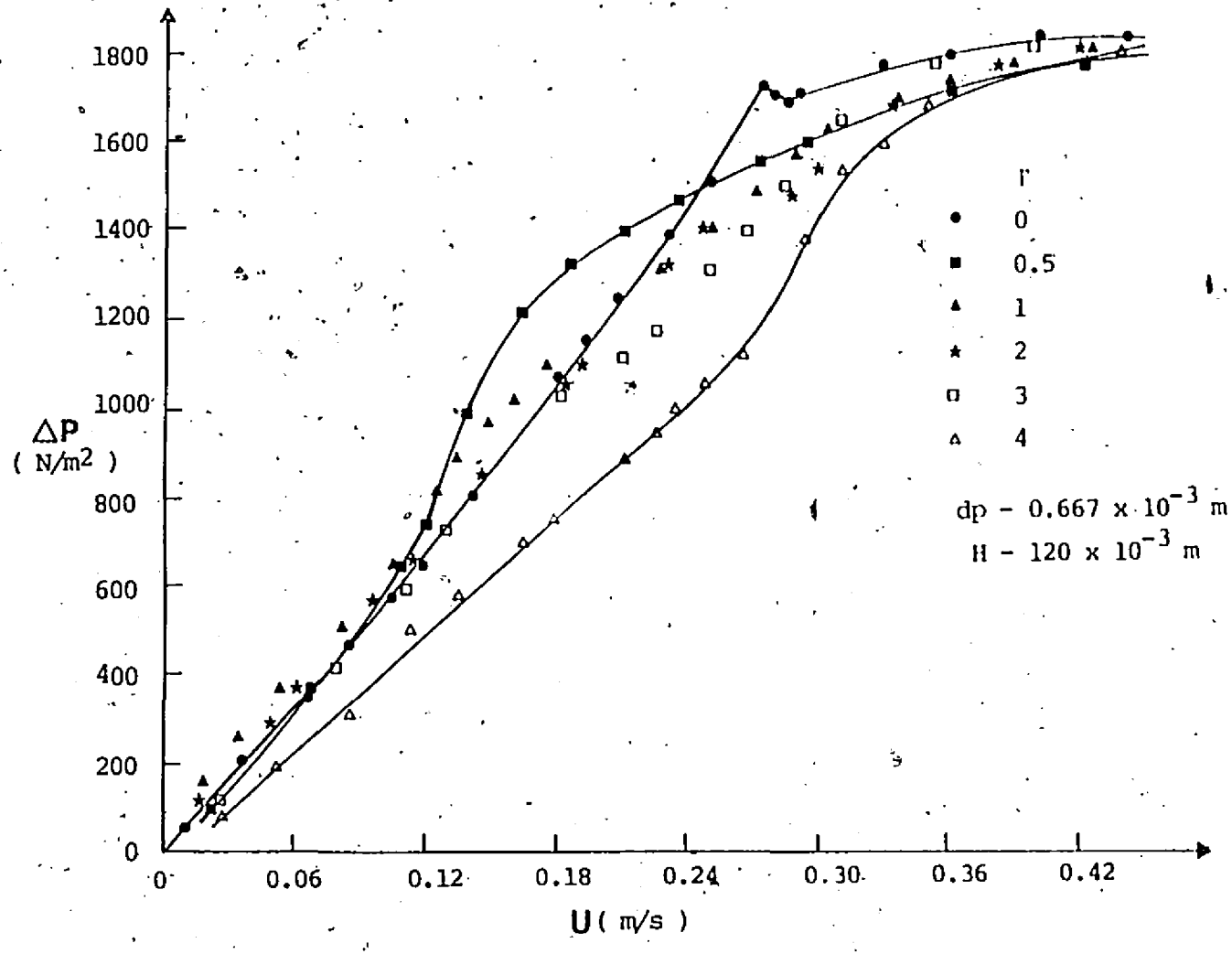

Figure 4-2 Effect of vibrational acceleration on a bed of dry glass ballotini at A=4.25 mm

vibration-induced bed compaction is more pronounced in the case of finer particles; higher compaction implies greater resistance to flow. Figure 4-3 confirms this statement in case of molecular sieves (dp=1.4 mm), where the bed pressure drop for $\Gamma>1$ is always lower than that for $\Gamma=0$.

The aforementioned results are in accordance with data presented by Gupta and Mujumdar (1980) for polyethylene particles (dp=3.1 mm) and Mujumdar (1984) for molecular sieve particles (dp=2.5 mm) where all the pressure drop versus velocity curves for $\Gamma>0$ lie below the $\Gamma=0$ curve over the entire air velocity range. Although the results presented by Gupta and Mujumdar (1980) are for very shallow beds (25 mm high) these results have also been further verified using polyethylene particles (dp=3.25 mm) for bed depths upto 120 mm.

In the case of finer particles, the initial compaction ($\Gamma<1.5$) is so significant that even vibrational acceleration $\Gamma\geq4$ and $U/Umf\geq0.7-0.8$ are inadequate to lower the pressure drop below the $\Gamma=0$ curve. It should be noted that the materials tested had different bulk densities. The effect of vibration decreases with a decrease in particle density (Gupta (1979)) and therefore for polyethylene and molecular sieve particles, the particle size effect is coupled with the density effect.

Figure 4-4 shows the effect of Γ on bed porosity for glass ballotini particles. The effect of vibrational acceleration on bed compaction, also shown in Figures 4-1 and 4-2 is clearly evident. For $U/Umf\leq0.6$ the bed always compacts for $\Gamma<1$; for $U/Umf=0$, vibration compacts the bed over the entire

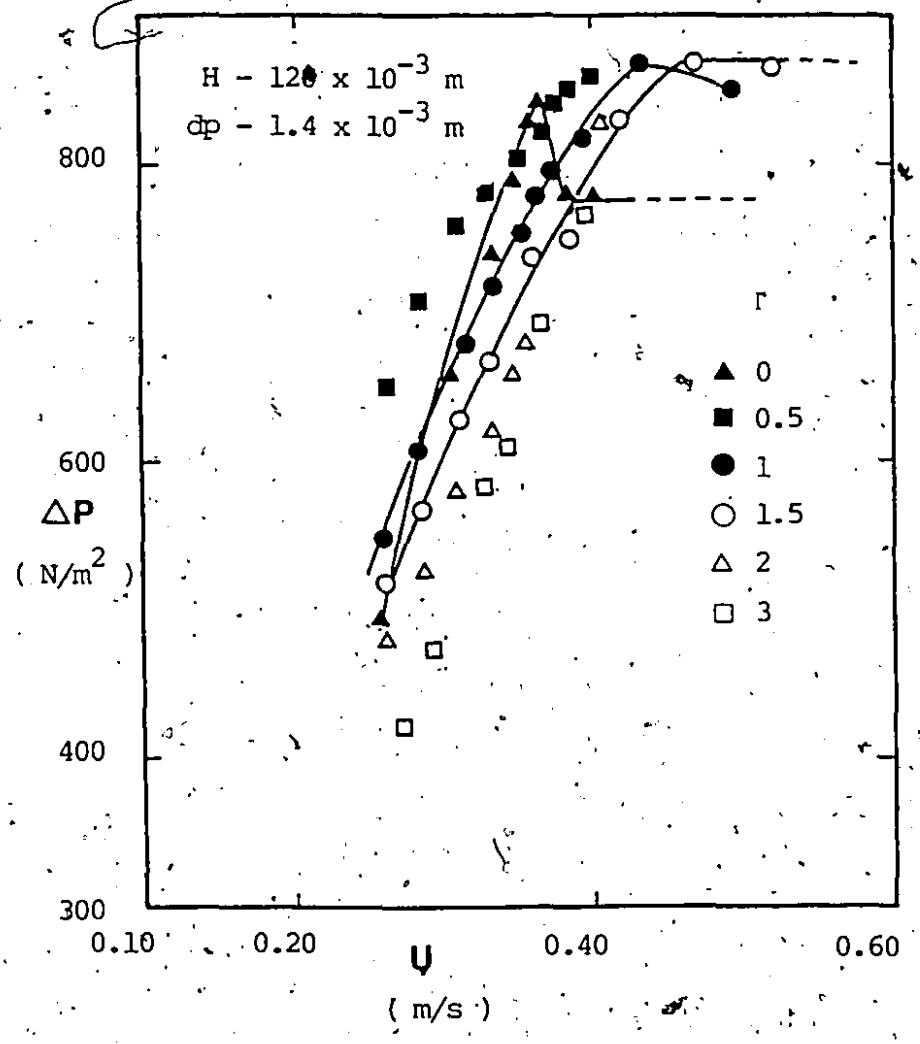

Figure 4-3 Effect of vibrational acceleration on a bed of dry molecular sieve particles at A=2.75 mm

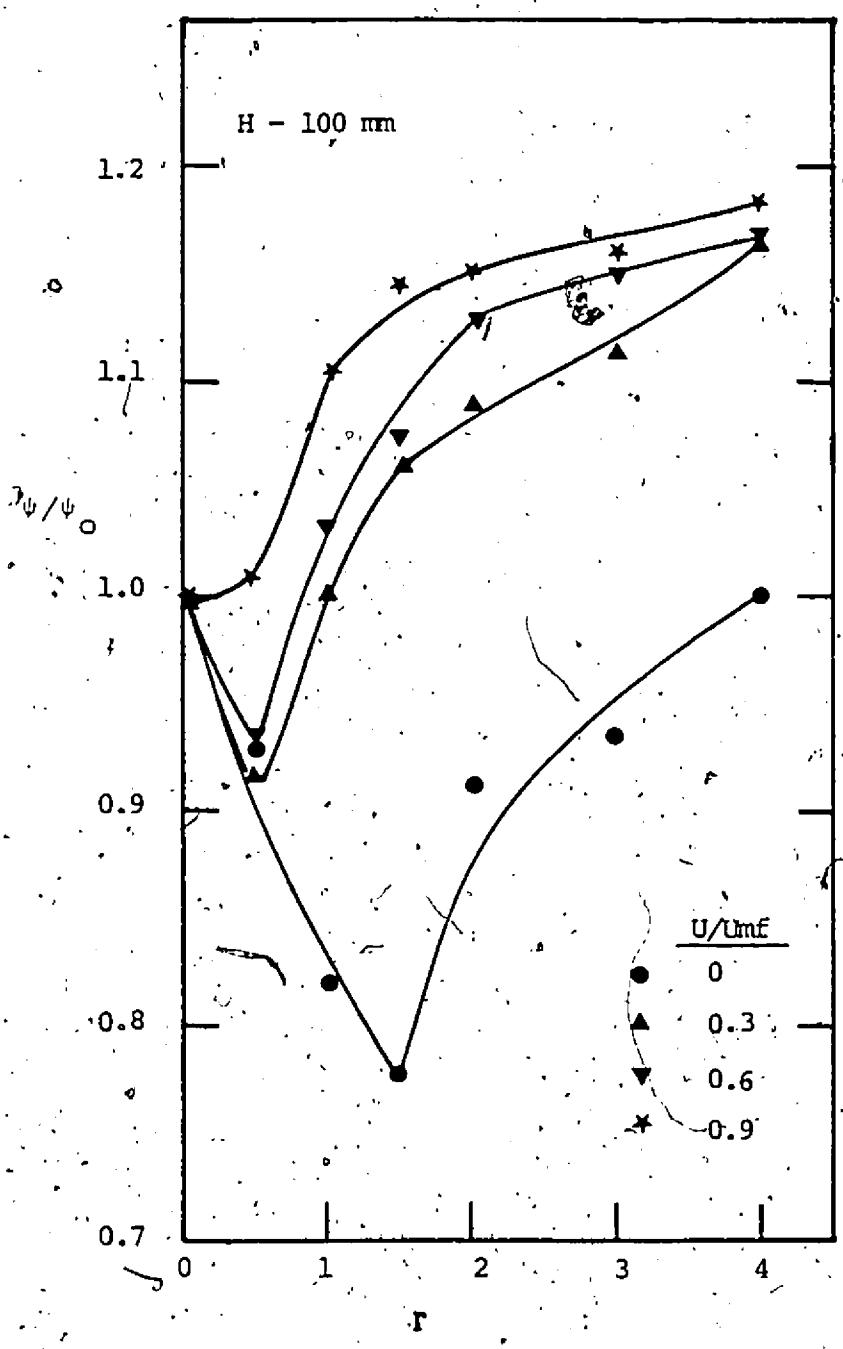

Figure 4-4 Effect of vibrational acceleration on bed porosity for glass ballotini

range tested although less severely for $\Gamma \geq 2$. Higher Γ values ($\Gamma \geq 2$) loosen up the bed for $U/Umf \geq 0.3$. At air flow rates close to minimum fluidization ($U/Umf \geq 0.9$) vibrational acceleration increases the bed porosity over the entire range. This is true in light of the fact that at higher air flow rates vibration aids in improving the bed structure (Bratu and Jinescu (1977)) rather than supporting it. A sharp rise in bed porosity between $\Gamma = 0.5$-1.5 for $U/Umf = 0.9$ is due to early fluidization of the bed under the influence of vibration, a fact also visually verified by the presence of bubbles.

Pakowski et al (1984) have reported initial compaction of bed for quartz sand particles ($dp = 0.210$-0.355 mm, $H = 40$ mm, $\Gamma = 0$-3) and more severely for smaller particles over a large range of Γ ($\Gamma = 0$-5). They also reported that higher amplitudes of vibration result in greater bed voidage at the same acceleration. Their results could not be verified due to the limitation on the frequency and amplitude of vibration in the current work.

It should be pointed out that the results presented in Figure 4-4 are visually determined average bed porosities at different sets of Γ and U/Umf. At higher Γ's ($\Gamma \geq 3$) and U/Umf ($U/Umf \geq 0.6$) the bed height and the pressure drop fluctuated very significantly. At high Γ's and U/Umf the average bed height was

determined, which was then used to calculate the average porosity from the following relationship (Kunii and Levenspiel (1967)):

$$= 1 - (H_{\Gamma=0} / H (1 - \psi_o))$$

4.2.2 Sticky Particles

Despite their extensive industrial applications, particularly for drying of sticky particulates, little is known about the aerodynamic behaviour of such systems. An attempt is made here to observe some flow behaviour of particles with surface stickiness, an important parameter in determining the bed characteristics in any drying process.

The fluidization curves for sticky particles are shown in Figures 4-5 through 4-7. It can be seen that curves for $\Gamma=0$ are very similar to those for conventional fluidization. Moderate stickiness (glycerine content less than 0.006 kg glycerine per kg dry ballotini) does not seem to have any effect on the shape of the fluidization curves although the minimum fluidization velocity increases and the bed structure is highly irregular. The shape of the ΔP - U curves for $\Gamma>0$ are similar to the ones reported by Gupta and Mujumdar (1980).

Seville and Clift (1984), who studied the effect of thin liquid layers on fluidization characteristics in a bed of glass ballotini using a light non-volatile oil (di-2-ethyl hexyl sebacate) reported an increase in the minimum fluidization velocity, Umf, with liquid loading. They also

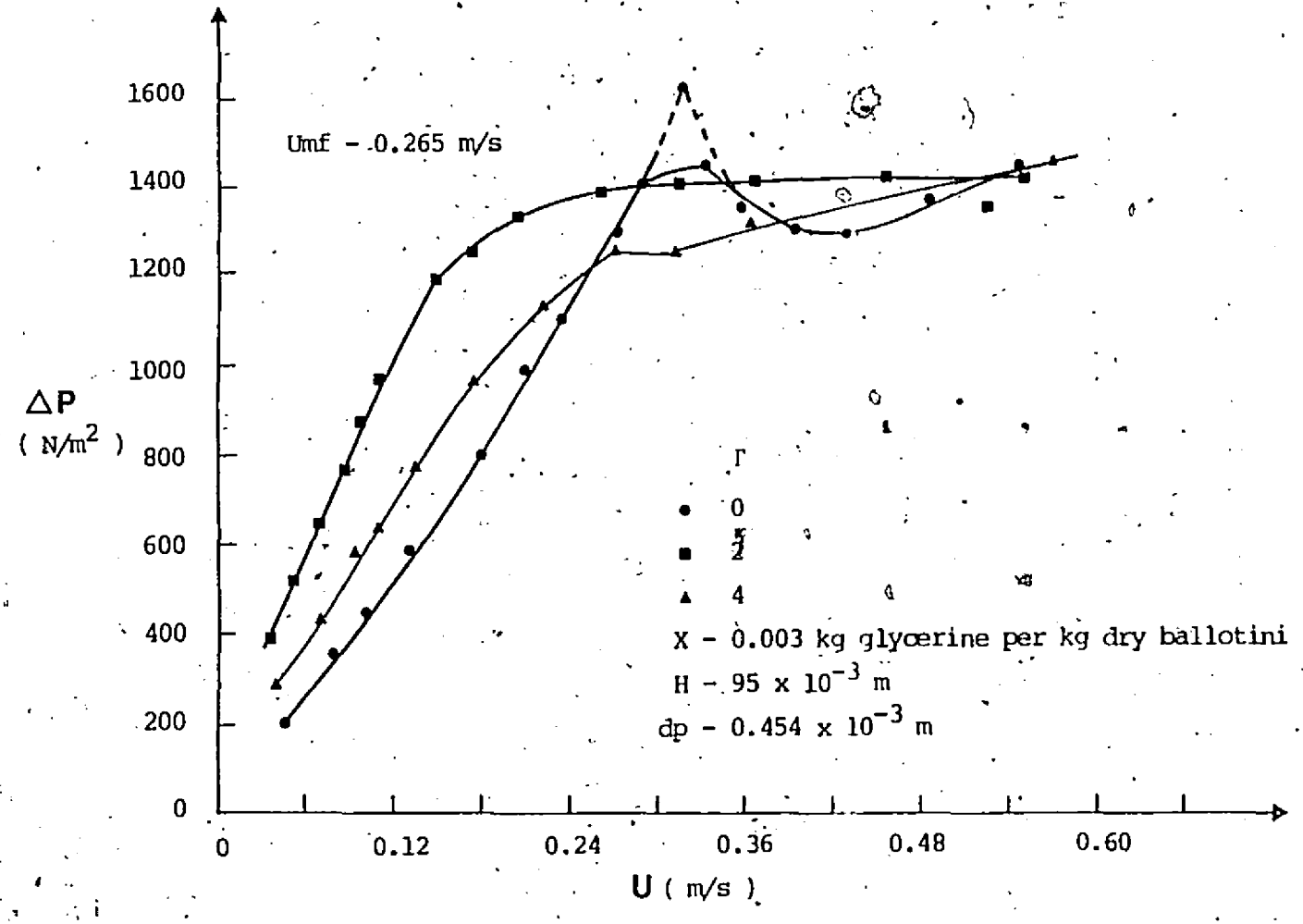

Figure 4-5 Effect of vibrational acceleration on a bed of sticky glass ballotini at A=2.75 mm

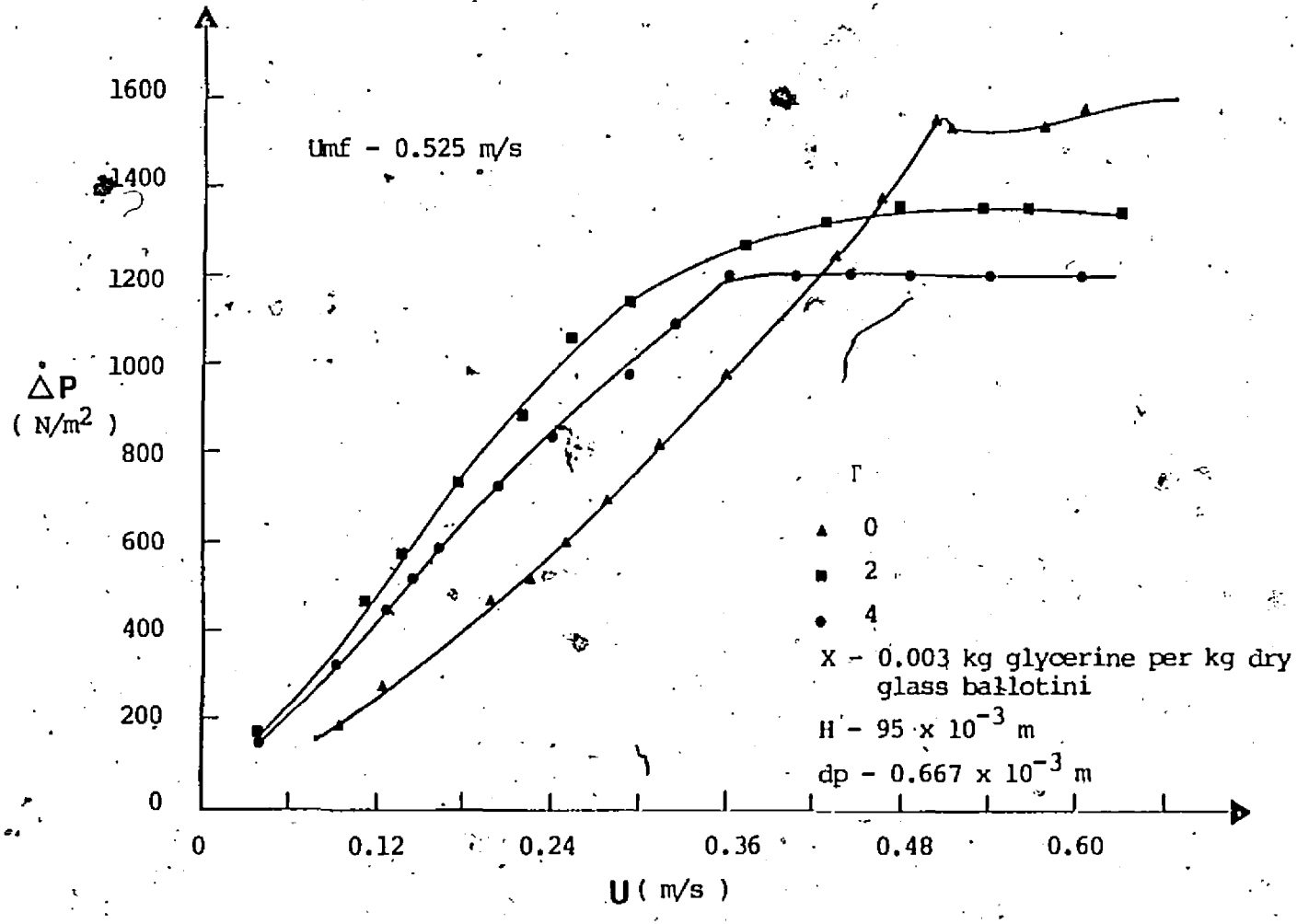

Figure 4-6 Effect of vibrational acceleration on a bed of sticky glass ballotini at A=2.75 mm

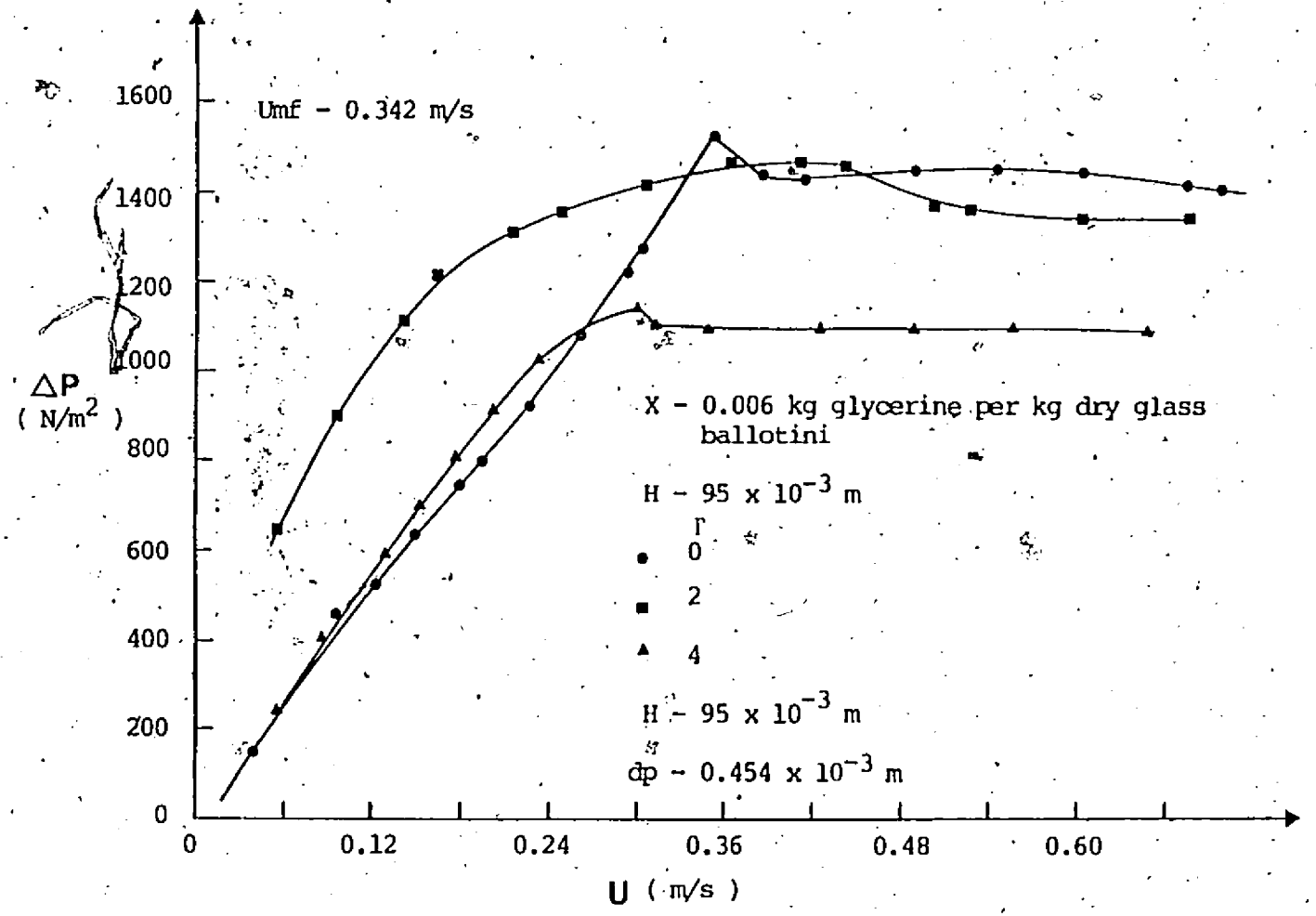

Figure 4-7 Effect of vibrational acceleration on a bed of sticky glass ballotini at A=4.25 mm

reported a shift in behaviour of the bed from Group B (sand like) through A (aeratable) to Group C (cohesive) of Geldart's (1973) classification i.e. from a regular to irregular bed structure (See Appendix B and Table 3.1(b) for classification of particles). Increasing interparticle cohesive forces in a bed of Group B material cause the fluidization characteristics to move through Group A to Group C. Increasing interparticle cohesion generally increases bed voidage and reduces the pressure gradient for given gas velocity (Seville and Clift (1984)) and hence increases the minimum fluidization velocity.

It should be noted from Figures 4-5 through 4-7 that with increasing Γ the pressure drop is always higher than that for $\Gamma=0$ over the aeration rate $U/Umf \leq 1$. It is also very important to note that beyond $U/Umf=1$, all flow curves reach a plateau. However, unlike the dry particle beds for which all flow curves reach a common plateau, for sticky beds the plateau levels are different and a function of X and Γ. This difference is more pronounced with increasing stickiness due to increased channelling in more sticky beds after fluidization has started. The pressure drop is consistently lower for higher Γ's after the plateau is reached. This may be attributed to a looser and more homogeneous structure of the bed as a result of applied vibration.

For non-vibrated beds highly irregular flow patterns were observed throughout the bed of sticky particles i.e. cracks and irregular channels covered the whole bed. For X=0.006 the bed

often separated as a whole from the distributor plate and remained suspended until it was ' tapped 'down. This irregular behaviour of the bed diminished with application of vibration; above Γ= 1.5, no discernible channelling occurred.

In Figure 4-5, the dotted line for Γ=0 represents a typical alternative ΔP versus U curve which is an indicator of the poor reproducability of the flow curves for sticky beds. The hump disappears when the bed is lightly tapped to break the bridges and channels formed due to stickiness of the particles. A very significant feature of the sticky beds was the absence of bubbling over the entire range of Γ's and air flowrates covered. For corresponding dry beds, there is considerable fluctuation in the bed pressure drop under similar conditions.

Another observation was the entrainment of particles at much lower superficial air velocities for sticky beds at Γ>2 viz., in the range of 1.4-2 times Umf (Note: Umf here is the measured value for the sticky (not dry) particles). For dry beds, there was no discernible entrainment under similar operating conditions. This is attributed to the formation of channels in the sticky bed; for a given superficial air velocity the air velocity within these channels and crevices can be high enough to cause localized entrainment of loose particles. Such local entrainment is aided by vibration which besides providing extra lift, breaks up some of the larger lumps into smaller ones which can be readily entrained.

4.3 MIXING

For efficient heat and mass transfer operations to take place in a VFB, it is important to accomplish good solids mixing in the bed. One of the main advantages of the VFB is that solids mixing commences at very low gas velocities and moderate vibrational accelerations. Gupta and Mujumdar (1980) studied the mixing phenomena in a VFB and defined a new " minimum mixing velocity ". Their observations were purely visual and provided no quantitative measure of onset of mixing.

Mixing besides affecting the heat transfer rates is also an indicator of the temperature gradients through out the bed and vice-versa. Therefore, the temperature variations in the bed provide a means of estimating the degree of particulate mixing as well as the circulatory patterns which are induced in a VFB under the joint action of vibration and aeration. The details of the procedure employed to obtain the mixing map are discussed in Chapter 3.

Figures 4-8 through 4-10 show the flow regimes in a VFB as far as solids mixing is concerned. It should be noted that all these figures are independent of the amplitude of vibration. Figure 4-8 shows the mixing characteristics for a bed of dry particles. The regions of moderate and vigorous mixing correspond to the "pseudo-fluidization" regime as reported by Gupta (1979).

Figure 4-8 also compares very well with the plot of minimum mixing velocity as a function of vibratory acceleration presented by Gupta and Mujumdar (1980). As discussed later in Chapter 5, the heat transfer rates are much higher for moderate

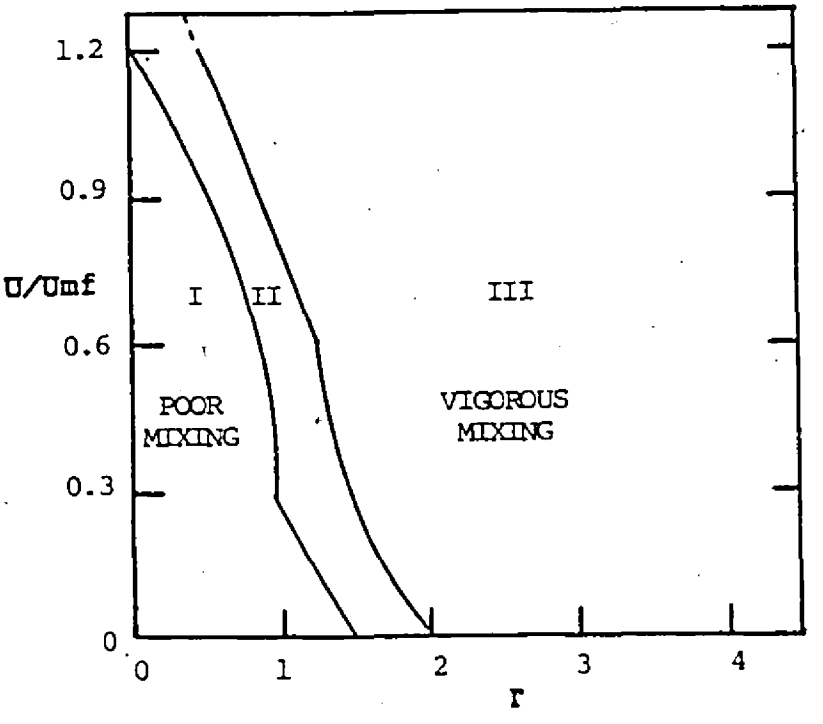

Figure 4-8 Map showing mixing characteristics for dry particles in a VFB

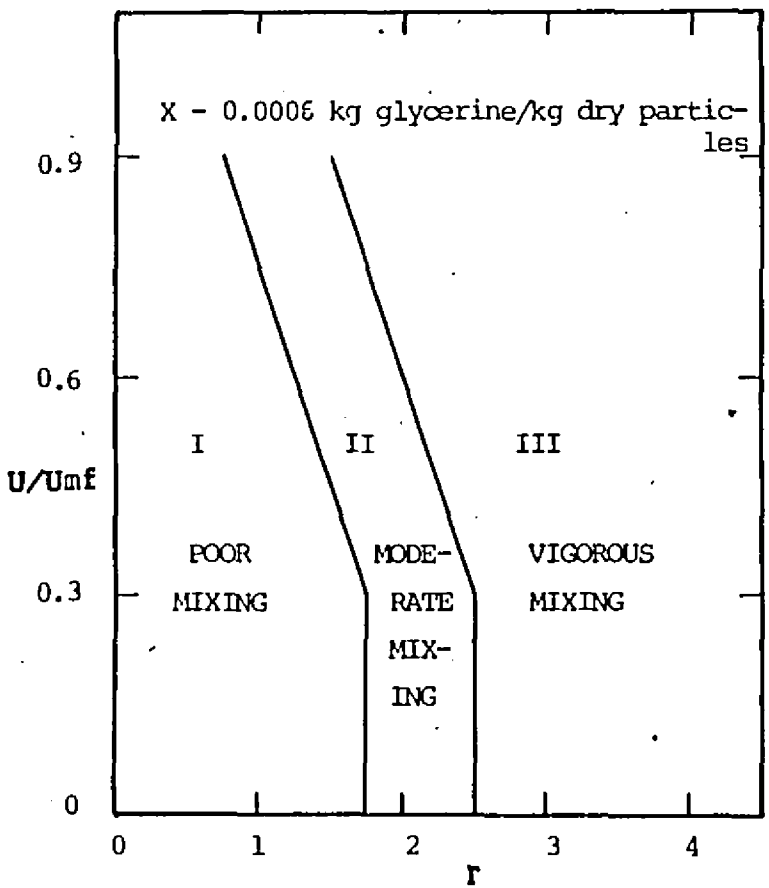

Figure 4-9 Map showing mixing characteristics for sticky particles in a VFB

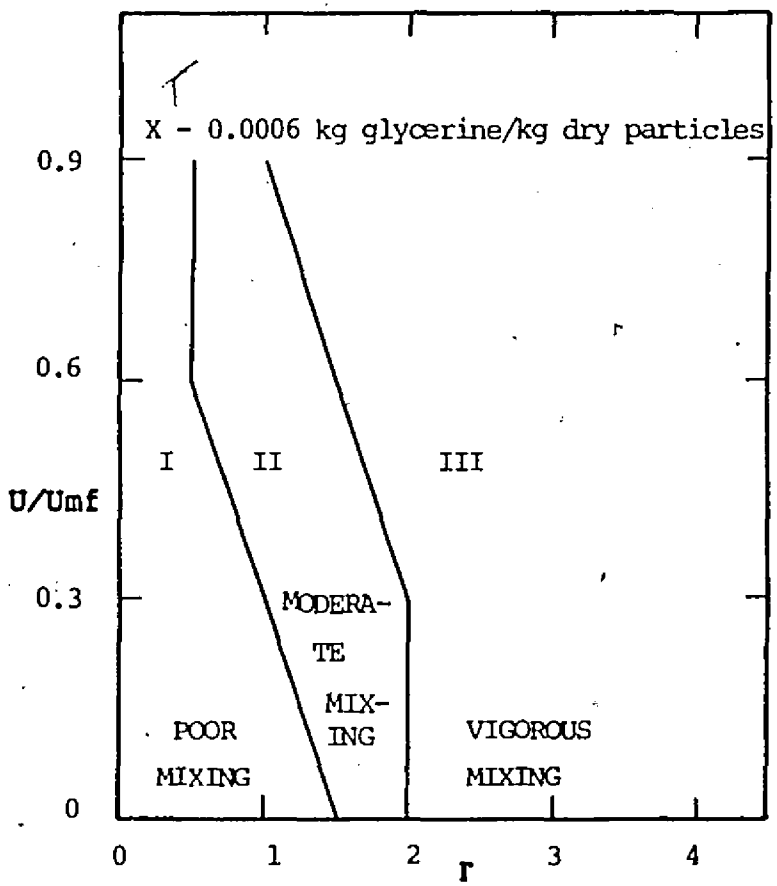

Figure 4-10 Map showing mixing characteristics for sticky particles in a VFB

and vigorous mixing regimes as compared to the region of poor mixing. These maps were developed on the basis of visual observations as well as the measured spatial variations in bed temperature with a heated cylinder in the bed. These results are semi-quantitative in nature.

Figures 4-9 and 4-10 show the mixing characteristics for sticky beds of glass ballotini. Comparison with Figure 4-8 shows that all the curves shift towards the right for a bed of sticky particles i.e. the region of poor mixing extends to higher Γ values. This can be explained in terms of the adhesive bonds formed between two particles which inhibit the initial mixing of bed by providing additional resistance to granular flow.

Figure 4-10 shows the mixing regime map for larger glass ballotini, but at the same stickiness level as in Figure 4-9. It can be seen that for larger ballotini the region of poor mixing is smaller as compared to the smaller ballotini, and vigorous mixing is initiated at lower values of Γ. In fact, at the stickiness level used Figure 4-10 is very similar to Figure 4-8 i.e. larger sized particles are less affected by stickiness as compared to the smaller ones.

The characteristic of Group B (sand like) particles of Geldart's (1973) classification is that, interparticle forces are negligible as compared to fluid drag. Seville and Clift (1984) have postulated a simple criterion for particles to be in Group B as:

$$g(\rho_p - \rho)(\Pi \, dp^3/6)/ F_h > \text{constant}$$

where F_h is the adhesion force transmitted in a single contact between two adjacent particles. The constant in the above equation is a function of particle characteristics.

Therefore, for a given stickiness level (i.e. F_h = constant) larger the particle size better are the structure and mixing characteristics of the bed. This probably explains why a bed of sticky glass ballotini (dp=1.017 mm) behaves much like a dry one as compared to a sticky bed of ballotini with dp=0.325 mm.

4.4 BED PRESSURE DROP

The operation at very low air flow rates leading to reduced pressure drops is a key hydrodynamic feature of the VFB. This leads to a more economic operation, due to requirements of smaller ducts, smaller dust collection equipment and reduced overall energy and power consumption. Since, rigidly mounted cylinders themselves act as distributed vibrators, the results presented are for a bed with a rigidly mounted horizontal immersed circular cylinder. The effects of amplitude and frequency of vibration, particle size, bed height and particle stickiness were examined in this study.

4.4.1 Effect of Vibrational Acceleration

The ΔP versus Γ results for beds of 0.454 mm and 0.667 mm glass ballotini, with a 25 mm diameter cylinder mounted centrally in the bed are presented in Figures 4-11 and 4-12, respectively. It can be seen from these figures that for

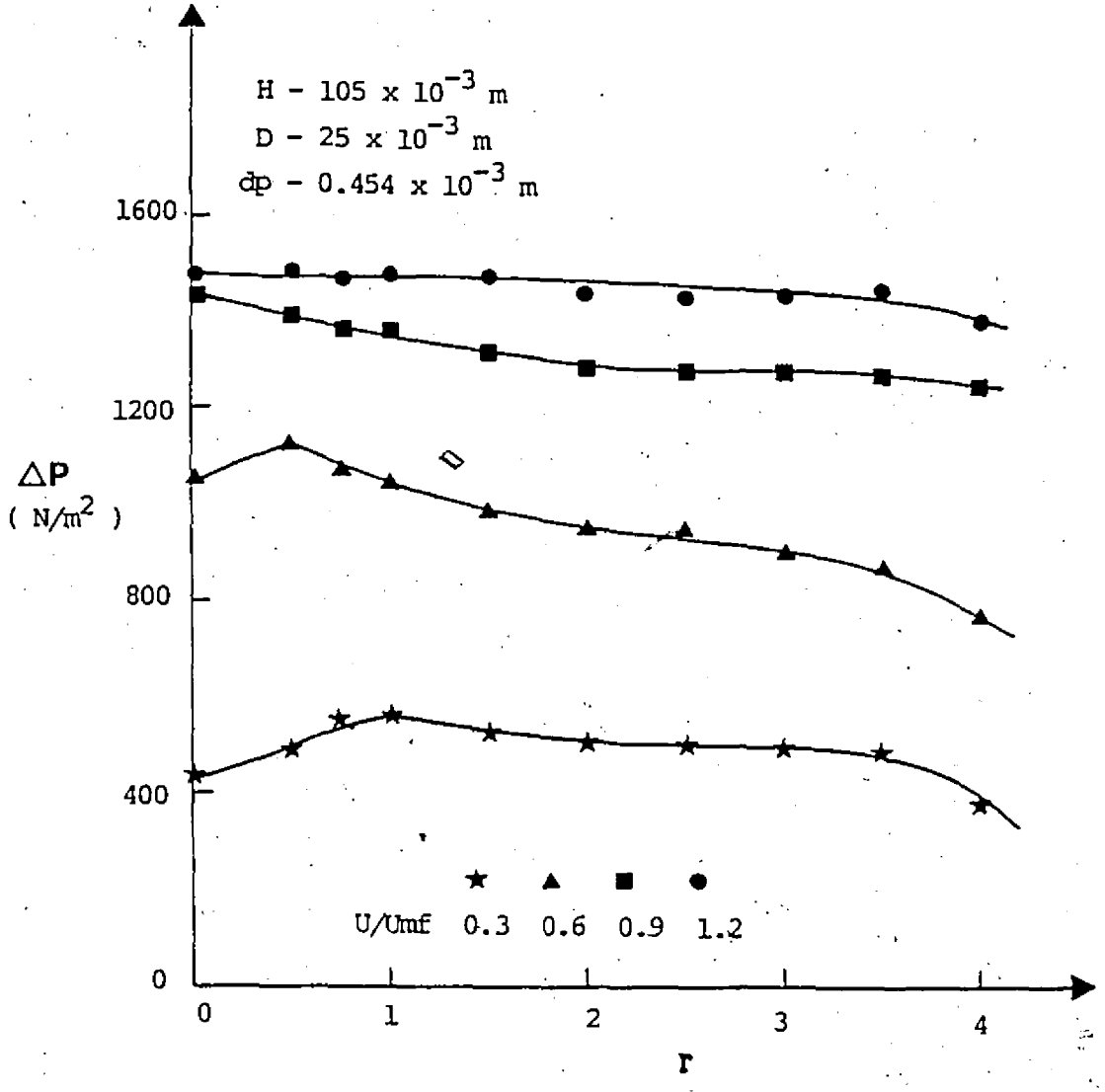

Figure 4-11 Effect of vibrational acceleration on ΔP for a bed of dry glass ballotini

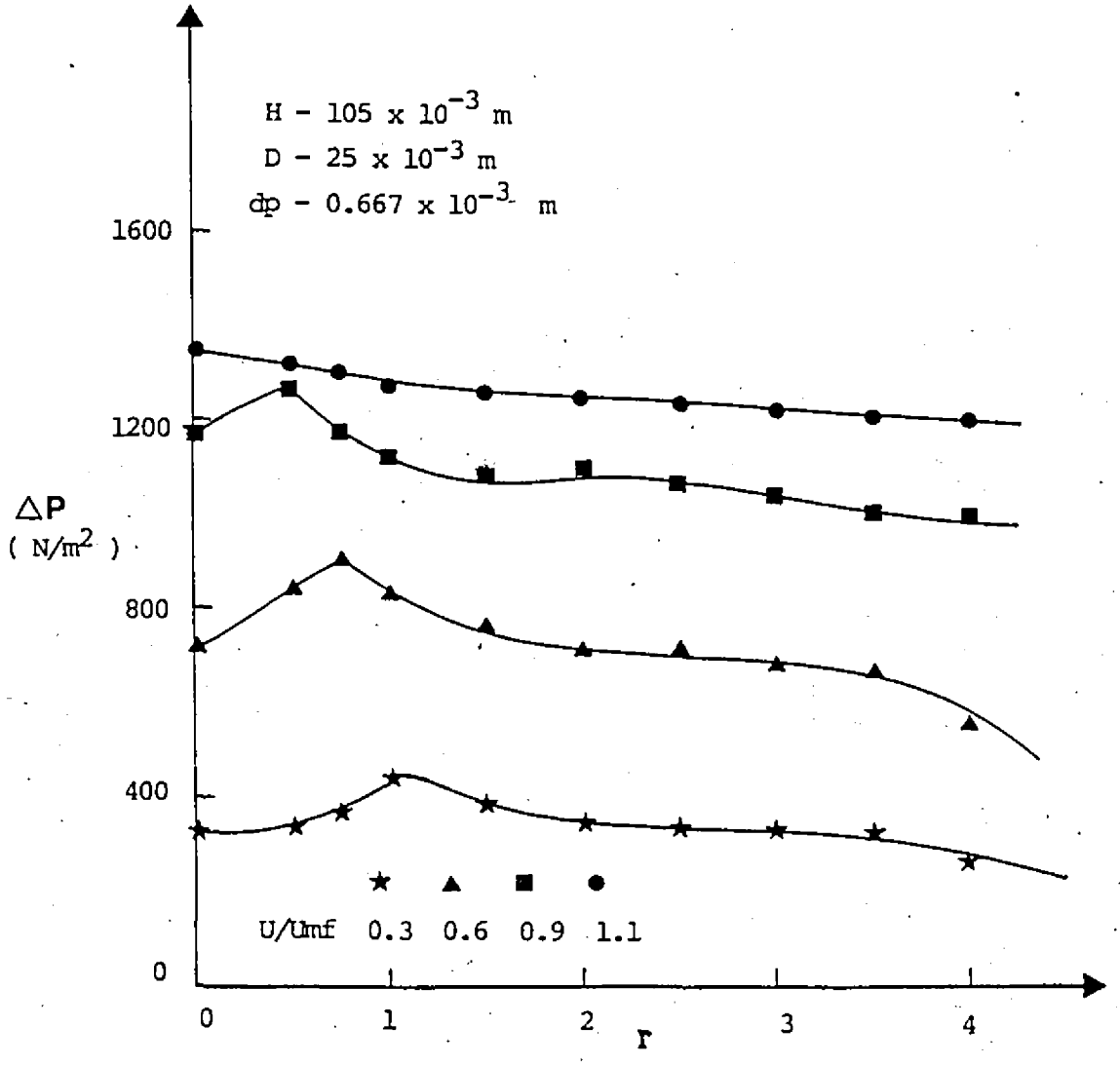

Figure 4-12 Effect of vibrational acceleration on ΔP for a bed of dry glass ballotini

U/Umf≤0.6 vibration first increases the pressure drop across the bed from Γ=0 through Γ=1 due to compaction, before lowering it gradually up to Γ= 3.5; beyond this value there is a considerable reduction in the bed pressure drop.

For U/Umf≥0.6, the initial phase of bed compaction is absent altogether and there is a monotonic decline in bed pressure drop from Γ=0 through Γ=4. This observation implies that at higher values of U/Umf the effect of air flow rate overrides the effect of vibration as stated among others, by Bratu and Jinescu (1971).

An important observation from Figures 4-11 and 4-12 is that the bed pressure drop is 10-20% lower in the case of larger ballotini as compared to the smaller one. Erdesz and Ormos (1984) carried out experiments with sand particles ranging from 0.15 mm to 0.8 mm in size and Γ=0-14. Their result that pressure drop curve for smaller particles is lower than that for beds of larger particles is contradictory to the present results. It should be noted, however, that Erdesz and Ormos (1984) used very small amplitude of vibration (1.85 mm), and their results in the Γ=1-4 range were very inconsistent. The exact cause for this discrepancy is not known.

Typical bed pressure drop versus Γ results for sticky beds are presented in Figures 4-13 through 4-15. As discussed earlier, for sticky particles the bed structure is very irregular. Each time the material was charged into the bed the starting pressure drop was different i.e. the flow pattern is not reproducible. Without vibration the whole bed often moved

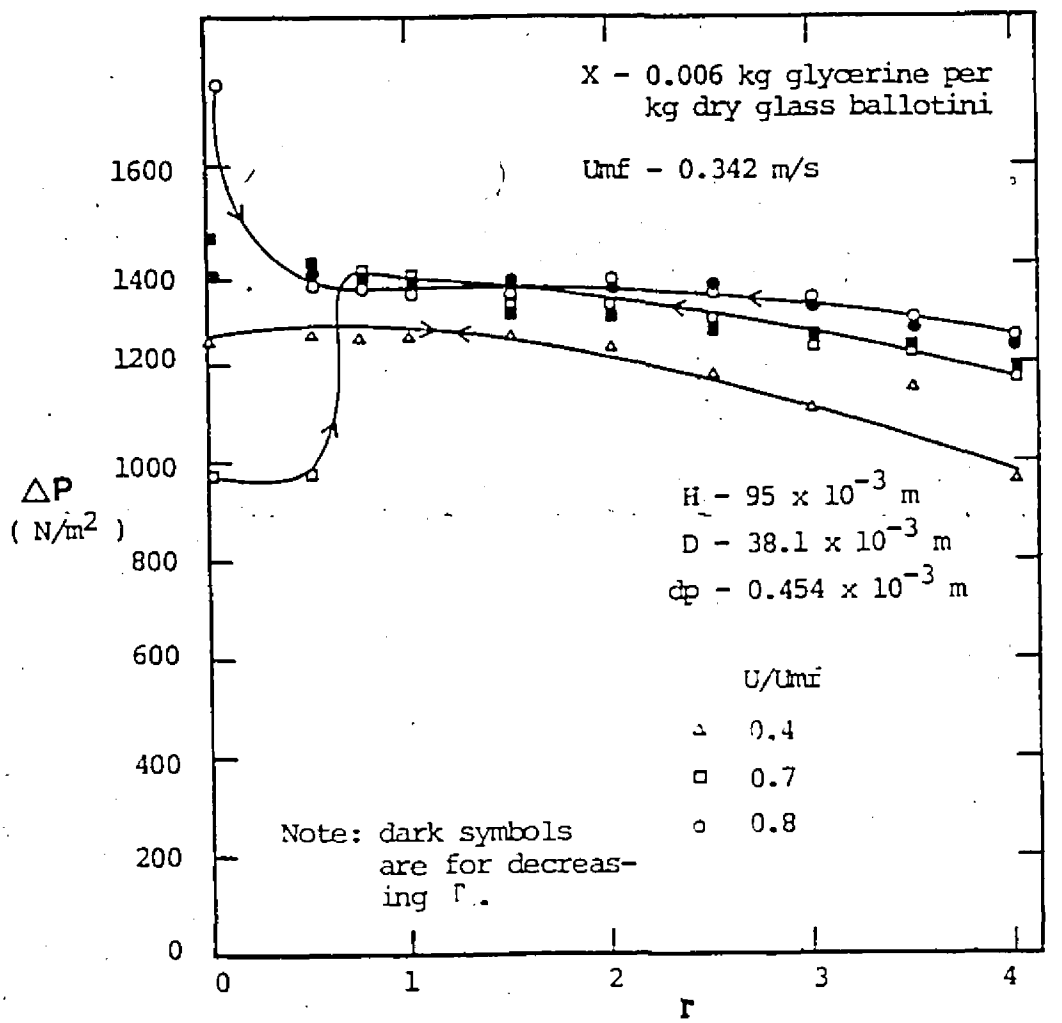

Figure 4-13 Effect of vibrational acceleration on ΔP for a bed of sticky glass ballotini

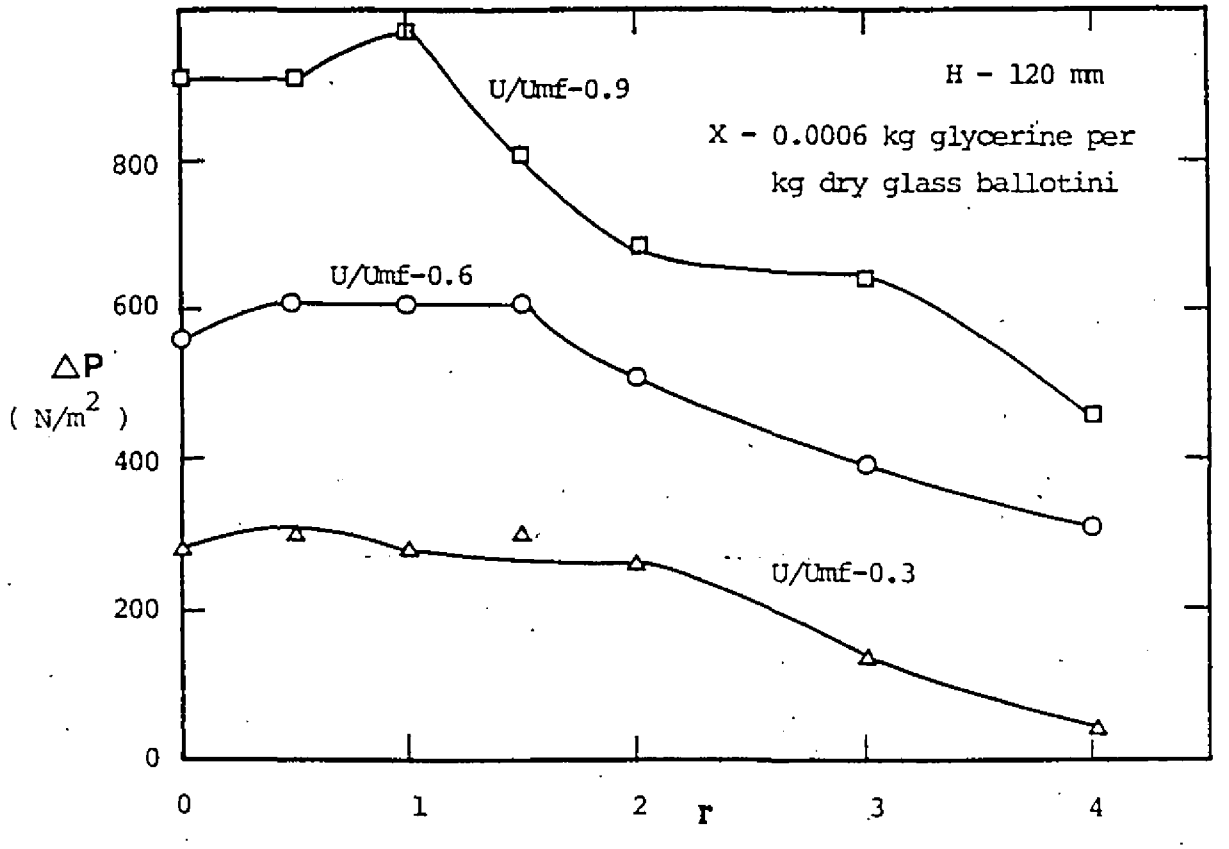

Figure 4-14 Effect of r on ΔP for sticky glass ballotini, dp=0.325 mm at A=4.25 mm

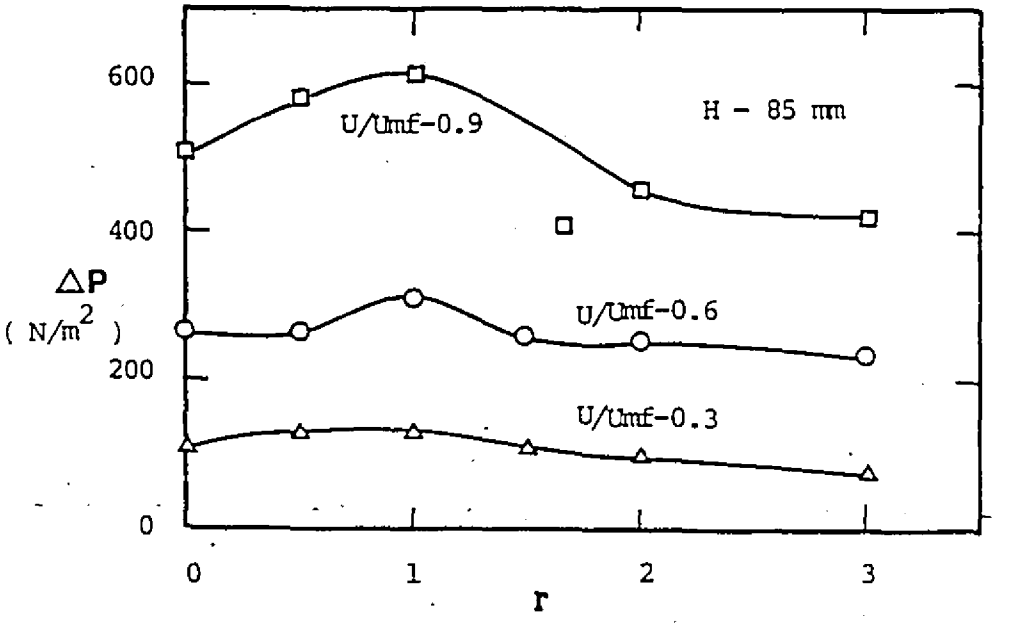

Figure 4-15 Effect of r on ΔP for sticky glass ballotini, dp=1.017 mm at A=4.25 mm and X=0.0006 kg glycerine per kg dry glass ballotini

as a piston, momentarily raising the pressure drop to very high values. To ensure uniformity, each time before the start of an experiment the bed was vibrated at $\Gamma=2$ to loosen it and obtain a nominally similar initial state of the bed structure. In many cases even this did not alleviate the problem of intial adjustment in the bed structure.

Figure 4-13 presents a typical case showing the influence the initial state of the bed of sticky particles has on bed pressure drop. Referring to the case of U/Umf=0.7, there was strong channelling initially (lower ΔP) followed by a sudden rise in pressure drop at $\Gamma=0.5-0.75$ due to vibration-induced homogeneity of the bed. For U/Umf=0.4 no initial period of adjustment was observed. At U/Umf=0.8 the whole bed moved as a piston raising the pressure drop considerably until at $\Gamma=1$ it suddenly disintegrated. It should be noted that in all cases an identical procedure was employed to obtain these data.

The curves for decreasing Γ are smooth right through $\Gamma=0$ because the bed is already in a homogeneous state. The trends of the pressure drop curves are similar to those those for dry glass ballotini except that the initial compaction is lower. This can be attributed to the interparticle forces due to stickiness which resist the initial "compacting" effect of vibration.

The magnitudes of pressure drop for sticky ballotini are about the same as compared to those for dry ballotini. However, in this case the Umf is much higher which means that the same pressure drop is obtained at the same U/Umf ratios but not at

the same absolute superficial velocity as compared to the case of dry ballotini. The increase in bed porosity due to cohesion as reported by Seville and Clift (1984) leading to formation of channels and an increase in minimum fluidization velocity is a probable explanation for this phenomenon.

Figures 4-14 and 4-15 show the effect of Γ on bed pressure drop for a bed of sticky particles but at much lower levels of stickiness (used in the heat transfer runs). It can be seen that unlike dry particles the maximum compaction and decrease in ΔP occurs for U/Umf=0.9 while it decreases for lower values of U/Umf. It is important to note that there is considerable reduction in pressure drop from Γ=1 to 4 (Figure 4-14) but not as much in Figure 4-15 which is for large glass ballotini (dp=1.017 mm) and at smaller amplitude of vibration.

4.4.2 Effect of Amplitude of Vibration

Figure 4-16 presents the effect of amplitude of vibration on the bed pressure drop. The results are plotted in a dimensionless form as Fv, vibration factor ($\Delta P/\Delta P_0$), versus Γ. It can be seen that higher is the amplitude greater is initial compaction and pressure drop reduction thereof.

For U/Umf=0.9, the effect of vibration is practically nonexistent. At U/Umf=0.3, the pressure reducing effect of vibration is greater for large amplitudes as reported earlier by Gupta (1979). It should be noted that the initial compaction of the bed is greater for higher amplitudes. For a bed of sticky glass ballotini, the pressure reducing effect of vibration is

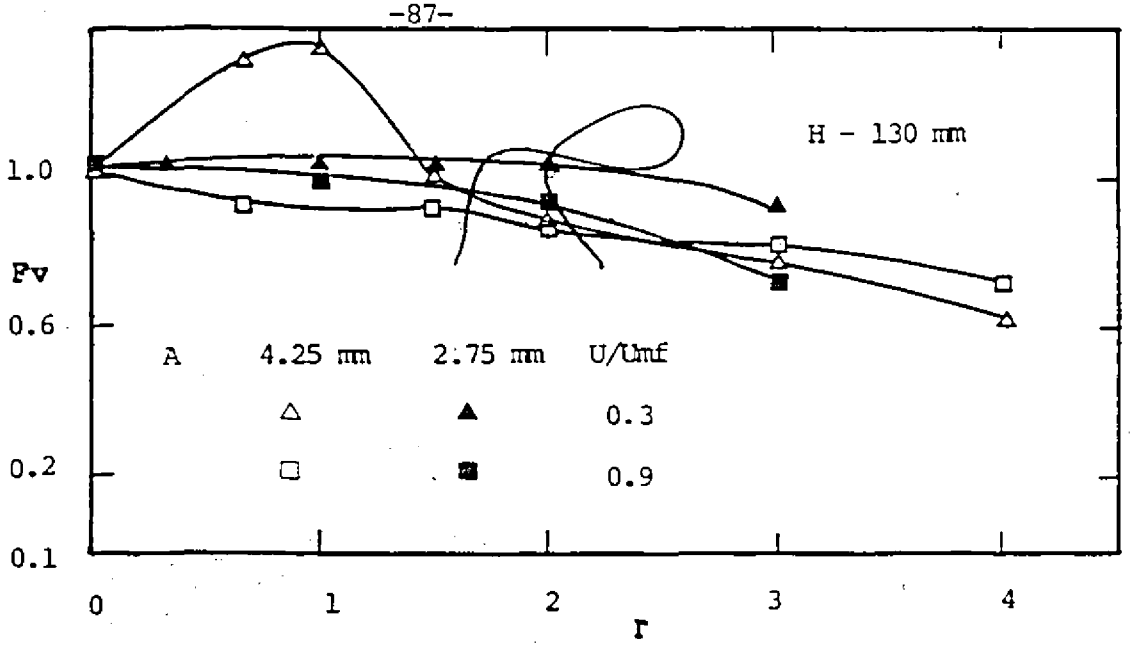

(a) glass ballotini, dp=0.595 mm

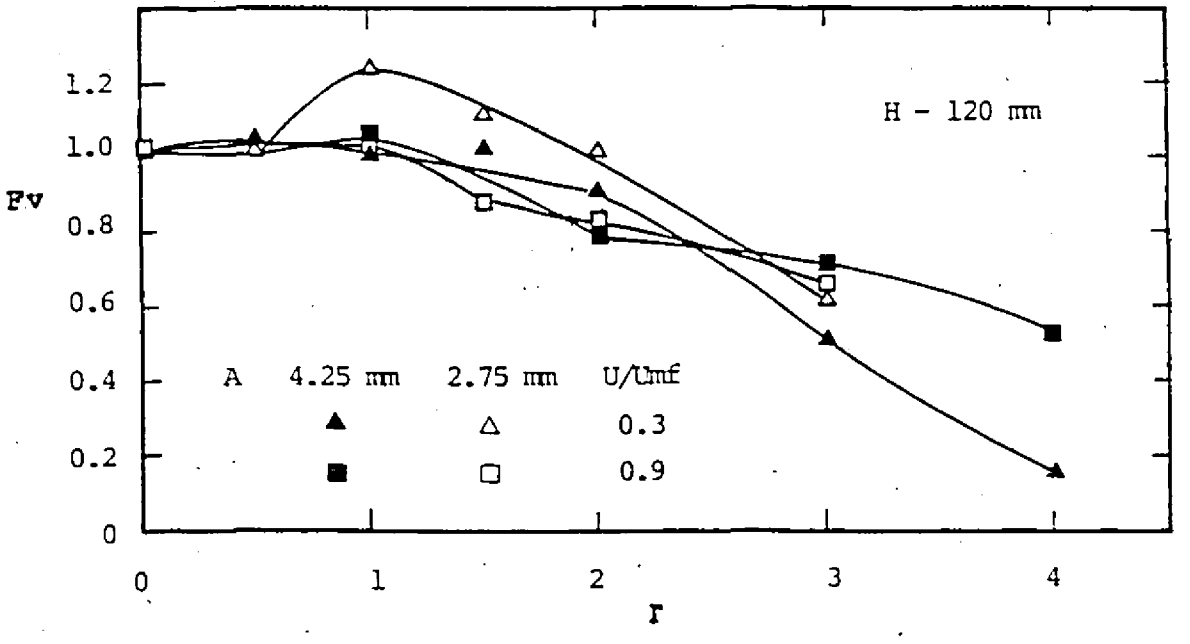

(b) glass ballotini, dp=0.325 mm

Figure 4-16 Effect of amplitude of vibration on ΔP

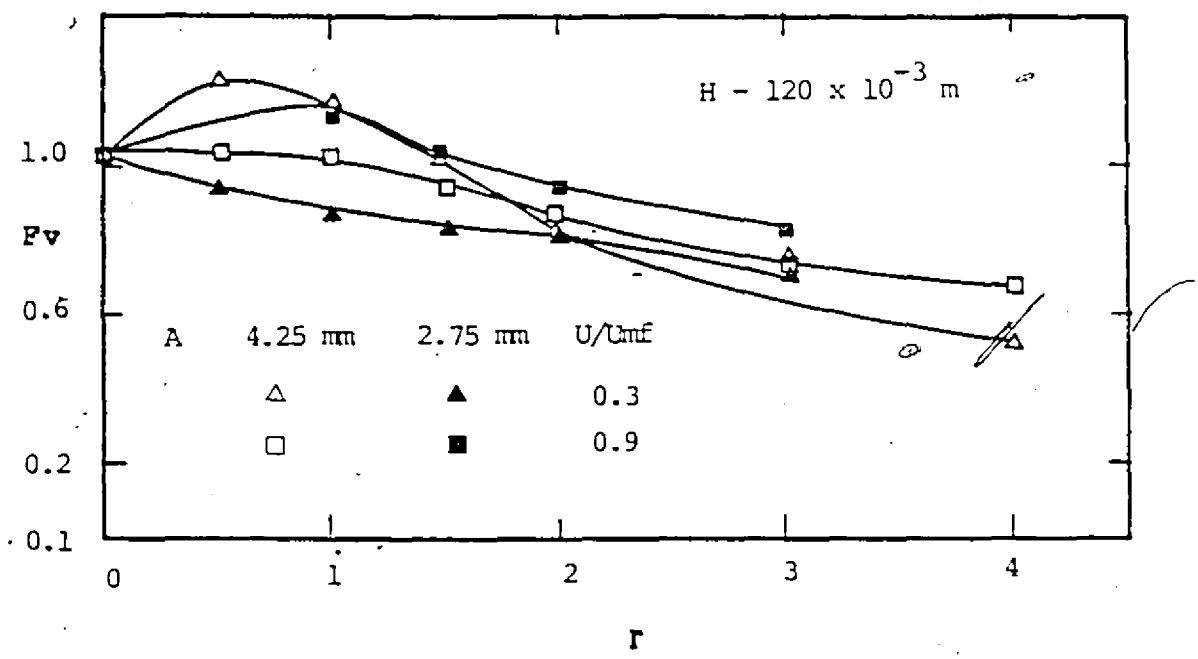

(c) molecular sieve particles, dp=1.4 mm

Figure 4-16 Effect of amplitude of vibration on ΔP

greater for higher amplitudes beyond $\Gamma>1.5$. On the other hand the initial compaction is more significant for smaller amplitude of vibration because the liquid bonds between the particles are not easily broken at smaller amplitudes. Such a mechanism can lead to the observed more appreciable initial compaction at lower Γ's for smaller amplitudes.

4.4.3 Effect of Bed Height

Figure 4-17 presents the effect of bed height on the bed pressure drop. As expected the effect of vibration diminishes with an increase in bed height, i.e. pressure reduction due to vibration is lower for deeper beds. Similar results were reported by Gupta and Mujumdar (1980) but with much smaller bed heights (12.5 - 37.5 mm). Beyond H=100 mm the effect of vibration on the bed pressure drop is marginal.

For sticky beds the trends are much the same except for some irregularities at higher air flow rates i.e. U/Umf=0.9 and $\Gamma<1.5$, when the bed is unstable and strong chanelling leads to non-reproducible results. Data presented for glass ballotini (dp=0.595 mm) indicate that the initial compaction of the bed is also reduced considerably with an increase in bed height possibly because the upper layers of the bed do not compact as much as the lower layers of the bed.

4.4.4 Effect of Particle Size

The effect of particle size on Fv versus Γ curves is presented for molecular sieves of two sizes in Figure 4-18. The

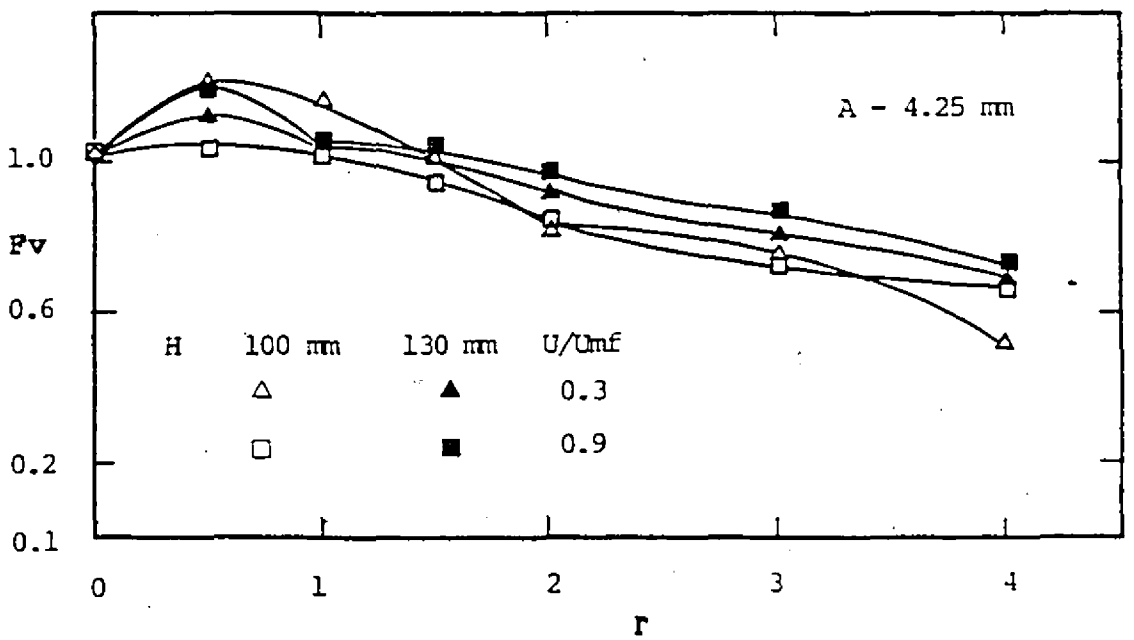

(a) molecular sieve particles, dp=1.4 mm

Figure 4-17 Effect of bed height on bed pressure drop

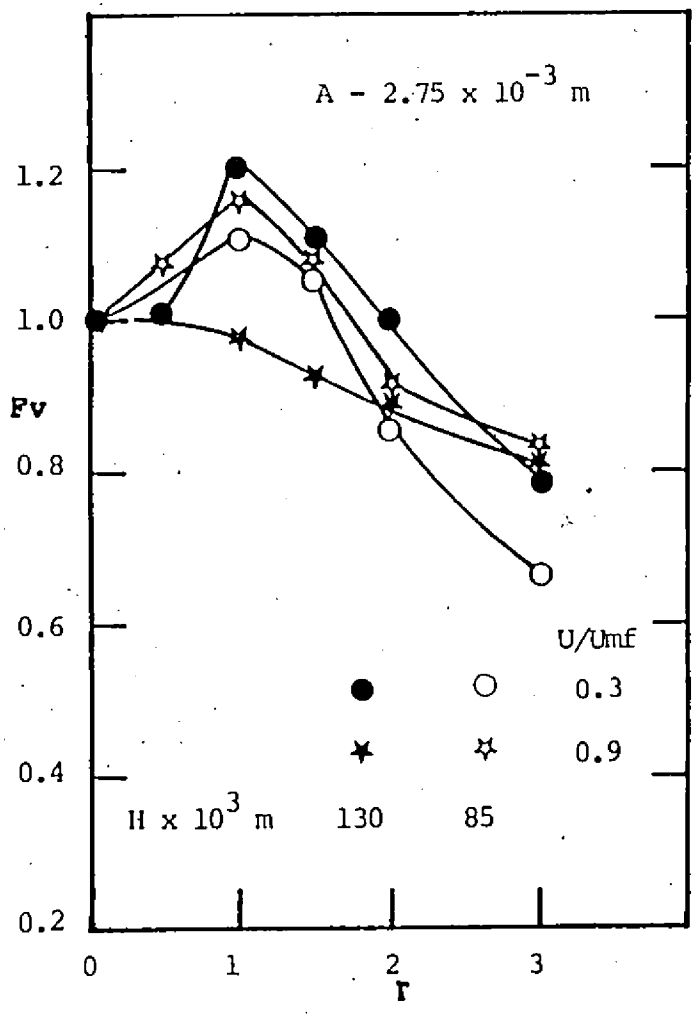

(b) sticky glass ballotini, dp=0.325 mm

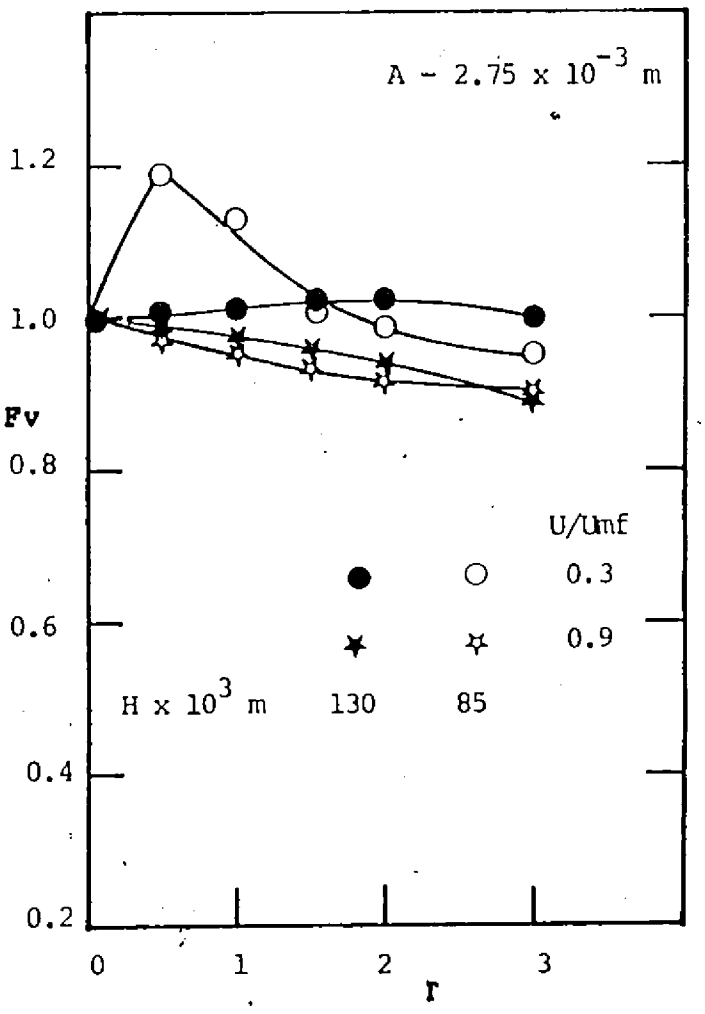

(c) glass ballotini, dp=0.595 mm

Figure 4-17 Effect of bed height on bed pressure drop

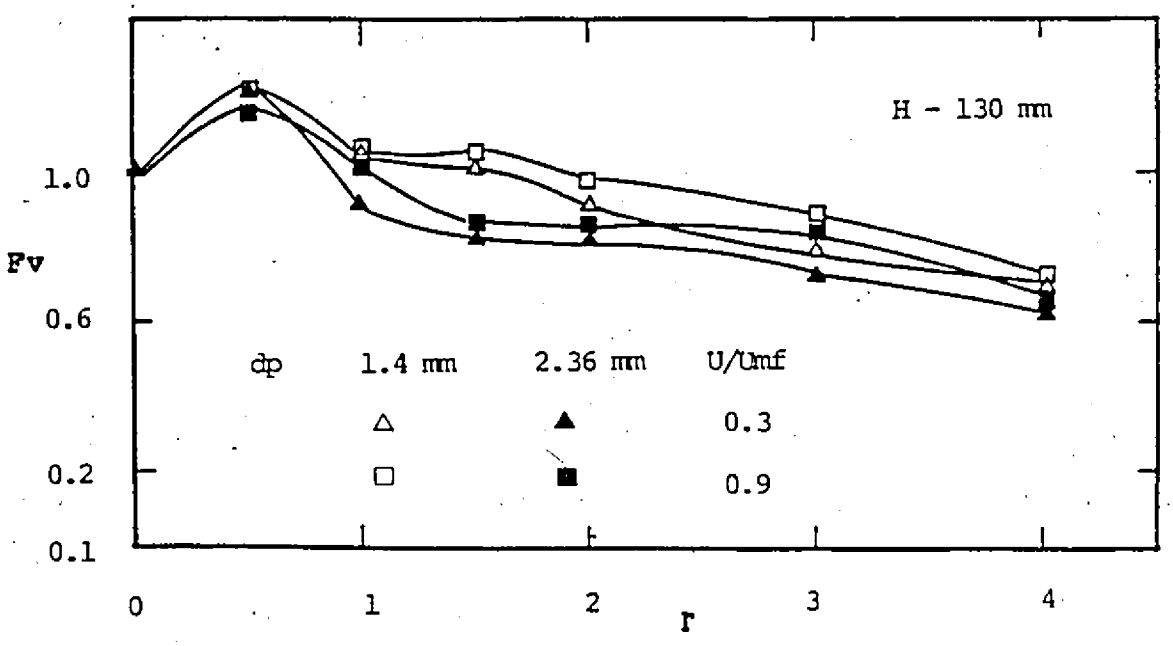

Figure 4-18 Effect of particle size on bed pressure drop for molecular sieve particles

pressure reducing effect of Γ is smaller for the smaller particle size. Gupta and Mujumdar (1980) reported similar observations and their explanation that the effect of vibration diminishes with an increasing H/dp ratio seems to be the most plausible one. A higher H/dp ratio, results in reduced transmission of vibration per unit length of the bed. It can be seen from Figures 4-11 and 4-12 that the magnitude of absolute pressure drop is also slightly lower for larger particles.

4.4.5 Effect of Frequency of Vibration

Figure 4-19 shows Fv as a function of vibrational frequency, ω. It can be seen that the pressure reducing effect of Γ is a stronger function of amplitude than of the frequency of vibration. The curves for higher amplitude are always lower than those for smaller amplitude. Further compaction of the bed occurs at lower Γ's in the case of higher amplitudes. From the definition of Γ and the fact that the bed compacts for $\Gamma \leq 1$, it is obvious that compaction would occur at lower frequencies for higher amplitudes.

4.5 FLOW OVER IMMERSED CYLINDERS

Heat transfer from heat exchange surfaces immersed in the bed is influenced by the particle and gas flow patterns around them. While the gas flow patterns cannot be readily visualized in the VFB, the more important particle flow patterns can be visualized relatively simply in the two-dimensional

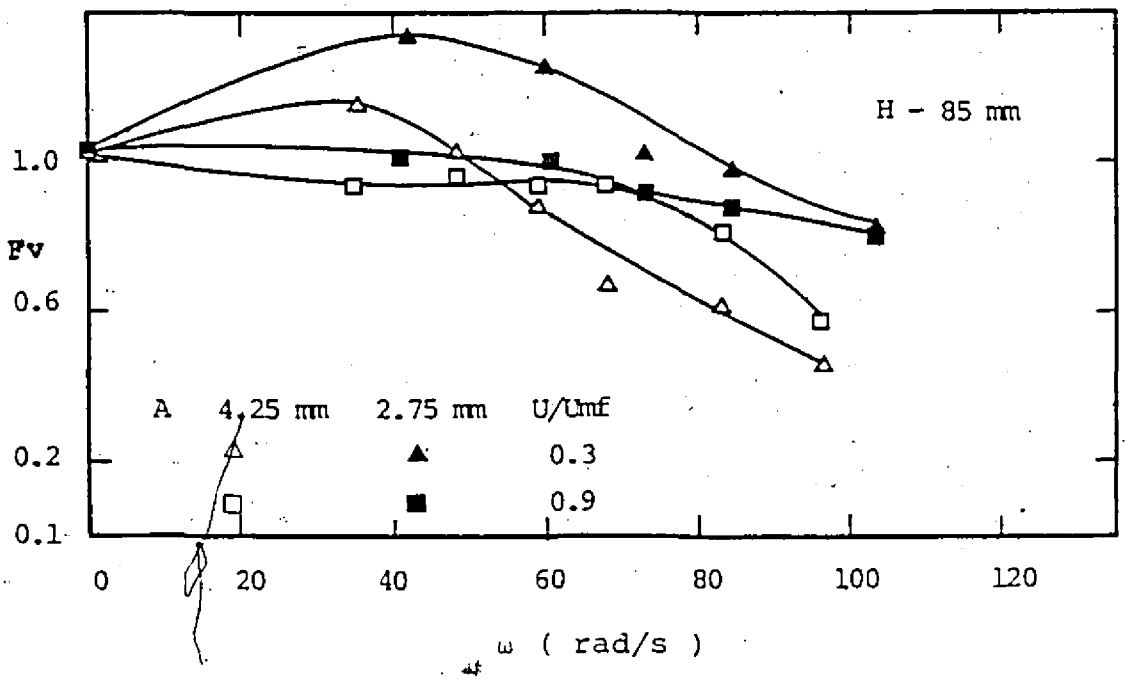

Figure 4-19 Effect of frequency of vibration on bed pressure drop for glass ballotini

configuration used. Since in engineering practice one is more interested in time averaged overall heat transfer rates, it was considered adequate to examine the time averaged spatial variation of the two-dimensional gaps (i.e. particle free zones) formed around immersed horizontal cylinders.

This does not necessarily imply that average heat transfer rates are directly and exclusively correlated to the time-averaged gap distributions around the cylinder. The particle flow patterns within the bed are equally important in determining the bed-to-surface heat transfer rates. The effect of flow patterns in the bed and average gaps around immersed cylinders on the average overall heat transfer rate is presented and discussed in the following chapter.

A typical sequence of gap formation around a rigidly mounted horizontal cylinder (25 mm diameter) immersed in a vibrated bed of glass ballotini (dp=0.454 mm) is shown in Figure 4-20. The cylinder axis was in the central midplane of the bed. For U/Umf=0.3 gap formation is initiated over the lower surface of the cylinder around r=1.5, while the gap on the top surface begins to develop only around r=2.5, beyond which both the upper and lower gaps grow in thicknesses nearly proportionately until r=4 - the upper limit of practical interest.

For U/Umf=0.6, the upper gap develops only about r=2 but with a rather unique shape i.e. two small symmetrically placed ears. These ears grow in size progressively with vibrational intensity until about r=3.5 when they merge to form a continuous

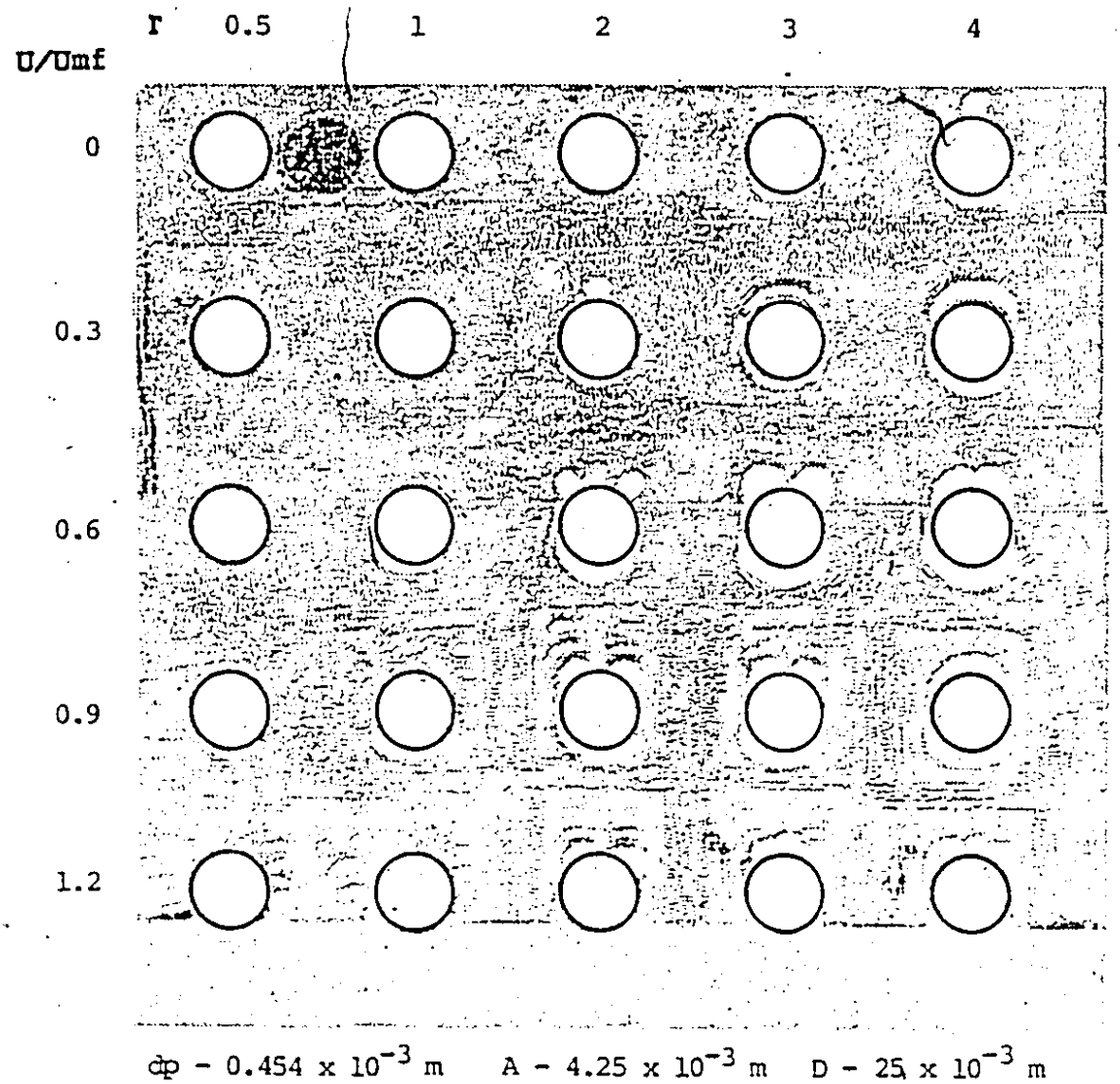

Figure 4-20 Gap formation around a single cylinder immersed in a bed of dry glass ballotini

gap on the upper surface. As the ratio of U/Umf is increased to 0.9, distinct bubbles appear at about Γ=0.5 with simultaneous gap formation on the lower surface.

It seems that until Γ=2 vibration aids bubbling, but beyond this value it progressively dampens it out. At vibrational accelerations beyond Γ=3.5 bubbling through the bed visibly vanishes. Vibration appears to aid bubbling by first loosening the bed (bubbling at U/Umf=0.9), but later the rapidly vibrating grid seemingly breaks up bubbles as they form. For example, at U/Umf=1.2 and Γ=4 no discernible bubbling occurred. At U/Umf=1.2 the lower gap initiates around Γ=0.5 while the top gap in the peculiar form of " ears " begins to develop around Γ=1-1.5. Also noticeable is the fact that even at Γ=4 the upper gap retaines its ear-like shape without disintegrating into a continuous gap.

Similar observations were recorded for the 38.1 mm diameter cylinder immersed in a bed of ballotini (dp=0.454 mm). An important observation was that, although the size of the cylinder increased 50%, the size of the gaps was only 10 - 15% larger than that for smaller cylinder, although the extent of the gaps were nearly the same.

For a small change in particle size, the magnitudes and trends of the air gaps did not change. For larger particles (dp>1 mm) as with molecular sieves, the gap formation was delayed and the magnitudes and extent of gaps were smaller. Figure 4-21 presents a graph of the maximum gap width, Y, versus Γ for dry glass ballotini (dp=0.667 mm) for a 25 mm diameter

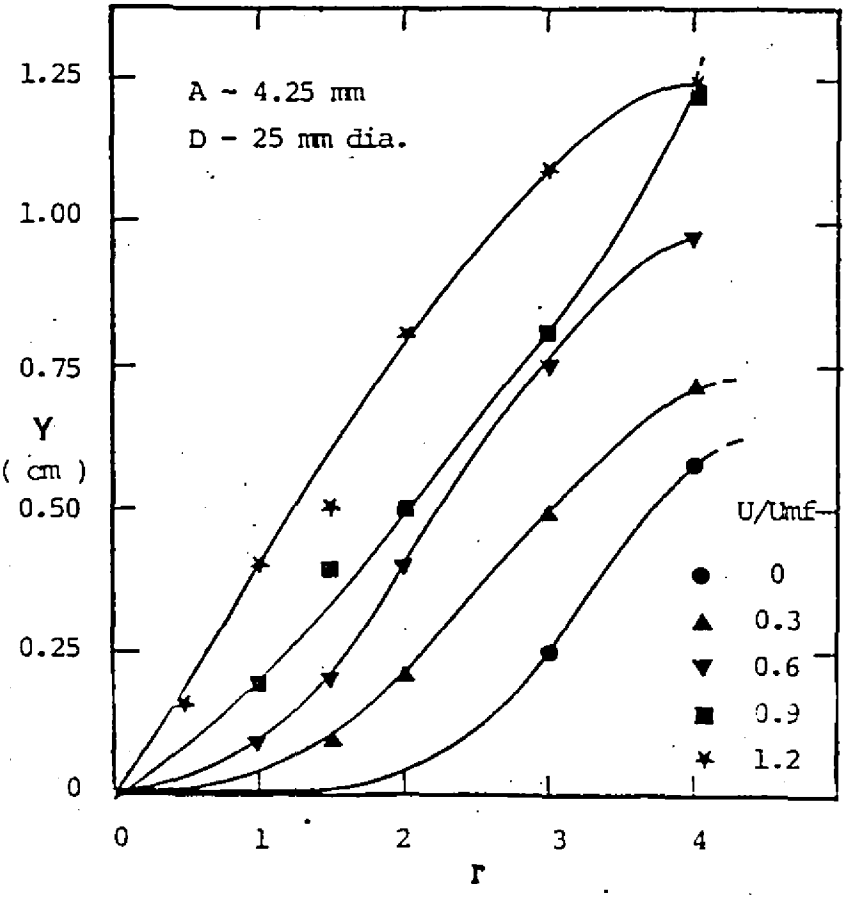

Figure 4-21 Effect of vibrational acceleration on gap widths around immersed cylinder in a bed of dry glass ballotini

immersed horizontal cylinder. These results were obtained, by visual measurements of the average gaps around the cylinder.

It can be seen from Figure 4-21 that with increasing U/Umf ratio the gaps start forming at lower values of Γ. The gap thickness increases with an increase in Γ for a fixed U/Umf ratio. The magnitudes of the gap widths at Γ=4 are different for all flow rates; the gap widths were greater with increasing U/Umf ratio. For U/Umf$\geq$0.9 the gap widths seemed to reach a common plateau at Γ=4 suggesting that at higher air flow rates and vibrational accelerations the effect of vibration on gap formation is negligible.

Figure 4-22 shows the angular coverage of the particle-free gap around the cylinder as a function of Γ. In determination of heat transfer rates it is the extent of the gap rather than its thickness that is important, because irrespective of the thickness the particle-free air gap acts as a poor thermal conductor for heat transmission.

It can be seen that for U/Umf$\geq$0.6 and Γ>1 the extent of gaps is unchanged while for U/Umf$\leq$0.3 the extent of gaps is lower, although for U/Umf=0.3 it is almost equal to those for higher U/Umf ratios at Γ=4. For Γ<1 there is almost no gap present for U/Umf$\leq$0.3 while for U/Umf$\geq$0.6 the extent of gap is greater at higher air flow rates. Figure 4-22 along with the mixing maps (Figures 4-8 through 4-10) are important starting steps towards understanding and physically modelling the surface-to-bed heat transfer process in a VFB.

A typical sequence of gap formation around a 25 mm

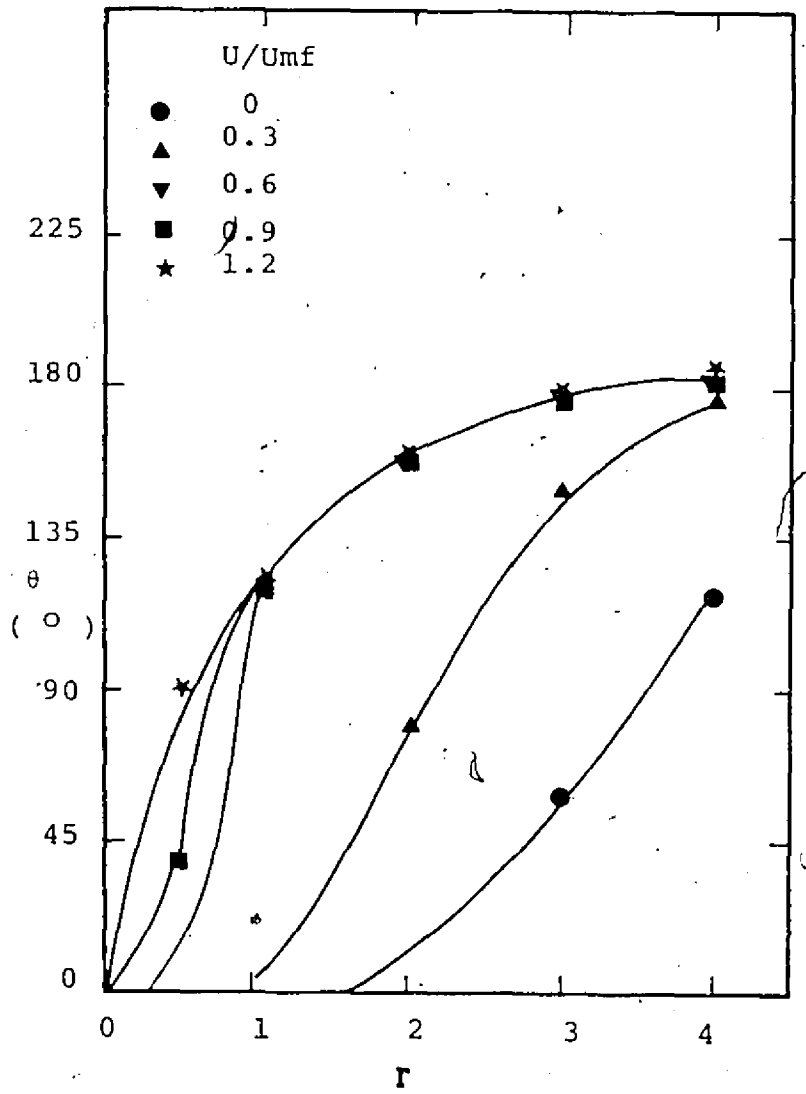

Figure 4-22 Extent of gap around an immersed cylinder as a function of r for a bed of dry glass ballotini

diameter immersed cylinder in a bed of smaller ballotini (dp=0.454 mm) and X= 0.003 kg glycerine per kg dry ballotini is shown in Figure 4-23. It is easy to see that the gap begins to form at Γ=2.5 for U/Umf=0.3 and that both the upper and lower gaps appear simultaneously with nearly the same size. For U/Umf=0.6 the gap formation initiated at Γ=2. For U/Umf=1 the gaps started forming at Γ=0.75 but the top gap was isolated from the cylinder surface and was above the cylinder in the shape of a well-defined crescent. Such a gap should conceivably have little effect on the heat transfer from the cylinder to the bed.

In all the aforementioned cases, the presence of particles within the air gaps was visually observed at Γ=3.5-4. These particles seemed to form a continuous shower in the gap. Similar trends were obtained with the larger diameter cylinder but with marginally larger gaps. For films exposed for over one or more seconds, the presence of particles in the gaps could not be seen as it was effectively washed out due to overexposure. Flash photographs did confirm the presence of particles in very dilute concentrations in the gap. These can be effective heat carriers and should be accounted for in a rigorous physical model.

Figure 4-24 shows the gap width plotted as a function of Γ for a bed of "sticky" glass ballotini. Note that the stickiness level is much lower in this case. It can be seen that for U/Umf$\geq$0.3 the gap widths are nearly the same after Γ>2. For Γ<2 lower U/Umf ratios have smaller gap thicknesses. For non-aerated case the gaps are much smaller for $\Gamma\leq$3 but at Γ=4

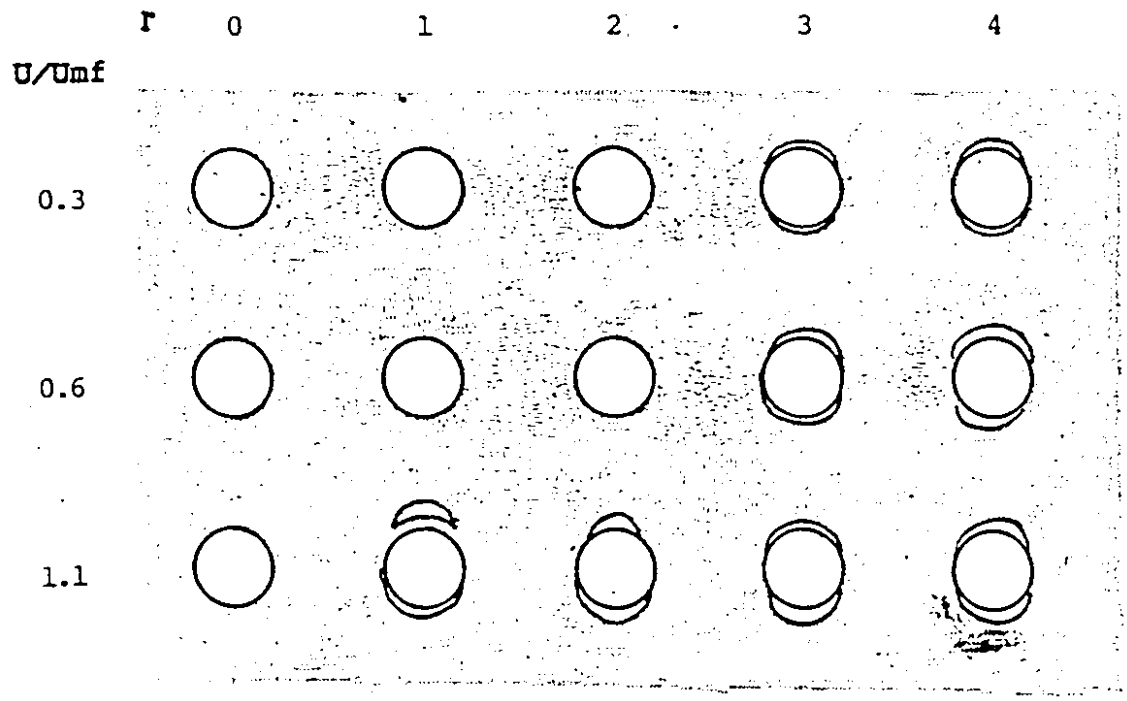

X - 0.003 kg glycerine per kg dry glass ballotini

dp - 0.454×10^{-3} m A - 4.25×10^{-3} m

Figure 4-23 Gap formation around a single cylinder (D=25 mm) immersed in a bed of sticky glass ballotini

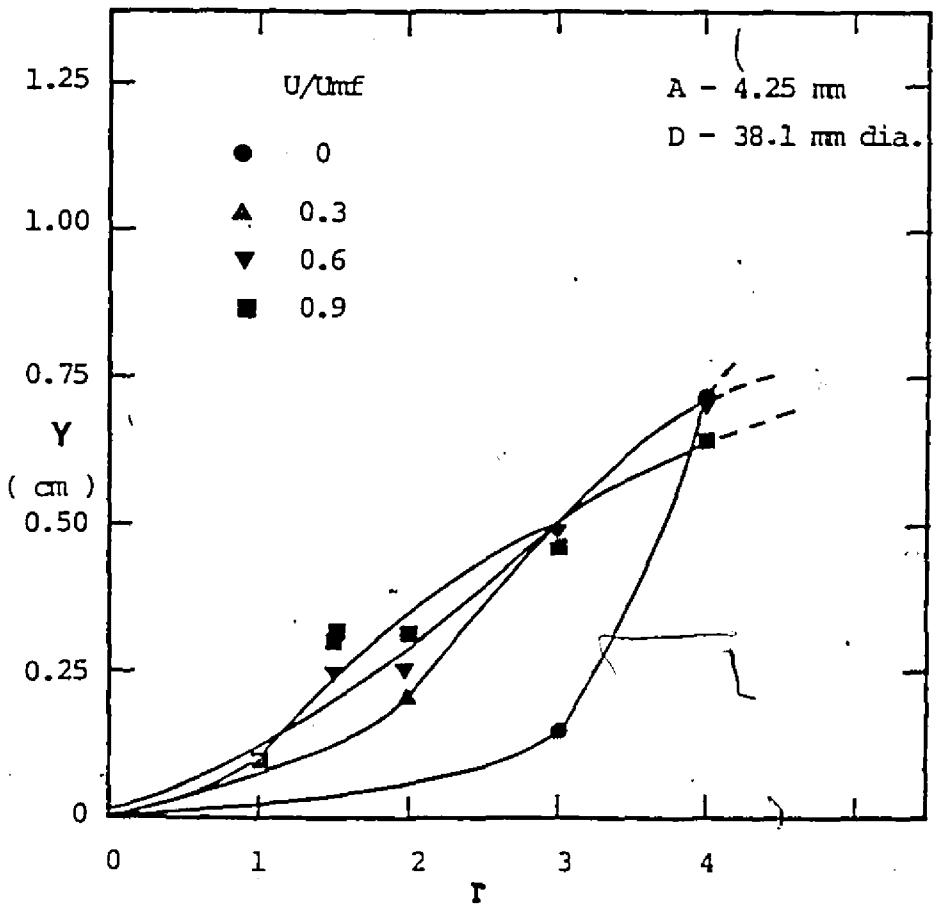

Figure 4-24 Effect of vibrational acceleration on gap widths around immersed cylinder in a bed of sticky glass ballotini

all the curves meet at the same level- a feature not observed for bed of dry particles.

4.6 EXTENDED VIBRATIONAL ACCELERATION NUMBER

Ringer and Mujumdar (1982) suggested the use of an extended vibrational acceleration number, Γ_{VFB} , for characterization of aerated vibro-fluidized beds. Γ_{VFB} takes into account the pressure drop and mass of the VFB. It is defined as:

$$\Gamma_{VFB} = \Gamma(Mg/(Mg - \Delta P_{mf} A_b))$$

where M is the mass of the bed, A_b the cross-sectional area of the bed and ΔP_{mf} is the bed pressure drop at minimum fluidization in presence of vibration.

According to Ringer and Mujumdar (1982) for VFB's the desired state of homogeneous fluidization is reached for Γ_{VFB} >1.4. They also proposed a relationship

$$Umf_{VFB} / Umf_{CFB} = (1 - \Gamma/\Gamma_{VFB})^{1/2}$$

where Umf_{VFB} is the minimum fluidization velocity for a VFB, while Umf_{CFB} is the minimum fluidization velocity for a conventional bed. It must be pointed out that due to non-availability of any reliable correlation to predict Umf_{VFB} it was visually determined as the point when the first disturbance (a small bubble) appears on the surface of the

bed. Due to the qualitative nature of determining Umf_{VFB} , the results although not exact, give a good insight as to the trends.

Tables 4.1 and 4.2 show the values obtained for Γ_{VFB} and corresponding experimental and theoretical values of Umf_{VFB}/Umf_{CFB} for glass ballotini and molecular sieve particles respectively. It can be seen from these tables that the theoretical correlation for prediction of the Umf does not predict the initial compaction and hence a rise in Umf_{VFB}/Umf_{CFB} ratio for a VFB. Beyond $\Gamma \geq 1$ the experimental and calculated values for glass ballotini are within 14% of each other.

In case of molecular sieves the experimental values are always higher than the calculated ones by 16-24%. It should be noted, however, that molecular sieves are almost twice as light as glass ballotini and the results of Table 4-2 were determined in the three-dimensional bed at a lower amplitude of vibration. For glass ballotini the correlation for predicting Umf_{VFB}/Umf_{CFB} works well as is shown in Figure 4-25 . The variation between experimental and calculated values for larger glass ballotini (dp=0.667 mm) in Figure 4-25 is within 10%. The correlation proposed by Ringer and Mujumdar (1982) is thus useful for engineering purposes since in practice one is interested only in $\Gamma > 1$.

4.7 CONCLUSIONS

The VFB helps in fluidization of sticky and agglomerating solids which are impossible to fluidize conventionally. There is

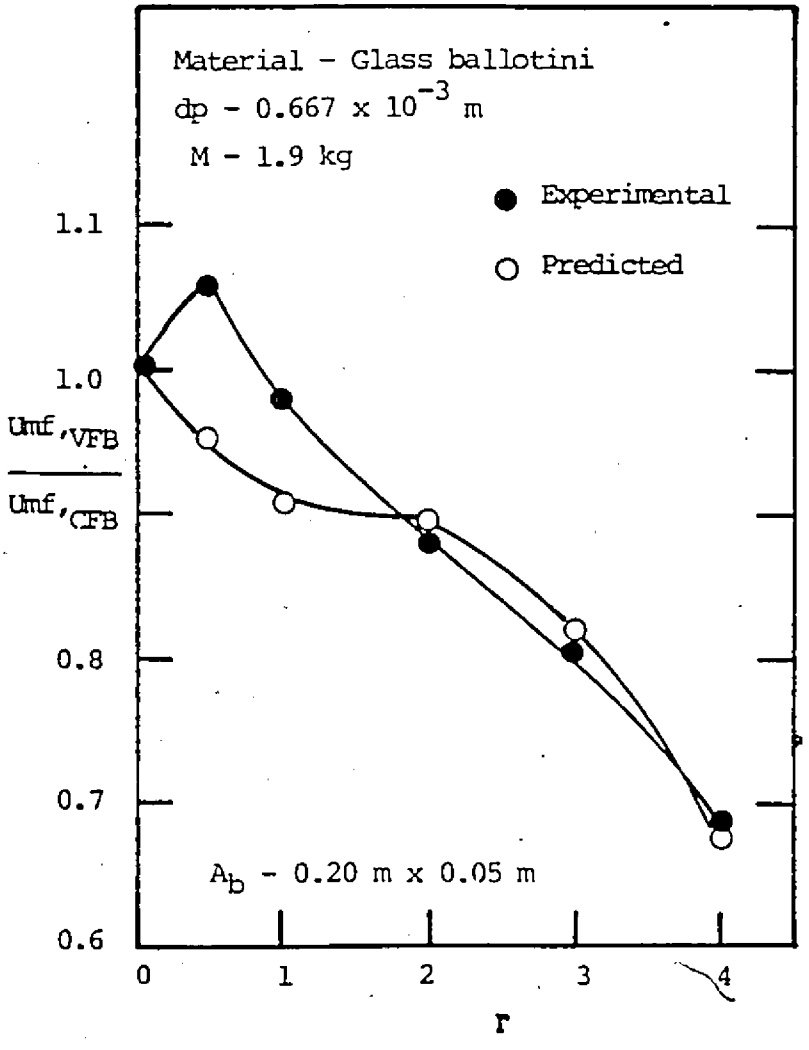

Figure 4-25 Effect of vibrational acceleration on the minimum fluidization velocity

a vibration-induced compaction for dry beds of particles in a VFB at low vibrational accelerations ($\Gamma \leq 1$). There is good solids mixing in a VFB at low aeration rates and moderate vibrational intensities ($U/Umf \leq 0.3$, $\Gamma \geq 1.5$). Addition of surface stickiness delays good solids mixing to higher Γ values, and larger sized particles are less affected by stickiness as compared to the smaller ones.

The bed pressure drop decreases with an increase in vibrational acceleration beyond $\Gamma > 1$ following an initial rise due to bed compaction. The effect of vibration attenuates with an increase in air flow and bed height and a decrease in particle size. The pressure reducing effect of vibration is a stronger function of the amplitude than of the frequency of vibration.

Flow patterns in a VFB show a presence of particle-free air gaps around the immersed circular cylinders for both dry and sticky beds of particles. These gaps increase in size with an increase in vibrational intensity and initiate at lower values of Γ with an increase in air flow rate.

The correlation proposed by Ringer and Mujumdar (1982) predicts the minimum fluidization velocity in presence of vibration better for glass ballotini as compared to molecular sieve particles and overlooks the effect of initial bed compaction.

TABLE 4.1

Effect of Vibrational Acceleration on Minimum Fluidization Velocity for a VFB

Material - Glass ballotini, Amplitude of Vibration- 4.25 mm

dp = 0.454 mm , A_b = 0.0101 m², M= 1.75 kg

r	0	0.5	1	2	3	4
ΔPmf (N/m²)	1618	1618	1520	1471	1398	1054
Umf (m/s)	0.146	0.156	0.140	0.133	0.113	0.101
$\frac{Umf_{VFB}}{Umf_{CFB}}$ (expt)	1.00	1.07	0.96	0.91	0.77	0.69
r	0.0	10.5	9.5	14.9	16.9	10.5
$\frac{Umf_{VFB}}{Umf_{CFB}}$ (pred)	1.00	0.97	0.94	0.93	0.90	0.79
%error	0.0	-9.4	-1.3	1.9	14.3	11.7

Effect of Vibrational Acceleration on Minimum Fluidization Velocity for a VFB

Material - Molecular sieve, Amplitude of Vibration- 2.75 mm

dp = 2.36 mm, A_b = 0.0408 m², M= 4.4 kg

Γ	0	0.5	1	1.5	2	3
ΔPmf (N/m²)	819	834	736	647	559	471
Umf (m/s)	0.50	0.52	0.491	0.484	0.458	0.421
$\frac{Umf_{VFB}}{Umf_{CFB}}$ (expt)	1.00	1.04	0.98	0.97	0.91	0.84
Γ	0.0	2.65	3.52	4.05	4.39	5.54
$\frac{Umf_{VFB}}{Umf_{CFB}}$ (pred)	1.00	0.90	0.85	0.79	0.74	0.67
%error	0	15.5	15.2	22.7	22.9	25.37

CHAPTER 5

RESULTS AND DISCUSSION - HEAT TRANSFER

5.1 INTRODUCTION

This chapter discusses the contact heat transfer results obtained experimentally for single, rigidly-mounted, horizontal circular cylinders immersed in a VFB. The results are presented in both dimensional and non-dimensional form. Effect of amplitude and frequency of vibration, aeration rate, particle diameter, particle stickiness and moisture content, on surface-to-bed heat transfer are examined experimentally. The effect of vibrational acceleration on heat transfer coefficient during a drying process is also discussed. Finally, an attempt is made to explain the experimental results, using existing theories on packed and fluidized bed heat transfer and information from the preceding chapter on mixing and flow patterns around immersed cylinders in a VFB. Note that without exception, heat transfer in this thesis refers to surface-to-bed heat transfer. All the heat transfer experiments were performed in a VFB fitted with a 18% free area distributor plate.

5.2 EXPERIMENTAL RESULTS

5.2.1 Effect of Vibrational Acceleration

Figures 5-1-a and 5-1-b show the effect of Γ on the heat transfer coefficient, h, for a VFB of glass ballotini vibrated at a constant amplitude of A=4.25 mm. For U/Umf=0 i.e. a non-aerated bed, vibration enhances the heat transfer

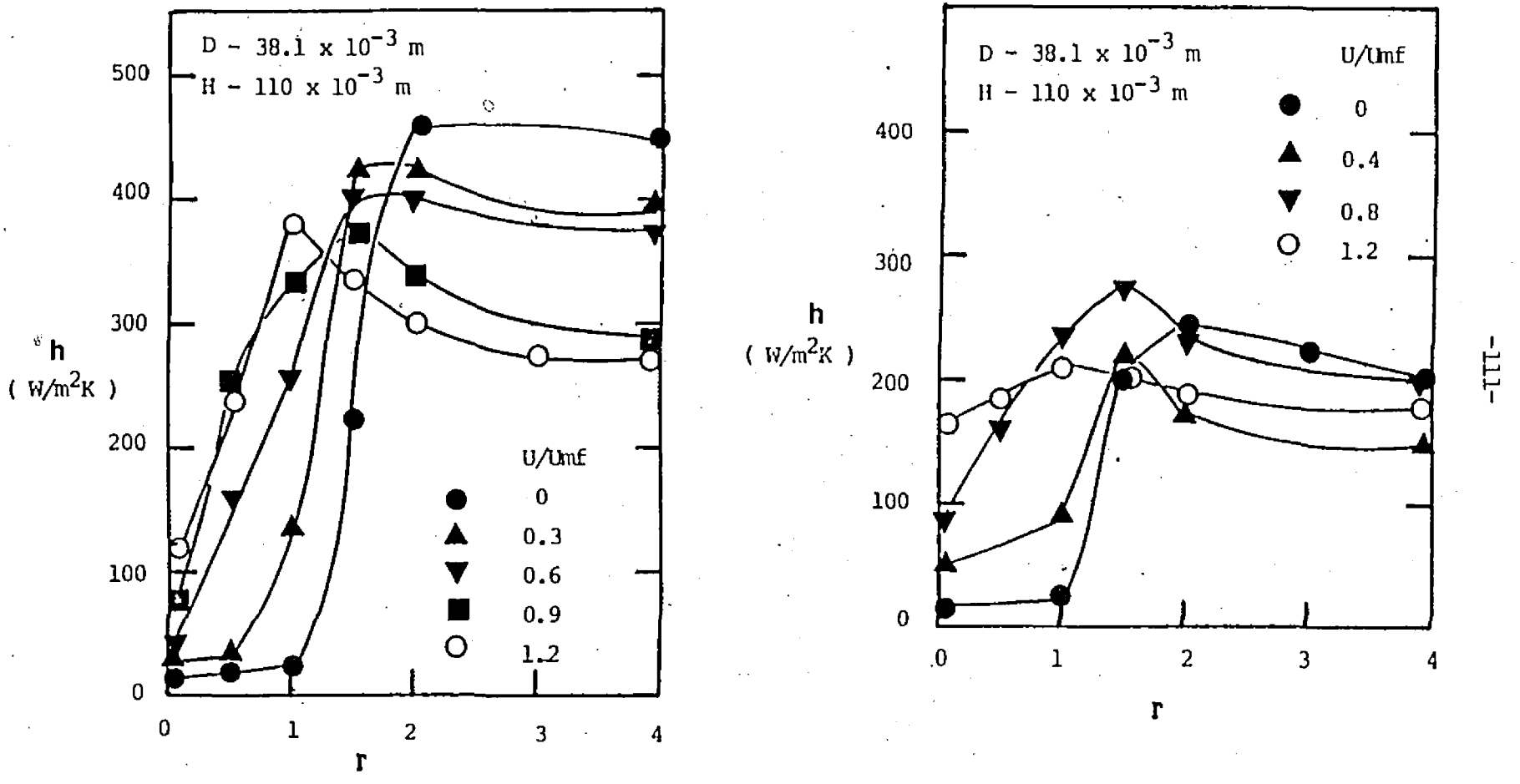

Figure 5-1 Effect of vibrational acceleration on heat transfer coefficient for dry glass ballotini (a) dp=0.325 mm (b) dp=1.017 mm at A=4.25 mm

coefficient by more than 20 times. The lower plateau of this S-shaped curve ends at $\Gamma=1$ while the upper plateau is fully formed at $\Gamma\geq2$. The increase in h, in the transition range, i.e. $\Gamma=1-2$, is associated with the transition from steady to vibro-fluidized bed and onset of vigorous particle mixing (transition from regime of poor mixing to one of vigorous mixing in Figure 4-8). Pakowski and Mujumdar (1984) and Bretsznajder et al (1963) have reported similar findings. Bretsznadjer et al(1963) also reported a heat transfer enhancement of 17-19 times for aluminum oxide, kaolin and zinc particle when vibrated moderately in non-aerated beds.

Superimposition of air flow on vibration makes the transition to higher levels of heat transfer to occur at lower values of Γ. Due to improved particle mixing induced by the air flow in the range $\Gamma<1.5$, h increases with increasing gas velocity. The peak reached by each curve also shifts progressively towards lower Γ values with an increase in U/Umf. A simple linear relationship was obtained from experimental observations correlating U/Umf to Γ_{max} (value of Γ at hmax) and is presented in Figure 5-2.

It is easy to notice from Figure 5-1 that for U/Umf=0 upper plateau values for h are larger than those for U/Umf>0. In fact the increase of gas velocity makes the bed expand and makes the transfer of vibration energy from the distributor less efficient. With increasing U/Umf the bed does not follow the vibration of the distributor grid but more or less levitates while the vessel vibrates.

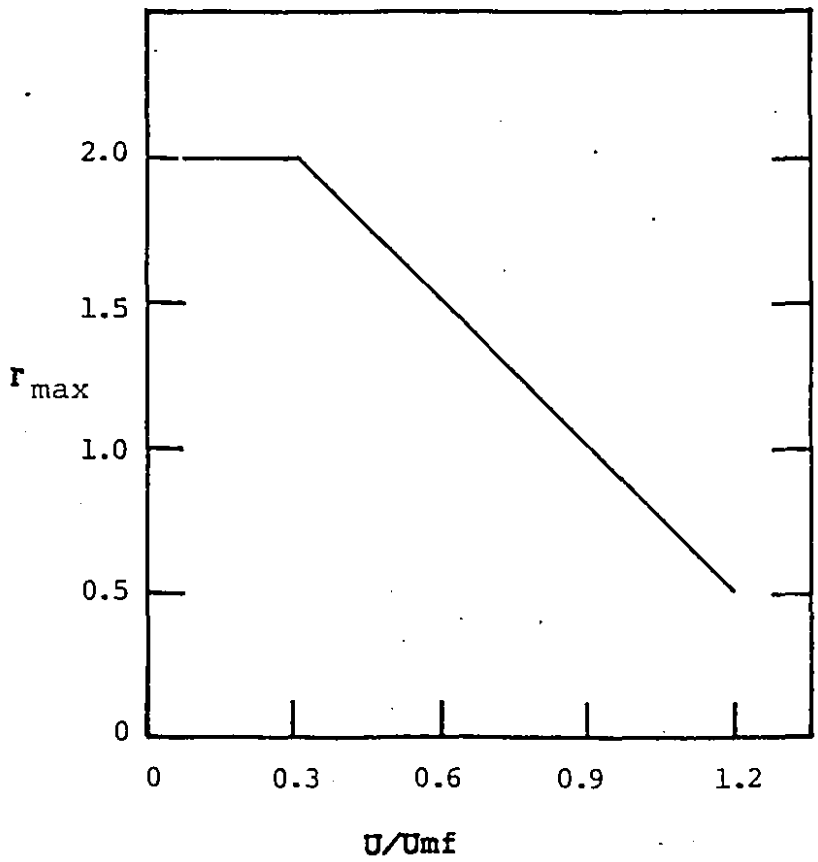

Figure 5-2 Effect of U/Umf on rmax for dry glass ballotini

Figure 5-1 shows that after reaching a maximum, around Γ=1.5 curves start to decline; this is attributed to the formation of stable particle-free air gaps around the immersed cylinder which inhibit the heat transfer (Pakowski and Mujumdar (1982), Mujumdar and Pakowski (1983)). Referring back to Figure 4-20 it is easy to notice that stable gaps form around the cylinders beyond Γmax. Although Γmax also corresponds to the onset of vigorous particle mixing in the bed (i.e. higher particle convective heat transfer), counteraction of the influence of mixing and air gap formation gives maxima in h versus Γ curves in the range Γmax=1-2.

The effect of vibrational acceleration on heat transfer coefficient for beds of molecular sieve particles is shown in Figure 5-3. Here the enhancement in heat transfer at U/Umf=0 is considerably lower than that for the smaller glass ballotini (dp= 0.325 mm). The values of Γmax are the same as those for glass ballotini, although the decline in the curves after the peaks is not as steep. This is ascribed to smaller particle-free air gaps around the cylinder for molecular sieve particles. Further, the heat transfer curves for lower U/Umf are always below the higher U/Umf curves, over the entire Γ range examined.

The reduction in the heat transfer enhancement for molecular sieve particles at U/Umf=0 is possibly related more to the theory of particle contact time and heat transfer rather than to the effect of vibration. At the condition of U/Umf=0 and Γ>2 (vigorous mixing), the particle contact time with the heat transfer surface is solely determined by frequency and amplitude

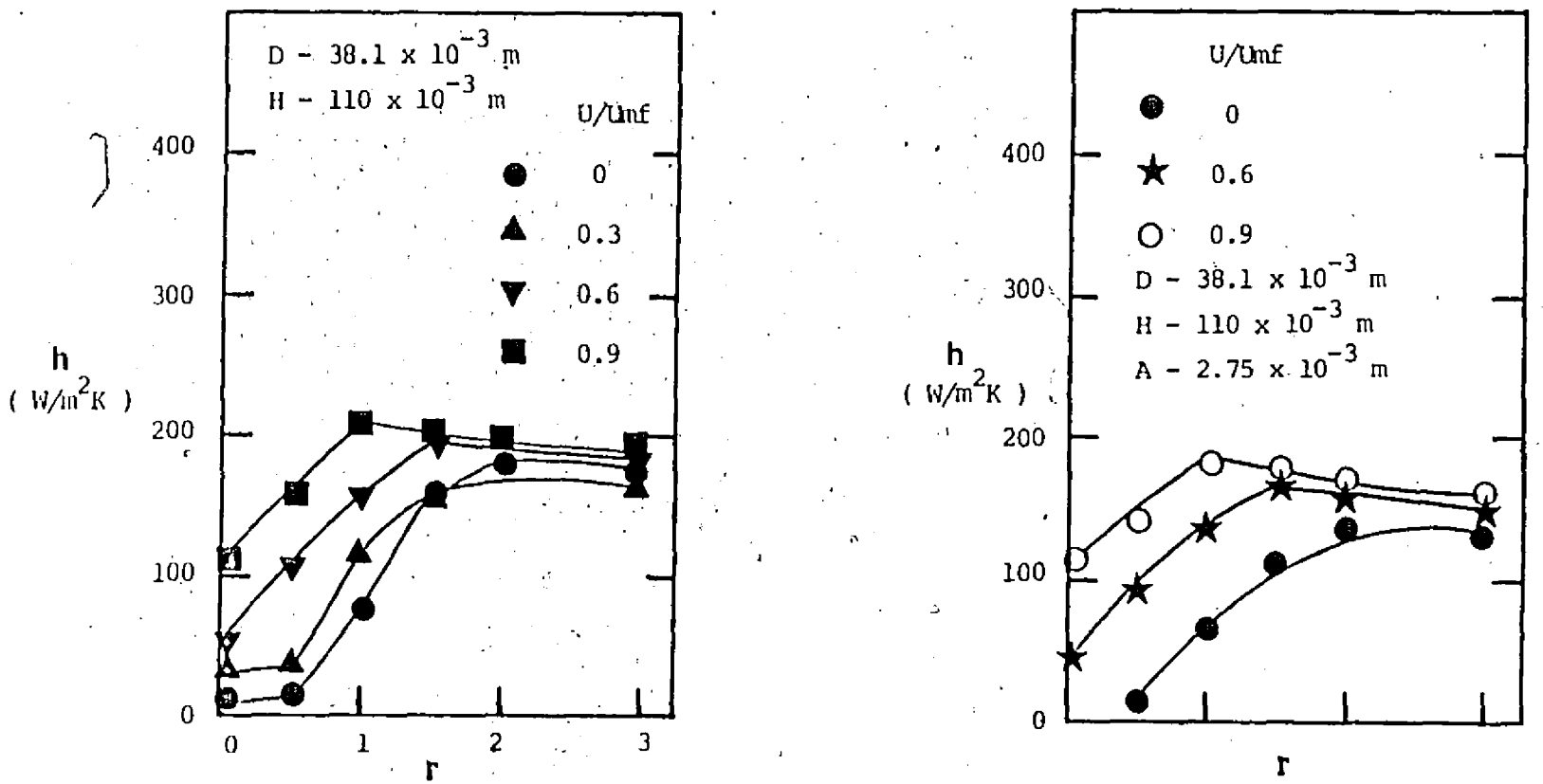

Figure 5-3 Effect of vibrational acceleration on heat transfer coefficient for dry molecular sieve particles

(a) dp=1.4 mm (b) dp=2.36 mm

of vibration. Hence, for a fixed value of Γ the contact times for all particles may be assumed to be uniform. However, the particle size and bed effective thermal conductivities are different. The particle contact heat transfer resistance proposed by Baskakov et al (1973) is

$$R_k = dp/(2Ks)$$

It can be seen from the above equation that an increase in particle size increases the thermal resistance lowering the heat transfer rate. Therefore the heat transfer enhancement at U/Umf=0 for larger glass ballotini (dp=1.017 mm) and smaller molecular sieves (dp=1.4 mm) is much smaller than glass ballotini, dp=0.325 mm. It should be noted that the thermal conductivity of beds of molecular sieve particles and glass ballotini are within 10-15% of each other as shown later in Table 5.1.

It is observed that heat transfer coefficients for molecular sieve particles at higher U/Umf's are larger than those for smaller U/Umf's over the entire Γ range and not so for glass ballotini. Although the minimum fluidization velocities for molecular sieve particles (dp=1.4 mm) and glass ballotini (dp=1.017 mm) and bed thermal conductivities are almost the same the reason for the above discrepancy could not be explained. It should however, be noted that molecular sieve particles are twice as light as glass ballotini.

An alternate representation of the enhancement in contact

heat transfer effected by mechanical vibration of a bed of dry glass ballotini and molecular sieve particles, aerated as well as non-aerated, is displayed in Figure 5-4. Here the heat transfer rates are normalized in terms of the heat transfer rate in the absence of vibration under otherwise identical conditions to yield enhancement factor, ϵ_h. It can be seen that the enhancement factor decreases with an increase in particle size and air flow. The effect of vibration diminishes with an increase in air flow rate, and is virtually negligible beyond U/Umf>1.2. The effect of vibration falls beyond Γmax, reaching asymtotic values for Γ>2. In fact Mujumdar and Pakowski (1983) reported a negative enhancement for glass ballotini particles (dp=0.454 mm) for U/Umf≥1.4 beyond Γ>2. No physical explanation could be given for this.

Traditionally the heat transfer data are presented in a dimensionless form viz. the Nusselt number. The data obtained in this study were also plotted as Nusselt number versus Γ. The Nusselt number was defined as Nu=hD/Ks, where D is the cylinder diameter and Ks the effective bed thermal conductivity. The bed effective thermal conductivities were calculated from the correlation proposed by Wakao and Kaguei (1982) as:

$$Ks = Ks^\circ + 0.1(Pr)(Rep)K_f \qquad \ldots\ldots\ldots 5.2.1$$

where Ks° is the thermal conductivity of the packed bed at no air flow or vibration. Ks° was determined from the correlation proposed by Wakao and Kaguei (1982) as:

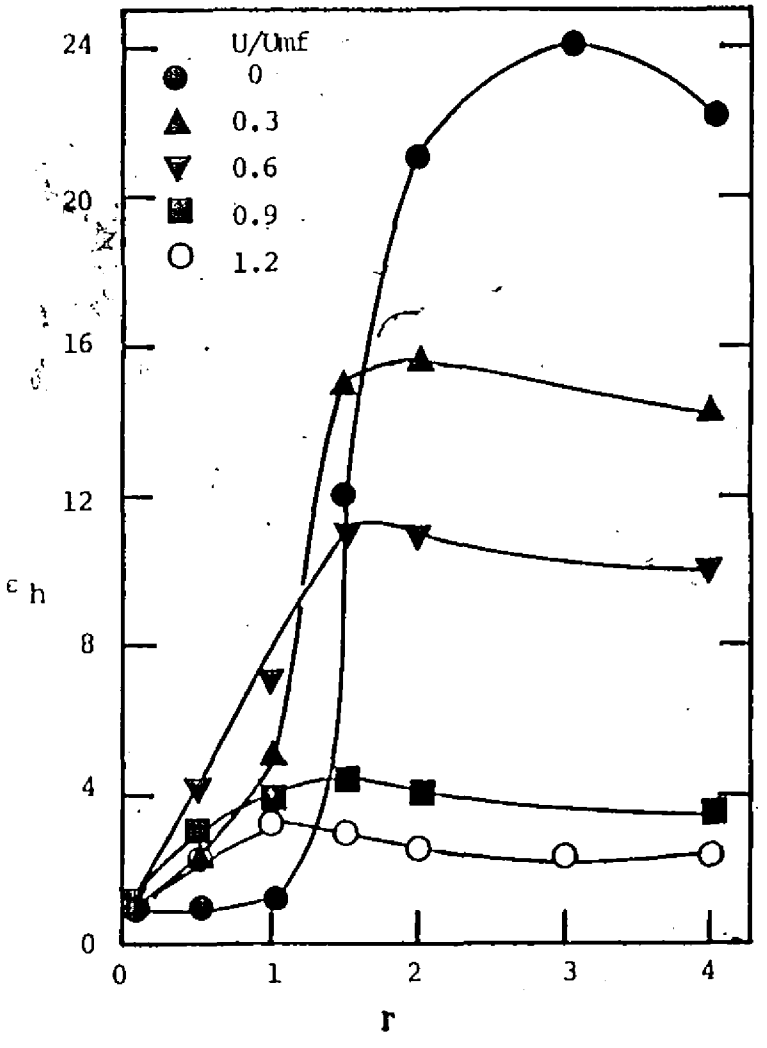

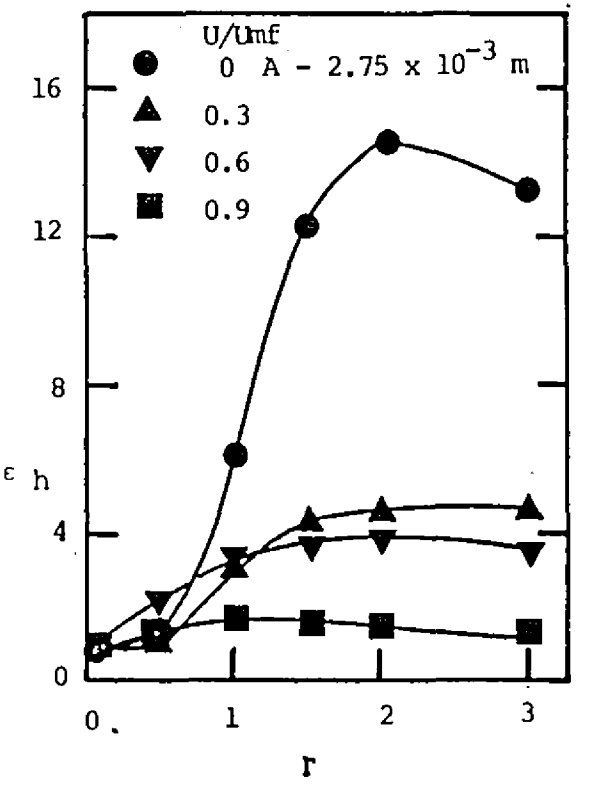

Figure 5-4 Heat transfer enhancement factor for

(a) glass ballotini, dp=0.325 mm

(b) molecular sieve particles, dp=1.4 mm

$$Ks^{\circ}/K_f = (2/(1-K_f/Kp))(\ln(Kp/K_f)/(1-K_f/Kp) - 1) \quad \ldots\ldots\ldots 5.2.2$$

Schlunder (1982) also proposed a more complex relationship to evaluate Ks° including the effects of thermal conductivity of particles and fluid, particle diameter, void fraction, particle shape factor, particle size distribution function and relative flattened particle surface contact area. The difference in thermal conductivities obtained by Schlunder's (1982) complex correlation and Equation 5.2.2 was found to be negligible. Hence Equation 5.2.2 was used because of its simplicity in evaluating Ks°.

In a conventional fluidized bed the thermal conductivity of the fluid is used in evaluating the Nusselt number, because at U>Umf, the gas convective heat transfer is the dominant heat transfer mechanism. Since this study is concerned with low aeration rates, i.e. U/Umf<1, the mixing maps (Figures 4-8 through 4-10) were used in the determination of the effective thermal conductivities. In the regime of poor mixing, Ks was used as the effective thermal conductivity of the bed; in regimes of moderate and vigorous mixing when the bed could be considered "fluidized", $0.5(Ks + K_f)$ was used as the effective bed thermal conductivity. Table 5.1 lists sample calculations for effective bed thermal conductivities for glass ballotini and molecular sieve particles respectively. Note that this representation of the Nusselt number is being presented for the first time in this thesis.

TABLE 5.1

Effective Bed Thermal Conductivity for Evaluation of the Nusselt Number

Glass ballotini, dp=1.017 mm, Umf=36.5 cm/s, K_f=0.0268 W/mK

Ks°=0.141 W/mK, $Ks = Ks° + 0.1(Pr)(Rep)K_f$ (5.1.1)

U/Umf | r	0	0.5	1	1.5	2	3	4
0	0.141	0.141	0.141	0.0839	0.0839	0.0839	0.0839
0.3	0.154	0.154	0.154	0.0904	0.0904	0.0904	0.0904
0.6	0.167	0.167	0.097	0.097	0.097	0.097	0.097
0.9	0.180	0.103	0.103	0.103	0.103	0.103	0.103

Molecular sieve particles, dp=1.4 mm, Umf=36.3 cm/s

Ks°=0.126 W/mK, $Ks = Ks° + 0.1(Pr)(Rep)K_f$ (5.1.1)

U/Umf | r	0	0.5	1	1.5	2	3	4
0	0.126	0.126	0.126	0.0764	0.0764	0.0764	0.0764
0.3	0.143	0.143	0.143	0.085	0.085	0.085	0.085
0.6	0.16	0.16	0.094	0.094	0.094	0.094	0.094
0.9	0.178	0.102	0.102	0.102	0.102	0.102	0.102

It should be noted from Table 5.1 that there is a discontinuity in the values of thermal conductivity when shifting from the regime of poor mixing to moderate mixing (Figure 4-8). The results for Nusselt number versus Γ for the regimes of poor, moderate and vigorous mixing (Figure 4-8) are plotted on the same figure in this thesis (Figures 5-5 and 5-6); however, due to the discontinuity in the values of thermal conductivities chosen the Nu versus Γ curves should be plotted separately for the regimes of poor mixing and moderate and vigorous mixing.

Figure 5-5 presents a typical Nusselt number versus Γ plots for beds of molecular sieve particles (dp=1.4 mm). It can be seen that the trends of the curves are the same as those of Figure 5-3-a, although the magnitudes have changed. The curves for higher U/Umf decrease in magnitude because of an increase in effective bed thermal conductivity as shown in Table 5.1. Similar results were obtained for other particles too.

Figure 5-6 presents heat transfer results in a normalized non-dimensional form which may be convenient in developing correlations in future. Biyikili, et al (1982) have also presented their data for heat transfer around a horizontal tube in the freeboard region of fluidized beds, in a normalized non-dimensional form. Figure 5-6 presents the heat transfer results plotted as $N=(Nu - Nu^{\circ})/(Numax - Nu^{\circ})$ versus $\Gamma/\Gamma max$, for glass ballotini and molecular sieves.

It can be noticed from Figure 5-6 that all curves in the range $\Gamma/\Gamma max<1$ (the practical range of interest) fall within a

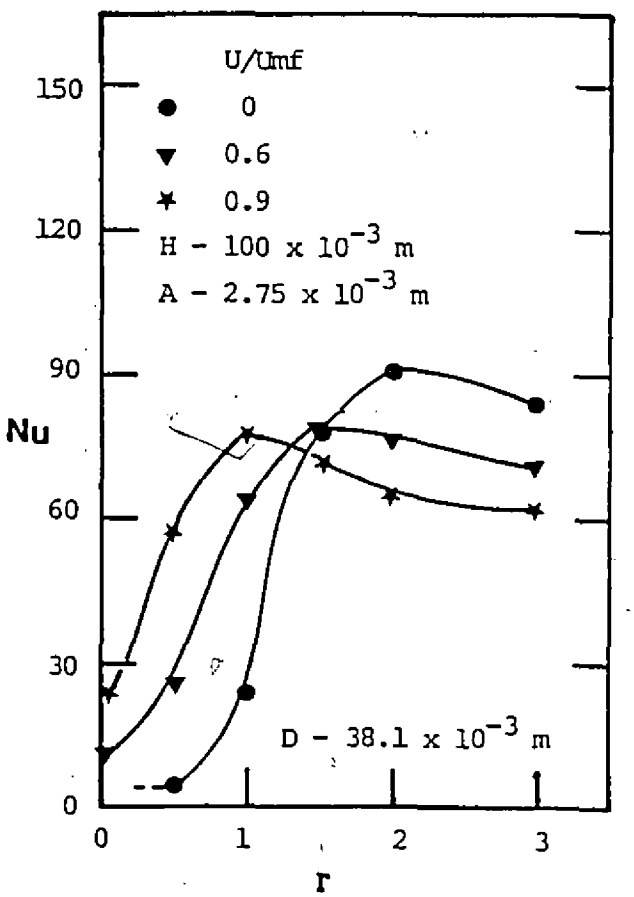

Figure 5-5 Nusselt number versus r for a bed of molecular sieve particles, dp=1.4 mm

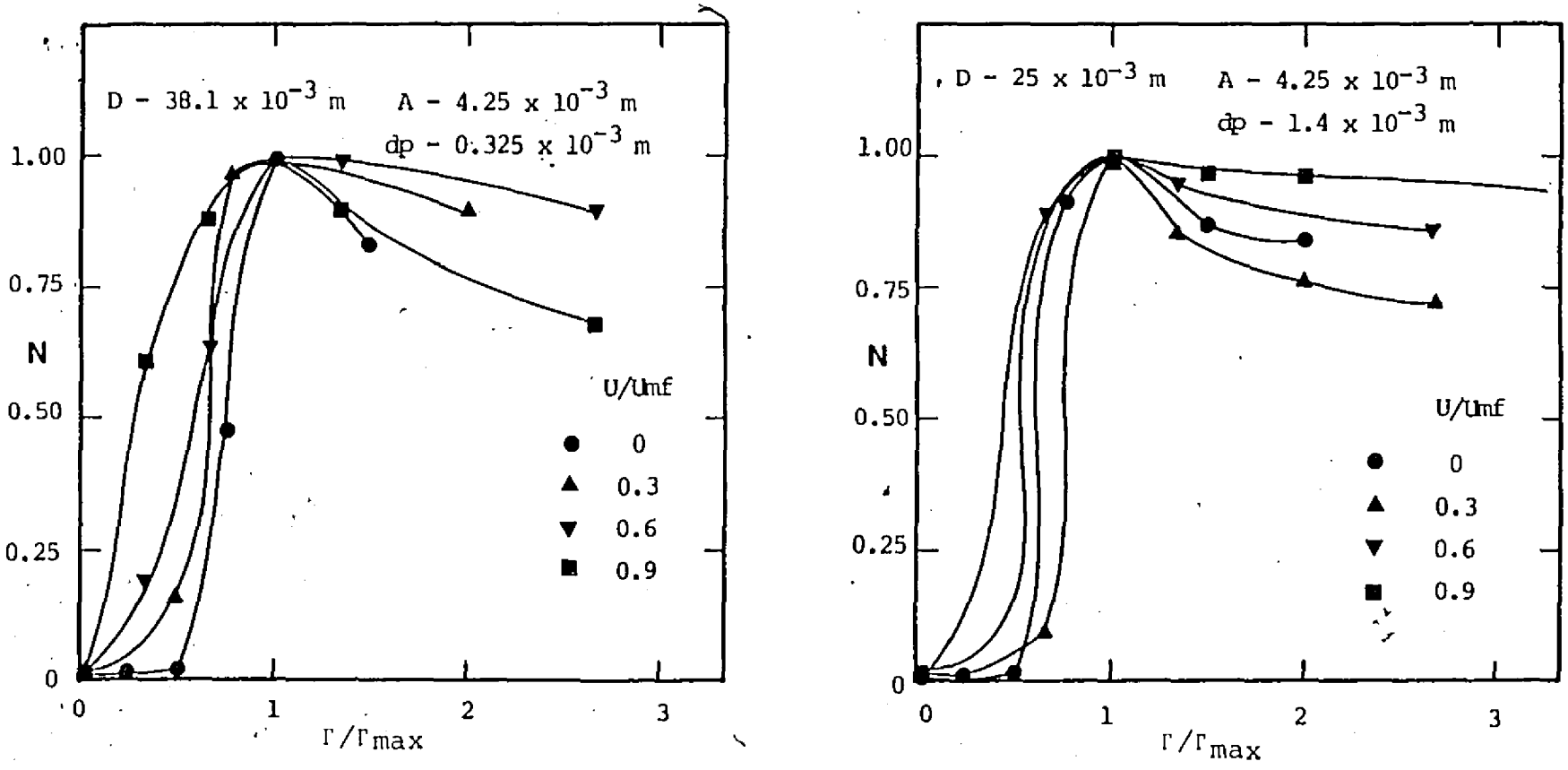

Figure 5-6 N versus Γ/Γmax for a bed of (a) glass ballotini, dp=0.325 mm (b) molecular sieve particles, dp=1.4 mm

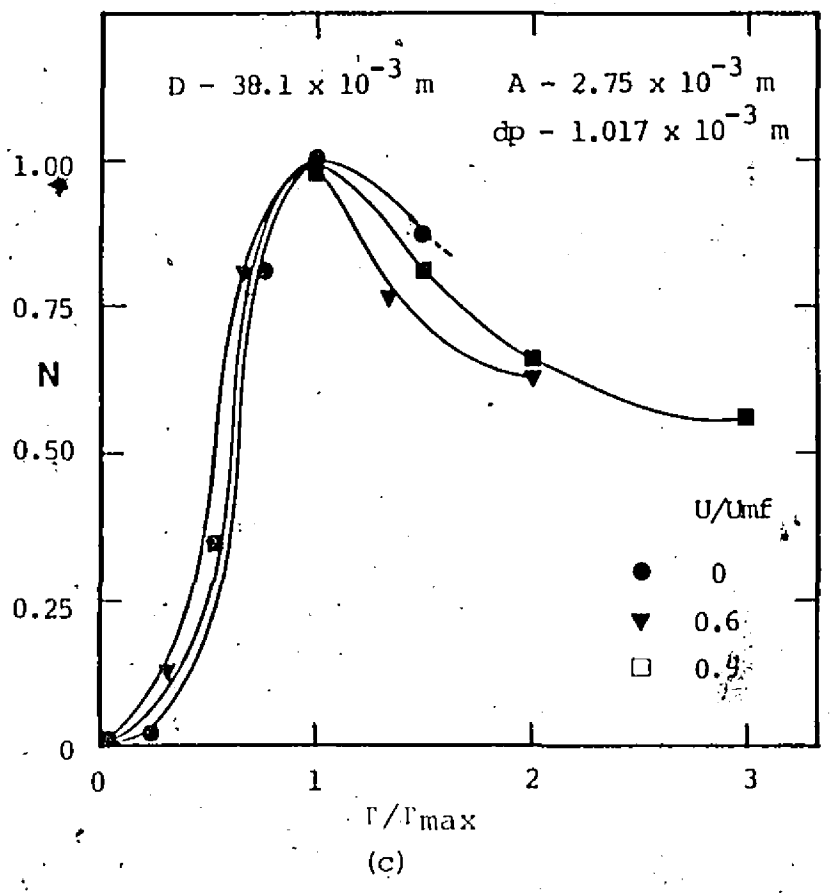

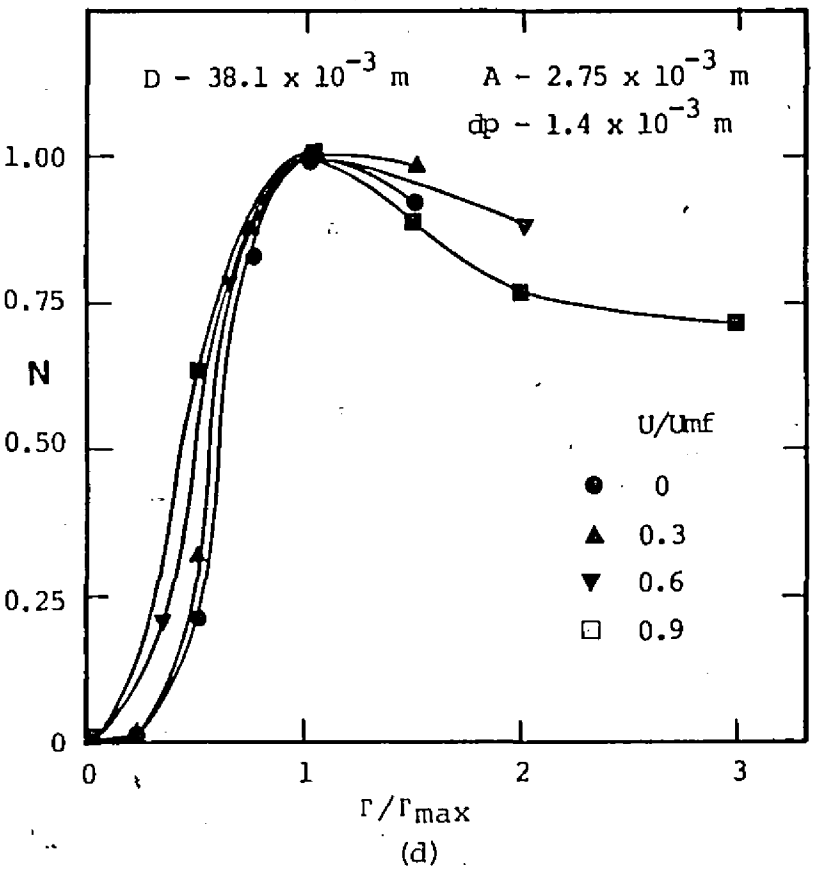

Figure 5-6 N versus Γ/Γmax for a bed of (c) glass ballotini, dp=1.017 mm (d) molecular sieve particles, dp=1.4 mm

very narrow bandwidth. The shape of all the curves in that range is also very similar. Knowing the values of Γ_{max} (Figure 5-2) and corresponding Nu_{max} and Nu°, it would be possible to generate an empirical correlation of the form:

$$Nu = f(N, \Gamma/\Gamma_{max}, U/U_{mf}) \qquad \ldots\ldots\ldots 5.2.3$$

The development of such a correlation was not a part of this study and further work in this area is needed.

5.2.2 Effect of Surface Stickiness

The objective in these experiments was to determine the effect of particle surface adhesion on the heat transfer rate in the absence of evaporation. This was achieved by wetting glass ballotini particles with controlled amounts of glycerine. The effect of drying on the contact heat transfer rate is presented in a later section.

Two levels of particle stickiness, X=0.0003 and 0.0006 were examined. Here X is kg glycerine/kg dry glass ballotini. It was found that X=0.0003 had no appreciable effect on heat transfer rates for large ballotini (dp=1.017 mm), while a slight decrease (5-10%) was observed for smaller glass ballotini (dp=0.325 mm). This can be attributed to stickiness affecting the smaller particles more strongly than larger ones, as discussed earlier in section 4.2.

Typical h versus Γ curves for beds of sticky glass ballotini , X=0.0006 kg glycerine/kg dry glass ballotini, are

presented in Figure 5-7. It can be noticed from this figure that the heat transfer coefficients for sticky particles are lower than those for corresponding dry beds under similar operating conditions. For smaller glass ballotini (dp=0.325 mm) the heat transfer coefficients are 40-50% lower as compared to dry beds; also no characteristic peaks (in the heat transfer curves) of dry beds can be observed. The lower plateau of all the curves is extended while the upper plateau is altogether absent. The heat transfer rate rises continuously although more slowly beyond $\Gamma>3$.

The aforementioned observation suggests that particle mixing is a dominant factor influencing the heat transfer rates in the Γ range examined. Moreover, for $U/Umf<0.9$ and $\Gamma\geq2$ the bed structure is homogeneous (no bubbling) and gap formations around the immersed cylinder are smaller. For larger ballotini, similar observations were recorded although the difference in heat transfer as compared to dry beds was smaller and the upper plateaus were fully formed.

Figure 5-8 shows a comparison between the heat transfer data for beds of sticky and dry glass ballotini. Clearly for smaller glass ballotini the heat transfer coefficient for sticky beds is lower than that for dry beds over the entire Γ range; for $U/Umf=0.9$, the value of h_c at $\Gamma=4$ was same for both sticky and dry glass ballotini. At such high levels of aeration and vibrational acceleration mixing in the bed is intense and is independent of the degree of inter-particle forces of adhesion; under these operating conditions the particle-to-particle

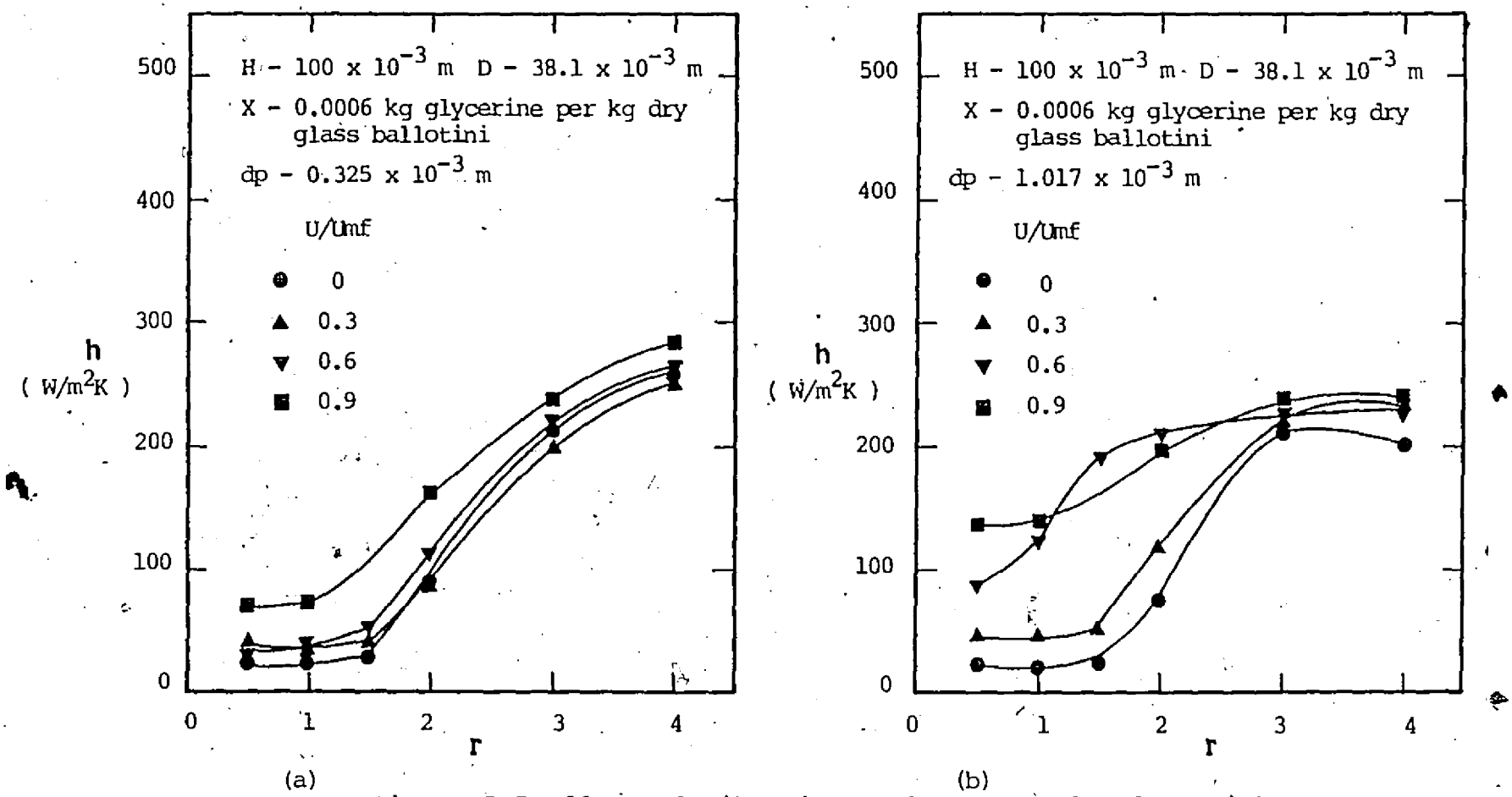

Figure 5-7 Effect of vibration on heat transfer for sticky glass ballotini (a) dp=0.325 mm (b) dp=1.017 mm

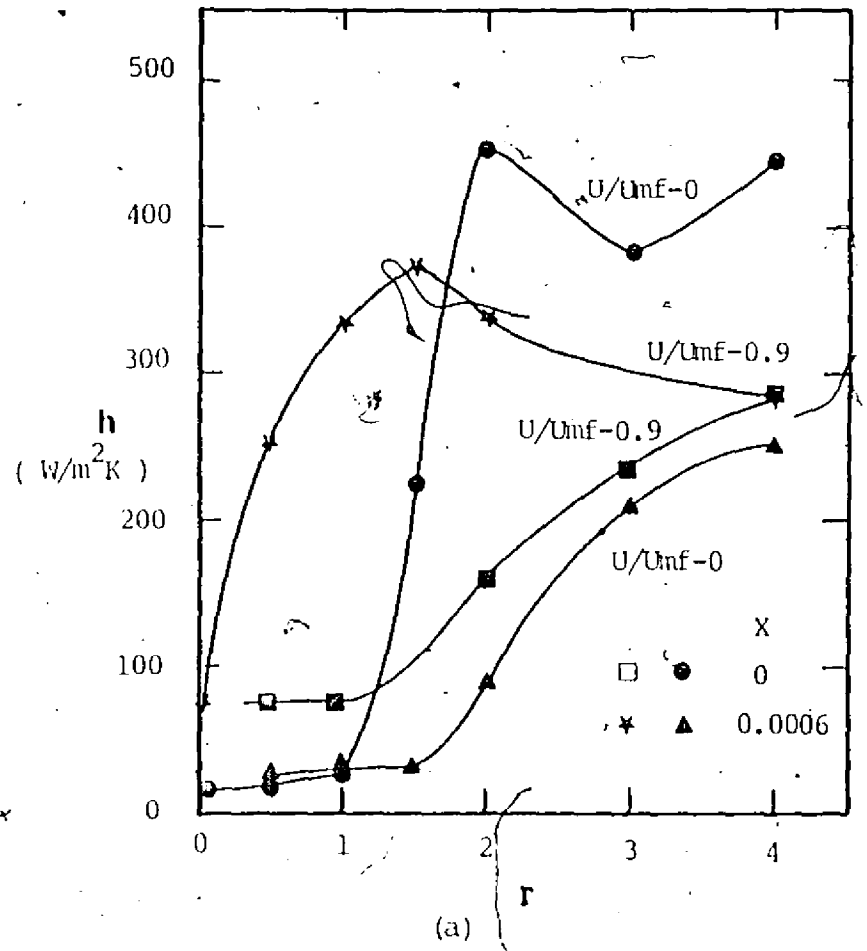

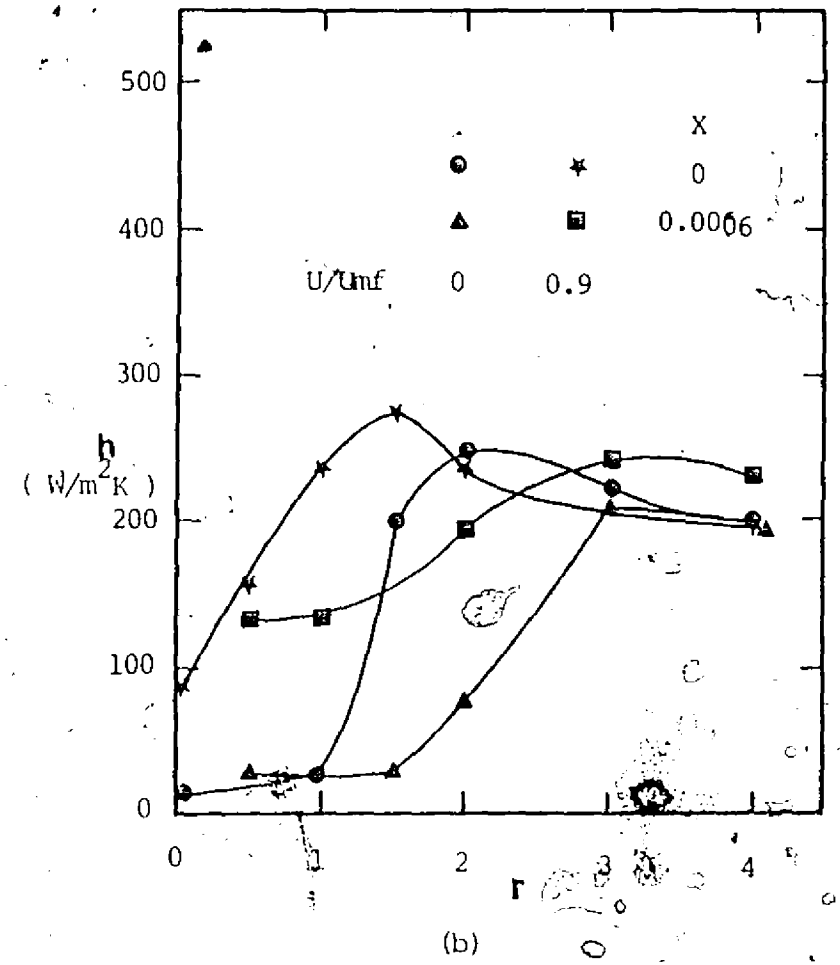

Figure 5-8 Effect of stickiness on heat transfer for sticky glass ballotini (a) dp=0.325 mm (b) dp=1.017 mm

contact is reduced to a minimum.

For larger glass ballotini the difference in h values between the dry and sticky particles is much less pronounced and beyond $\Gamma \geq 3$, a common plateau is reached for all the curves. In fact, for U/Umf=0.9 and $\Gamma \geq 2.5$, sticky beds displayed higher heat transfer rate. The above observation could be attributed to the following facts. Firstly, stickiness affects larger particles less severely than smaller ones (because of fewer interparticle contacts per unit bed volume) and secondly, once the interparticle bridges are broken(i.e. $\Gamma \geq 3$), beds with low stickiness levels were observed more homogeneous when compared to dry beds.

Figure 5-9 presents the same results as above, but at a lower amplitude of vibration. Since stickiness bonds are broken more efficiently at higher amplitudes of vibration to induce particle mixing, smaller amplitudes have a lower heat transfer rate at a given value of Γ and U/Umf>0.

5.2.3 Effect of Particle Size

Figures 5-10-a through 5-10-d display for VFB's the well known trend verified repeatedly for conventional fluidized beds viz. h is higher for smaller particles. Examination of Figures 5-10-a through 5-10-c leads to the conclusion that decrease of h with increase in particle size is more significant at lower U/Umf and larger particle sizes (dp=0.595 mm to dp=1.017 mm) as compared to that for smaller particles (dp=0.325 mm to dp=0.595 mm).

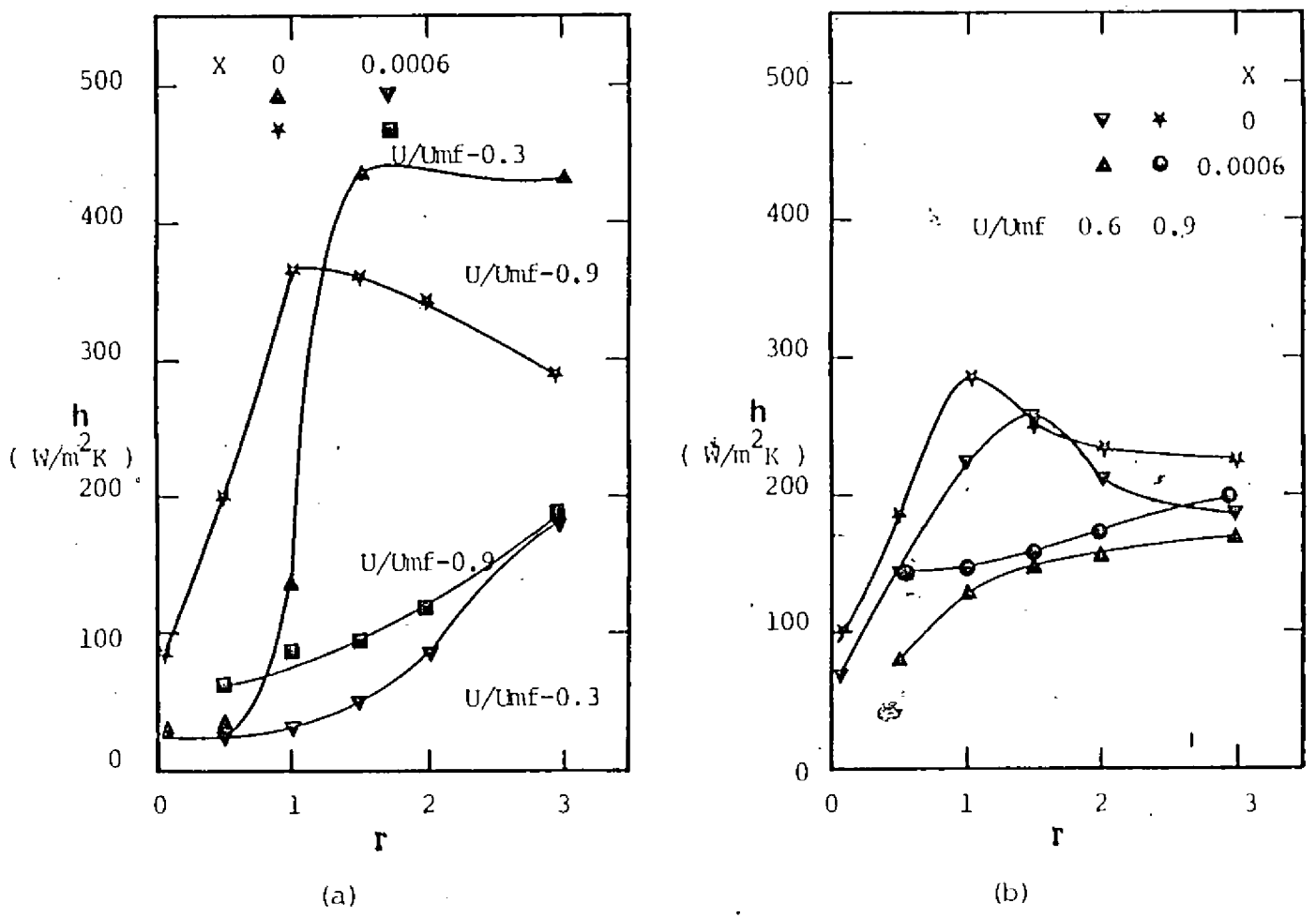

Figure 5-9 Effect of stickiness on heat transfer for glass ballotini (a) dp=0.325 mm (b) dp=1.017 mm

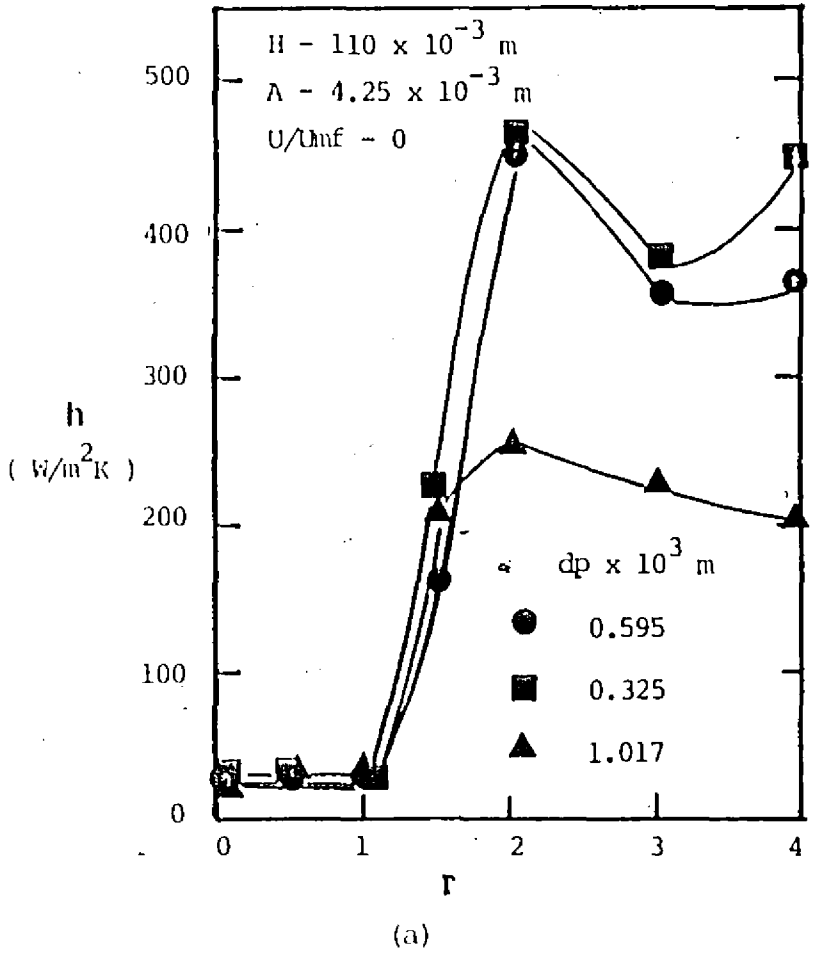

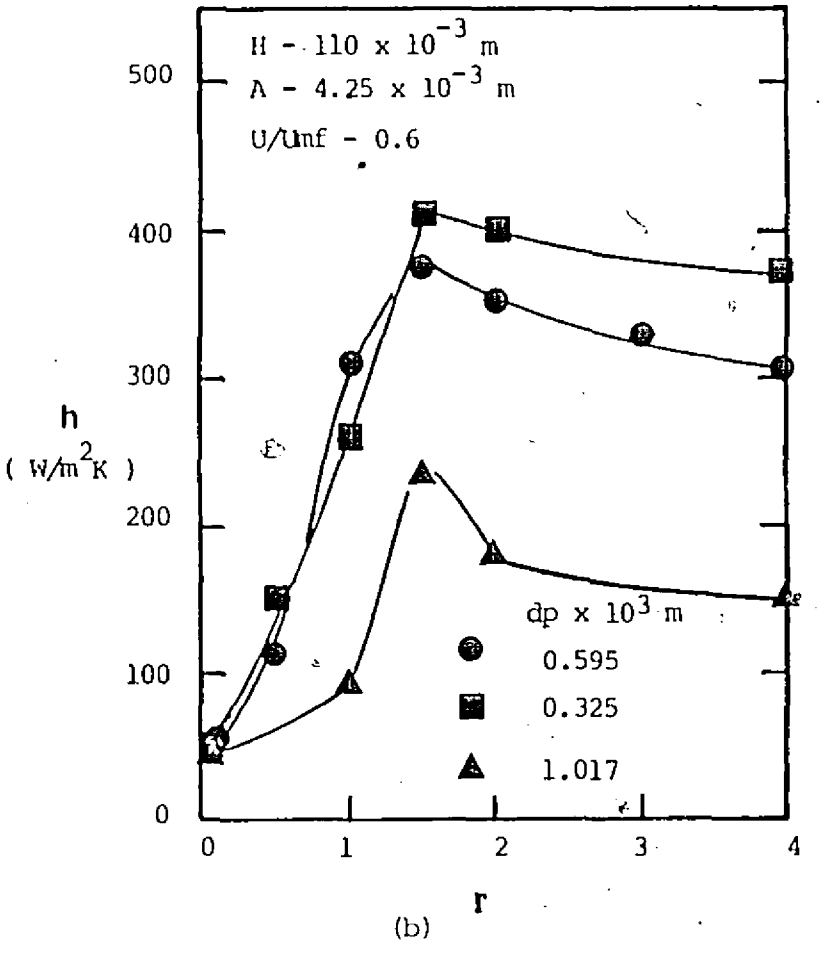

Figure 5-10 Effect of particle size on heat transfer coefficient

(a) glass ballotini (b) glass ballotini

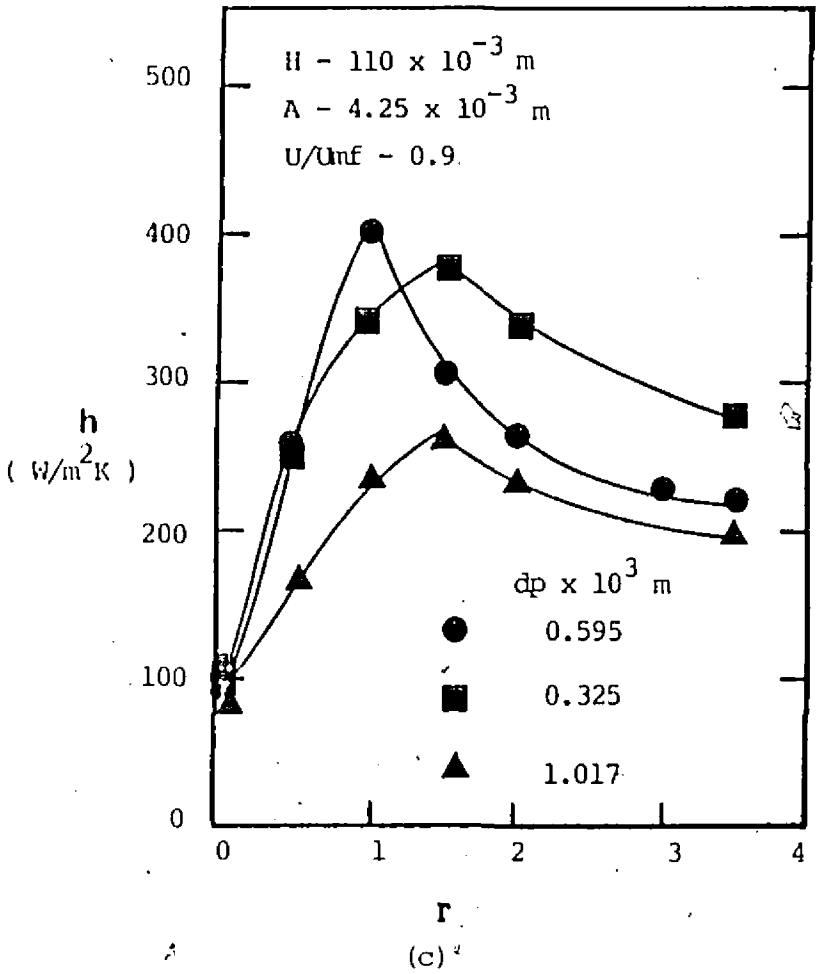

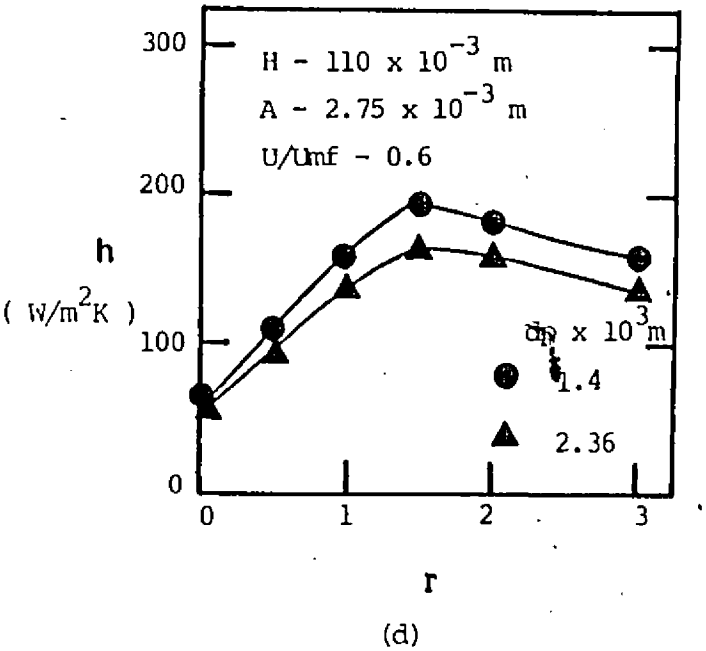

Figure 5-10 Effect of particle size on heat transfer coefficient

(c) glass ballotini (d) molecular sieve particles

Chandran et al (1980) and Biyikili and Chen(1982) reported a 16% decrease in h from dp=0.325 mm to dp=0.595 mm, and a 25% decrease from dp=0.595 mm to dp=1.017 mm, in conventional fluidized beds. From Figure 5-10-c, at U/Umf=0.9 and r=1.5 (initiation of bubbling in a VFB), h decreased by 19% from dp=0.325 mm to dp=0.595 mm and 17% from dp=0.595 mm to dp=1.017 mm. The difference in h between smaller and larger particles is much less pronounced at higher U/Umf; at higher U/Umf the gas convective term becomes significant for larger particles as compared to the smaller ones.

The effect of particle size on heat transfer diminishes with increasing particle size until, beyond dp=3 mm it disappears completely as reported for conventional fluidized beds, by Baskakov et al (1973) and verified by Biyikili and Chen (1982) and Chandran, et al (1980). Figure 5-10-d verifies this for a VFB of molecular sieve particles, where the difference in h between dp=1.4 mm and dp=2.36 mm is reduced considerably.

The decrease in h with increase in particle diameter (dp<1 mm) is explained predominantly due to an increase in the average gas conduction paths between the heat transfer surface and the first row of particles and between particles. The increase in the gas conduction path increases the resistance to heat flow, as shown by Schlunder (1982), Heyde and Klocke (1980), Martin (1981) and Baskakov et al (1973). Baskakov et al (1973), reported the thermal resistance between the first row of particles and the surface to be half of that between

adjacent layer of particles in the lattice and equal to:

$$R_k = dp/2Ks \qquad \ldots\ldots 5.2.4$$

It can be seen that this resistance is directly proportional to the particle diameter. Further, the particle surface area per unit volume of the bed is larger for small particles and therefore small particles are more efficient in exchanging heat with the surface.

Another way of examining the effect of dp is in terms of ε_h. Figure 5-11 shows that ε_h decreases with increase in dp, regardless of U/Umf. The actual decrease depends upon U/Umf too. Thus larger particles are less sensitive to vibration-induced enhancement of heat transfer. Pakowski and Mujumdar(1982) also reported a decrease in heat transfer coefficient with an increase in particle size in a VFB, although the difference between particles of glass ballotini of sizes dp=0.454 mm and 0.667 mm is larger in their case (38% for U/Umf=0 and 20% for U/Umf=0.6) as compared to this study.

Figure 5-12 shows the effect of particle size on the contact heat transfer for beds of sticky glass ballotini. It can be noticed that , unlike the beds of dry particles, beds of sticky larger particles have a higher heat transfer rate for U/Umf>0 and r<3. This is attributed to stronger interparticle forces for smaller particles (dp=0.325 mm) as compared to larger ones (dp=1.017 mm). Thus strong liquid bridges inhibit initial particle convective heat transfer process for small

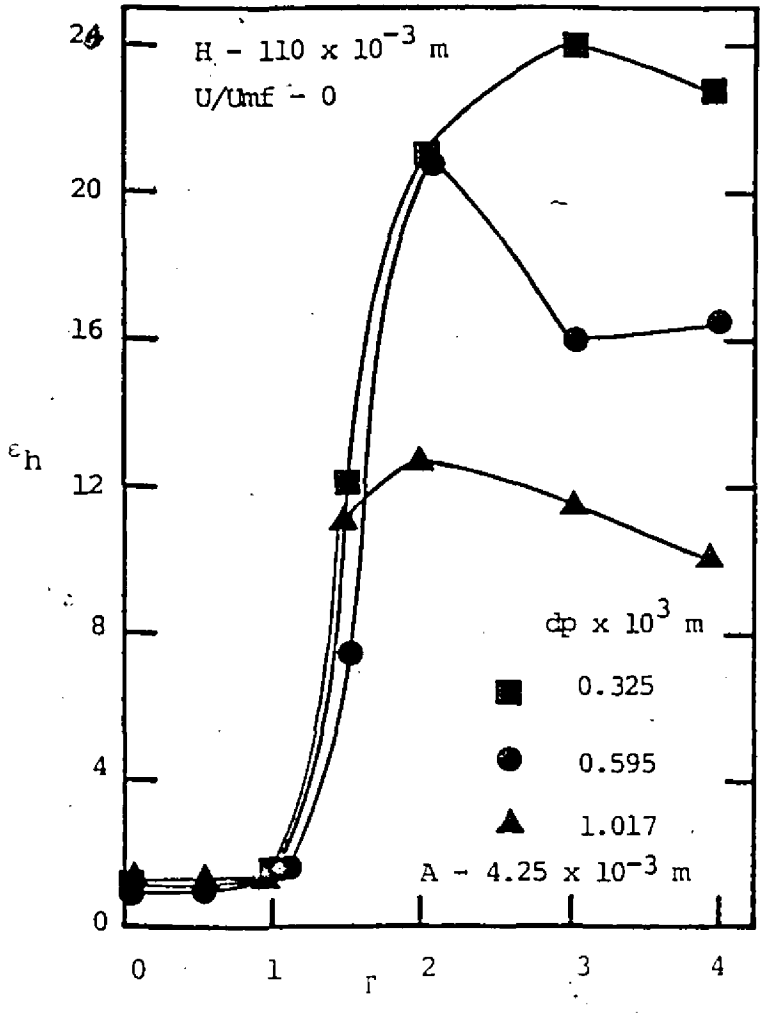

Figure 5-11 Effect of particle size on heat transfer enhancement factor for glass ballotini

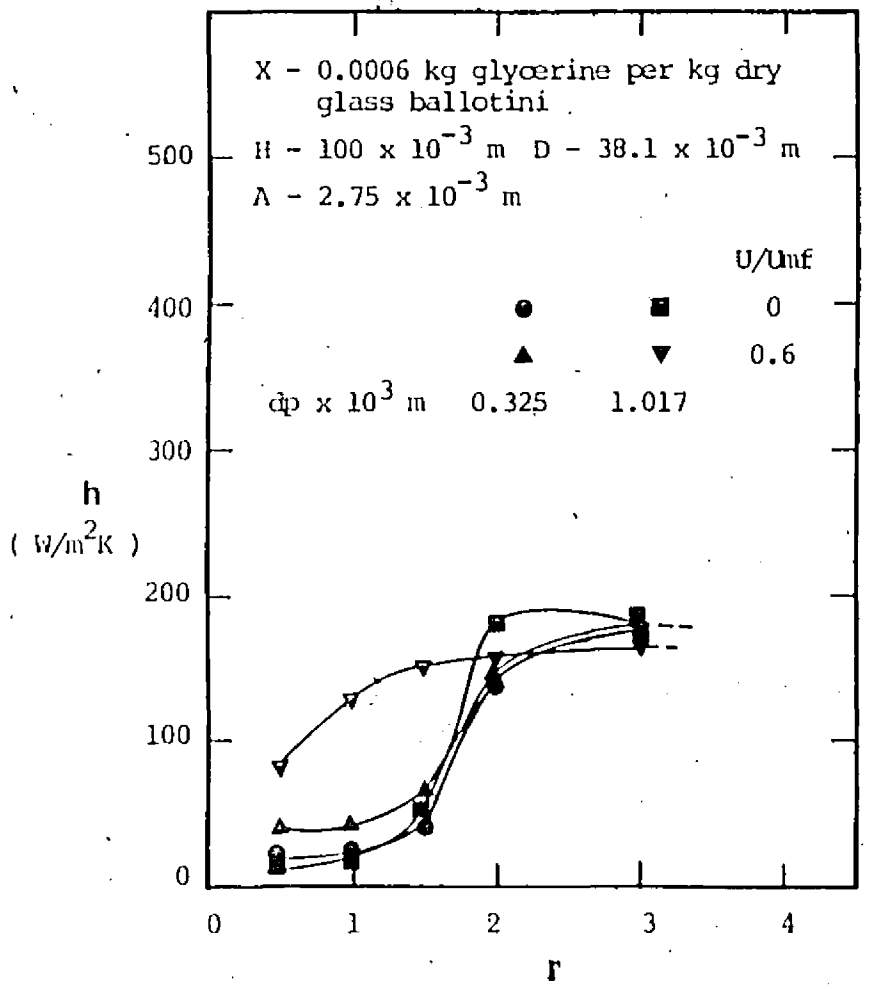

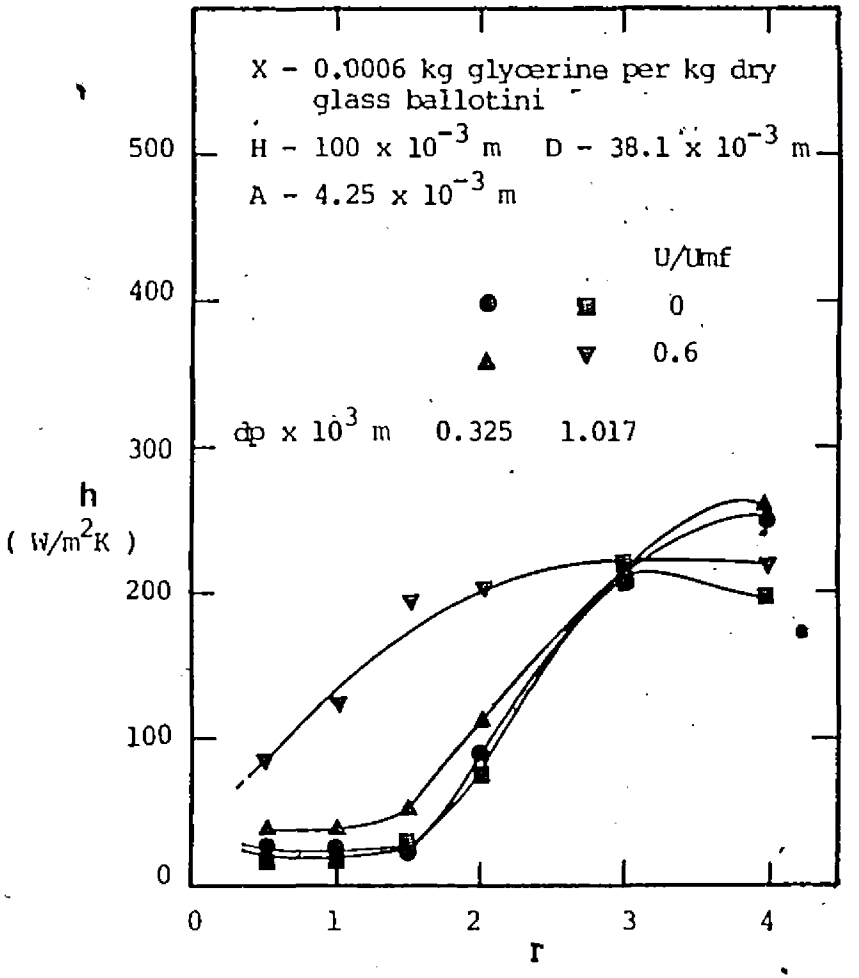

Figure 5-12 Effect of particle size on heat transfer coefficient for sticky glass ballotini

particles. Beyond $\Gamma>3$, when the bed is homogeneous and well mixed, the smaller particles have a higher heat transfer coefficient as can be seen from Figure 5-12-b.

For non-aerated beds, the difference in heat transfer coefficients for both particle sizes is negligible for $\Gamma\leq2.5$, since the heat transfer mechanism for U/Umf=0 is predominantly due to particle convective heat transfer which is inversely proportional to the particle size. Therefore, the effects of stickiness (to reduce heat transfer for smaller particles) and particle heat transfer (higher for smaller particles) cancel each other out to a great extent.

Pakowski and Mujumdar ,(1982) reported no significant effect of particle size on heat transfer coefficient at X=0.0006 for glass ballotini, dp=0.454 mm and dp=0.667 mm. It should be noticed that the difference in these particle sizes is half of what was used in the current study.

5.2.4 Effect of Amplitude of Vibration

Three amplitudes of vibration- 1.5 mm, 2.75 mm and 4.25 mm, were examined. It should be noted that this study was limited to lower Γ's at smaller A's since the upper frequency level of the vibratory mechanism was fixed. Figures 5-13-a through 5-13-d portray the effect of amplitude of vibration. At higher U/Umf, Γ values seem to couple effectively the combined influence of A and ω (Figures 5-13-c and 5-13-d).

Figure 5-13-a shows that for U/Umf=0 heat transfer is higher for A=4.25 mm as compared to A=2.75 mm, but lower as

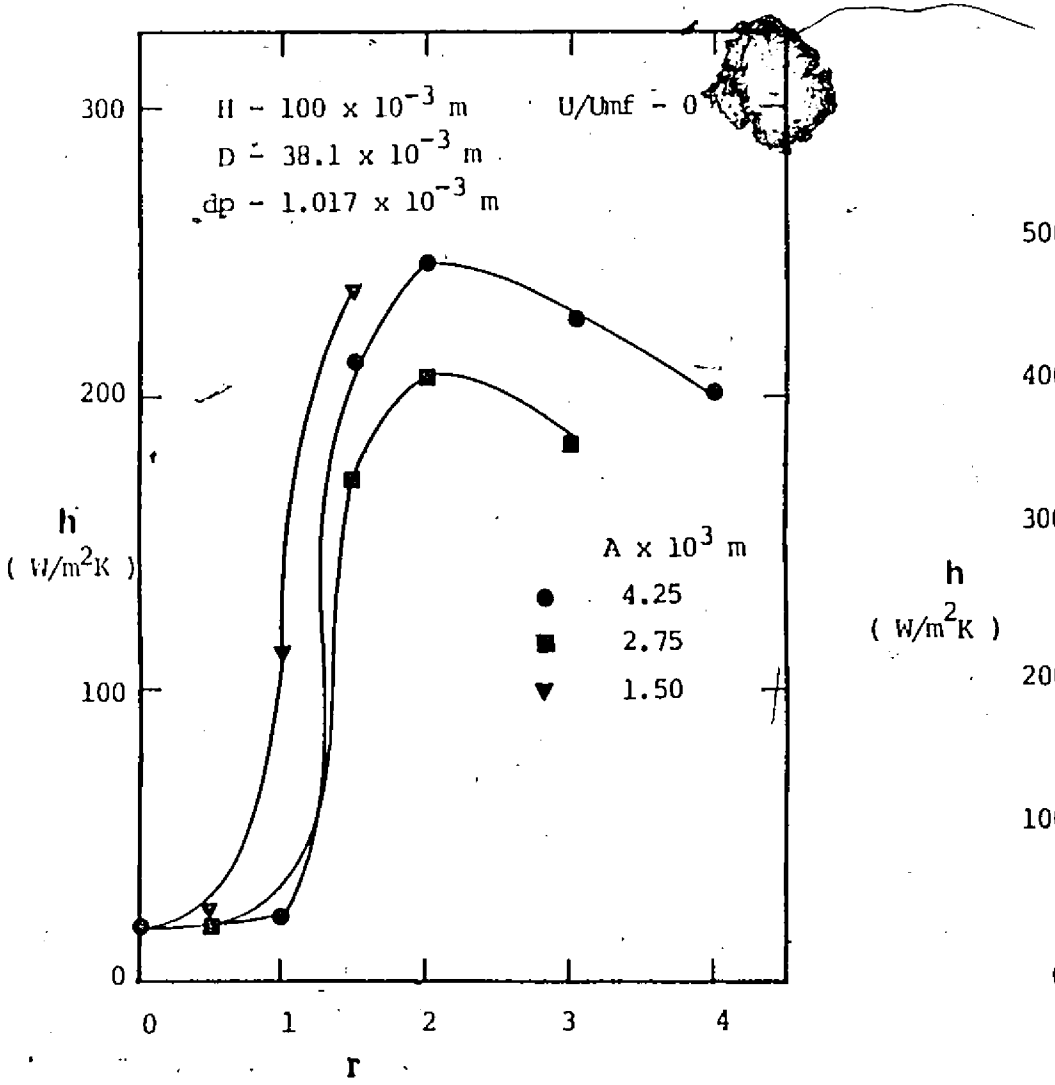

(a) glass ballotini, dp=0.325 mm

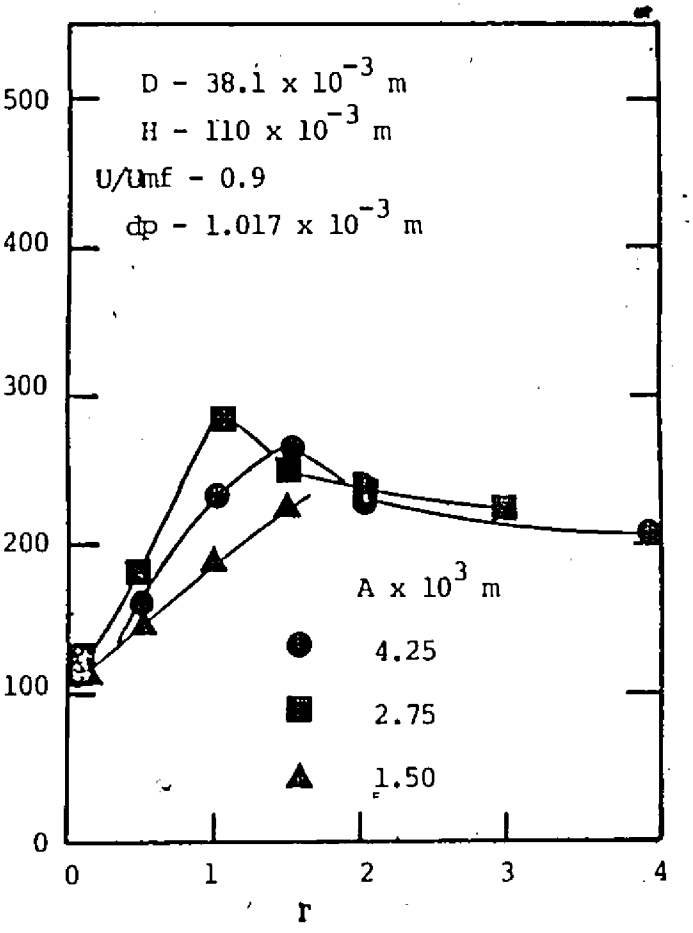

(b) glass ballotini, dp=0.325 mm

Figure 5-13 Effect of amplitude of vibration on heat transfer

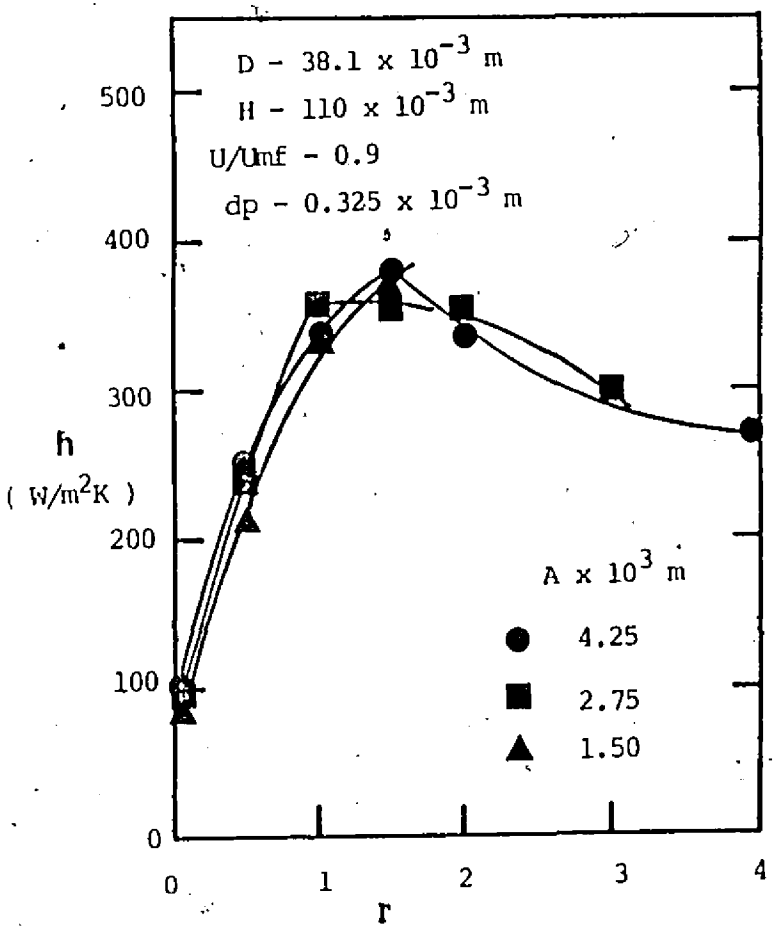

(c) glass ballotini, dp=0.325 mm

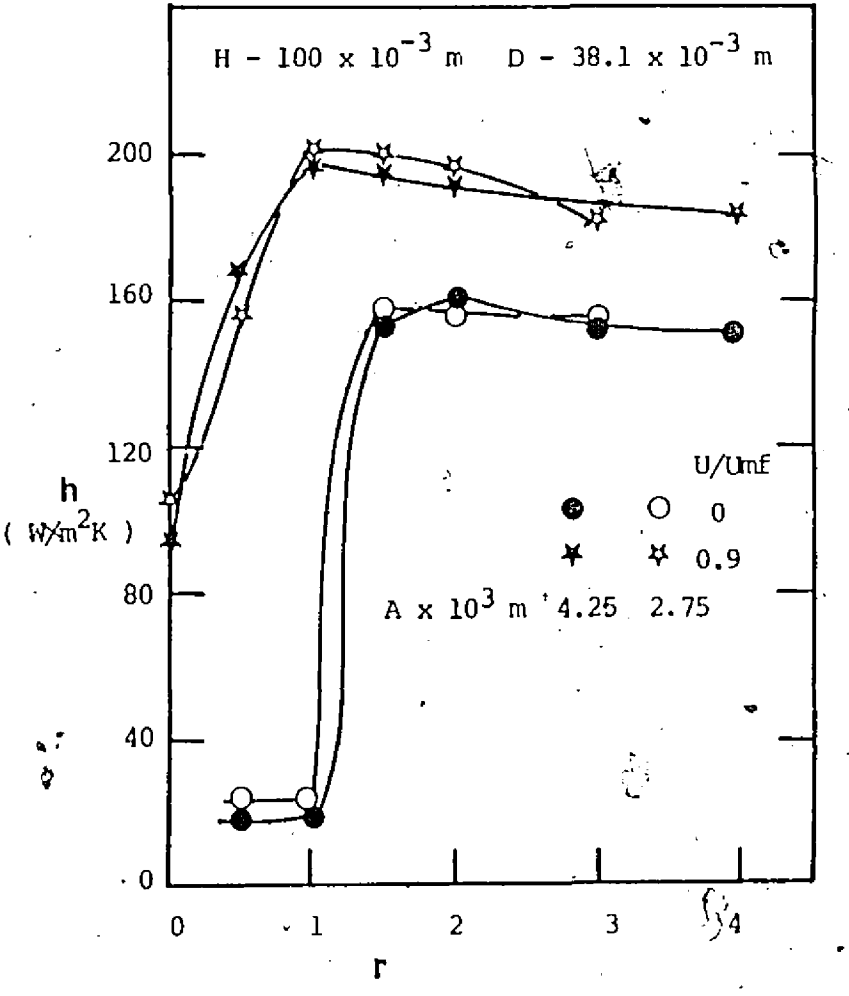

(d) molecular sieve particles, dp=1.4 mm

Figure 5-13 Effect of amplitude of vibration on heat transfer

compared to A=1.5 mm. This observation can be attributed to the effect of the frequency of vibration, ω. It can be seen from Figure 5-14-a, that heat transfer is higher for higher amplitudes at same value of ω, although when represented on h versus Γ plot, h is higher for A=1.5 mm. Moreover, the curve for A=1.5 mm in Figure 5-14-a rises above the other two curves beyond ω>95 rad/s due to the fact that gap formation at Γ=1.5 and A=1.5 mm is much smaller as compared to that at higher amplitudes.

Similar h versus ω plots were obtained for higher air flow rates as shown in Figure 5-14-b and 5-14-c, although at higher aeration rates the bandwidth of h versus Γ curves narrows down.

Increase in amplitude, for a given frequency, reduces the contact time of the particles with the vibrating surface (since particles are projected at an earlier part of the vibration cycle). This enhances the heat transfer rates since particle contact heat transfer is inversely proportional to the square root of contact time. Gupta (1979) also postulated that increase in amplitude results in a decrease in the "emulsion density" around the immersed vibrating surface and hence results in reduction in bed thermal diffusivity which in turn decreases the heat transfer coefficient. With the present knowledge, it is not possible to quantitatively predict the aforementioned effects or to determine to what extent these two mechanisms counteract each other. It is clear that the effect of amplitude must be examined in some detail over a wider range of A and Γ.

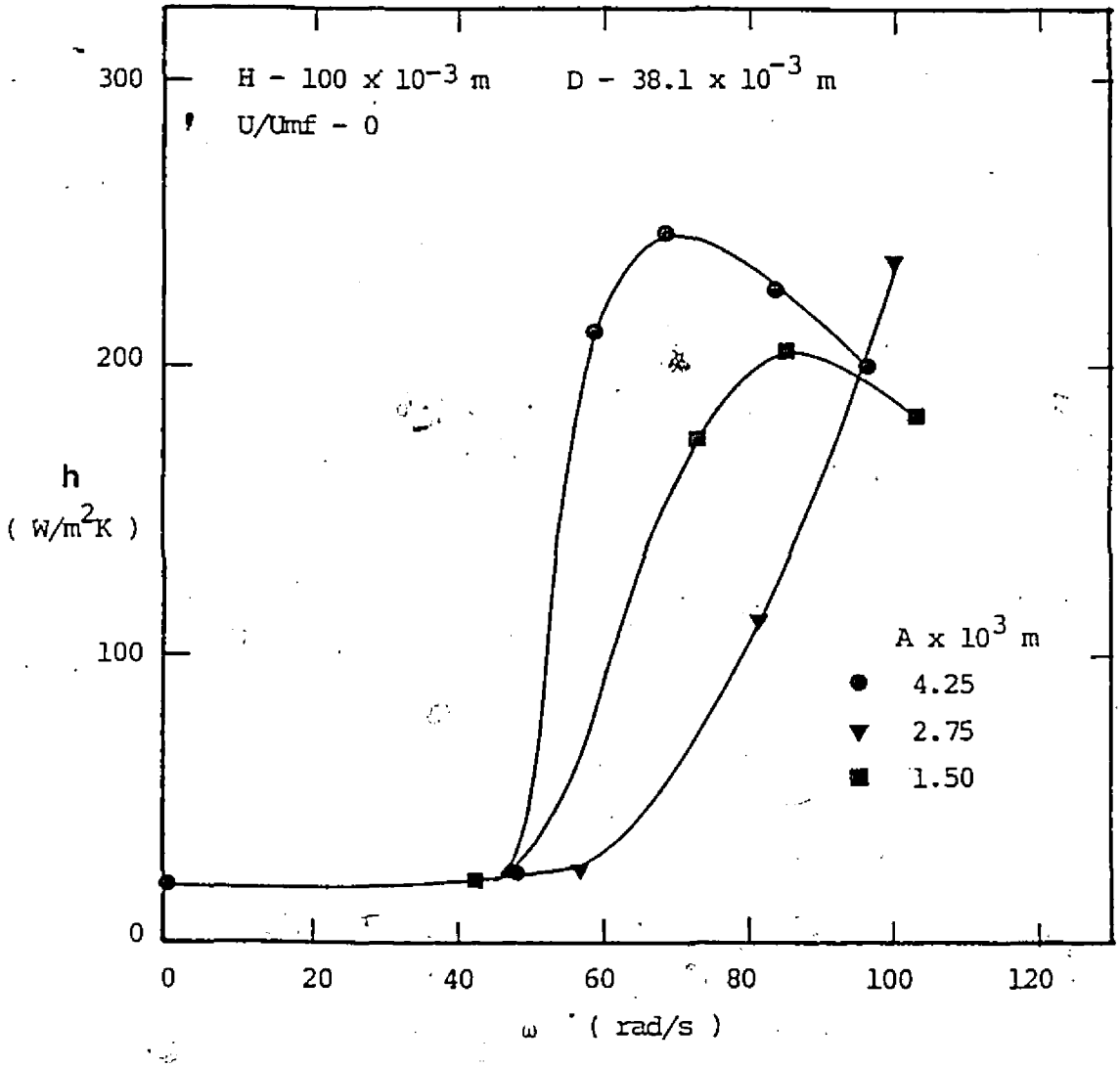

Figure 5-14 Effect of ω on heat transfer for (a) glass ballotini dp=1.017 mm

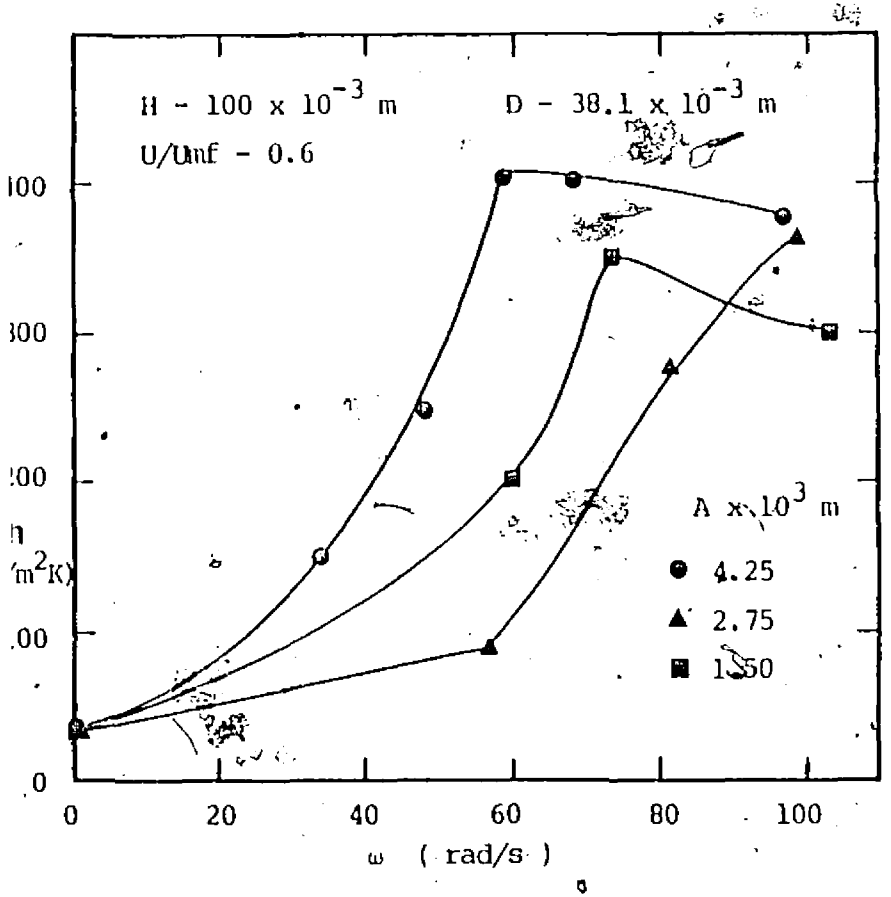

(b) glass ballotini, dp=0.325 mm

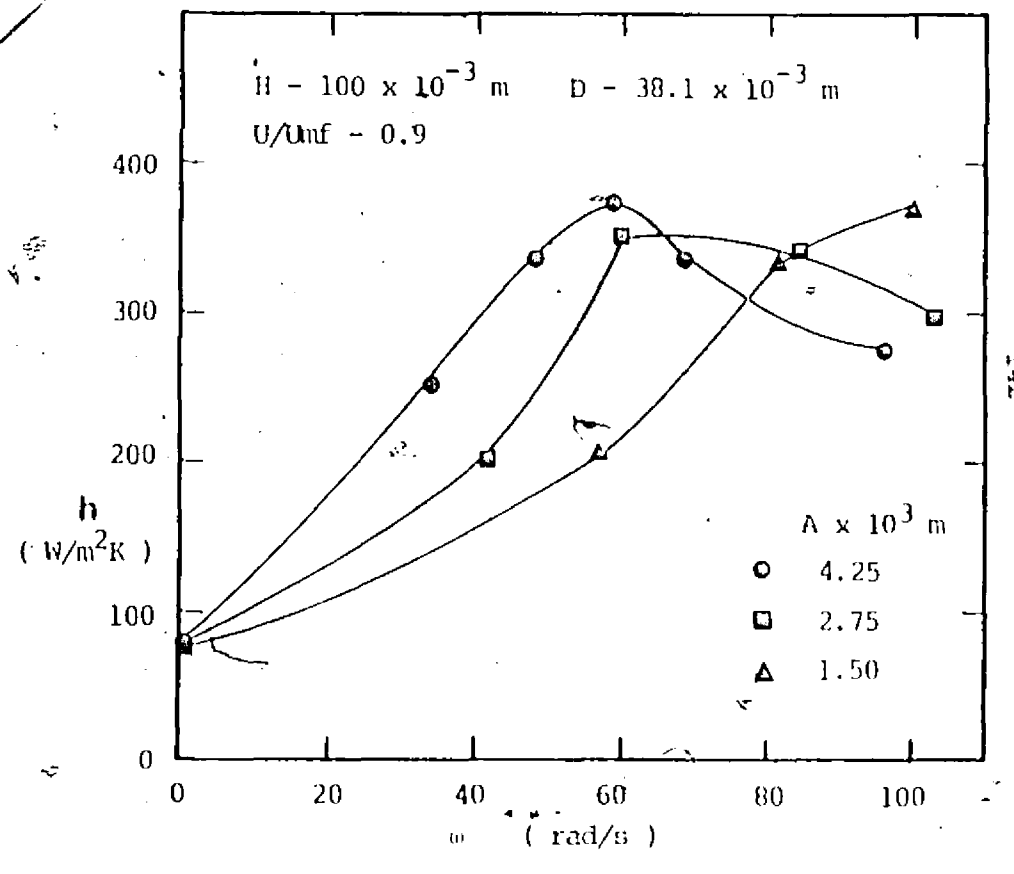

(c) glass ballotini, dp=0.325 mm

Figure 5-14 Effect of ω on heat transfer

The effect of amplitude of vibration on heat transfer for sticky particles is displayed in Figure 5-15. At higher air flowrates, i.e. U/Umf=0.9 higher amplitudes of vibration resulted in higher heat transfer coefficients, while at U/Umf=0, the lower amplitude of vibration displayed higher heat transfer rates till Γ≤2.5. The value of hmax was always higher for A=4.25 mm as compared to A=2.75 mm. Figure 5-16 showing the h versus Γ curve for sticky glass ballotini, confirms the fact that higher amplitudes of vibration induce higher heat transfer rates at a given value of Γ (once the liquid bridges are broken).

5.2.5 Drying

The drying experiments were performed with molecular sieve particles (porous) of two sizes (dp=1.4 mm and 2.36 mm) at two amplitudes of vibration (A=2.75 mm and 4.25 mm). The mass of the bed and the heat input were kept constant. Ambient air (28-30°C) was employed to minimize the rate of drying so that quasi-steady state could be attained permitting measurements of h° (heat transfer coefficient for wet molecular sieve particles) without resorting to the more complex transient technique. A typical drying run took about 2 hours. Furthermore, since only the average moisture content could be measured by sampling the bed during operation, the choice of Γ and U/Umf was dictated by the requirement of good mixing in the bed. No data could be obtained at low Γ's and U/Umf values.

The following observations were recorded during the course of an experiment. Smaller molecular sieve particles (

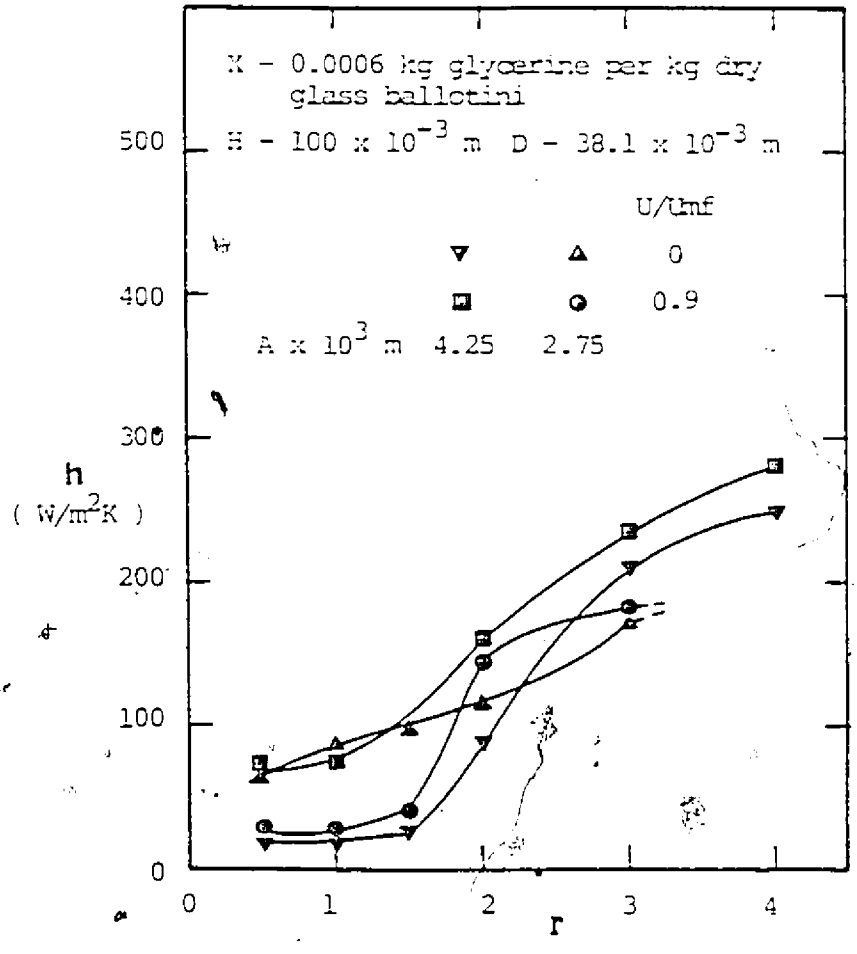

Figure 5-15 Effect of amplitude of vibration on heat transfer for a bed of sticky glass ballotini, dp=0.325 mm

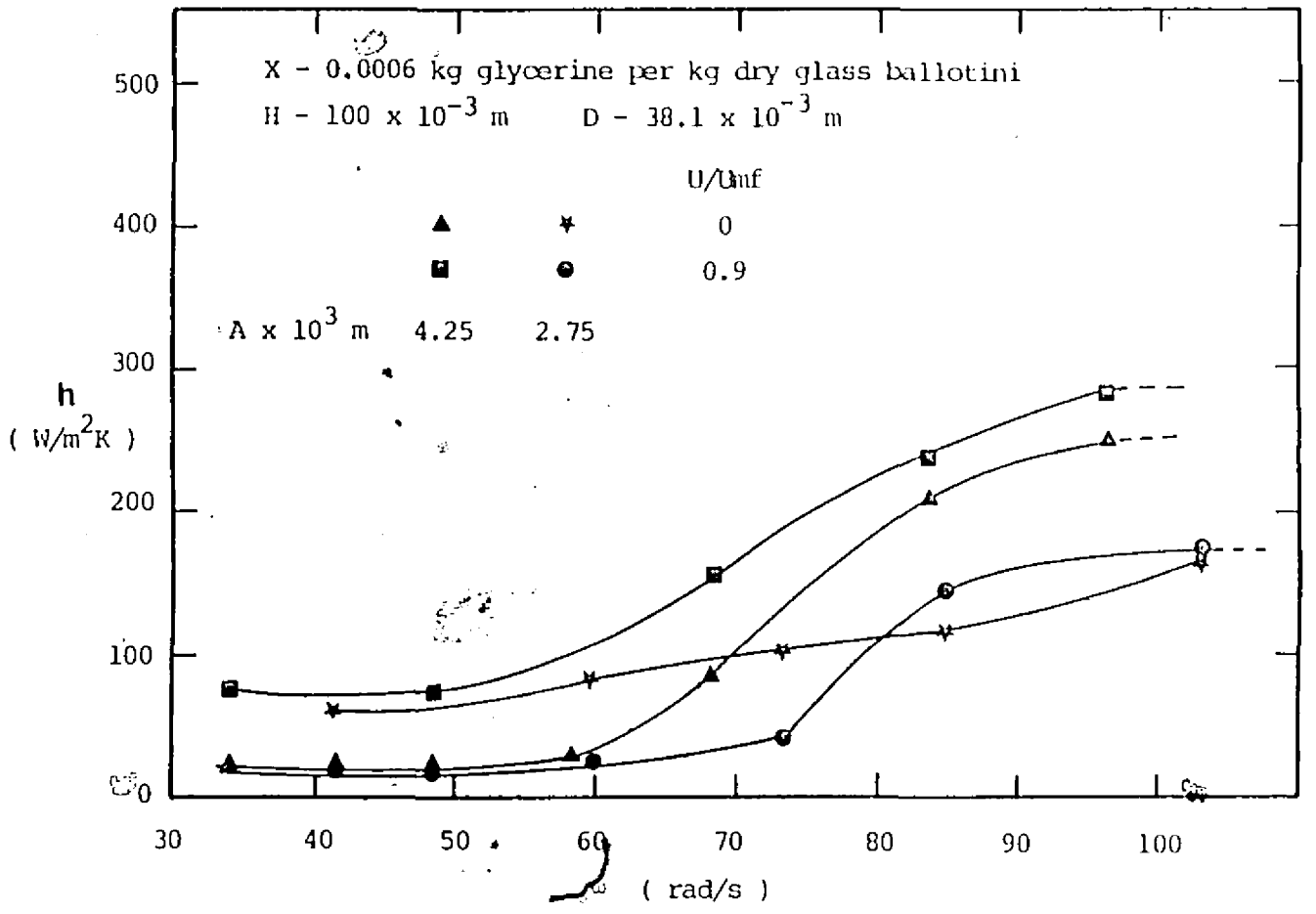

Figure 5-16 Effect of frequency of vibration on heat transfer for a bed of sticky glass ballotini, dp=0.325 mm

dp=1.4 mm) formed lumps initially (X=0.33-0.42 kg water/kg dry particles) hampering good mixing of the bed. The larger particles (dp=2.36 mm) were free flowing over the entire range of X. Strong interparticle liquid bonds for smaller particles account for the above effect. In the range $0.30 \leq X \leq 0.39$ vibration caused interparticle moisture to free itself, which on many occasions distorted the actual average moisture content of the collected samples. Note, X here is kg water/kg dry particles and not stickiness level as before.

Due to poor initial solids mixing, smaller particles took longer to reach steady state as compared to larger ones. It was impossible to "fluidize" the bed homogeneously with good particle mixing without the help of vibration. Both the particles retained their original physical properties- size, shape and appearance, on completion of an experiment. Elutriation and attrition were negligible, due to gentle handling of the particles. Another important observation was the presence of a thin film of molecular sieve material on the test cylinder during the experiment, leading to lower heat transfer rates.

Figures 5-17 through 5-19 display the appreciable increase in h° due to presence of moisture. When surface evaporation takes place (Xc for molecular sieve particles is about 24% dry basis) evaporation of unbound water causes a significant rise in h°. In the range $0.30 \leq X \leq 0.35$ vibration causes interparticle moisture to free itself. As it is removed physically the bed mobility rises which is probably responsible

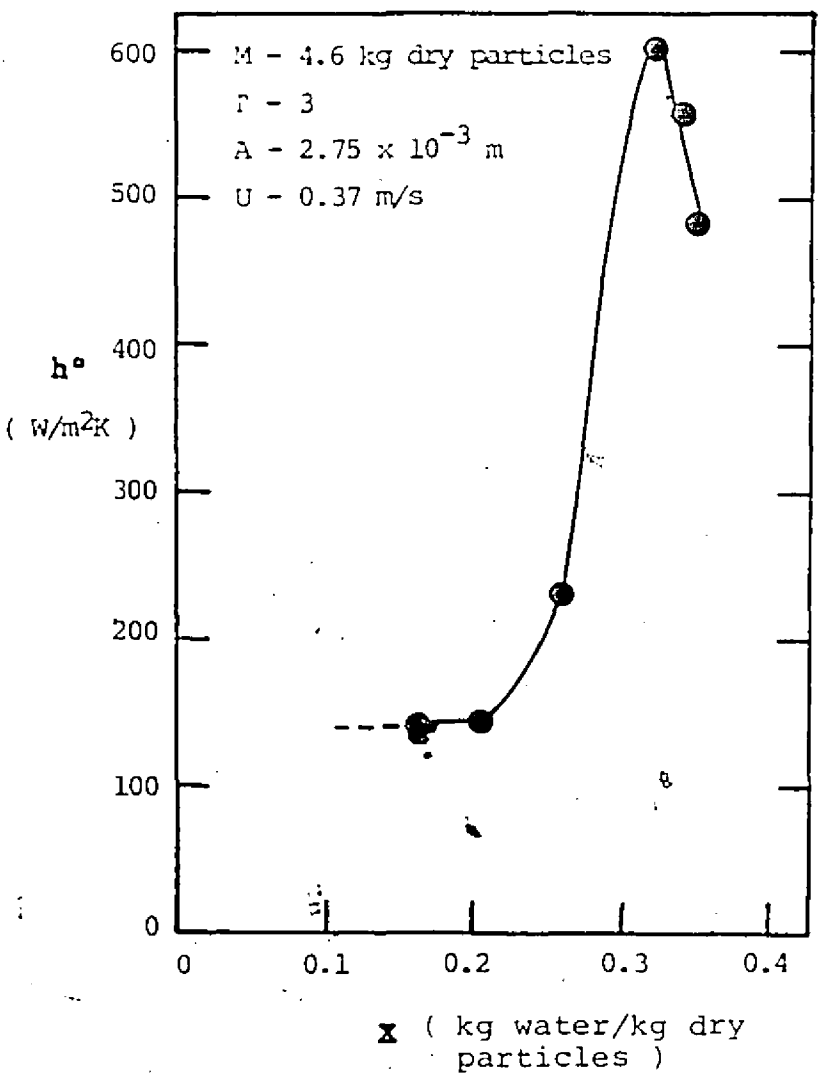

Figure 5-17 Effect of moisture content on heat transfer coefficient for molecular sieve particles, dp=1.4 mm

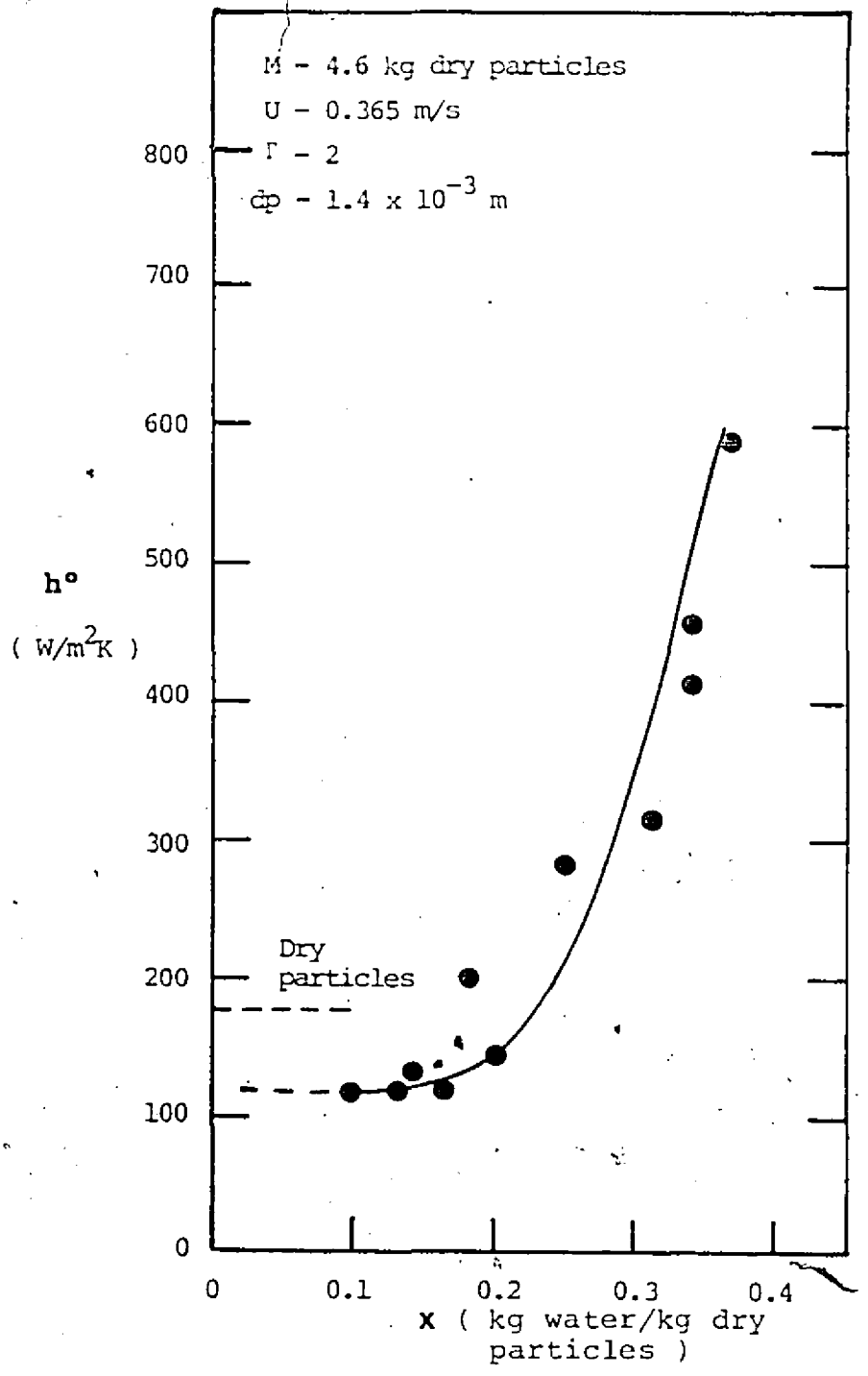

Figure 5-18 Effect of moisture content on heat transfer coefficient for molecular sieve particles

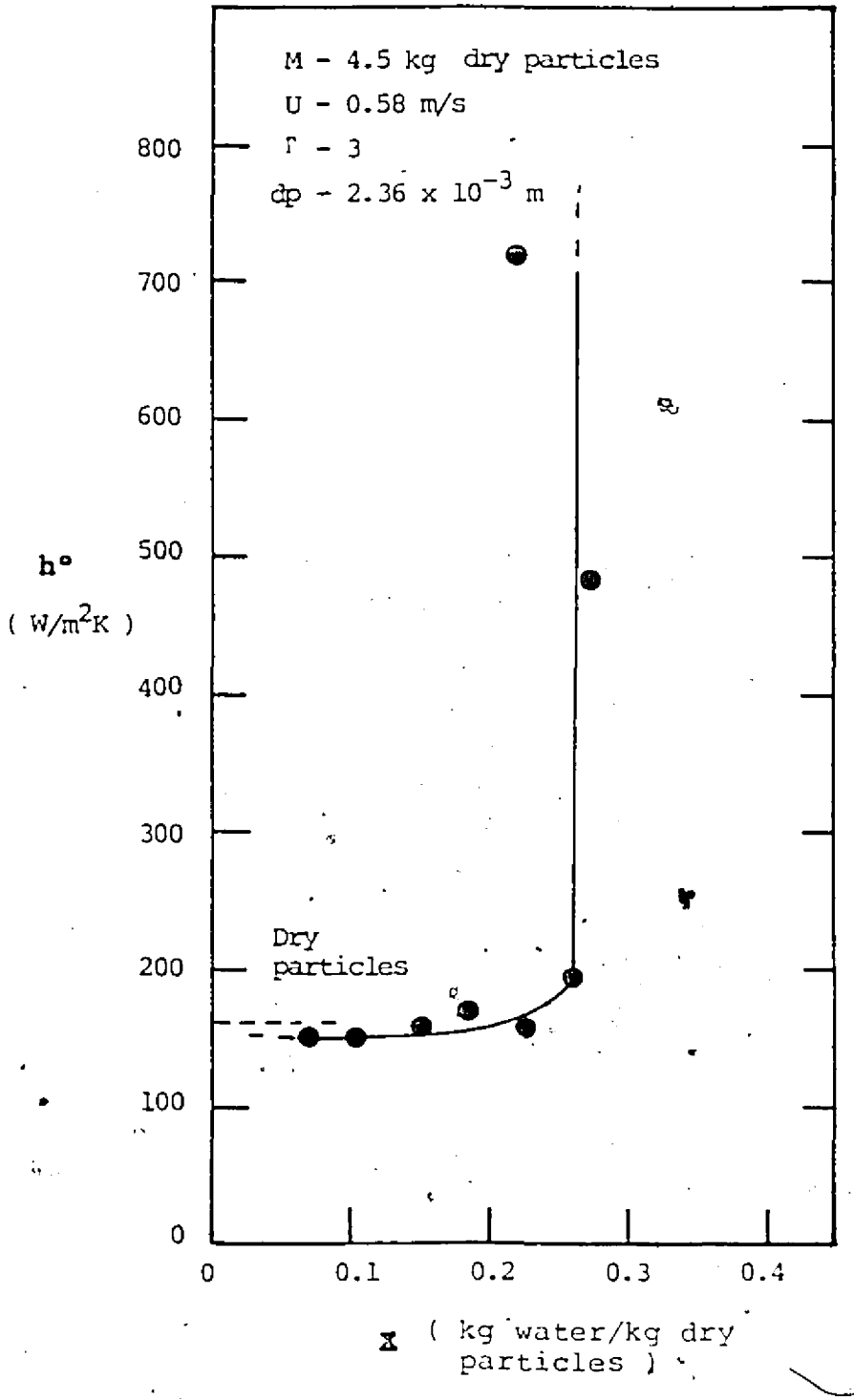

Figure 5-19 Effect of moisture content on heat transfer coefficient for molecular sieve particles

for the increase of h° from 475 W/m²K at X=0.35 to about 600 W/m²K at X=0.30 as can be seen from Figure 5-17. Note that this effect was not observed in all the runs. With decrease in X, h° also decreased markedly.

Presence of moisture is expected to increase the effective thermal conductivity of the porous molecular sieve material, although not very significantly (thermal conductivity of water is only 4% higher than that of molecular sieve particles), as demonstrated by Toei (1984). Therefore the moisture and thermal diffusivity values are not expected to increase h° significantly with an increase in X.

It is noteworthy that the decrease in h° occurs in the vicinity of the critical moisture content of the particles. Below X=0.20, the heat transfer values approach those obtained earlier for dry particles. Indeed, in the experiments the measured values were slightly lower than those obtained for dry particles, due to formation of a thin film of molecular sieve material on the cylinder as mentioned earlier. The fact that below X≤Xc h° approaches h substantiates the proposed argument that the rise in h° is predominantly due to the presence of surface moisture and evaporation mechanism, rather than to the internal particle characteristics.

Figures 5-20 and 5-21 depict the effect of air flow and vibrational acceleration on h° versus X curves respectively. It may be noticed from Figure 5-20 that the shape of the h° versus X curve remains unaltered with an increase in air flow. As expected the final value of h° is greater for higher air flow

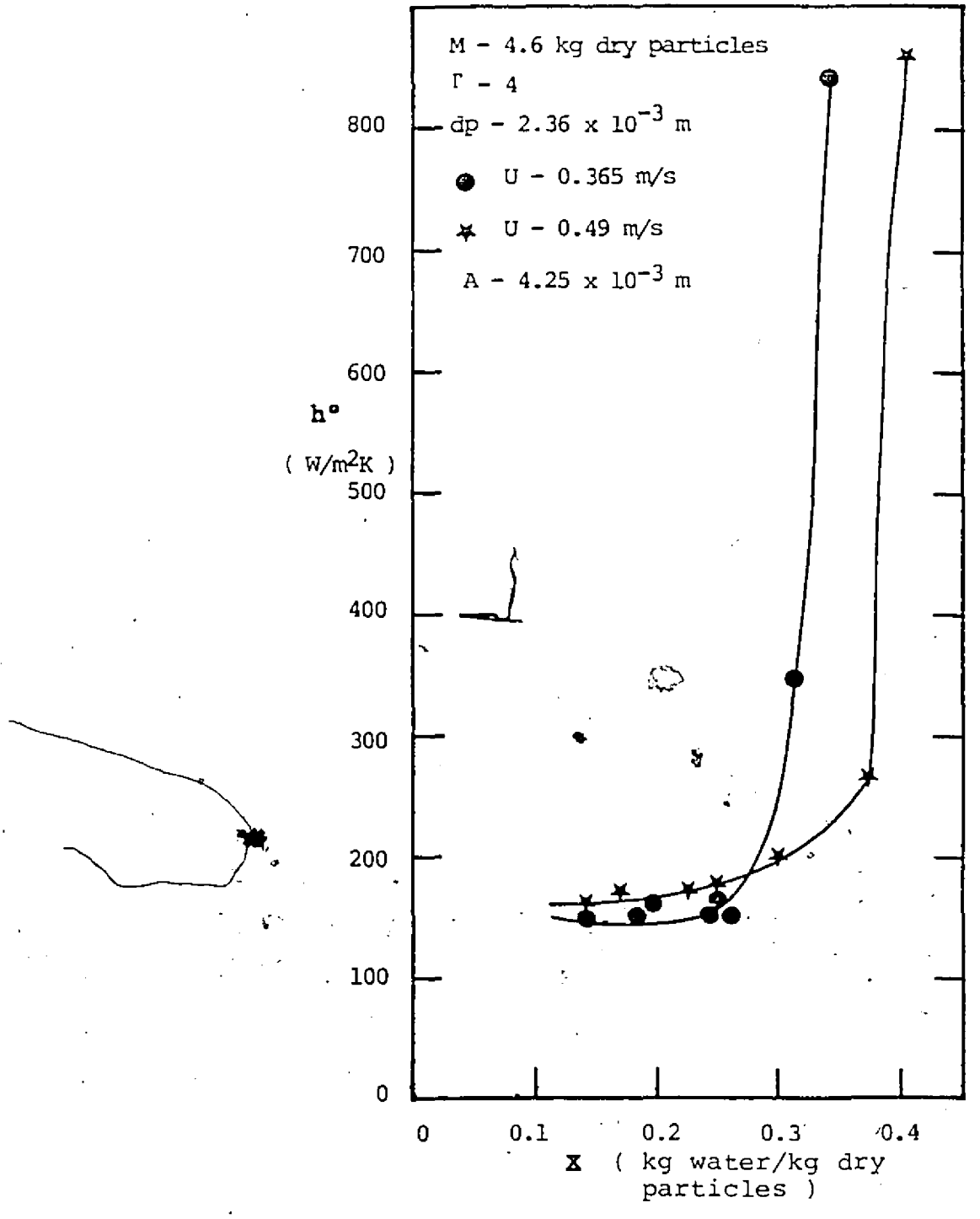

Figure 5-20 Effect of air flow on heat transfer for wet molecular sieve particles

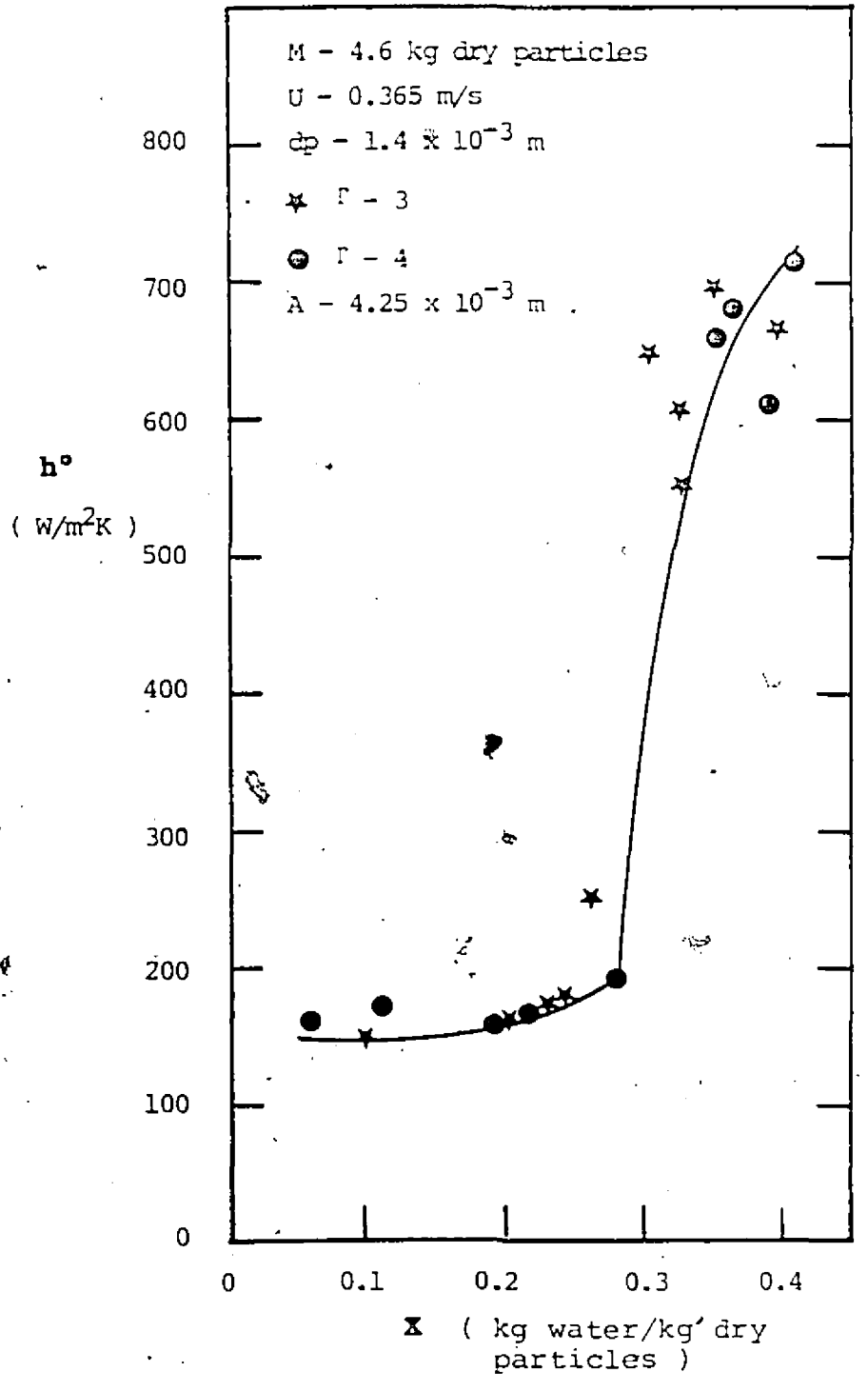

Figure 5-21 Effect of vibrational acceleration on heat transfer for wet molecular sieve particles

rate. Due to different initial moisture distribution in the bed the two curves do not match at high values of X although the heat transfer coefficients are almost identical.

Figure 5-21 shows that vibrational acceleration beyond the level required for good mixing has no apparent effect on h°. From the above discussions it can be concluded that effect of vibrational acceleration ($\Gamma \geq 2$) and air flow ($U/Umf \leq 1$) on h° is insignificant.

It is observed from Figures 5-17 through 5-21 that the maximum value of h° for $X > Xc$ is greater for larger particles as compared to smaller ones; reduced initial mixing in beds of smaller particles leads to a lower heat transfer as compared to larger particles.

Only exploratory experiments were carried out in this study to demonstrate the rather dramatic effect of water evaporation on contact heat transfer- a phenomena that has apparently not been examined at all in the open literature. Further work is needed to quantify and then model this very important practical problem in contact drying of granular solids.

5.3 HEAT TRANSFER MECHANISM

5.3.1 Introduction

The average overall wall-to-bed heat transfer coefficient for any granular bed (packed, agitated or fluidized) consists of three parallel mechanisms: particle convection, gas convection and radiation.

$$h = he + hg + hr$$

A brief description for each of the above mentioned heat transfer components is given in Chapter 2. For beds operating at low temperatures (<800 K) radiative component of heat transfer is negligible as compared to the others.

At low aeration rates i.e. U/Umf≤1 and small particle sizes (dp<1 mm) the gas convective heat transfer component contributes marginally (less than 5%) towards the overall heat transfer. At higher aeration rates (U/Umf≥3) and large particle sizes (dp>3 mm) the particle convective heat transfer becomes small (<15%) as compared to the gas convective heat transfer.

A detailed explanation of the particle and gas convective heat transfer mechanism is presented later in this chapter.

5.3.2 The Model

In a VFB particle-free air gaps are observed around the immersed surfaces as discussed in depth in the preceding chapter. These particle-free air gaps act as poor conductors of heat, lowering the efficiency of the system. On the other hand these gaps effectively reduce the contact time between the bed and the surface as shown in Figure 5-22. Moreover, it is postulated that it is the extent of coverage of the gaps rather than its width that is important in determining the overall heat transfer rate.

The following assumptions were proposed in modelling the

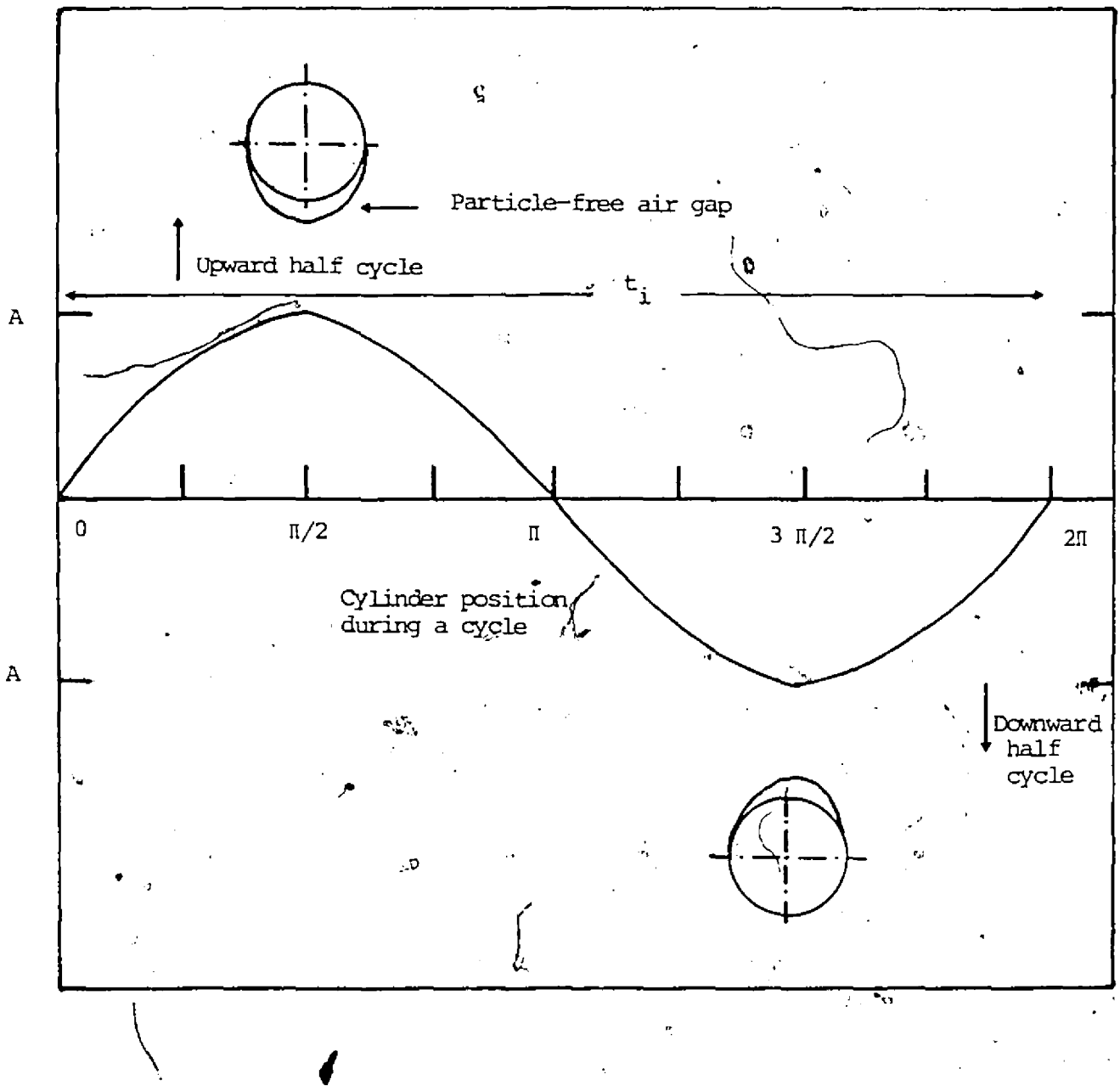

Figure 5-22 Extent of gap around a circular cylinder as a function of cylinder position

immersed surface-to-bed heat transfer in A VFB.

1. The model is applicable for well-mixed beds i.e. in regimes of moderate and vigorous mixing (Figure 4-8).
2. The particles are assumed to be spherical.
3. The air gaps around the immersed cylinder are assumed to be particle-free.
4. The extent and width of gaps used in calculations are at the peak positions of cylinder vibration cycle i.e. at $\pi/2$ and $3\pi/2$ in Figure 5-22. These measurements were made visually and are subject to uncertainty of at least 10-15 %.
5. The amplitude of vibration has no effect on the heat transfer rate (contact time) and the contact time is only a function of frequency of vibration. (This is clearly an oversimplification for the purpose of development of a simple model.)
6. The bed porosity is assumed to be independent of the amplitude of vibration.
7. The gas convective component of heat transfer is neglected for $U/Umf \leq 0.6$.
8. Radiative heat transfer is negligible because of the low temperature differences used.
9. The extent of the gap is assumed to remain the same and only the gap width changes with position in the vibration cycle.

In order to include the effect of particle-free air gaps

that develop in a VFB the overall heat transfer equation can be written as:

Overall heat transfer = (particle convective heat transfer in surface-to-particle contact region) + (gas convective heat transfer in surface-to-particle contact region) + (heat transfer in particle-free gap zone)

$$he = (1 - \theta/360)(he + hg) + hv\theta/360 \quad .... \ 5.3.1$$

where θ is the extent of coverage of gap in degrees around the cylinder, during one half cycle of the cylinder vibration and hv is the heat transfer coefficient for the particle-free air gaps (Figure 4-20).

The heat transfer coefficient for the gaps, hv, was calculated using the following correlation (Perry and Chilton (1973)).

$$hv = Cr (Re)^{m} (Pr)^{1/3} Ks/D \quad ..... \ 5.3.2$$

where

Cr = 0.911, m = 0.385 for Re = 4 - 40

Cr = 0.683, m = 0.466 for Re = 40 - 4000

Equation 5.3.2 predicts the heat transfer coefficient for gas flow over a circular cylinder with its axis perpendicular to flow. The observation that the air gaps around the immersed cylinder are essentially particle free allows the use of above correlation to determine hv.

The evaluation of particle and gas convective heat transfer components of equation is discussed below.

Suarez et al (1983) determined experimentally and modelled instantaneous azimuthal heat transfer coefficients for a heated horizontal cylinder immersed in a three-dimensional air fluidized bed. They also performed flow visualization studies in a two-dimensional bed to evaluate the applicability of the heat transfer model. The model consisted of two regions around the submerged cylinder - fluidized and unfluidized., The heat transfer from the fluidized region was evaluated by determining the particle convective heat transfer coefficient,, he, while the unfluidized region was assumed to behave like a moving bed.

5.3.3 Particle Convective Heat Transfer

The particle convection model presented by Schlunder (1982) proposes three basic mechanisms as follows:

(i) wall-to-particle heat transfer

(ii) heat conduction in packed beds

(iii) heat convection by particle motion

Wall-to-Particle Heat Transfer

The minimum heat transfer resistance between a rigid wall and an adjacent sphere is built up by heat conduction through the gaseous gap between the wall and the sphere. Taking into account the discontinuity effect at the interfaces, Schlunder(1982) proposed the local wall-to-particle heat transfer coefficient due to heat conduction as:

$$hp,loc = (K_f/(S + \; + 6)) \qquad .... \; 5,3.3$$

where

$$\; = 2\Lambda(2/\gamma - 1)$$

where K_f is the thermal conductivity of the interstitial gas, S is the local gap width between the surfaces of the wall and sphere, 6 is the sum of the roughnesses of both the surfaces, Λ is the mean free path of the gas molecules and γ is the accomodation coefficient.

Integration of Equation 5.3.3 yields the average value hp with respect to the projection area of the sphere as :

$$hp = 4K_f/dp((1 + 2(\sigma + 6)/dp)\ln(1 + dp/2(\sigma + 6)) - 1) \qquad ..... \; 5.3.4$$

The above equation gives the maximum possible surface-to-bed particle heat transfer coefficient i.e. under the condition of contact time tending to zero (Schlunder (1982), Martin (1981), Bock and Molerus (1980)).

The mean free path of the gas molecules is given by

Martin (1981) as

$$\Lambda = 16/5 \left(RT/2\pi m \right)^{1/2} \left(\mu/p \right) \qquad \ldots\ldots 5.3.5$$

Martin (1981) has also given an empirical equation for the accomodation coefficient γ. For air γ (310 K) = 0.9.

Equation 5.3.4 is valid for heat exchange between a single particle and a wall. For heat transfer to a fixed bed, it is necessary to take into account the voids which exist between the particles at the wall and which contribute only negligibly to heat exchange. On the average the voids are approximately equal to the bed porosity, i.e. the ratio of the free volume between the particles to the total volume of the fixed bed. Therefore the maximum heat transfer coefficient between a fixed bed and the wall can be written as (Heyde and Klocke (1980), Martin (1981), Bock and Molerus (1980), Bock (1981)):

$$hs = hp(1 - \psi) \qquad \ldots\ldots 5.3.6$$

Heat Conduction in Packed Beds

The heat transfer coefficient for the heat conduction in packed beds was first proposed by Mickley and Fairbanks (1955) under the condition of isothermal wall as

$$hc = 2(KsCp\rho p(1 - \psi)/(\pi t))^{1/2} \qquad \ldots\ldots 5.3.7$$

where t is the contact time between the bed and the wall.

It should be pointed out that the Ks value used in this

equation is the thermal conductivity of the bed over the entire r range and not the average of the fluid thermal conductivity and bed thermal conductivity as was the case for evaluating the Nusselt number, in the appropriate mixing regime in VFB's.

The effect of heat convection by particle motion on the heat transfer can be neglected if the bulk material particles are mixed perfectly (Toei et al (1984)). This limits the application of the proposed heat transfer model to regimes of moderate and vigorous mixing (Figure 4-8) i.e. when the temperature gradients in the bed are almost negligible.

Overall Particle Convective Heat Transfer

The overall particle convection heat transfer can be considered to comprise of a resistance in the wall-to-bed heat transfer in series with that of heat conduction in packed beds. The average particle convective heat transfer coefficient can then be written as (Bock and Molerus (1981), Heyde and Klocke (1980), Martin (1981), Toei et al (1984)):

$$1/he = 1/hs + 1/hc$$

or

$$1/he = 1/(hp(1-\psi) + (\pi^{1/2}/2)(t/(KsCp\rho p(1-\psi))^{1/2}) \quad \ldots\ldots\ldots 5.3.8$$

It should be noted from Equation 5.3.8 that for low contact times ($t<<1$) the second term on the right hand side

becomes insignificant compared to the first one, i.e. the contact resistance of the gaseous gap dominates and the heat transfer coefficient depends upon the thermal conductivity of the gas, particle size and bed voidage (Equation 5.3.4). For large contact times (t>>1) the value $KsCp\rho p(1 - \psi)$ of the emulsion phase is the dominant factor. Therefore in the limiting cases we have:

$$he = hp(1 - \psi) \qquad \text{as } t - 0$$

and

$$he = 2/(\pi)^{1/2}((\ KsCp\rho p(1-\psi))/t\ )^{1/2} \qquad \text{as } t - \infty$$

Equation 5.3.8 is a general one and can be applied for packed, agitated, moving or fluidized beds. Since in a conventional fluidized bed there are two phases- bubble and emulsion, Equation 5.3.8 has to be modified slightly. Bubbles act as voids and contribute almost nothing towards the heat transfer process and therefore the overall particle convective heat transfer coefficient for a CFB can be written as (Bock and Molerus (1980), Martin (1981), Heyde and Klocke (1980)):

$$1/he' = (1/(1 - \psi)(1/he) \qquad \ldots\ldots 5.3.10$$

where ψ is the mean volume fraction of the bubbles in the bed and around the immersed surface and he' is the particle convective heat transfer coefficient for CFB's.

It can be seen from Equation 5.3.10 that in a CFB an

increase in bubble fraction decreases the heat transfer rate. On the other hand an increase in porosity (higher air flowrates) is accompanied by reduced contact time which enhances the heat transfer rate. The counteracting effects of these two phenomena give rise to an optimum heat transfer coefficient for CFB's.

Contact Time

The most important step in evaluation of he is the calculation of contact time. For conventional fluidized beds a number of correlations are available. Martin (1981) considers the contact time to be proportional to the time taken to cover a path with length of one particle diameter in free flight (i.e. t = dp/Up, where Up is the particle velocity).

Bock and Molerus (1981) defined the contact time of the emulsion phase in a CFB as

$$t = (1 - \varepsilon)/f_B \qquad \ldots\ldots$$

where f_B is the local bubble frequency in vicinity of the immersed surface.

In the above equations for contact time the problem lies in evaluating Up or f_B. Baskakov et al (1973) proposed a very comprehensive empirical correlation for evaluating the contact time as

$$t = 0.44(dp\ g/(Umf^2(U/Umf-a)^2)^{0.15}(dp/D)^{0.225}\ s \qquad \ldots\ldots \quad 5.3.11$$

where 'a' is an empirical constant allowing for effects of probe diameter and particle shape. It tends to diminish as the probe diameter increases and as the particles become more spherical.

Baskakov et al (1973) also determined an empirical correlation for ψ - the fraction of the total time when the probe is shrouded by gas bubbles, as

$$\psi = 0.33((Umf^2(U/Umf-a)^2/dp.g)^{0.14} \quad \ldots\ldots 5.3.12$$

The advantage of Equations 5.3.11 and 5.3.12 lies in the fact that $t \neq \infty$ and $\psi \neq 0$ at U=Umf. This is attributed (Baskakov et al (1973)) to a tendency for a void to form beneath the cylindrical obstruction even at U≤Umf. Bubbles periodically form from this void and rise along the probe surface causing particle movement even before the bed is fluidized. Equation 5.3.11 was thus used to evaluate contact time for U/Umf≥0.9 and r>1 for a vibrated bed, when the effect of vibration diminishes and bubbling initiates throughout the bed (Figure 4-20).

For a rigidly mounted cylinder in a VFB, the contact time of the particles with the immersed surface is dependent upon the frequency of vibration and the formation of particle-free air gaps around the immersed surface. Figure 5-22 displays the proposed mechanics of bed and immersed surface interaction.

Figure 5-22 shows one full oscillation of the immersed cylinder. On the upward swing there is a particle-free air gap below the cylinder and a particle free air gap above it on its

downwards swing. The gaps shown are the peak gaps observed at cylinder positions $\pi/2$ and $3\pi/2$. It is assumed that during the upper half of the cycle there is always a lower gap present and for the bottom cycle there is always a top gap present. The variations of these gaps as a function of cylinder position was not examined; it is recognized that this might play an important role in determining the exact mechanism of heat transfer. In the current study only the peak gaps were used in all model calculations. High speed cine photography may be employed to examine this aspect in depth in future.

It can be seen from Figure 5-22 that in the upper half cycle only the top half of the cylinder contacts the bed while in the lower cycle the bottom half contacts the bed. Since the time period of oscillation, t_o, is

$$t_o = 1/f$$

the contact time can be written as

$$t = 1/2f \qquad \ldots\ldots 5.3.13$$

It should be pointed out that this model completely ignores the amplitude of vibration - a parameter which has a significant effect on heat transfer as verified experimentally (Malhotra and Mujumdar (1984)). Equation 5.3.13 was used to evaluate the contact time for $U/U_{mf}<0.9$ over the entire range of r in for well mixed beds.

Equation 5.3.13 is only valid for regimes of moderate and

vigorous mixing when gaps start forming. This model is therefore not valid for poorly mixed beds as stated earlier.

Suarez et al (1983) defined the contact time for the fluidized region around the immersed cylinder as the time between successive minimum values of the experimentally determined instantaneous heat transfer coefficients. The discrepancy between their predicted and experimental results was about 17 percent.

Heat Transfer in a Poorly Mixed VFB

In the region of poor mixing the bed can be considered as cyclically moving past the immersed cylinder and the corresponding contact times calculated knowing the particle circulation rates. Toei et al (1984a, 1984b) have performed studies in a bed agitated by a circumferentially moving heat source (impeller). They calculated the particle contact time as the ratio of the length of circumference to the impeller speed. However, in the current study the particle circulation rates were not determined and therefore a theoretical approximation of the heat transfer coefficient in the poorly mixed regime could not be obtained.

The case of $r=0$ and $0 \leq U/Umf \leq 0.9$ is the packed bed with/without air flow. Correlations to predict the heat transfer coefficients have been given by Adams (1981), Perry and Chilton (1973), Wakao and Kaguei (1982) and Gabor (1970), among others.

Gabor (1970) proposed the following correlation to

predict the heat transfer coefficient from immersed circular cylinders to packed beds:

$$h = (4KsC_f U\rho /(\pi L))^{1/2} + Ks/D \qquad \ldots\ldots\ldots 5.3.14$$

where L is the heater length.

The above correlation predicts very low values of h as compared to experimentally obtained values. Table 5.2 shows the experimental and predicted values of immersed surface heat transfer coefficient for packed beds. The large deviation for smaller particles as compared to larger ones can be seen from Table 5.2.

For U/Umf=0 and Γ=0 Equation 5.3.14 reduces to

$$h = Ks/D \qquad \ldots\ldots\ldots 5.3.15$$

This means that for U/Umf=0 and Γ=0 the heat transfer coefficient is a function of bed thermal conductivity and cylinder diameter only.

5.3.4 Gas Convective Heat Transfer

The second component in evaluation of the overall heat transfer coefficient is the gas convective one (hg). Gas convection is the direct wall-to-bed heat transfer over those parts of the surface which are not in contact with particles. An increase in particle size leads to an increase in Umf and hence an increase in the convective heat transfer for a given

TABLE 5.2

Comparison Between Experimental and Predicted (Gabor (1970))

Values for h at r=0

Particle Type	dp mm	U/Umf	h(pred) W/m²K	h(expt) W/m²K
Glass ballotini	0.325	0	3.7	18.0
Glass ballotini	0.325	0.3	13.5	28.5
Glass ballotini	0.325	0.6	17.5	36.5
Glass ballotini	0.325	0.9	21.0	84.5
Glass ballotini	1.017	0	3.7	19.5
Glass ballotini	1.017	0.4	29.0	54.0
Glass ballotini	1.017	0.8	37.5	86.0
Molecular sieve	1.4	0	3.3	----
Molecular sieve	1.4	0.3	24.0	37.0
Molecular sieve	1.4	0.6	35.0	49.0
Molecular sieve	1.4	0.9	44.0	114.0
Molecular sieve	2.36	0	3.3	7.0
Molecular sieve	2.36	0.6	45.0	39.0
Molecular sieve	2.36	0.9	59.0	87.0

U/Umf value.

Baskakov et al (1973) measured the rate of sublimation from napthalene coated cylindrical surfaces immersed in fluidized beds to evaluate the gas convective heat transfer coefficient. The best fit to their experimental data for hg yielded

$$hg = (K_f/dp)\ 0.009\ Pr^{0.33}\ Ar^{0.5}\ (U/Uopt)^{0.3} \qquad \ldots\ldots\ldots 5.3.16$$

The above equation is valid for U>Umf. However, this equation was used for evaluating hg for U/Umf≥ 0.6 for large particles (dp> 1 mm) in this thesis. This assumption did not lead to any significant error due to low air flowrates used because of the relative insignificance of the gas convective heat transfer as compared to particle convective heat transfer in a VFB as shown later.

It can be seen from Equation 5.3.16 that hg is proportional to dp while he decreases with an increase in particle diameter. Therefore at high air flowrates (U≥Uopt) in a CFB of large particles (dp>3 mm) the average heat transfer coefficient, h, is made up primarily of hg (> 75%). For dp>4.5 mm, h is nearly entirely made up of the gas convective heat transfer term.

5.3.5 Radiation Heat Transfer

The third component making up the overall heat transfer

coefficient is the radiative one. Since radiative heat transfer becomes significant only at high temperatures (T>800 K) as reported by Baskakov et al (1973), it will not be discussed here. The maximum bed and surface temperatures in this study are less than 330 K. Correlations predicting the radiative heat transfer coefficient can be found in Martin (1981), Baskakov et al (1973) among others.

5.3.6 Theoretical Prediction of Overall Heat Transfer Coefficient

Table 5.3 summarizes the equations used in modelling the immersed surface-to-bed heat transfer in a VFB.

Tables 5.4 through 5.8 tabulate the various parameters used in predicting the overall heat transfer coefficient. The average bed porosity and the extent of gaps have been estimated from Figures 4-4 and 4-22. It should be noted that the model employed overlooks the effects of amplitude of vibration and cylinder diameter.

The deviation between experimental and predicted values of h is very significant at U/Umf=0 and r=1.5 for all the particles. This deviation is less significant for larger size particles possibly due to the much lower values of hp for larger particles as compared to the smaller ones, i.e. the second term in Equation 5.3.8 is comparable to the first one for larger particles. The above discrepancy is explained in details as follows.

It can be seen from Table 5.3 that when the extent of the

TABLE 5.3

Comparison of CFB and VFB Heat Transfer Models

Conventional Fluidized Bed

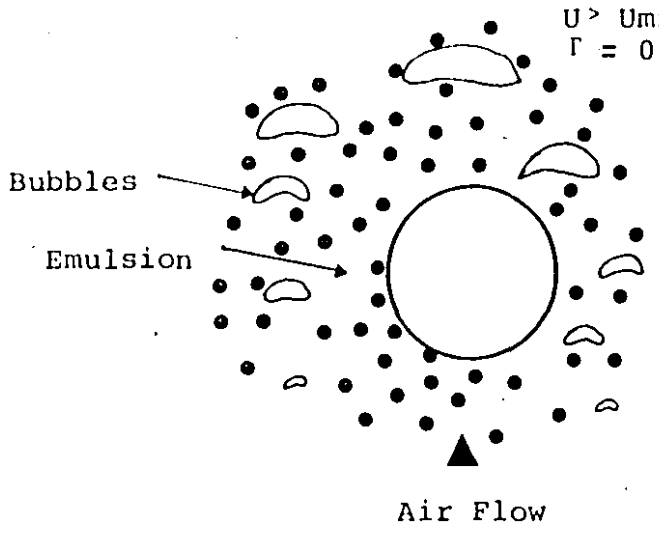

Overall Heat Transfer Coefficient

$$h = he + hg$$

Particle Convective Heat Transfer

$$1/he' = (1/(1 - \psi_B)(1/he)$$

..... 5.3.10

Vibrated Fluidized Bed

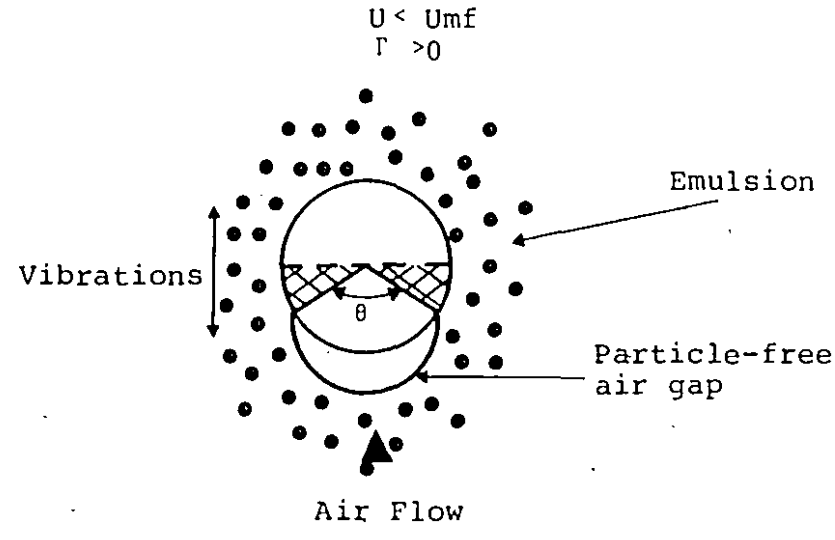

Overall Heat Transfer Coefficient

$$h = (1 - \theta/360)(he + hg) + hv\theta/360$$

.... 5.3.1

Particle Convective Heat Transfer

$$1/he = 1/(hp(1-\psi) + (\pi^{1/2}/2)(t/(KsCp\rho p(1-\psi))^{1/2}$$

..... 5.3.8

-continued-

TABLE 5.3 (CONTINUED)

Gas Convective Heat Transfer Coefficient

$$hg = (K_f/dp)\ 0.009\ Pr^{0.33}\ Ar^{0.5}\ (U/Uopt)^{0.3}$$

U > Umf 5.3.16

Contact Time

$$t = 0.44(dp\ g/(Umf^2(U/Umf-a)^2)^{0.15}(dp/D)^{0.225}\ s$$

..... 5.3.11

U >Umf

Contact Time

$$t = 1/2f$$ 5.3.13

U/Umf $\leq$0.6

Mixing regimes II & III
(Figure 4-8)

$$t = 0.44(dp\ g/(Umf^2(U/Umf-a)^2)^{0.15}(dp/D)^{0.225}\ s$$

..... 5.3.11

U/Umf $\geq$ 0.9

Bubble Fraction in the Bed

$$\Psi_B = 0.33((Umf^2(U/Umf-a)^2/dp\ g)^{0.14}$$

..... 5.3.12

Heat Transfer Coefficient for Particle-Free Air Gaps

$$hv = Cr\ (Re)^m (Pr)^{1/3} Ks/D$$ 5.3.2

where

Cr = 0.911, m = 0.385 for Re = 4 - 40

Cr = 0.683, m = 0.466 for Re = 40 - 4000

TABLE 5.4

Theoretical Prediction of Overall Heat Transfer Coefficient

Glass ballotini, dp=0.325 mm, D=38.1 mm dia

A=4.25 mm, U/Umf=0

r	1.5	2	3	4
hp (W/m^2K)	1875	1875	1875	1875
Ks (W/mK)	0.141	0.141	0.141	0.141
t (s)	0.053	0.046	0.0375	0.0325
ψ	0.35	0.40	0.41	0.44
he (W/m^2K)	761	731	746	730
hg (W/m^2K)	0	0	0	0
hv (W/m^2K)	0	0	0	0
θ	0	15	60	120
h (W/m^2K)	761	701	622	487
h(expt) (W/m^2K)	225	458	400	390
% error	238	53	55	22

U/Umf=0.3

r	1.5	2	3	4
hp (W/m^2K)	1875	1875	1875	1875
Ks (W/mK)	0.142	0.142	0.142	0.142
t (s)	0.053	0.046	0.0375	0.0325
ψ	0.466	0.477	0.489	0.513
he (W/m^2K)	651	653	662	649
hg (W/m^2K)	0	0	0	0
hv (W/m^2K)	3	3	3	3
θ	40	80	150	180
h (W/m^2K)	579	509	387	326
h(expt) (W/m^2K)	431	443	--	401
%error	34	15	--	19

TABLE 5.4 (CONTINUED)

U/Umf=0.6

r	1	1.5	2	3
hp (W/m^2K)	1875	1875	1875	1875
Ks (W/mK)	0.143	0.143	0.143	0.143
t (s)	0.065	0.053	0.046	0.0375
ψ	0.45	0.47	0.497	0.506
he (W/m^2K)	641	645	633	644
hg (W/m^2K)	0	0	0	0
hv (W/m^2K)	4	4	4	4
θ	120	145	160	180
h (W/m^2K)	429	387	353	324
h(expt) (W/m^2K)	268	409	404	--
%error	60	5.1	12.5	--

U/Umf=0.9

r	0.5	1	1.5	2	3	4
hp (W/m^2K)	1875	1875	1875	1875	1875	1875
Ks (W/mK)	0.144	0.144	0.144	0.144	0.144	0.144
t' (s)	0.140	0.133	0.200	0.200	0.200	0.200
ψ	0.44	0.484	0.501	0.506	0.513	0.525
he (W/m^2K)	547	526	465	461	456	448
hg (W/m^2K)	25	25	25	25	25	25
hv (W/m^2K)	5	5	5	5	5	5
θ	40	120	145	160	180	190
h (W/m^2K)	509	369	294	272	243	215
h(expt) (W/m^2K)	253	338	376	341	--	271
%error	100	9.25	22	20	--	21

TABLE 5.5

Theoretical Prediction of Overall Heat Transfer Coefficient

Glass ballotini, dp=0.595 mm, D=38.1 mm dia

A=4.25 mm, U/Umf=0

r	1.5	2	3	4
hp (W/m^2K)	1132	1132	1132	1132
Ks (W/mK)	0.141	0.141	0.141	0.141
t (s)	0.053	0.046	0.0375	0.0325
ψ	0.35	0.40	0.41	0.44
he (W/m^2K)	540	513	517	501
hg (W/m^2K)	0	0	0	0
hv (W/m^2K)	0	0	0	0
θ	0	15	60	120
h (W/m^2K)	540	491	431	335
h(expt) (W/m^2K)	175	440	400	367
%error	208	12	8	9

U/Umf=0.6

r	1	1.5	2	3	4
hp (W/m^2K)	1132	1132	1132	1132	1132
Ks (W/mK)	0.149	0.149	0.149	0.149	0.149
t (s)	0.065	0.053	0.046	0.0375	0.0325
ψ	0.45	0.47	0.497	0.506	0.513
he (W/m^2K)	458	455	441	444	445
hg (W/m^2K)	0	0	0	0	0
hv (W/m^2K)	6	6	6	6	6
θ	120	145	160	180	190
h (W/m^2K)	307	274	248	225	213
h(expt) (W/m^2K)	312	375	530	325	310
%error	1.45	27	29	31	31

TABLE 5.6

Theoretical Prediction of Overall Heat Transfer Coefficient

Glass ballotini, dp=1.017 mm, D=38.1 mm dia

A=4.25 mm, U/Umf=0

r	1.5	2	3	4
hp (W/m²K)	687	687	687	687
Ks (W/mK)	0.141	0.141	0.141	0.141
t (s)	0.053	0.046	0.0375	0.0325
↓	0.37	0.408	0.417	0.43
he (W/m²K)	356	340	341	337
hg (W/m²K)	0	0	0	0
hv (W/m²K)	0	0	0	0
θ	0	15	60	120
h (W/m²K)	356	326	284	224
h(expt) (W/m²K)	215	245	228	198
%error	66	33	25	13.5

U/Umf=0.4

r	1.5	2	3	4
hp (W/m²K)	687	687	687	687
Ks (W/mK)	0.158	0.158	0.158	0.158
t (s)	0.053	0.046	0.0375	0.0325
↓	0.458	0.468	0.477	0.495
he (W/m²K)	313	311	311	303
hg (W/m²K)	0	0	0	0
hv (W/m²K)	6.5	6.5	6.5	6.5
θ	90	120	160	180
h (W/m²K)	236	210	175	155
h(expt) (W/m²K)	238	177	--	156
%error	0.6	19	--	0.5

TABLE 5.6 (CONTINUED)

U/Umf=0.8

r	1	1.5	2	3	4
hp (W/m^2K)	687	687	687	687	687
Ks (W/mK)	0.176	0.176	0.176	0.176	0.176
t (s)	0.065	0.053	0.046	0.0375	0.0325
ψ	0.468	0.481	0.495	0.501	0.503
he (W/m^2K)	305	303	298	299	301
hg (W/m^2K)	43	43	43	43	43
hv (W/m^2K)	9	9	9	9	9
θ	120	145	160	180	190
h (W/m^2K)	236	210	193	175	172
h(expt) (W/m^2K)	212	207	180	--	172
%error	11	2	7.5	--	3

TABLE 5.7

Theoretical Prediction of Overall Heat Transfer Coefficient

Molecular sieve particles, dp=1.4mm, D=38.1 mm dia

A=2.75 mm, U/Umf=0

r	1.5	2	3
hp (W/m²K)	546	546	546
Ks (W/mK)	0.126	0.126	0.126
t (s)	0.043	0.037	0.030
↓	0.385	0.40	0.415
he (W/m²K)	280	295	274
hg (W/m²K)	0	0	0
hv (W/m²K)	0	0	0
θ	90	135	160
h (W/m²K)	210	184	152
h(expt) (W/m²K)	158	184	170
%error	33	0.25	10.5

U/Umf=0.3

r	1.5	2	3
hp (W/m²K)	546	546	546
Ks (W/mK)	0.143	0.143	0.143
t (s)	0.043	0.037	0.03
↓	0.412	0.424	0.435
he (W/m²K)	271	269	268
hg (W/m²K)	0	0	0
hv (W/m²K)	5.5	5.5	5.5
θ	120	145	170
h (W/m²K)	183	164	144
h(expt) (W/m²K)	158	175	174
%error	15.5	6.5	17

TABLE 5.7 (CONTINUED)

U/Umf=0.6

r	1	1.5	2	3
hp (W/m^2K)	546	546	546	546
Ks (W/mK)	0.160	0.160	0.160	0.160
t (s)	0.055	0.043	0.037	0.030
ψ	0.408	0.415	0.425	0.437
he (W/m^2K)	270	272	270	269
hg (W/m^2K)	0	0	0	0
hv (w/m^2K)	8	8	8	8
θ	90	135	160	180
h (W/m^2K)	204	173	154	138
h(expt) (W/m^2K)	160	195	189	175
%error	26	11.5	18	22

U/Umf=0.9

r	0.5	1	1.5	2	3
hp (W/m^2K)	546	546	546	546	546
Ks (W/mK)	0.178	0.178	0.178	0.178	0.178
t' (s)	0.150	0.141	0.227	0.227	0.227
ψ	0.40	0.432	0.45	0.46	0.47
he (W/m^2K)	249	219	216	212	239
hg (W/m^2K)	36	36	36	36	36
hv (W/m^2K)	9.5	9.5	9.5	9.5	9.5
θ	90	120	135	160	180
h (W/m^2K)	216	163	144	129	187
h(expt) (W/m^2K)	157	194	176	168	209
%error	37	16	18	23	10.5

TABLE 5.8

Theoretical Prediction of Overall Heat Transfer Coefficient

Glass ballotini, dp=0.325 mm, D=38.1 mm dia

A=2.75 mm, U/Umf=0.3

r	1.5	2	3
hp (W/m^2K)	1874	1874	1874
Ks (W/mK)	0.142	0.142	0.142
t (s)	0.043	0.037	0.030
ψ	0.466	0.477	0.489
he (W/m^2K)	672	676	685
hg (W/m^2K)	0	0	0
hv (W/m^2K)	3	3	3
θ	120	150	180
h (W/m^2K)	449	396	343
h(expt) (W/m^2K)	440	437	430
%error	2	9.5	20

gap, θ, is less than 180° the contact time t=1/2f is applicable only to the sector of the cylinder covered by the angle θ i.e. the section of the cylinder shown by crossed hatched lines has a contact time different from t=1/2f. In that region the contact time can be determined from the frequency of vibration and particle circulation rates. The contact times in this case are expected to be 10-20 times higher giving much lower heat transfer rates. Unfortunately no quantitative measurements are available to verify this postulate.

The above situation can be considered analogous to heat transfer in a bed moving across a fixed heat source or a moving heat source in a fixed bed as examined by Toei et al (1984a, 1984b). Unfortunately, the particle circulation rates were not measured and therefore predictions for heat transfer coefficient using the proposed model are inaccurate for low values of θ (<120°).

A sample of the heat transfer coefficients obtained by using contact times of the order of the ones obtained in moving beds (Toei et al (1984a, 1984b)) is given below.

t = 0.5 s	h = 428 W/m²K
t = 1 s	h = 337 W/m²K
t = 2 s	h = 259 W/m²K
t = 3 s	h = 220 W/m²K

The above values of h were predicted from Equation 5.3.1 and 5.3.8 at U/Umf=0 and r=1.5 for glass ballotini particles (

dp=0.325 mm). The experimental value for the corresponding case is 225 W/m^2K (Table 5.4). It should be noted that at Γ=1.5 moderate mixing just onsets in the bed (Figure 4-8) and therefore the particle circulation velocities are low.

Pakowski and Mujumdar (1982) have reported angular velocities of circulation as high as 0.17 revolutions per sec at Γ=4 i.e. ω_p=6.28 rad/s for a cylinder immersed in the central midplane of a bed of cross section 0.20 m x 0.20 m and H=100 mm. Therefore the contact time for Pakowski and Mujumdar's (1982) case can be estimated to be $t=\omega_p/2\pi$ = 1 s (Toei et al (1984b)). Hence the contact time for Γ<4 must be higher than 1 s. For the case of Γ=1.5 the contact time can be estimated to be between 2-3 s. It can be seen from the results presented above that for t=2-3 s the predicted and experimental values of h are within 10% of each other. Therefore the knowledge of particle circulation rates can lead to good prediction of h using Equation 5.3.8.

The assumption that the extent of the gap remains constant throughout the entire cycle of vibration (Figure 5-22) is a very tentative one. It is conceivable that the gap extent as well as its width both change with the cylinder position during one oscillation and this is expected to affect the heat transfer rate significantly, i.e. the fractional area available for heat transfer changes continuously and the extent of gap at cylinder positions $\pi/2$ and $3\pi/2$ cannot be used in a more comprehensive model.

Further work to determine the instantaneous extent of gap

as a function of cylinder position during one cycle of vibration and measurements of particle circulation rates is essential to get a better insight into the mechanism of heat transfer and to develop a better physical and mathematical model of the phenomenon.

In view of the aforementioned assumptions and the fact that at $\theta<180°$ the particle contact time, $t=1/2f$, is valid only for the cylinder surface covered by angle θ, the model should not predict the results accurately for $\theta<180°$. However, the predicted and experimental values of h for $\theta>120°$ were found to be within 25% of each other for all the particles i.e. the heat transfer coefficients for the moving bed region (the surface of the cylinder covered by angle $(180-\theta)°$) are not low enough to affect the overall heat transfer coefficient significantly. Therefore, the model seems to predict the overall heat transfer coefficient reasonably well for $\theta>120°$ (the regimes of moderate and vigorous mixing for $U/Umf\geq 0.3$).

The relative significance of the three components of the overall heat transfer coefficient - he, hg and hv can be seen from Tables 5.4 through 5.8. For non-aerated beds h is made up entirely of he while for $U/Umf\leq 0.6$ hg and hv are negligible compared to he. At higher air flow i.e. $U/Umf=0.9$ the contribution of hg towards h is 5% for smaller particles and 12% for larger particles. Heat transfer through the gaps makes up less than 2% of the total contribution, according to the proposed model.

The effect of amplitude of vibration on predicted values

of h for glass ballotini(dp=0.325 mm) at U/Umf=0.3 can be seen from Tables 5.4 and 5.8. It can be observed that predicted values of h are greater for higher amplitude (A=4.25 mm.) as compared to the smaller amplitude (A=2.75 mm), although the contact times are lower for smaller amplitude at the corresponding values of Γ.

The above effect can be attributed to the fact that at lower amplitude the extent of gaps is larger (although the width is smaller) as compared to higher amplitude for corresponding values of Γ. On the other hand the bed porosity is assumed to remain constant for both amplitudes of vibration.

The overall heat transfer coefficient is primarily dependent on the particle convective heat transfer. The parameters affecting the particle convective heat transfer, he are - particle size, bed porosity, contact time, bed thermal conductivity, particle density and particle heat capacity. For given particle specifications the heat transfer coefficient is primarily a function of bed porosity and contact time. A 10% increase in bed porosity leads to a 5% decrease in heat transfer while a 10% increase in contact time decreases the heat transfer by 2%, for glass ballotini, dp=0.325 mm.

However, it should be noted that discrepancy in estimation of contact times may be as high as 50 - 100% (changes heat transfer rates by 8-12%) and therefore it is essential to estimate the contact time and bed porosity both as accurately as possible. Moreover the bed porosity is a function of bed height a phenomenon not examined in this study.

It should however be noted that the effect of contact time on overall heat transfer becomes more significant with an increase in particle size. For example a 50% increase in the contact time for glass ballotini (dp=1.017 mm) leads to a decrease of 14% in overall heat transfer coefficient as compared to 8% for the smaller glass ballotini (dp=0.325 mm).

Comparison of Table 5.7 and Figure 5-3 shows that the theoretical model does not predict higher heat transfer coefficients for higher U/Umf ratios over the entire range of r for molecular sieve particles. The model based on gaps and contact time predicts a slight decrease in heat transfer coefficient with an increase in U/Umf for all particles due to an increase in bed porosity. This discrepancy for the molecular sieve particles could not be accounted for in terms of the assumptions and the model used.

Figures 5-23 through 5-25 show a graphical representation of some typical results of Tables 5.4 through 5.8. The experimental and predicted values are marked on the figures. It should be noted that only the lower gaps are shown in these figures i.e. these figures refer to the upper half of the vibration cycle. No predictions could be made for the zone of poor mixing, while the predicted values for r=0 were obtained from Equations 5.3.14 and 5.3.15.

The model presented in Table 5.3 can in principle, be applied also to wet and sticky particles. The domain of its application shrinks due to an expanded region of poor mixing for sticky particles. Moreover, it is essential to obtain the

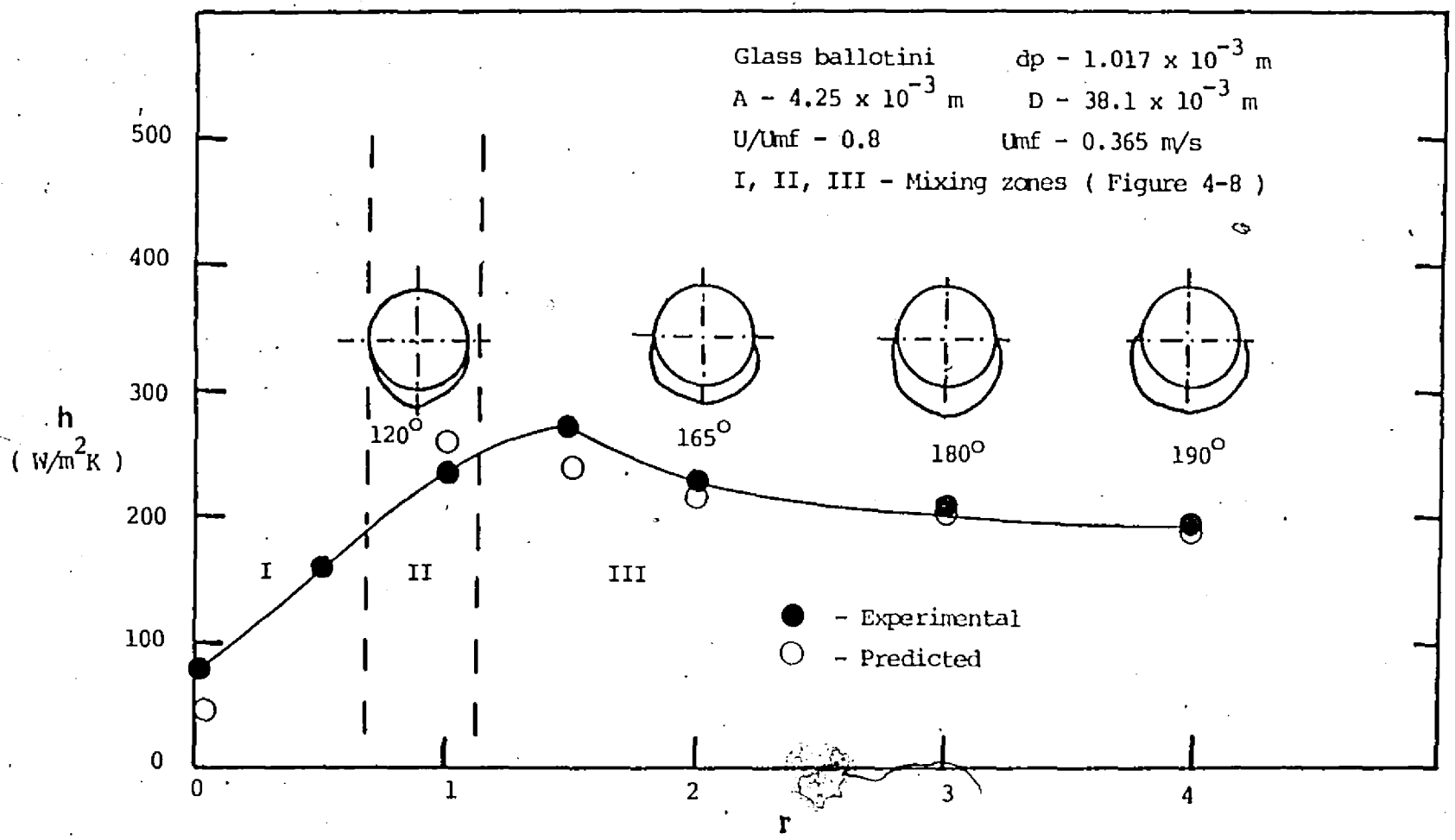

Figure 5-23 Comparison between experimental and predicted values of h

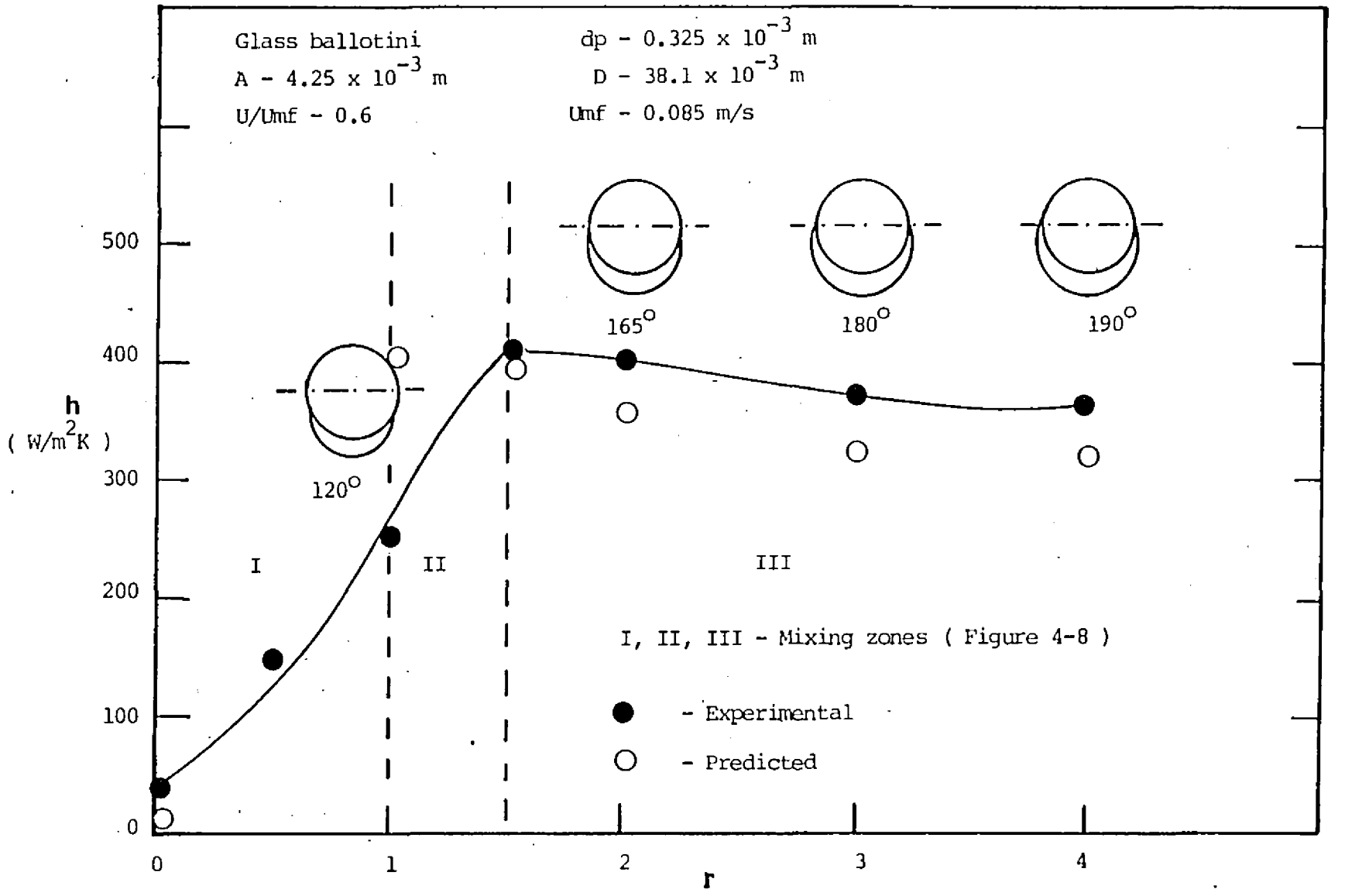

Figure 5-24 Comparison between experimental and predicted values of h

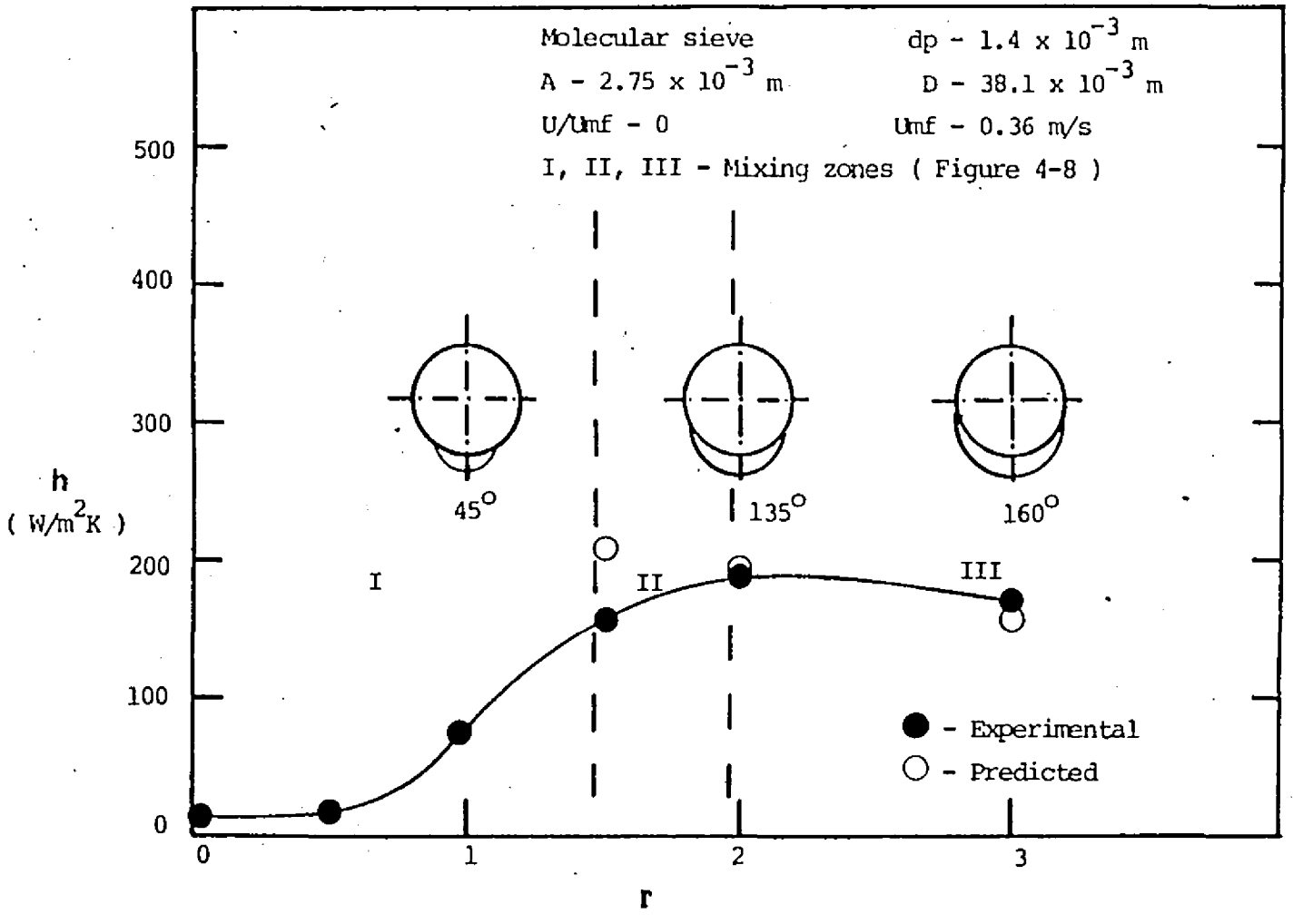

Figure 5-25 Comparison between experimental and predicted values of h

effective bed thermal conductivity in presence of surface stickiness and the bed porosity for wet or sticky beds. Since in the current study limited data were obtained on gap formation around cylinders immersed in beds of sticky particles, bed porosity and bed thermal conductivity, the heat transfer coefficient could not be predicted for beds of sticky or wet particles. Another key unknown at this time is the estimation of thermal conductivity of beds of wet and sticky particles.

5.4 CONCLUSIONS

In conclusion it can be said that vibration enhances the heat transfer rates considerably for beds of dry and sticky particles. The enhancement decreases with an increase in air flow and surface stickiness. The heat transfer coefficient decreases with an increase in particle size more significantly at smaller particle sizes ($d_p < 1$ mm) as compared to the larger particle sizes ($d_p \geq 1$ mm). At a given frequency of vibration higher amplitudes of vibration lead to higher heat transfer rates.

Presence of surface moisture enhances the heat transfer considerably for molecular sieve particles. Below the critical moisture content the heat transfer coefficient is same as that for the bed of dry particles.

The proposed model for evaluating h, predicts results within 25% for well mixed beds and $\theta > 120°$. The knowledge of particle circulation rates is essential for prediction of the heat transfer coefficient in the regime of poor mixing.

CHAPTER 6

CONCLUSIONS

This study presents experimental results of the effect of vibration on flow and immersed surface-to-bed heat transfer in a vibrated fluidized bed.

Immersed heat transfer surfaces mounted horizontally and rigidly to the bed allow use of deeper beds as compared to suspended surfaces because rigidly mounted surfaces themselves act as vibrators.

This study was divided into two sections - flow and heat transfer. The flow experiments were performed to obtain data in order to explain the heat transfer results. The flow experiments were conducted in a two-dimensional bed (0.20 m x 0.05 m) to allow easy visual observation of flow and mixing patterns around the immersed surfaces. The heat transfer experiments were performed in a bed of square cross-section (Figure 3-3). Glass ballotini and molecular sieve particles were selected as model particles and Table 3.1 lists their physical properties. Table 3.2 presents the range of operating parameters.

The important conclusions reached with regard to the flow behaviour of VFB's are:

1. Application of vibration facilitated homogeneous fluidization of sticky and agglomerating solids beyond $\Gamma>1$. For $X>0.006$ kg glycerine per kg dry glass ballotini, even vibrational acceleration of $\Gamma=4$ was

not enough to obtain homogeneous fluidization of sticky particles.

2. The bed pressure drop decreased with an increase in vibrational acceleration beyond $\Gamma>1$ following an initial rise due to bed compaction for $\Gamma\leq1$. The effect of vibration attenuated with increase in the air flow rate and bed height and a decrease in particle size. The amplitude of vibration exerts a stronger influence on the bed characteristics as compared to the frequency of vibration at a given vibrational acceleration.

3. Semi-quantitative maps for solids mixing in a VFB are presented for dry and sticky particles (Figures 4-8 through 4-10). Addition of surface stickiness delayed the onset of good solids mixing to higher Γ values. Small particles were more affected by stickiness as compared to the larger ones.

4. Depending upon the aeration rate and vibrational acceleration , application of vibration gives rise to particle-free air gaps around the immersed circular cylinders for beds of both dry and sticky particles (Figures 4-20 and 4-23). These gaps, which act as poor conductors of heat increased in size with an increase in Γ. At higher aeration rates these gaps formed at lower values of Γ.

The important conclusions reached from experimental studies on heat transfer are:

1. Vibration enhanced the overall heat transfer coefficient severalfold (upto 20 times) when the bed shifted from the regime of poor mixing to that of moderate and vigorous mixing of Figure 4-8. This enhancement was maximum for a non-aerated bed and decreased with an increase in the U/Umf ratio. Addition of surface stickiness caused the heat transfer enhancement to be more gradual and lower in magnitude.

2. Addition of surface stickiness decreased the heat transfer rate. Smaller particles were more affected by stickiness as compared to the larger ones. The heat transfer coefficient decreased with an increase in particle size. Higher amplitudes of vibration increased the heat transfer rate at the same value of vibrational frequency.

3. The heat transfer coefficient increased 4-8 times for wet molecular sieve particles in the region of unbound moisture. Below the critical moisture content of the particles the heat transfer coefficient approached that for dry particles. Once good solids mixing is achieved, vibrational acceleration and air flow rate had negligible effect on the shape of the heat transfer curves for wet

molecular sieve particles, over the entire range of parameters examined.

4. The proposed elementary model (Table 5.3) for evaluating the immersed surface-to-bed overall heat transfer coefficient predicted results with reasonable accuracy (±25%) in the regimes of moderate and vigorous mixing. In the regime of poor mixing knowledge of particle circulation rates is essential for predicting the heat transfer results. The model failed to predict the results for cases where less than one-third of the cylinder surface was covered with particle-free air gaps. The proposed model does not incorporate the effect of amplitude of vibration.

APPENDIX-A

EXPERIMENTAL UNCERTAINTY

A.1 Definitions and Terminology

ACCURACY refers to the fixed amount an instrument reading deviates from its known or calibrated input, regardless of how many times the measurement is made. Accuracy error is a fixed one.

PRECISION ERROR refers to the ability of an instrument to replicate its readings. Measurements may be precise or imprecise depending on how well an instrument can reproduce subsequent readings of an unchanged input. Precision error is not a fixed one.

ERROR is a number, 2 rpm, 0.6°C etc, and is defined as the calibrated or known input reading minus the instrument reading. Error is thus known or predicted only when we can calibrate or otherwise check the test apparatus.

UNCERTAINTY, like error, is a number that would be if it could be measured by calibration.

In this project the errors referred to are, the ones supplied by the manufacturers or are estimated by the method suggested by Kline and McClintock (1953) and Schenck (1968). The rule of thumb in estimation is, that the maximum possible error is equal to one half the least count of the instrument. The probability of the readings lying between this error bound is 95%.

A.2 Error and Uncertainty in Complete Experiments

In most of the situations, the final result of an experiment is dependent on measurements from several instruments combined through some mathematical process. In dealing with several instruments, the error whether uncertainty error or precision error shall be treated on a common basis. The general method of estimating error in the final result is shown below.

Consider the general case of a result E which is a function of the two measured variables V and W:

$$E + e = f(V+v, W+w) \qquad \text{A.2.1}$$

If this function is continuous and has derivatives, it can be expanded in a Taylor series and using the first two terms only and with

$$R = f(V, W)$$

the result is

$$e = \left(\partial E/\partial V \right)_W v + \left(\partial E/\partial W \right)_V w \qquad \text{A.2.2}$$

(the lower case letters apply to deviations from the correct reading).

$$\Sigma e^2 = \left(\partial E/\partial V \right)_W^2 \Sigma v^2 + 2\left(\partial E/\partial V \right)_W \left(\partial E/\partial W \right)_V \Sigma vw + \left(\partial E/\partial W \right)_V^2 \Sigma w^2$$

The term Σvw goes to 0 and $s^2 = \Sigma e^2/n$ (standard deviation) so that,

$$s^2 = \left(\partial E/\partial V \right)_W^2 s_V^2 + \left(\partial E/\partial W \right)_V^2 s_W^2 \qquad \text{A.2.3}$$

and for any uncertainty interval q,

$$q^2 = \left(\partial E/\partial V \right)_W q_V^2 + \left(\partial E/\partial W \right)_V q_W^2 \qquad \text{A.2.4}$$

Equation A.2.4 is very important in determining experimental error. A few equations of error determined from Equation A.2.4 are given in the table below.

Equations of Error

Function E	Error in Result q
$K (V \pm W)$	$(q_V^2 + q_W^2)^{1/2}$
KVW	$E((q_V/V)^2 + (q_W/W)^2)^{1/2}$
KV/W	" "
KV^b	bEq_V/V
Kexp(V)	Eq_V
Kln(V)	$Eq_V/(V\ln V)$
KSinV	$Eq_V/\mathrm{Tan}V$

(K is a constant of proportionality)

A.3 Sample Calculation

The average surface-to-bed heat transfer coefficient is defined as:

$$h = Q/(Ac\ \Delta T) \qquad A.3.1$$

Assuming no error in determining the heater surface area, Ac,

$$q_Q / Q = \pm 0.5\% = \pm 0.005$$

$$\Delta T = Ts - T_b$$

$$q_T = \pm 0.67°C \text{ (error in thermometer reading)}$$

The maximum error in average heater or bed temperatures is therefore ±0.67°C.

Referring to Appendix-D for the experimental values of the variables:

$$Ts = 36.67°C$$

$$T_b = 26°C$$

$$\Delta T = 10.67°C$$

Equation A.3.1 and the Equations of Error give:

$$q_T = ((0.67)^2 + (0.67)^2)^{1/2}$$

$$= 0.94°C$$

Therefore,

$$q_h/h = ((q_Q/Q)^2 + (q_T/\Delta T)^2)^{1/2}$$

$$q_h/h = ((0.005)^2 + (0.94)^2)^{1/2}$$
$$= 0.088$$
$$= 8.8\%$$

Thus, the maximum error in the heat transfer coefficient is about 8-9%. It should be noted that this is the maximum possible error due to the fact that temperature gradients used in the experiments were always greater than 10°C.

APPENDIX-B

AERODYNAMIC CLASSIFICATION OF PARTICLES

The behaviour of solids fluidized by gases falls into four clearly recognizable groups, characterized by density difference ($\rho_p - \rho$) and mean particle size. A general criterion for distinguishing between bubbling (aggregative, heterogeneous) and non-bubbling (particulate, homogeneous) fluidization, by the way of classifying powders into four different groups is presented below.

Group A- Materials having a small mean size and/or a low particle density (less than about 1.4 gm/cm^3) generally fall in this group (e.g. some cracking catalysts). Beds of powders in this group expand considerably before bubbling commences. When the gas supply is suddenly cut-off the bed collapses slowly, typically at a rate of 0.3-0.6 cm/s, this being similar to superficial velocity of the gas in the dense phase. Gross circulation of the powder (akin to convection currents in liquids) occurs even when few bubbles are present, producing rapid mixing.

Group B - This group contains most materials in the mean size and density ranges 40 m < dp < 500 m, 4 gm/cm^3> ρ_p > 1.4 gm/cm^3, sand being the most typical powder. In contrast with group A powders, naturally occuring bubbles start to form in this type of powder at or only slightly above minimum

fluidization velocity. Bed expansion is small and the bed collapses very rapidly when the gas supply is cut-off. There is little or no powder circulation in the absence of bubbles and the bubbles burst at the surface of the bed as discreet entities.

Group C - Powders which are in any way cohesive belong in this category. "Normal Fluidization " of such powders is extremely difficult; the powder lifts as a plug in small diameter tubes , or channnels badly, i.e. the gas passes up voids extending from distributor to bed-surface. This is due to the interparticle forces being greater than those which the fluid can exert on the particle, and these are generally the result of very small particle size, strong electrostatic charges or the presence in the bed of very wet or sticky material. Particle mixing and consequently heat transfer between a surface and the bed is much poorer than with the powders of groups A or B.

Group D - This group is confined to large and/or very dense particles which are readily spoutable. The gas velocity in the dense phase is high, solids mixing relatively poor; consequently back mixing of the dense phase gas is small.

A powder classification diagram for fluidization by air (ambient conditions) is shown in Figure B-1. This diagram derived from theoretical considerations, matches very well with experimental results and is widely accepted.

REFERENCES

1. Geldart, D. " Types of Gas Fluidization", Powder Technology, 7, pp 285 - 292, 1973.

2. Geldart, D. " The Effect of Particle Size and Size Distribution on the Behaviour of Gas-Fluidized Beds ", Powder Technology,Vol 6, pp 201 - 215, 1972.

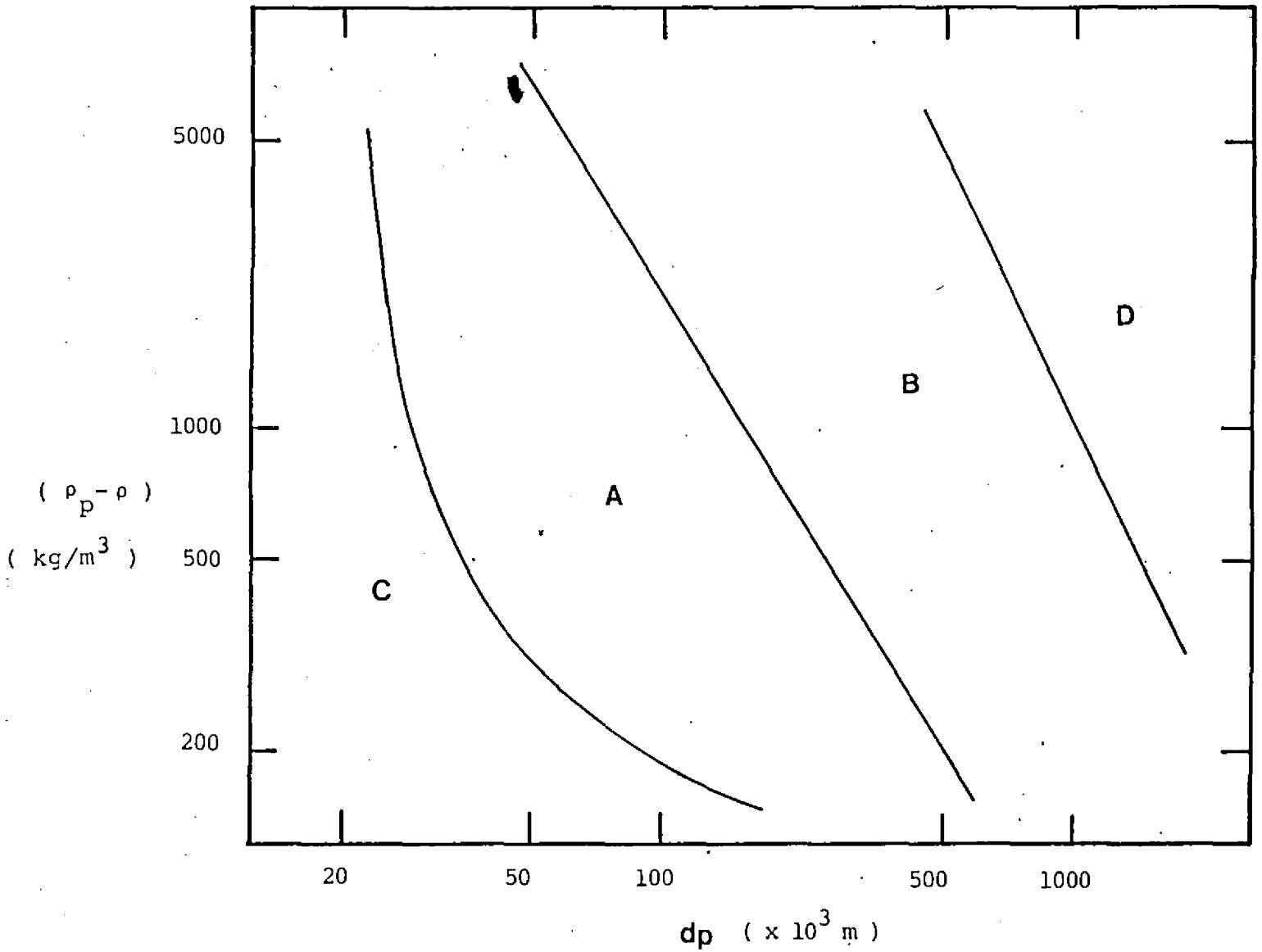

Figure B-1 Aerodynamic classification of particles

APPENDIX-C

THERMAL CLASSIFICATION OF PARTICLES

Geldart's (1973) classification of particles addresses only the fluid dynamic aspect of fluidization. Although fluid dynamics is important for bed behaviour, particles could be classified according to their performance in heat transfer, solids mixing and other types of processing characteristics for fluidized beds. Thermal classification of particles is made on the basis of the heat transfer component contributing most to the overall heat transfer between the bed and an immersed surface. Jovanic and Catipovic (1983) verified experimentally that thermally large particles remain essentially isothermal while in contact with the surface.

In a fluidized bed heat is transferred from (to) an immersed surface by packets of particles, by gas percolating between the particles of the packet and the surface and by gas bubbles. When smaller particles contact a hot heat transfer surface several rows of particles are heated and the emulsion packet is considered a continuum having a certain effective thermal conductivity. However, with increasing particle size, only one or few rows are heated during the time of packet contact, and the effective thermal conductivity begins to approach the thermal conductivity of the solid. Very large particles constitute a packet by itself.

The packets rest on the surface for a short time and are constantly replaced by fresh emulsion from the bed. This

constant particle motion is a mechanism of " particle convective mode of heat transfer " discussed in depth by Schlunder (1982). The surface-to-packet heat transfer is viewed in terms of two resistances in series: a) the contact resistance and b) the resistance within the emulsion packet phase. With increasing particle diameter the contact resistance constitutes a rapidly increasing portion of the total particle convective resistance. Therefore, regardless of the gas velocity, the contact resistance can be used in place of the total resistance for sufficiently large particles, i.e. the particle convective component is independent of the emulsion behaviour at the surface. This argument has been used by Jovanovic and Catipovic (1983) as a definition of thermally large particles. For small particles, the emulsion packet resistance is significantly greater than the contact resistance.

Jovanovic and Catopovic (1983) used the particle thermal time constant, $tp = \rho_p Cp\, dp^2 / 18\, Kf$ to thermally classify the particles. The particles are large if tp is significantly larger than the average packet residence time, t, and they are small if $tp < t$; as a consequence, the heat transfer coefficient is a function of t.

Figure C-1 shows the thermal classification of particles as a function of three dimensionless groups, as proposed by Jovanovic and Catipovic (1983).

REFERENCES

1. Jovanovic, G. and N. Catipovic," A New Approach in Classifying Solids in Bubbling Gas-Fluidized Beds ", Proceedings of the 4th International Conference on Fluidization, Japan, Vol 1, 9, 1983.

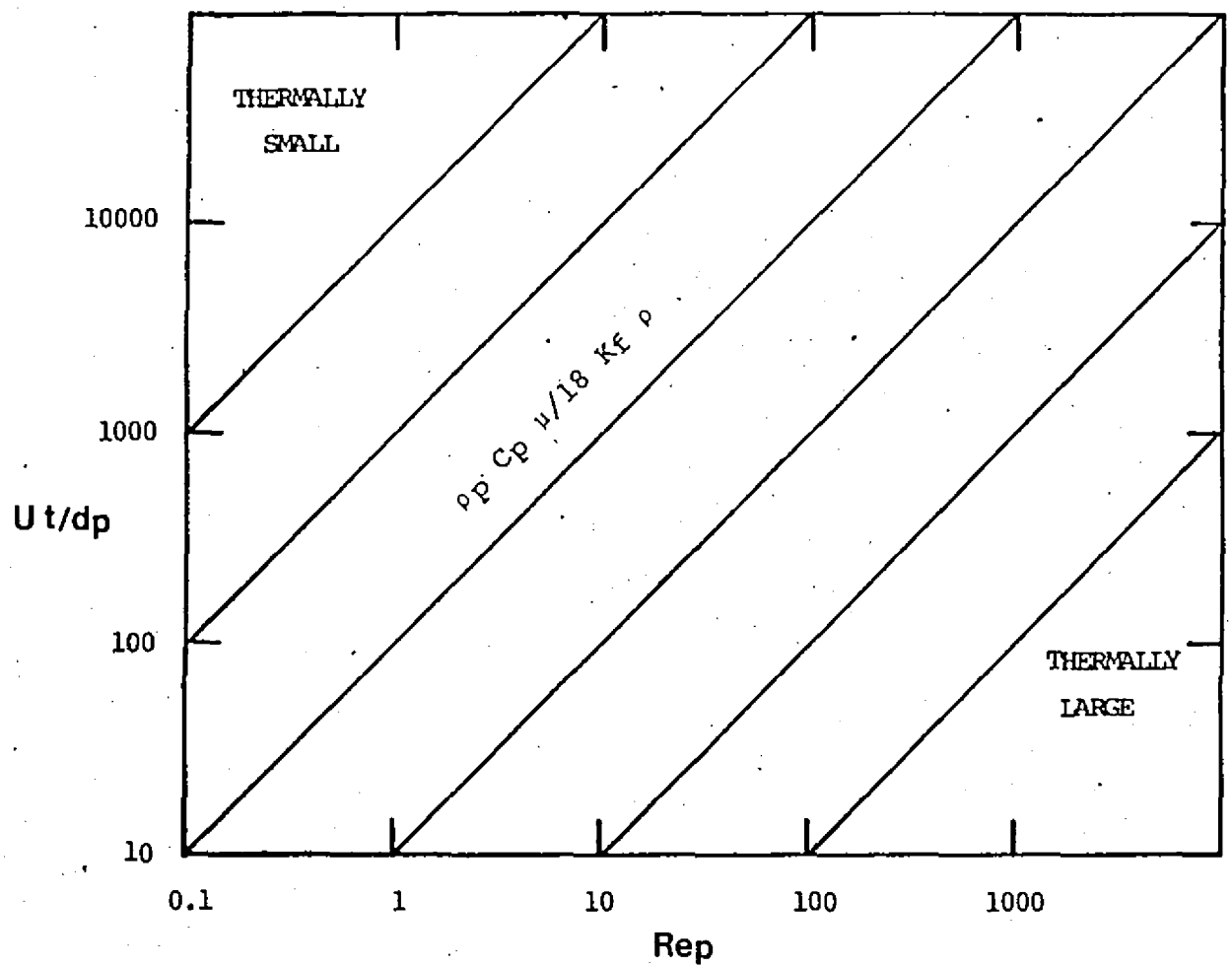

Figure C-1 Thermal classification of particles

APPENDIX-D

SAMPLE DATA SHEET

Date: 24 Nov 1983 Data Sheet Time:60 min

Cylinder Diameter: 38.1 mm Particle Type: Glass Ballotini
Size: dp=0.595 mm

Heat Transfer Area (Ac): 67.15×10^{-4} m^2 ΔPo (N/m^2):117

Distributor Type: 18% free area Flowmeter Reading:--

Umf (m/s): 0.201 Bed Height: 110 mm

U/Umf: 0.6 Temperature (°C)

r:0.5 Thermocouple No:

Wattmeter Reading: 33

Multiplying Constant: 0.2534

Actual Heat Input (Q): 8.3622 W

Bed Pressure Drop (ΔP): 902 N/m^2

Heater:	Bed:
1: 36.7	33: 32.1
4: 36.7	35: 26
7: 36.8	37: 30
10: 36.7	Bed Exit:
13: 36.7	26: 25.7

Average Bed Temperature (T): 26°C

Average Heater Temperature(Ts): 36.67°C

Temperature Gradient (ΔT): 10.67°C

Average Surface-to-Bed Heat Transfer Coefficient (W/m^2K): 116.7

REFERENCES

Abubakar, M.Y., J.D. Tarasuk, M.A. Bergougnou and J.L. Sullivan," Local and Overall Heat Transfer Coefficients on a Horizontal Tube Inside a Shallow Gas Fluidized Bed by Means of a New Two Sector Heat Transfer Probe", Proceedings of the Fourth International Conference on Fluidization, 5, 7, 1983.

Adams, R.L.," An Approximate Formula for Gas Convection Dominant Heat Transfer in Large Particle Fluidized Beds", ASME Journal of Heat Transfer, Vol 103, pp 395-397, 1981.

Adams, R.L.," Extension of Adams-Welty Fluid Bed Heat Transfer Model to the Packed Bed Case", ASME Journal of Heat Transfer, Vol 103, pp 602-604, 1981.

Adams, R.L. and J.R.Welty," An Analytical Study of Bubble and Adjacent Tube Influence on Heat Transfer to a Horizontal Tube in a Gas Fluidized Bed", ASME Journal of Heat Transfer, Vol 104, pp 205-209, 1982.

Adams, R.L.," An Approximate Model for Bubble Phase Convective Heat Transfer to a Horizontal Tube in a Large Particle Fluid Bed", ASME Journal of Heat Transfer, Vol 104, pp 565-567, 1982.

Adams, R.L.," Coupled Gas Convection and Unsteady Conduction Effects in Fluid Bed Heat Transfer Based on a Single Particle Model", Int.J.Heat Mass Transf.,Vol 25, 12, pp 1819-1828, 1982.

Adams, R.L.," Heat Transfer in Large Particle Bubbling Fluidized Beds", ASME Journal of Heat Transfer, Vol 106, pp 85-90, 1984.

Arai, N. and S. Sugiyama," Studies of Fluidization of Moist Particles", Journal of Chem.Eng.of Japan, Vol 7, 4, pp 247-251, 1974.

Baker, G.W.," Flow Properties of Powdered Shortenings", J.Food Science, Vol 45, pp 1370-1375.

Baskakov, A.P., B.V. Berg, O.K. Vitt, N.F. Fillipovsky, V.A. Kirakosyan, J.M. Goldobin and V.K. Maskaev," Heat Transfer to Objects Immersed in Fluidized Beds", Powder Technology, Vol 8, pp 273-282, 1973.

Biyikili, S. and J.C. Chen," Effect of Mixed Particle Sizes on Local Heat Transfer Coefficients Around a Horizontal Tube in Fluidized Beds", Presented at the 7th International Heat Transfer Conference, Munich, 1982.

Biyikili, S., K. Tuzla and J.C. Chen," Heat Transfer Around a Horizontal Tube in Freeboard Region of Fluidized Beds", Presented at the AIChE Annual Meeting, Los Angeles, 1982.

Bock, H.J. and O. Molerus," Influence of Hydrodynamics on Heat Transfer in Fluidized Beds", Fluidization 1980, Eds. J.R. Grace and M. Matsen, Plenum Publishing Corpn., N.Y.

Bock, H.J.," Effect of Bubble Flow on Heat Transfer Between Immersed Surfaces and Gas/Solid Fluidized Bed", German Chemical Engineering, Vol 4, 1, pp 23-30, 1981.

Bock, H.J.," Dimensioning of Vertical Heat Transfer Surfaces in Gas/Solid Fluidized Beds", German Chemical Engineering, Vol 4, 6, pp 356-362, 1981.

Bock, H.J.," Heat Transfer in Fluidized Beds", Proceedings of the Fourth International Conference on Fluidization, 5, 8, 1983.

Botterill, J.S.M., Y. Teoman and K.R. Yuregir," Temperature Effects on the Heat Transfer Behaviour of Gas Fluidized Beds", AIChE Symposium series, Vol 77, 208, pp 330-340, 1981.

Bratu, E. and G.I. Jinescu," Effect of Vertical Vibrations on the Pressure Drop in a Fluidized Layer", British Chem. Eng., Vol 16, 8, pp 691-695, 1971.

Bretsznajder, S., M. Jaszczak and W. Pasiuk," Increasing the Rate of Certain Industrial Chemical Processes by the Use of Vibration", International Chem. Eng., Vol 3, 4, pp 496-502, 1963.

Bukarwa, M.F., V.A. Chelenov and N.V. Mikhailov,"Investigations of Heat Transfer Between Heating Surfaces and Vibrofluidized Bed", Int. Chem. Eng., Vol 9, pp 119-121, 1969.

Catala, V.A. and P.F. Maupsey," Thermal Conductivity of Porous Bodies at Low Pressures", Presented at 7th Int. Congress of Chem. Eng. Chem. Equipment Design and Automation, Czechoslovakia, 1981.

Cermak, B.," Thermodynamic Models of Moist Material", Presented at 7th Int. Congress of Chem. Eng. Chem. Equipment Design and Automation, Czechoslovakia, 1981.

Cermak, B.," Thermogravimetric Determination of the Dried Material Properties", Presented at 7th Int. Congress of Chem. Eng. Chem. Equipment Design and Automation, Czechoslovakia, 1981.

Chandran, R., J.C. Chen and F.W. Staub," Local Heat Transfer Coefficients Around Horizontal Tubes in Fluidized Beds", ASME Journal of Heat Transfer, Vol 102, pp 152-157, 1980.

Chandran, R. and J.C. Chen," Bed-Surface Contact Dynamics for Horizontal Tubes in Fluidized Beds", AIChE Journal,Vol 28, 6, pp 907-913, 1982.

Chelenov, V.A. and N.V. Mikhailov," Properties of a Vibrating Fluidized Bed",Inzh. Fiz. Zhurn., Vol 9, 2, pp 196-200, 1965.

Coelho, M.C. and N. Harnby," The Effect of Humidity on the Form of Water Retention in a Powder", Powder Technology, Vol 20, pp 197-200, 1978.

Coelho, M.C. and N. Harnby," Moisture Bonding in Powders", Powder Technology, Vol 20, pp 201-205, 1978.

Danielsen, S. and S. Hovmand," Drying of Granulated Product in a Vibrated Fluid Bed", DRYING'80, Vol 1, Ed. A.S. Mujumdar, Hemisphere Publishing Corpn., N.Y., pp 194-199, 1980.

Delker, N.A. and L.R. Glicksman," Conduction Heat Transfer at the Surface of Bodies Immersed in Gas Fluidized Beds of Spherical Particles", AIChE Symposium series, Vol 77, 208, pp 341-349, 1981.

Downton, G.E., J.L. Flores-Luna and C.J. King," Mechanism of Stickiness in Hygroscopic Amorphous Powders", I&EC Fundamentals, 21, pp 447-451, 1982.

Endoh, K. and H. Hirano," Heat Transfer from a Sphere and a Cylinder in a Sinusoidally Vibrating Air Stream", Kagaku Kogaku, 37, pp 815-820, 1973.

Engelmann, E.W.," The Utah Electric Vibrating Dryer", Mining and Metallurgy, pp 477-478, November 1958.

Erdesz, K. and Z. Ormos," Bed Expansion and Pressure drop in Vibro-Fluidized Layers", DRYING'84, Ed. A.S. Mujumdar, Hemisphere/Springer Verlag, N.Y., pp 169-177, 1984.

Feddors, R.F. and R.F. Landel," Effect of Surface Adsorption and Agglomeration on the Packing of Particles", Powder Technology, Vol 23, pp 219-223, 1974.

Gabor, J.D.," Heat Transfer to Particle Beds with Gas Flows Less than or Equal to that Required for Incipient Fluidization," Chem. Eng. Science, Vol 25, pp 979-984, 1970.

Geldart, D.," Types of Gas Fluidization", Powder Tech-

nology, Vol 7, pp 285-292, 1973.

Geldart, D. and A.R. Abrahamsen," Homogeneous Fluidization of Fine Powders Using Various Gases and Pressures", Powder Technology, Vol 19, pp 133-136, 1978.

Geldart, D., N. Harnby and A.C. Wong," Fluidization of Cohesive Powders", Powder Technology, Vol 37, pp 25-37, 1984.

Goel, I., S.C. Saxena and A.F. Dolidovich," Heat Transfer from Rough and Finned Horizontal Tubes in a Gas Fluidized Bed", ASME Journal of Heat Transfer, Vol 96, pp 91-97, 1984.

Grewal, N.S. and S.C. Saxena," Heat Transfer Between a Horizontal Tube and a Gas-Solid Fluidized Bed", Int. J. Heat Mass Transfer, Vol 23, pp 1505-1519, 1980.

Grewal, N.S.," A Generalized Correlation for Heat Transfer Between a Gas-Solid Fluidized Bed of Small Particles and an Immersed Staggered Array of Horizontal Tubes", Powder Technology, Vol 30, 2, pp 145-154, 1981.

Grewal, N.S. and S.C. Saxena," Experimental Studies of Heat Transfer Between a Bundle of Horizontal Tubes and a Gas Solid Fluidized Bed of Small Particles", Ind. Eng. Chem. Process Des. Dev., 22, pp 367-376, 1983.

Gupta, R.," Aerodynamic and Drying Characteristics of a Vibrated Fluidized Bed", Master's Thesis, McGill University, Montreal, Canada, 1979.

Gupta, R. and A.S. Mujumdar," Aerodynamics of a Vibrated Fluid Bed", The Can. J. of Chem. Eng., Vol 58, pp 332-338, 1980.

Gutman, R.G.," Vibrated Beds of Powders, Part I: A Theoretical Model for the Vibrated Bed", Trans. Inst. Chem. Engrs., Vol 54, pp 174-183, 1976.

Harrison, D. and L.S. Leung,"Bubble Formation at an Orifice in a Fluidized Bed," Trans. Inst. Chem. Engrs., Vol 39, pp 409-414, 1961.

Hasatani, M., N. Arai and K. Hori," Drying of Granular Particles in a Multistage Inclined Fluidized Bed with Mechanical Vibration", Proceedings of 4th International Drying Symposium, Vol I, Eds. R. Toei and A.S. Mujumdar, pp 228-235, 1984.

Heyde, M and H.J. Klocke," Heat Transfer Between Fluidized Beds and Heat exchange Installations", International Chemical Engineering, Vol 20, 4, pp 583-599, 1980.

Hoelen, Q.E.J.J.M. and S. Stemerding," Heat Transfer in a Fluidized bed", Powder Technology, Vol 30, 2, pp 161-184, 1981.

Holman, J.," Experimental Methods for Engineers", McGraw-Hill Book Co., NewYork, 1966.

Jinescu, G., C. Balaban and T. Dobre," Drying of Granulated Polymers in Vibrated Fluidized Beds", DRYING'82, Ed. A.S. Mujumdar, Hemisphere/McGraw-Hill, N.Y., pp 42-47, 1982.

Jinescu, G. and C. Balaban," Drying of Granulated Polymers in Vibrofluidized Bed", Proceedings of 3rd International Drying Symposium, Univ. of Birmingham, Vol 2, Ed. J.C. Ashworth, pp 124-129, 1982.

Jovanovic, G.N. and N.M. Catipovic," A New Approach in Classifying Solids in Bubbling Gas-Fluidized Beds", Proceedings of the Fourth International Conference on Fluidization, Japan, 1, 9, 1983.

Kavetskii, G.D., L.V. Nikonov, V.N. Kartechin, N.G. Krokhin and M.K. Kosheleva," Aerodynamics of Flow in Vibro-Aero Fluidized Bed", Chem and Tech. of fuels and Oils, 11, pp 717-721, 1975.

Kazachinskaya, N.V. and O.I. Bilyk," Multifactorial Experiment on Drying of Common Salt in a Vibrated Fluidized Bed with Conductive Heating", Heat Transfer-Soviet Research, Vol 7, 6, 1975.

Keey, R.B.," Drying Principles and Practice", Pergamon Press, 1972.

Kendall, K.," Sticky Solids", Contemporary Physics, Vol 21, pp 277-297, 1980.

Kitano, K., H. Hirano and K. Endoh," Flow Pattern in a Vicinity of a Sphere or Disk Sinusoidally Vibrating in Liquid", Memoirs of Faculty of Engineering, Hokkaido University, Japan, Vol XV, 1(66), 1979.

Kline, S.J. and F. McClintock," Describing Uncertainties in Single Sample Experiments", J. Mech. Engineering, 1953.

Kunii, D. and O. Levenspiel," Fluidization Engineering", Wiley Publications, 1967.

Kwamya, J. and A.S. Mujumdar," Heat Transfer for a Horizontal Tube Suspended in a Vibrated Fluid Bed", To be presented at the Can. Chem. Eng. Conf., Quebec City, October 1984.

Malhotra, K., L. Law-Kwet-Cheong and A.S. Mujumdar,

" Pressure Drop Characteristics for Vibrated Beds of Dry and Sticky Particles", Powder Technology, Vol 39, 1, pp 101-105, 1984.

Malhotra, K. and A.S. Mujumdar," Single Tube Heat Transfer in Aerated Vibrated Beds", Proceedings of the Fourth International Drying Symposium, Vol II, Eds. R.Toei and A.S. Mujumdar, pp 681-689, 1984.

Malhotra, K. and A.S. Mujumdar," Flow Patterns for Cylinders Immersed in an Aerated Vibrated Bed", Accepted for publication in The Can. J. of Chem. Eng., 1984.

Martin, H.," Fluid-Bed Heat Exchangers- A New Model for Particle Convective Energy Transfer", Chem Eng. Communn., Vol 13, pp 1-16, 1981.

Mersmann, A.B. and R. Wunder," Heat Transfer Between a Dispersed System and a Vertical Heating or Cooling Surface", Presented at ITHC, Toronto, 1978.

Mickley, H.S. and D.F. Fairbanks," Mechanism of Heat Transfer to Fluidized Beds", AIChE Journal, Vol 1, pp 374-384, 1955.

Molerus, O.," Interpretation of Geldart's Type A,B,C and D Powders by Taking into Account Interparticle Cohesion Forces", Powder Technology, Vol 33, 1, pp 81-88, 1982.

Mujumdar, A.S.," Recent Developments in Drying of Solids", J. Indian Institute of Chemical Engineers, Vol 4, pp 100-103, 1981.

Mujumdar, A.S. and Z. Pakowski," Effect of Vibration on Immersed Surface Heat Transfer in a Fluidized Bed", Presented at the ASME-JSME Joint Thermal Engineering Conference, Honolulu, 1983.

Mujumdar, A.S.," Aerodynamics, Heat Transfer and Drying in Vibrated Fluid Beds", Lat.Am. J. Heat Mass Transfer, Vol 7, pp 99-110, 1983.

Mujumdar, A.S.," Aerodynamic Characteristics of a Vibrated Bed of Particles", DRYING'84, Ed. A.S. Mujumdar, Hemisphere/ Springer-Verlag, N.Y., pp 178-185, 1984.

Mujumdar, A.S.," Aerodynamics and Heat Transfer Measurement in Aerated Vibrated Beds", Presented at VIIth All Union Heat and Mass Transfer Conference, Minsk, USSR, 1984.

Ozkaynak, T.F. and J.C. Chen," Emulsion Phase Residence Time and its Use in Heat Transfer Models in Fluidized Beds", AIChE Journal, Vol 26, 4, pp 544-549, 1980.

Pakowski, Z. and A.S. Mujumdar," Heat Transfer from a Horizontal Cylinder to a Vibrated Bed of Wet Particles", Presented at the Third Drying Symposium, Birmingham, 1982.

Pakowski, Z., A.S. Mujumdar and C. Strumillo," Theory and Application of Vibrated Bed and Vibrated Fluid Bed for Drying Process", Advances in Drying, Ed. A.S. Mujumdar, Vol 4, Hemisphere/Springer-Verlag, pp 245-306, 1984.

Perry, R.H. and C.H. Chilton," Chemical Engineer's Handbook", Vth ed., McGraw-Hill Kogakusha Ltd, Tokyo.

Pye, E.W.," Vibration Shakes up Thinking on Fluid Bed Drying", Process Engineering, pp 61-63, March 1974.

Rietema, K.," Fluidized Bed Drying", Lecture notes, Technical University, Eindhoven, The Netherlands.

Ringer, D.U. and A.S. Mujumdar," Immersed Surface-to-Particle Heat Transfer in a Vibro-Fluidized Bed", DRYING'82, Ed. A.S. Mujumdar, Hemisphere/McGraw-Hill, N.Y., 1982.

Ringer, D.U. and A.S. Mujumdar," Surface-to-Particle Heat Transfer in Vibro-Fluidized Beds", Accepted for publication in Powder Technology, 1984.

Ringer, D.U. and A.S. Mujumdar," Analysis of Aerodynamics and Heat Transfer in Vibrofluidized Beds", Drying Technology- An International Journal, Vol 2, 4, 1984.

Schlunder, E.U.," Particle Heat Transfer",Presented at the 7th Int. Heat Transfer Conference, Munich, 1982.

Schenck, H.," Theories of Engineering Experimentation", 2nd edition, Published by McGraw-Hill Book Co., N.Y., 1968.

Schubert, H.," Capillary Forces- Modelling and Application Particulate Technology", Powder Technology, Vol 37, pp 105-116.

Seville, J.P.K. and R. Clift," The Effect of Thin Liquid Layers on Fluidization Characteristics", Powder Technology, Vol 37, pp 117-129, 1984.

Shah, M.M.," Generalized Prediction of Maximum Heat Transfer to Single Cylinders and Spheres in Gas-Fluidized Beds", Heat Transfer Eng., An International quarterly, Vol 4, 3-4, pp 107-122, 1983.

Shah, P.J., S.N. Upadhyay and S.N. Saxena," Heat Transfer from Smooth Horizontal Tubes Immersed in Gas Fluidized Beds", AIChE Symposium series, Vol 77, 208, pp 350-355, 1981.

Simpson, H.C. and B.W. Rodger," The Fluidization of Light Solids by Gases Under Pressure and Heavy Solids by Water", Chem. Eng. Science, Vol 16, pp 153-180, 1963.

Skilbeeck, J.P.," Tracer Study Characterisation of Polymer Dryer Performance", Chem. Eng. Communn., Vol 4, pp 207-218, 1980

Strumillo, C. and Z. Pakowski," Drying of Granular Products in Vibro Fluidized Beds", DRYING'80, Ed. A.S. Mujumdar, Hemisphere Publishing Corpn., N.Y., pp 211-226, 1980.

Suarez, E., R.S. Figloiola and D.R. Pitts," Instantaneous Azimuthal Heat Transfer Coefficients from a Horizontal Cylinder to a Mixed Particle Size Air-Fluidized Bed", ASME paper, 83-HT-93, 1983.

Sunderland, P. and I. Ahmed," Mass Transfer in a Vibration Mixed Reactor", Trans. I. Chem Eng., Vol 59, pp 95-99, 1981.

Suzuki, K., H. Hosaka, R. Yamazaki and G. Jimbo," Drying Characteristics of Particles in a Constant Drying Rate Period in Vibro-Fluidized Bed", J. of Chem Eng. of Japan, Vol 13, 2, pp 117-122, 1980.

Suzuki, K., A. Fujigama, R. Yamazaki and G. Jimbo," Some Investigations of Falling Rate Period of Vibro-Fluidized Bed Drying", J. of Chem Eng. of Japan, Vol 13, 6, pp 493-495, 1980.

Suzuki, K., A. Fujigama, R. Yamazaki and G. Jimbo," Characteristics of Vibro-Fluidized Bed for Drying of Wetted and Agglomerated Particles", J. of Chem Eng. of Japan, Vol 13, 6, pp 495-498, 1980.

Suzuki, K., R. Yamazaki and G. Jimbo," Incipient Fluidization Condition for a Vibro-Fluidized Bed", Kagaku-Kogaku Ronbunshu, 8, pp 307-311, 1982.

Suzuki, K., M. Ikeda, M. Esaka and K. Kubota," Characteristics of Vibro-Fluidized Bed Freeze Drying", Proceedings of the Fourth International Drying Symposium, Vol II, Eds. R. Toei and A.S. Mujumdar, pp 433-438, 1984.

Szentgyorgyi, S., K. Molnar and M. Orvos," The Second Falling Rate Period of the Capillary Porous Materials", Presented at the 7th Int. Chem. Eng. Chem. Equipment Design and Automation, Czechoslovakia, 1981.

Toei, R.," Drying Mechanism of Capillary Porous Bodies", Advances in Drying, Vol 2, Ed. A.S. Mujumdar, Hemisphere/ McGraw-Hill, N.Y., pp 267-297, 1984.

Toei, R., T. Ohmori, T. Hiruta and M. Okazaki," Heat Transfer

Coefficient Between Heating Wall and Agitated Granular Bed", Proceedings of the 4th International Drying Symposium, Vol II, Eds. R. Toei and A.S. Mujumdar, pp 495-500, 1984.

Toei, R., T. Ohmori and M. Okazaki," Heat Transfer from Submerged Body Moving in Granular Bed", Proceedings of the 4th International Drying Symposium, Vol II, Eds. R. Toei and A.S. Mujumdar, pp 501-506, 1984.

Varsayni, E.P. and Z. Puskas-Nadai," Hydrodynamic Aspects in the Choice Between Vibrational and Spouted Bed Drying Processes", Hungarian Journal of Industrial Chemistry, Vol 5, pp 415-422, 1977.

Wakao, N. and S. Kaguei," Heat and Mass Transfer in Packed Beds", Gordon and Breach Science Publishers, N.Y., 1982.

Yamazaki, R., Y. Kanagawa and G. Jimbo," Heat Transfer in Vibro-Fluidized Bed- Effect of Pulsated Gas Flow", J. of Chem Eng. of Japan, Vol 7, 5, pp 373-378, 1974.

Zabrodsky, S.S.," Hydrodynamics and Heat Transfer in Fluidized Beds", M.I.T. Press, 1966.